Novel Mechanisms of Endothelial-Epithelial Interactions Underlying Cancer Metastasis

by

Yamicia Doyasi Connor

B.S., Chemical-Biological Engineering, Massachusetts Institute of Technology (2007)

B.S., Biology, Massachusetts Institute of Technology (2007)

Submitted to the Department of Health, Sciences, and Technology in partial fulfillment of the requirements for the degree of

Doctor of Philosophy in Medical Engineering and Medical Physics

at the

MASSACHUSETTS INSTITUTE OF TECHNOLOGY

September 2013

Author .....
Department of Health, Sciences, and Technology
August 26, 2013

Certified by .....
Shiladitya Sengupta, Ph.D.
Assistant Professor
Thesis Supervisor

Accepted by .....
Emery N. Brown, M.D., Ph.D.
Director, Harvard-MIT Program in Health Sciences and Technology/Professor of Computational Neuroscience and Health Sciences and Technology

Novel Mechanisms of Endothelial-Epithelial Interactions Underlying Cancer Metastasis

by

Yamicia Doyasi Connor

Submitted to the Department of Health, Sciences, and Technology
on August 26, 2013, in partial fulfillment of the
requirements for the degree of
Doctor of Philosophy in Medical Engineering and Medical Physics

Abstract

Elucidation of molecular mechanisms underlying metastasis is the final frontier in cancer biology research. Identifying individual pathways in the metastatic cascade could lead to development of metastasis-specific therapeutics; however, current *in vivo* metastasis model systems are not efficient tools for isolating a single molecular event from the network of complex biological pathways. In response to these needs, we have developed a 3D *in vitro* co-culture system that isolates molecular and physical interactions between metastatic cells and the endothelium, which are prerequisite for invasive spread. We have used this model to identify key mediators of epithelial-endothelial cell interactions, to screen metastasis specific therapeutics, and most significantly, to elucidate a novel form of intercellular communication through thin cytoskeletal projections called nanoChannels (nCs) that is involved in pathological angiogenesis and that may prime metastatic spread. Metastatic cells preferentially form nCs with the endothelium, enabling rapid and directed transfer of intracellular contents. Proteins, small cytoplasmic dyes, nanoparticles, and most interestingly, functional microRNAs (miRNAs) are transported through these structures. Communication of miRNAs through nCs presents a novel mechanism of pathological angiogenesis and the angiogenic switch. NanoChannel-mediated communication introduces a new paradigm of cancer progression in which tumor cells can directly transform surrounding cell populations in order to facilitate cancer pathogenesis.

Thesis Supervisor: Shiladitya Sengupta, Ph.D.
Title: Assistant Professor

Acknowledgments

I would like to thank Professor Sengupta for his guidance throughout my PhD and for kindly providing the resources necessary for completion of this project. Thank you to all my committee members for their mentorship and greatly appreciated feedback. I would like to especially thank, Professor Dvorak and Professor Zetter for always graciously giving their time and support to meet with me throughout the semesters. Next, I would like to thank Professor Harris for being an exceptional mentor, who throughout the years has provided steadfast guidance to Yonatan and I in our professional and academic careers. Lastly, I would like to thank Amjad Husain. It has has been a pleasure working with you this last year and I look forward to our continued collaborations in the future.

I have had the privilege of working with several exceptional scientists during my PhD. I hope that I was able to teach you all a fraction of the things I have learned from you. I would like to especially thank Michael Oh. Together we tirelessly performed many of the initial, often unsuccessful, experiments for the project. It's funny to think you will actually be a doctor before I am. Congratulations and I am so happy to have worked with you. I would next like to thank Taylor Lloyd. Both in the lab and throughout medical school you have been a constant source of support. I am so blessed to have you as a friend and look forward to many more years of friendship, as we navigate the next steps of our careers. I would like to thank Divya Bharat. Your cheerful disposition was always a bright spot in my day. I would like to thank Shyama Nandakumar. Even though we have worked together for the shortest amount of time, it's like you have always been a member of the group. Your support and hard work, particularly during a difficult period, was absolutely remarkable. I am extremely impressed on how quickly you were able to learn the material, but more importantly how seamlessly you integrated into our team never complaining when asked to do almost impossible tasks. Hopefully we will be able to work with each other again in the future. I would next like to thank Cherelle Walls. We have known each other since MITES.

Can you believe that?!?! I am so happy that you were able to work with us on this project and I know it's been difficult balancing your volunteer work in the lab with a full time job. Thank you again for all your hard work. We are in the home stretch now.

Last, I would like to thank those who have supported me in almost every way imaginable, both academically and personally. I would like to start by thanking Sarah Tekleab. You have been such a blessing in my life. What started out with me providing you an opportunity has transformed into you giving me so much more. Your work in the lab on this project has been tireless. You have supported me as well as others in the group, many times carrying an unequal share of the burdens. Your willingness to selflessly serve those around you in a humble and genuine way is a quality few people possess and one I can learn much from. I love you and I thank you. I would next like to thank my fianc Yonatan Tekleab. It's hard to find words to describe how blessed I am to have you in my life. You have supported in every possible way a human being can support another. Through every step of my academic, professional, and personal life beginning with my freshmen year at MIT, you have selflessly given of your time, love, and companionship. I unequivocally would not be here today if it wasnt for your love and support. I love you with all of my heart. And finally to my family my mother, father, and brother without your selfless love I would not be where I am today. You are the anchor that I need in order to undertake all the challenges in my crazy life. I thank you from the bottom of my heart. I love you and I am so blessed to have such a wonderful family.

Contents

List of Figures

6-2 **Nanochannel (nC)-mediated transfer of intercellular contents in an *in vivo* metastatic breast cancer model.** MDA-MB-231 cells were loaded with CFSE (green) and injected into the tail vein of CD1 nude mice. The mice were sacrificed at the indicated time points and the lungs were removed, fixed, and stained. Endothelial cells (red) were triple-stained with vWF, CD34, and PECAM-1 (white dashed outline). 3D confocal reconstructions demonstrate nCs penetrating the endothelial cells and transferring CFSE dye (white solid outline). Examples of intercellular transfer are indicated with yellow arrowheads. MDA-MB-231 cells can be seen migrating out of the endothelial vessels 24hrs post-injection. Micrometastases began to form by 72hrs (yellow dashed outline). 304

6-3 ***In vivo* nanoChannel projections captured with SEM micrographs.** The figure shows a metastatic breast epithelial cell, highlighted in yellow, extending an nC projection to the endothelium, highlighted in purple. The endothelium is identified due to the presence of red blood cells in the endothelial cell lumen. Metastatic breast epithelial cells are loaded with gold nanoparticles in order to identify these cells in the tissue. 305

6-4 **High magnification view of nanoChannels *in vitro*.** High magnification SEM micrographs show nanoChannels extending from metastatic breast epithelial cells to the endothelium in *in vitro* cultures. These nanoChannels look similar to structures observed *in vivo*, which further confirms that the structures observed in the *in vitro* model system are similar to the structures that are formed *in vivo*.306

6-5 ***In vivo* intercellular transfer was reduced after pre-treatment with cytoskeletal polymerization inhibitors.** Endothelial cells were isolated from mouse lungs 48hrs post-injection and the level of transfer was quantified using FACS. Intercellular transfer was reduced by 43% ($p<0.001$). 307

List of Tables

Chapter 1

Introduction

Cancer cell metastasis is the highest cause of cancer-related mortality, responsible for 90% of all cancer-associated death[7–9]. More than 1 in 3 individuals will be diagnosed with cancer over their lifetime, resulting in greater than 500,000 US deaths annually[10]. Decades of research in cancer biology have brought the field tremendous understanding of the disease; however metastasis remains the most poorly understood aspect of cancer progression[7,9,11]. Limited treatment options exist for patients with metastatic cancer, and surgical interventions are rarely successful[7,8,12]. Despite aggressive treatment, only 20% of patients who receive a diagnosis of metastatic cancer will survive more than 5 years[8,10,12] compared to a nearly 70% survival rate upon early diagnosis[10]. Limited understanding of the mechanistic steps that underlie metastasis imposes the rate-limiting step in the development of future generations of successful cancer therapies[8,9]. Metastasis is a complex cascade involving genetic, environmental, and physical forces that transform a single tumor-initiating cell into wildly invasive disease[7–9,12–15]. One of the major limiting factors in the study of cancer metastasis is development of appropriate *in vivo* and *in vitro* model systems that allow for the isolation and probing of discrete steps of the metastatic cascade[8]. An understanding of the individual steps that underlie metastatic progression will allow for the development of therapeutic interventions directly targeting invasion[7].

Much of the insight into cancer metastasis has been gained through the de-

velopment of *in vivo* model systems or retrospective analysis of metastatic tissues removed from human patients[8,16]. However, these approaches suffer from unique weaknesses. The greatest limitation of animal model systems is their inability to decouple individual stages of metastasis. Retrospective analyses of human metastatic tumors also suffer from a similar weakness due to difficulty in determining *de novo* site-specific roles that a genetic anomaly may have served[16]. Appropriate *in vitro* model systems would create a platform for the direct observation and manipulation of cellular processes involved in metastasis not easily allowed by the currently available tools[16,17].

Each stage in the metastatic cascade presents unique therapeutic opportunities. Beginning with formation of the primary tumor, the steps of metastatic invasion can be summarized into breakdown of the basement membrane and local tissue invasion, systemic dissemination through the vasculature, and finally seeding of a secondary tumor site. Each of these stages presents an opportunity for intervention[12]. However, current insight into the mechanisms that control colonization are less well developed than our understanding of the initial stages of metastasis which are formation of the primary tumor and interactions with the endothelium. While the majority of current drug therapies target the biology of the primary tumor, arguably one of the most promising, yet untapped, opportunities for therapeutic intervention within the metastatic cascade is disruption of interactions between metastatic cells and the endothelium that are prerequisite for formation of secondary tumor sites. Disruption of the events underlying these interactions may introduce new therapeutic strategies for both early and late stages in metastasis.

The complexity of cancer underlies the need to develop physiologically relevant platforms that mimic tumor development *in vivo*. Previous studies have shown that 3D culture systems provide a more structurally appropriate context to study cancer progression, offering superior recapitulation of the tumor environment compared to traditional 2D systems. The advantage of 3D systems is best epitomized in breast cancer research. Standard two-dimensional model systems are limited in their ability to accurately capture the molecular mediators underly-

ing breast cancer and cannot be used to study interactions between multiple cell types[18]. The utility of 3D cultures to better capture cancer physiology has been well demonstrated[18]; 3D cultures allow for the recapitulation of native cellular morphology and architecture, which affect cellular gene expression, behavior, and response to external environment[16]. The use of 3D mammosphere cultures for the study of breast cancer has been widely adopted by the research community[16]. However, a limitation of these current systems is their exclusive focus on the development of the primary tumor: the model systems do not capture the molecular events underlying more advance stages of cancer, specifically the interactions with the endothelium that precede invasive spread throughout the body.

In an attempt to address these needs, this thesis describes the engineering of a 3D *in vitro* co-culture system which captures molecular and physical interactions between metastatic cells and the endothelium that allow for the discovery of metastasis-promoting pathways. I begin the thesis with a review of literature in **Chapter 2** which discusses biological mechanisms involved in formation of a primary tumor with specific emphasis on the role of the endothelium and tumor microenvironment in cancer progression. I end with a perspective into mechanisms of cell-cell communication, emphasizing modes of intercellular communication that enable to spread of genetic material.

The review of literature is followed in **Chapter 3** by a deep characterization and discussion of the model system. Interactions between metastatic cells and the endothelium are pre-requisite for the development of metastatic disease, presenting a key point of therapeutic intervention motivating the development of our co-culture system. This powerful model has enabled discovery of important mediators of epithelial-endothelial cell (EEC) interactions by providing a high-throughput platform to study interaction phenotypes and screen anti-angiogenic and anti-tumorigenic therapies. Characterization of EEC interaction phenotypes reveals stark differences between primary, tumorigenic non-metastatic, and metastatic cells. Interestingly, metastatic cells derived from several tissue types preferentially align and incorporate within vessels, while primary and tumorigenic cells have

low to moderate interaction with the endothelium, respectively. From our analysis of these cultures arose a two-parameter interaction index that can differentiate metastatic capacity of breast epithelial cells by examining EEC interaction phenotype. We have used this model to identify key mediators of EEC interactions, such as FAK and $\beta 1$ integrins. RNAi inhibition of FAK and $\beta 1$ integrins resulted in the disruption of the architecture, leading to 3.4 ($p<0.001$) and 8.6 ($p<0.001$) fold change in cell interactions, respectively. Small molecule inhibitors of the FAK-$\beta 1$ signaling pathway were used to perturb this architecture, resulting in a 68% ($p<0.05$) decrease in invasive capacity while enhancing the susceptibility to the metastatic cells to the cytotoxic agent doxorubicin.

The co-culture model enabled drug screening of metastatic specific therapeutics. However, the most interesting finding from characterization of the model system was the discovery of a novel form of intercellular communication between metastatic cells and the endothelium through thin cytoskeletal projections called nanoChannels (nCs). The remainder of this thesis focusses on describing this communication in order to understand its functional significance in cancer.

Chapter 4 introduces communication through nCs. Unlike classical modes of cell-cell communication (i.e. paracrine, endocrine, and autocrine signaling), nCs allow for both rapid and directed transfer of intracellular contents from metastatic breast cancer cells to the endothelium. We have found that metastatic cells, unlike primary and tumorgenic cells, preferentially form nCs with the endothelium. nCs form quickly ($\sim$ 1.0hrs) mediating transfer of intercellular contents to 20-60% ($p<0.0001$) of the endothelial cell population. Functional nCs have been identified in both *in vitro* cultures and *in vivo* metastatic mouse models. Proteins, small cytoplasmic dyes, nanoparticles, and most interestingly, functional microRNAs (miRNAs) are transported into the endothelium through these structures. Transport of microRNAs through nCs is the subject of focus in **Chapter 5**. Metastatic cell communication of miRNAs presents a new mechanism for pathological angiogenesis and the angiogenic switch as presented in **Chapter 6**. nC-mediated communication leads to a 26x and 2x increase in pathological angiogenesis markers CD137

($p<0.001$) and CD276 ($p<0.001$), respectively. nCs are composed of cytoskeletal proteins and can be disrupted by low-dose actin-tubulin small molecule inhibitors, presenting potential drug candidates for metastasis specific therapies. Combination of 500pM Docetaxel with 30nM Latrunculin A or 50nM Cytoclasin D resulted in a 3x ($p<0.01$) disruption of TNT structures, reducing TNT-mediated communication by 42% ($p<0.0001$) and 56.6% ($p<0.0001$), respectively.

NanoChannel-mediated communication introduces a new paradigm of cancer progression where tumor cells can directly manipulate surrounding cell populations to facilitate cancer pathology. **Chapter 7** discusses the potential role of nCs in metastasis and the future work required to further our understanding of the role these structures may play in cancer progression. We have shown that nCs function in both early and late stages of cancer. Therefore, we propose that in the future, nCs may be a therapeutic target for the treatment of invasive disease.

Chapter 2

Review of Literature

2.1 Cancer: A Historical Perspective

Cancer has plagued the human body throughout history and remains the second leading cause of death in the United States, exceeded only by cardiovascular disease **(Figure 2-1)**. Approximately, 50% of men and 33% of women will develop cancer over their lifetimes. Earliest descriptions of cancer can be found in the Edwin Smith Papyrus a selection from an ancient Egyptian trauma surgery textbook dating back to 3000 BCE[19]. Over the centuries development of the scientific method and advances in technology have transformed our understanding of cancer as an imbalance of the four humors to a genetically based disease with heritable and environmental (e.g. chemical, radiation and viral exposures) causes. **Figure 2-2** provides a timeline of milestones occurring throughout the history of cancer.

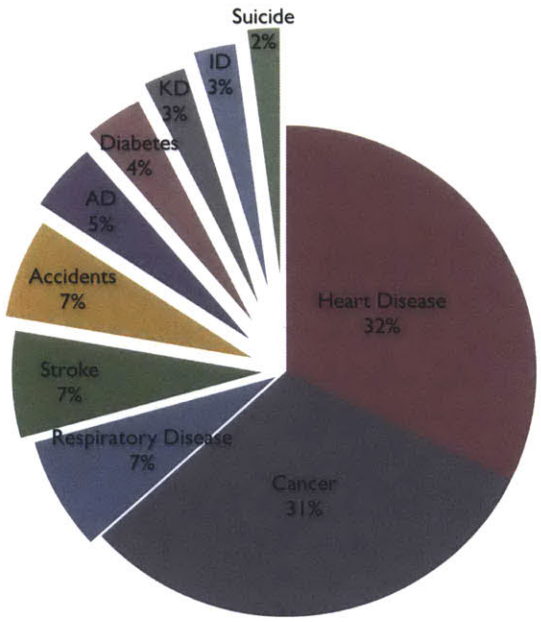

Figure 2-1: Leading causes of death. Cancer is the 2nd leading cause of death in the US after cardiovascular disease.

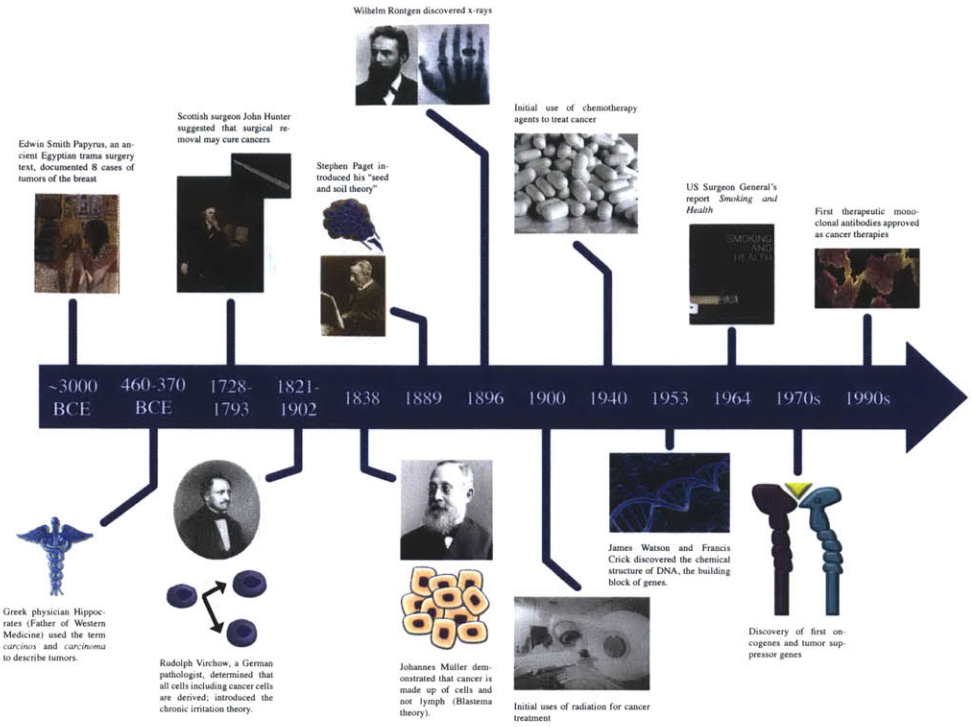

Figure 2-2: Milestones throughout the history of cancer.

2.2 Cancer Metastasis

Although decades of research in cancer biology have brought the field tremendous progress and understanding about this disease, metastasis remains the most poorly understood aspect of cancer progression. Limited understanding of the mechanistic steps underlying metastasis imposes the rate-limiting step in development of future generations of successful cancer therapies. The path from a single cell the acquires sufficient genetic hits for tumorigenesis, to the development of wildly invasive disease involving many secondary sites, has yet to be clearly paved. Although critical pieces of the puzzle have been discovered, and viable therapies developed, there remains much to be understood.

2.2.1 Stages of Metastatic Progression

Metastasis is a hidden process that occurs deep within the body, making each of the individual stages difficult to observe. Furthermore, cancer metastasis is difficult to study due to dynamic and reciprocal system-wide interactions that define advanced stages of cancer[20]. Cancer metastasis can be broken down into three distinct stages outlined in **Figure 2-3**. The first is tumor initiation and development into an invasive lesion. This is followed by metastatic cell migration and interaction with lymph and endothelial vessels; this stage is defined by intravasation, survival and migration through the vasculature, and finally extravasation into surrounding tissue. The final stage is seeding of secondary sites and the development of micrometastases[7–9,12].

2.2.1.1 Development of the Primary Tumor

Over the centuries, there have been several theories developed to explain the complex origins of cancer. For example, Otto Warburg in his manuscript *On the Origin of Cancer Cells* proposed that cancer is a metabolic disease[21], while others have attributed the origins of cancer to a failure of organogenesis[22–26]. However, the discovery of the double-helix structure of DNA in 1953 by Watson and Crick and the subsequent identification of the first oncogenes and tumor suppressors in the 1970s concluded many of these debates, replacing these theories with a general consensus that cancer is primarily a genetic disease[7,27,28]. Nevertheless, proponents of other theories remain active today[22–25].

It is widely accepted that cancer results from successive genetic mutations that lead to disruption of proliferation pathways and other elements of normal cellular physiology. These principles form the foundation of the somatic mutation theory[13,14]. Tumorigenesis is a multistep process that occurs once a sufficient number of genetic alterations have occurred. These genetic alterations result in uncontrolled cell growth and other hallmark characteristics of cancer pathology[14]. Generally, cancer is an age-dependent disease requiring four-to-seven indepen-

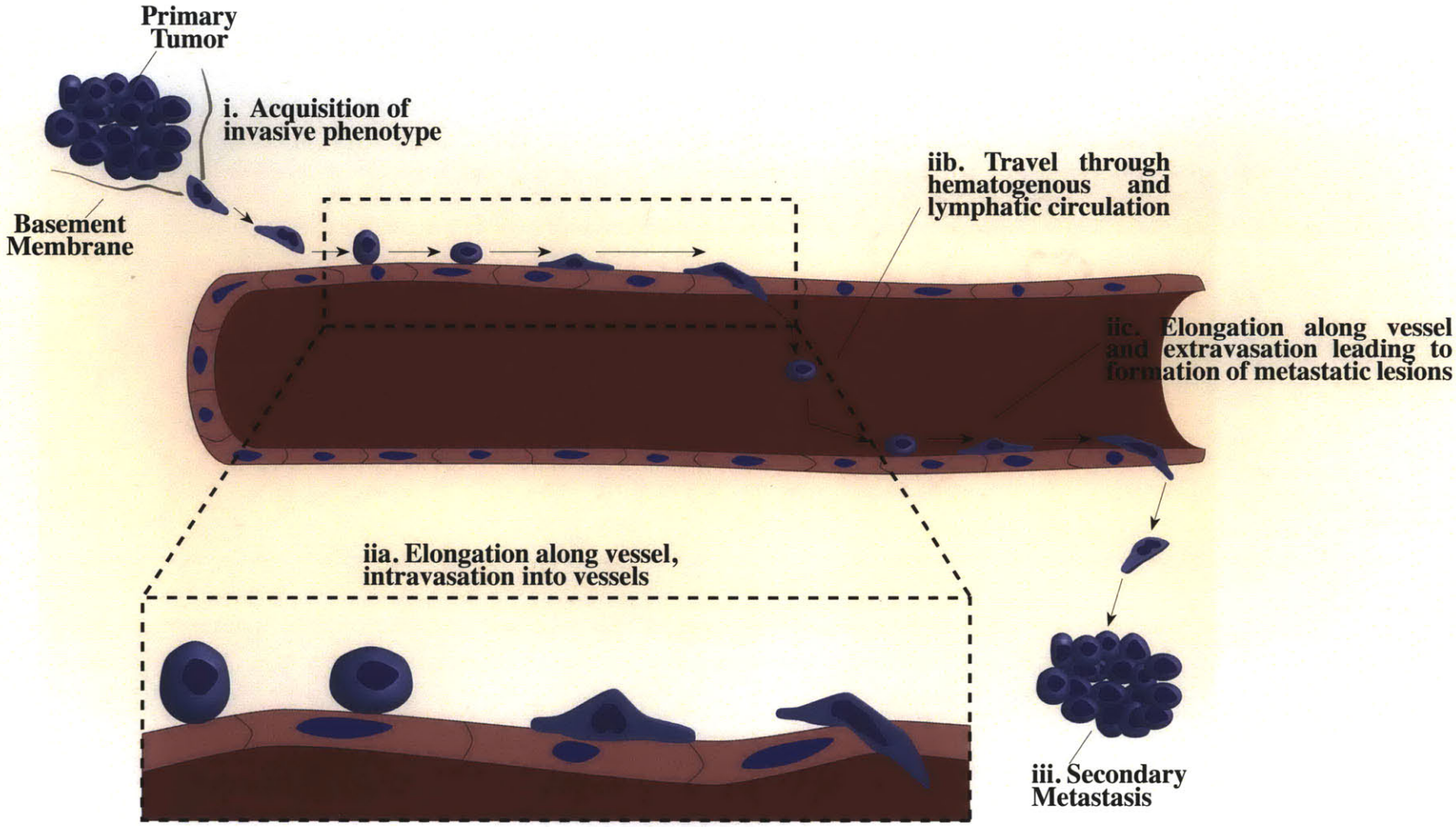

Figure 2-3: Overview of the metastatic cascade. Cancer metastasis can be broken down into three general phases, (i) development of the primary tumor and acquisition of an invasive phenotype, (ii) interactions with the endothelium, and (iii) formation of a secondary tumor site.

dent, stochastic, and rate-limiting events to incite tumorigenesis[13]. The confluence of characteristics may provide insight into why cancer is relatively rare over the human lifetime. Early analysis of tumor pathology samples showed that cancer evolves through a series of states beginning with normal tissue morphology and ending with highly invasive disease[29]. In a hallmark paper in 2000, Hanahan and Weinberg outline six characteristic features underlying cancer formation and progression: (1) unlimited replication potential, (2) self-sufficiency in growth signals, (3) insensitivity to antigrowth signals, (4) escape of apoptosis signals, (5) angiogenesis, and (6) tissue invasion and metastasis **(Figure 2-4)**.

Unlimited replication potential Cancer cells are uniquely capable of sustaining unlimited replicative capability. A tumor is able to accomplish this through defects in regulatory pathways that normally control cellular proliferation and homeostasis. Contrast this to most cells in the body which exhibit limited replicative capacity.

There are two natural barriers to cellular proliferation in healthy cells. The first is senescence which refers to a shift from a proliferative to nonproliferative state, maintaining cellular viability[14]. The second state is crisis which ends in cell death[14]. In normal cells continued cellular proliferation induces senescence and in some cell populations cellular crisis and apoptosis.

Induction of senescence and cellular crisis is regulated by telomeres. Telomeres are repetitive hexanucleotide sequences present at the ends of each chromatid[14]. They function in protecting the chromosome during cellular replication by preventing shortening, deterioration, or fusion with neighboring chromosomes[14]. The length of telomeres controls the number of replicative cycles that a cell can undergo before entering cellular crisis. In normal cells continuous proliferation results in shortening of telomeres, which leads to chromosomal instability[30]. However, immortalized cells and cancer cells are able to escape this process, partly with the aid of telomerase. Telomerase is a specialized DNA polymerase that functions in lengthening telomere repeat units. Telomerase is expressed in many human can-

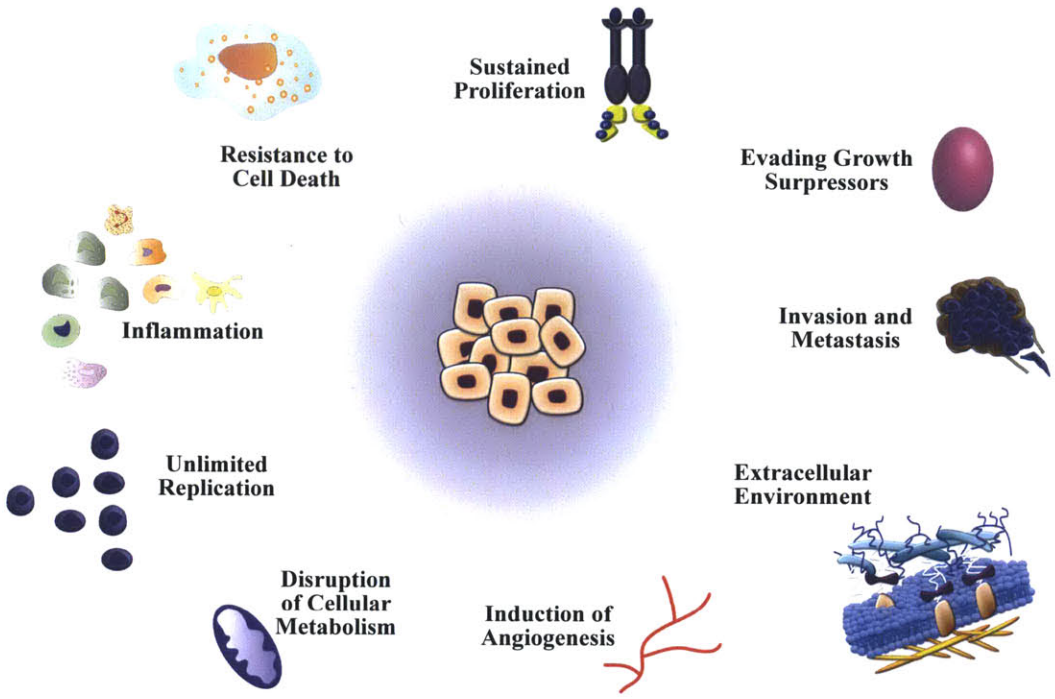

Figure 2-4: Hallmarks of Cancer. Cancer results from perturbations in normal physiological pathways.

cers and in 90% of immortalized cells. Its activity has been shown to prevent senescence and crisis, the hard-wired cellular defenses against cancer[14,31].

Regulation of telomeres in tumor cells is complex. Tumor cells are able to maintain telomeric DNA at significant lengths to prevent initiation of senescence or apoptosis. However, early in tumor progression in certain cancers a transient telomerase deficiency occurs[14]. For example, early breast cancers experience telomere shortening undergoing telomere crisis due to loss of telomerase function. Telomere crisis in turn leads to genomic instability that promotes the acquisition of tumor-promoting mutations[32]. In late tumors, telomerase function is restored stabilizing the genome leading to frank tumor growth resulting form the genetic mutations gained during telomere crisis[32].

Senescence can also be triggered by excessive growth signaling. Studies examining Ras, Myc, and Raf overexpression demonstrated that prolonged upregulation of growth promoting pathways can trigger senescence in cells. Cancer cells are able to successfully regulate expression of oncogenes in order to achieve high

levels of growth while still avoiding induction of anti-proliferative mechanisms[14].

Self-sufficiency in growth signals Proliferation in normal cells is tightly regulated and directly linked to appropriate biological stimuli[13,14]. A key characteristic of cancer cells is the decoupling of cellular proliferation from appropriate growth signals. Growth signals typically come from growth factors which initiate normal cellular proliferation through binding of intracellular tyrosine kinase domains[13,14]. However, growth signals can also come from components of the extracellular matrix (ECM) or cellular adhesion molecules. These signals are transmitted into the cell through transmembrane receptors, which regulate cellular pathways controlling growth, survival and energy metabolism. Determining the exact source of these growth signals is difficult due to tightly regulated temporal and spatial paracrine signaling which are difficult to probe experimentally[13,14]. The complexity is further heightened because regulation of growth promoting signaling is superimposed on chaotic mechanisms controlling the bioavailability of growth factors, such as unpredictable enzymatic liberation of soluble factors sequestered in the extracellular matrix (ECM) or pericellular spaces by proteases and sulfatases.

Cancer cells develop self-sufficiency of growth signals through a variety of different mechanisms. Normal cells require mitogenic growth signals before they can move from a quiescent to an active proliferative state. However, cancer cells can avoid this requirement by creating their own growth signals. Tumors characteristically show a reduced requirement for exogenous growth signals because they are able to generate their own growth cues.

Roughly five general mechanisms enable tumors to maintain self-sufficiency of growth. The first is autocrine proliferative stimulation. Tumor cells themselves produce growth factors that support their continued proliferation. One example is platelet-derived growth factor (PDGF) autocrine signaling implicated in sarcomas and glial-derived neoplasms. Another example of tumor autocrine signaling is basic fibroblast growth factor (bFGF) signaling in melanoma[33].

The second mechanism used to maintain self-sufficiency of growth in cancer is release of growth activating signals by the stroma. For example, fibroblast, a significant component of the tumor microenvironment, commonly secreting ECM proteins, growth factors, and angiogenic factors, have been shown to enhance invasive disease[34]. For example, in breast tumors, conditional deletion of type II transforming growth factor-β (TGF-β) receptor in fibroblast led to increased hepatocyte growth factor signaling which enhanced the invasive behavior of the mammary carcinoma cells[34].

The third mechanism utilized by cancer cells to achieve self-sufficiency of growth signals is increasing the number of receptor proteins on cancer cells. Therefore, even in the setting of normal growth factor signaling, the tumor cells elicit a hyperresponsive effect. Common examples of this mechanism are EGF-R/erbB overexpression in stomach, brain, and breast tumors or HER2/neu receptor overexpression in stomach and mammary carcinomas[13]. In the extreme, high levels of growth factor receptor expression can results in ligand independent signaling, such as ERB-2 overexpression in mammary tumor cells[35].

The fourth mechanism underlying unregulated tumor growth are structural mutations in receptors that enable ligand-independent signaling. In many tumors, deletions of the epidermal growth factor receptor (EGFR) external domain leads to constitutive signal activation independent of ligand binding. Similar ligand independent signal have been observed for RET, Trk, and Met receptors[33]. Alternatively, cancers can also express growth stimulating ECM integrin receptors[13].

Lastly, growth independent signaling can be achieved by completely bypassing the receptor by activating downstream targets. For example, approximately 40% of human melanomas exhibit B-Raf activating mutations that lead to constitutive signaling from Raf to the mitogen activated protein kinase (MAPK) pathway[14]. Furthermore activating mutations in the phosphoinositide 3-kinase (PI3K) pathway have been identified in several tumor types[14].

Negative regulators of proliferation signaling also play critical roles in cancer. For example, RAS mutations result in uncontrolled growth due to defects in RAS

GTPase activity that disable its ability to turn off G-protein signaling[14]. Another example is, phosphatase and tensin homolog (PTEN) protein negative regulation of PI3K function through the degradation of phosphatidylinositol (3,4,5) trisphosphate (PIP_3). Therefore mutations in PTEN function result in unchecked PI3K signaling[14]. The presence of these negative feedback loops can also play unintentional roles in drug therapy. For example, through a negative feedback loop pharmacological inhibition of mammalian target of rapamycin (mTOR) leads to up-regulation of the PI3K pathway counteracting the growth inhibitory effects of mTOR inhibition[14].

Insensitivity to antigrowth signals The ability to regulate cellular proliferation is essential to maintaining normal cellular homeostasis. Therefore, cells have adapted many anti-proliferative signaling pathways. These pathways are typically under the control of tumor suppressor genes. Common examples are PT53 and RB tumor suppressor proteins. These proteins function as gateways of cellular division. In order for cancer cells to thrive they must develop mechanisms for circumventing these negative proliferation signals. For example, almost all human cancers have defects in the p53 pathway. P53 is commonly known as the "guardian of the genome." It's activated in response to a variety of cellular stresses including DNA damage, hypoxia, and expression of oncogenes[36]. In response, it triggers changes in cellular proliferation cues leading to apoptosis, cell cycle arrest, or senescence[36]. P53 has diverse cellular functions including repair and recombination, chromatin modification, participation in genome stabilizing protein complexes, or acting directly as a transcription factor[37]. As a result of its diverse roles, p53 functions in varied biological functions including, but not limited to, cellular metabolism, cell-cycle regulation, immune response, angiogenesis, cellular differentiation, cell-cell communication, and cellular motility. Due to its diversity of roles disruption of p53 function leads to devastating and widespread cellular consequences[37]. Not surprisingly, p53 mutations are present in most human cancers. Approximately 50% of cancer p53 mutations alter transcriptional activity[37]. In the remainder of

cases, p53 mutational defects lead to reduction in nuclear p53[37].

Escape of apoptosis signals In addition to overexpression of pro-growth stimuli, tumor cells have also adapted mechanisms for circumventing cellular death signals. Apoptotic pathways are initiated by physiological stresses such as DNA damage or deregulation of oncogene signaling. There are two distinct apoptotic pathways for extracellular and intracellular stresses. The intrinsic pathway, or mitochondrial pathway, is activated by intracellular stresses acting through caspase-9[38]. Extracellular stresses are received via binding of tumor necrosis factor (TNF) family of ligands to cell surface 'death receptors' which activate the extrinsic pathway through caspase-8[38]. Activation of caspases initiates apoptotic machinery directing cells toward cell death.

The intrinsic pathway regulated by the B-cell lymphoma 2 (Bcl-2) family of proteins is the primary apoptotic pathway implicated in cancer pathogenesis[14,38]. Apoptosis via the intrinsic pathway is regulated by pro- (i.e. Bax, Bak) and anti-apoptotic (i.e. Bcl-2 family) signals[14]. The Bcl-2 family of proteins are inhibitors of apoptosis. By binding to Bax and Bak, the two pro-apoptotic regulators, Bcl-2 proteins prevent them from disrupting the outer mitochondrial membrane and releasing pro-apoptotic signaling proteins such as cytochrome C[14]. Cytochrome C release in turn activates proteolytic caspases that lead to cellular destruction. Bcl-2 disregulation has been implicated in human cancers, primarily human lymphomas[38].

Tumor cells have adapted several mechanisms in order to avoid cell death through apoptosis. The most common is loss of TP53, circumventing its role as a sensor of damaged DNA[14]. In normal cellular physiology in response to DNA breaks and chromosomal abnormalities, p53 increases expression of Noxa and Puma BH3-only proteins[14]. BH3-only proteins inhibit apoptosis by directly inhibiting Bcl-2 proteins or increasing pro-apoptotic proteins[14]. BH3 mimetics may act as potential cancer therapeutics[38]. Tumor cells also avoid cell death by directly up-regulating anti-apoptotic regulators like Bcl-2, increasing growth factor survival

signals, or decreasing pro-apoptotic regulators[14].

Similar to apoptosis, cancer cells also exhibit defects in autophagic programs. Autophagy refers to the breakdown of cellular components such as organelles that allows for the recycling of the components in a resource limited setting[14]. The role of autophagy in cancer is complex and paradoxical. Autophagy can increase tumor cell survival by allowing cancer cells to better withstand metabolic stress like hypoxia[39]. Similarly, in response to drug therapies an increase in autophagy seems to protect cancer cells[40]. Paradoxically however, cancer cells also up-regulate growth promoting pathways which inhibit autophagic signaling pathways.

Autophagy is regulated through similar mechanisms as apoptosis. For example, BH3 regulatory proteins such as Beclin-1 can trigger autophagy. In mice inhibition of Beclin-1 increases susceptibility to cancer[14]. Tumor cells with defects in both apoptotic and autophagic pathways may trigger necrotic cell death which through a pro-inflammatory environment can promote tumor growth and survival[39].

In contrast to apoptosis and autophagy, necrosis cell death is tumor promoting. Necrosis is unregulated cell death characterized by increased membrane blebs, cell membrane rupture, and release of intracellular contents. Necrosis creates a pro-inflammatory state that leads to endothelial cell recruitment and angiogenesis, increased tumor cell invasiveness, and growth stimulation[14]. Necrotic cells can also directly secrete growth signals such as IL-1α directly stimulating neighboring tumor cell proliferation[14].

Angiogenesis Angiogenesis, the process of forming new blood vessels from pre-existing vasculature, is critical for cancer progression. The growth of both the primary tumor and secondary metastatic lesion requires the recruitment of an adequate blood supply to support the metabolic demands of the growing cancer. These vessels also serve a dual role functioning as conduits of escape for metastatic cells from the primary tumor.

The pioneering work of Juda Folkman introduced the concept that angiogenesis is critical for tumor development. An "angiogenic switch" occurs in cancers

where tumor cells constitutively activate angiogenesis[41]. This contrasts the transient activation seen in normal physiology for example in wound healing or in the female reproductive cycle[42]. Folkman established the requirement that angiogenesis is necessary to support tumor expansion beyond 2-3mm[41]. This was supported by work showing that early lesions in the breast and cervix display characteristics of the angiogenic switch[43].

Physiological angiogenesis is regulated through a delicate balance of pro-and anti-angiogenic signals[44]. The first discovered angiogenesis factor was a chondrosarcoma-derived growth factor[45] later identified as basic fibroblast growth factor (bFGF or FGF-1)[44]. BFGF was described as a growth factor derived from chondrosarcomas that stimulates proliferation of endothelial cells, which was purified due to its strong affinity for heparin[45]. However, the most potent and ubiquitous pro-angiogenic factor is vascular endothelial growth factor-A (VEGF-A)[14,44].

VEGF-A functions in both physiological and pathological angiogenesis, regulating growth of new blood vessels during embryogenesis and the maintenance of endothelial cells homeostasis in the adult[14]. VEGF-A was initially discovered as a vascular permeability factor released from hepatocarcinoma cells[46,47]. VEGF-A belongs to the vascular permeability factor (VPF)/VEGF family which regulates angiogenesis along with other growth factors such as TGF-β, PDGF, ephrins, and angiopoietins[48]. There are several types of growth factors in the VPF/VEGF family including VEGF-B, VEGF-C, VEGF-D, placenta growth factor (PIGF), and VEGF-E. VEGF-B functions in coronary artery development, VEGF-C and D are primarily implicated in lymphangiogenesis, but they can also induce angiogenesis and demonstrated to increase vascular permeability[48]. PIGF is highly expressed in the placenta, but not in normal embryonic or adult tissues. Tumors, however, have high expression of PIGF, which is believed to aid VEGF-A in inducing pathological angiogenesis[48].

Development of normal healthy endothelium requires the complex interplay of many of these growth factors. However, formation of tumor endothelium is much more simplistic, dependent on a limited subset of cytokines. Tumor endothelium

can be induced by VEGF-A alone[48].

The VPF/VEGF family exert their biological effects by binding three high affinity tyrosine kinase receptors, VEGFR-1, VEGFR-2, and VEGFR-3. VEGFR-1 and VEGFR-2 are normally expressed on endothelial cells *in vivo* and *in vitro*. VEGFR-1 functions in monocyte and macrophage migration and negatively regulates VEGFR-2 function through a soluble variant that binds to VEGF preventing its binding to VEGFR-2[49]. VEGFR3 primarily functions in lymphatic endothelial cell biology[49]. VEGF receptors are also present on non-endothelial cell types including both normal and tumor epithelial cells indicating the possibility that autocrine stimulation pathways are involved in VEGFR signaling.

Angiogenesis is critical for all stages of tumor growth[43], initiation[48], development, invasion and metastasis[44]. Angiogenesis is a multistep process requiring integration of many biological phenomena such as endothelial cell proliferation, migration, organization, recruitment of pericytes, etc.; therefore to effectively study pathological angiogenesis requires an *in vivo* system. The development of pathological angiogenesis models have been primarily elucidated in an *in vivo* mouse ear model using adenoviral vectors to overexpress an isoform of VEGF-A, $VEGFA^{164/5}$ that can singly induce pathological angiogenesis[48].

Tumor endothelium is poorly organized with little basement membrane and decreased intercellular junctional complexes, presenting convenient opportunities for tumor cells to exit from the primary site into the bloodstream[44]. As many as $2 * 10^6$ mammary carcinoma cells can be found in the circulation of a breast cancer patient, although few of these cells will become tumors[44]. Angiogenesis is strongly correlated with metastasis and tumor progression. Decreasing angiogenesis results in decreased metastatic lesion[44]. There are also correlations between angiogenic factors and relapse and prognosis of invasive cancers[44]. For example, high levels of bFGF in renal cancer leads to poor survival rates[44]. In breast cancer, VEGF has been linked to early relapse[44]. Furthermore in several cancers (e.g. breast, prostate, lung, stomach, cervix, ovary, and squamous cell carcinoma of the head and neck) density of the vasculature is correlated with disease outcomes, highlighting the

role of angiogenesis in tumor progression[44].

There is diversity among tumors regarding the requirement for angiogenesis[14,44]. Some tumors are highly vascular, such as human renal and pancreatic neuroendocrine carcinomas, while others have little vasculature, such as pancreatic ductal adenocarcinomas[14]. Differences in neovascularization patterns may be partly regulated by tissue-dependent induction of angiogenesis by tumor stromal microenvironments[50]. Angiogenesis signals may also be regulated directly by oncogenes like Ras and Myc or indirectly by stromal cells or immune inflammatory cells[14].

Due to the high dependence of tumor cells on angiogenesis, not surprisingly, treatment of tumor cells with angiogenesis inhibitors has shown great efficacy in cancer[44]. Anti-angiogenesis drugs work against the tumor through a variety of mechanisms. Several studies have demonstrated that pro-apoptotic, anti-angiogenesis drugs, can overcome the growth advantages conferred to tumor cells by oncogenes and loss of tumor suppressors[51]. Furthermore, anti-angiogenesis drugs have been shown to normalize tumor vasculature, which makes delivery of chemotherapeutic drugs more efficient[52].

There are a variety of natural and synthetic angiogenesis inhibitors, which have been tested as possible therapeutic agents in cancer. The best characterized endogenous inhibitor of angiogenesis is thrombospondin-1 (TSP-1)[44]. Another example is interferon. Interferon is a potent inhibitor of angiogenesis through the inhibition of capillary endothelial cell migration[44]. Metallic proteinase inhibitors exhibit anti-angiogenic properties. Naturally occurring matrix metallic proteinase inhibitors referred to as TIMPS (tissue inhibitors of metallic proteinases) inhibit angiogenesis by preventing successful migration of endothelial cells when forming new vasculature[44].

Anti-angiogenesis inhibitors have also effectively been used in the clinic. The first approved anti-angiogenesis drug was Avastin[53]. Avastin is an anti-VEGF antibody commonly used in the treatment of breast cancer[53]. Following the approval of Avastin there has been an explosion in the development of additional

anti-angiogenesis agents. Tarceva is an epidermal growth factor tyrosine kinase inhibitor that can block VEGF-B, FGF, and TGF-α signaling that is used for treatment of lung cancer[53]. Linomide has been shown to inhibit angiogenesis induction through various pro-angiogenic factors, such as VEGF, FGF, and TNF-alpha[53]. Celecoxib is an inhibitor of the inducible prostaglandin G/H synthase COX2[53]. Is used in treatment of familial adenomatous polyposis (FAP) and has been shown to reduce the number of colorectal polyps in patients with familial FAP. COX2 inhibitors function as anti-angiogenesis agents by decreasing FGF and VEGF signaling, which are both pro-angiogenic factors. Their use for the treatment of prostate and cervical cancer is currently being explored[53].

Combinations of anti-angiogenesis drugs and chemotherapy are commonly used in the clinic for the treatment of cancer and have demonstrated enhanced therapeutic efficacy. These improvements have lead to the development of anti-angiogenic chemotherapy[53]. Anti-angiogenesis chemotherapy optimizes the dose and schedule of chemotherapy in order to optimally to target endothelial cells, and not cancer cells. Surprisingly, these treatment strategy has shown increased efficacy[53]. In addition, combination of multiple anti-angiogenesis drugs may also improve treatment outcomes. For example, combination of Tarceva and Avastin led to better clinical outcomes than either drug alone[53].

Tissue invasion and metastasis The development of an invasive phenotype cannot be modeled as a simple linear set of sequential, discrete steps. Instead it is better represented as a complex algorithm with many inputs of overlapping and parallel steps **(Figure 2-5)**. This algorithm is dictated by the confluence of numerous chaotic genetic alterations, angiogenic contributions, and influences from the microenvironment. An invasive phenotype can generally be characterized by alterations in tumor cell adherence to both neighboring cells and the ECM, increased migratory capacity, and change in cellular morphology. These changes are mediated by the inappropriate activation of a developmental regulatory program referred to as epithelial-mesenchymal transition. Its unclear if cancer cells slowly

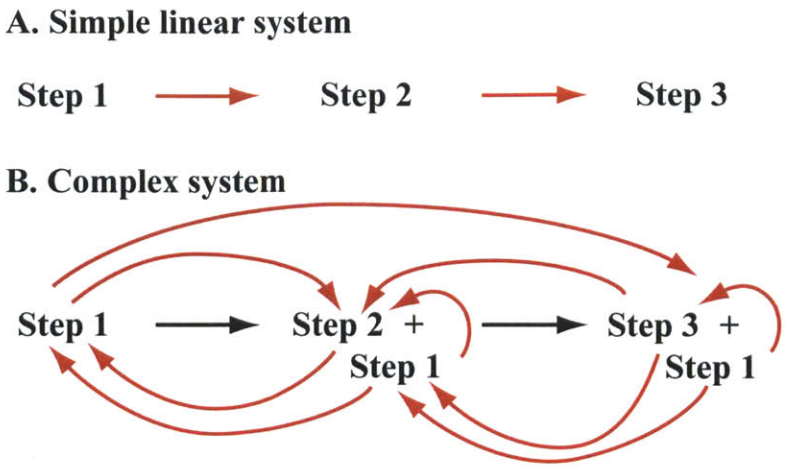

Figure 2-5: Development of an invasive phenotype is complex. Development of an invasive phenotype is a complex algorithm with many inputs of overlapping and parallel steps.

develop an invasive phenotype or if some cancers are invasive from their initiation. There is likely a combination of both factors. However, one thing that remains clear is that the transition of cancer from a localized proliferative disease into an invasive migratory disease represents an important and disease outcome altering change. To address all of the elements of development of an invasive phenotype would be overly exhaustive, however, I will highlight the most critical elements: loss of contact inhibition, epithelial-mesenchymal transitions (EMT), and cellular migration.

Loss of contact inhibition: Adhesion molecules are critical regulators of normal cell physiology. Integrins function primarily as mediators of cellular adhesion to the ECM. They are heterodimeric cell surface proteins composed of a combination of α and β subunits[54]. There are 24 distinct heterodimers formed from 18 α and 8 β subunits[54]. The extracellular domains of integrins bind to specific sequences in EMC proteins such as fibronectin and collagen. Binding of integrins to the ECM results in conformational changes which promote linkage of their cytoplasmic tails with the actin cytoskeleton[55]. Integrins exert their cellular functions by recruiting scaffolding and signaling proteins like paxillin and focal adhesion kinase (FAK) **(Figure 2-6)**. There are two models of initiation of adhesion complexes[55]. The first

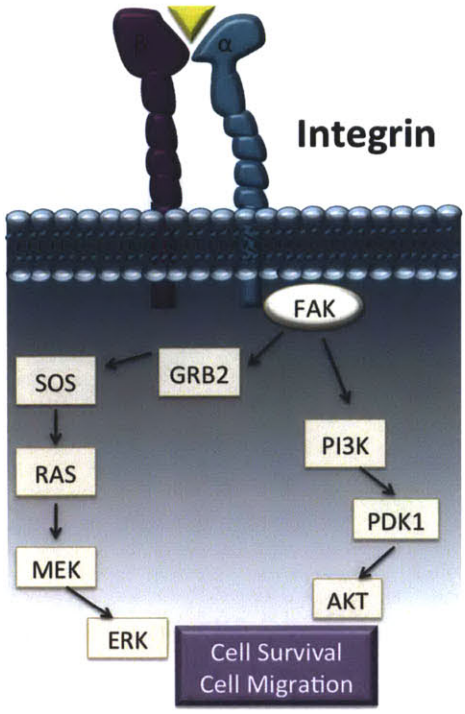

Figure 2-6: Schematic of FAK-Ingrin signaling axis. Integrins mediate cell-ECM adhesion by forming adhesion complexes typically through focal adhesion kinase (FAK). The FAK-integrin signaling axis signals through critical survival and proliferation pathway such as PI3K and MAPK pathways. Not surprisingly aberrations in FAK-integrin signaling is implicated in cancer pathogenesis and invasion.

is binding of integrins to the ECM leading to assembly of adhesion complexes. The second is initiated by actin polymerization. In this model, dendritic actin is use as the template for the formation of adhesion complexes[55]. Formation of adhesion complexes is regulated by the Rho family of GTPases[56]. The best characterized members, Rac, Rho, and Cdc42, have been implicated in cancer progression. They function by regulating guanine nucleotid exchange factors (GEF) and GTPase activation proteins (GAP) in adhesion complexes[55].

The morphology of migrating tumor cells varies considerably from benign cells. The most important factors regulating this is compliance of the substrate (i.e. the ECM) and the intrinsic contractility of the cells[55]. For example, tumor cells with weak adhesion are rounded, similar to the shape of lymphocytes[55]. Contrast this morphology with fibroblasts and endothelial cells which are highly spreading due to tight adhesions[55]. The force balance between the ECM and the surface of the cell

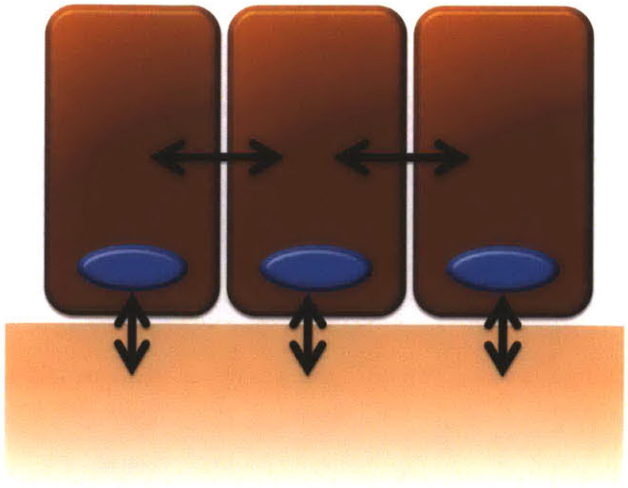

Figure 2-7: Force balance between cells and ECM. In normal tissues cells experience mechanical forces from neighboring cells and the ECM. The force balance between the ECM and the surface of the cell are critical regulators of cellular morphology.

are critical regulators of this dynamic[55] **(Figure 2-7)**.

Cadherins mediate cell-cell adhesions. E-cadherin is a calcium dependent cell-cell adhesion molecule that is the primary mediator of adhesion in epithelial cells[57]. E-cadherin forms complexes with β-catenin, and α-E-catenin in order to establish connections at the junction between two neighboring cells[57]. The E-cadherin-catenin complex (CCC) is linked to the cytoskeletal system[57]. Cancer is characterized by aberrations in cell matrix adhesions and cell-cell adhesions. Proliferation in normal cells is regulated by a phenomenon called contact inhibition. Contact inhibition refers to the normal physiological response where formation of dense populations of normal cells, suppress cell proliferation. This phenomenon leads to confluent cell monolayers of cultured cells. Tumor cells, however, no longer exhibit this phenotype.

NF2 pathway regulates contact inhibition through the actions of merlin[58,59]. Merlin functions in contact inhibition, by coupling cell surface adhesion molecules to transmembrane receptor tyrosine kinase (e.g. E-cadehrin to EGFR receptor)[58,59]. Through this mechanism, merlin strengthens the adhesiveness of cadherin mediated cellular attachments. Loss or defects in merlin therefore may result in a reduc-

tion of contact inhibition[58,59]. An alternative contact inhibition pathway is through LKB1 protein[60–62]. LKB1 epithelial polarity protein is responsible for organization of epithelial structures. Its important for the maintenance of tissue integrity. When LKB1 function is disrupted, epithelial cells become susceptible to Myc transformation[60] . Both LKB1 and merlin are tumor suppressors[58–62].

Epithelial-Mesenchymal Transition: Epithelial-mesenchymal transition describes a complex developmental program that epithelial cells undergo as they lose their differentiated characteristics and acquire mesenchymal features, that results in an invasive phenotype. It's characterized by loss of adhesion molecules, increased motility, enhanced resistance to apoptosis, expression of matrix degrading proteases, and alterations in cellular shape from a polygonal to a spindly fibroblastic morphology[14,63]. For example, invasive cancers show a characteristic loss of E-cadherin, the primary adhesion molecule responsible for cell-cell adhesion in epithelial cells, accompanied by an up-regulation of N-cadherin[14]. N-cadherin is normally expressed on migrating neurons during development and is associated with embryogenesis and inflammation[14]. The switch in cadherin expression from E-cadherin, which promotes cell-cell adherence in the tumor, to N-cadherin, expressed on migrating mesenchymal cells, facilitating tumor cell binding to the stoma, is a hallmark feature of invasive tumors.

Mesenchymal-epithelial transitions (MET) refers to the reversal of EMT that seems to occur following seeding of the secondary site. Both EMT and MET are critical regulatory programs in normal embryonic development. However, inappropriate initiation of these programs underlies cancer pathology and other human diseases[63]. There have been several studies that have linked expression of EMT related proteins and the acquisition of an EMT phenotype with the development of metastatic disease. For example, in patients with tumorigenic breast cancer expression of invasive gene signatures correlated with patient survival and the occurrence of metastatic disease[64]. In another study, the presence of a progenitor-like phenotype in differentiated mammary epithelial cells correlated with invasive

cell populations[65,66].

EMT is orchestrated by a set of transcription factors functioning in migratory processes during embryogenesis, such as Snail, Slug, Twist, and Zeb1/2[14]. These transcription factors seems to regulate the entire metastatic cascade with the exception of colonization[63]. For example, Snail1 in epithelial cells represses E-cadherin expression by regulating Zeb2, a transcriptional repressor of E-cadherin that is up-regulated in Snail-induced EMT[67]. There is dynamic interplay between these transcription factors, therefore induction of one set of these factors commonly leads to up-regulation of the others[66].

There are many factors that contribute to initiation of the EMT program including interactions between cancer cells and the tumor stroma, genetic and epigenetic changes, aberrant growth factor and developmental pathway signaling, and environmental stimuli such as hypoxia. Not surprisingly, the inherent genetic and epigenetic instability of cancer cells promotes EMT programming in cancer. Genetic instability allows for the development of diverse heterogeneity in a tumor, increasing the likelihood that one cell will have the genetic alterations necessary to progress through EMT. For example, in mammary epithelial cells, induction of EMT results in epigenetic changes which in turn lead to *de novo* methylation of other gene promoters that maintained the EMT state[68].

Interactions between tumor cells and the microenvironment also contribute to EMT program initiation. For example, in colon cancer, there are spatial distinctions between mesenchymal-like and non-mesenchymal like tumor cells that are believed to be the result of differential interactions with the microenvironment. In these tumors, mesenchymal-like cells were found at the invasive front, while cells in central areas of the tumor and at secondary metastatic sites express features characteristic of differentiated cells. These differences have been linked to changes in localization of β-catenin, the primary oncogene in colon cancer, from the nucleus to the membrane/cytoplasm, which are associated with a mesenchymal-like and epithelial-like phenotype, respectively[69]. This data is further supported by higher expression of Snail in peripheral tumor cells versus central tumor cells in several

epithelial cancers. The Snail gene is believed to function as a critical regulator of EMT through repression of E-cadherin[70].

The microenvironment also seems to function in mediating MET, restoring an epithelial phenotype in the secondary metastases. For example, co-culturing prostate carcinoma cells with normal hepatocytes increased expression of E-cadherin, similar to E-cadherin expression at the primary and secondary tumor sites, but higher than E-cadherin expression in cells during the initial invasive phase[71].

Matrix degrading proteases such as MT1-matrix metalloptoteinase (MMP)/MMP-14 are implicated in ECM remodeling[72]. These proteases provide a mechanism of escape for tumor cells by re-patterning of collagen fibers in the ECM to create tube-like microtracks that allow for collective mass movement of cancer cells[20].

Signaling pathway such as transforming growth factor-β (TGF-β), Wnt, Notch, and Hedgehog pathways have been implicated as critical regulators of EMT program[63]. The TGF-β pathway is one of the best characterized regulators of EMT in both normal physiology and tumor progression[73]. The cytokine members of the TGF-β pathway regulate EMT directly through ligand-receptor interactions or indirectly through involvement with Notch, Wnt, and integrin signaling pathways[63]. TGF-β exerts its function in EMT through Par6. Par6 is a regulator of epithelial cell polarity and tight junction formation[38,74]. Par6 is a substrate for the type II TGF-β receptor. Binding of Par6 to the TGF-β receptor controls interaction with Smurf1 which targets RhoA for degradation, in turn leading to loss of tight junctions[74]. TGFβ also exerts its role in EMT through effects on the immune system. Through systemic immune suppression it inhibits anti-tumor immune responses[75]. In addition, TGFβ indirectly regulates EMT by directing tumor stromal cells to initiate invasion-promoting changes in the tumor[75]. Cancer stem cells are also key hallmark features of EMT. In human mammary epithelial cells, EMT promotes development of stem-cell like properties[76–78]. Interestingly the TGF-β pathway is also highly active in these stem-cell like populations in mammary cancers[79].

EMT is a developmental regulatory mechanism therefore it's not surprising that initiation of EMT in cancer is associated with aberrant signaling of important de-

velopmental pathways, such as Wnt, Notch, and Hedgehog[80]. Constitutive activation of the Wnt signaling pathways have long been linked to tumorgenesis in colon cancer and has recently been linked to EMT[63]. β-catenin acts a transcription factor leading to activation of EMT promoting genes[63]. There are studies suggesting that therapeutic targeting of the Wnt signaling pathway with inhibitors may be a potential strategy for modifying EMT in cancer[81]. However, β-catenin expression alone cannot induce EMT, highlighting the complex regulator pathways required to orchestrate this transition[63].

A second developmental pathway, Notch, has also been implicated in EMT pathways both in normal physiological development and tumorigenesis[63]. In pancreatic cancer cells, Notch induces EMT by regulating the NF-κB (NF-κB) pathway, VEGF signaling, and MMP release[82]. The Notch pathway can also directly alter TGF-β activity.

Finally, although less frequently cited, the Hedgehog pathway also regulates tumor metastasis and EMT progression[63]. The best characterized ligand of the Hedgehog pathway, Sonic hedgehog, is known to be a mediator of angiogenesis. Mutations in the SHH pathway are commonly linked to increased cellular proliferation and tumorigenesis[83]. In pancreatic cancer, high SHH expression has been linked to initiation of EMT programming which can be reversed by the SHH inhibitor cyclopamine[83].

External stimuli such as hypoxia can also result in EMT initiation[63]. Hypoxia leads to EMT through induction of Hypoxia Inducible Factors (HIFs), regulating a variety of EMT stimulating mechanisms including signaling pathways such as Notch and NF-κB, induction of epigenetic modification, or direct up-regulation of EMT transcription factors such as Snail and Twist[63,84].

Lastly, miRNAs have been shown to be critical regulates of EMT[63]. The miR-200 family (miR-200a, miR-200b, miR-200c, miR-141, and miR-429) and miR-205 have been shown by several group to be primary miRNA regulators EMT, acting on E-cadherin respressor proteins zinc-finger E-box-binding homeobox factors ZEB1 and ZEB2[85,86]. These miRNA also act through the TGF-β pathway[87].

Migration The cytoskeleton plays critical roles in basic cellular functions (e.g. cell motility, cell division, wound healing, cellular integrity, and transport)[88–90]. Understanding cytoskeletal dynamics provides insight into principles underlying both normal and pathological disease states[88,89,91,92]. Through the use of molecular biology, biochemistry, and engineering models, there has been significant progress in understanding the principles that define dynamic morphogenesis: how the cytoskeleton works to change cell shape, transport of intercellular contents, and maintain cell integrity[88,90]. Complex interactions between microtubules and actin form the basic underpinnings of this dynamic system[88].

The cytoskeleton accomplishes complex cellular tasks using three basic constituents: microfilaments (actin filaments), intermediate filaments, and microtubules[90]. Although each of these structures play varying roles, actin filaments generally are more involved in motility and maintaining cellular integrity, while microtubules play larger roles in cell division and transport of macromolecules[90]. Intermediate filaments are primarily responsible for mechanical support acting as cytoplasmic and nuclear scaffolds[93]. Cytoskeletal filaments combined with regulatory proteins, such as capping proteins and severing proteins (e.g. actin depolymerizing factor (ADF)/cofilin family), work through signaling pathways (e.g. Ras/Rho family of small GTPases) to achieve varied cellular functions[89,91].

Lamellipodia, filopodia, blebs, and invadopodia are four classically defined plasma membrane protrusions[88,92]. Lamellipodia function primarily in cellular migration extending long distances to form attachments with the ECM that anchor the cell and provide the traction required for movement through tissues[92]. Filopodia are important for guidance and sensing in the cellular environment. Membrane blebs are important for regulating directional cell migration that may play a role in development. Invadopodia are protrusions optimized for matrix degradation. Vesicles carrying matrix-degrading proteases are targeted to these projections by the exocyst complex[92]. **Figure 2-8** provides a schematic of cellular cytoskeletal projections.

Each of these structures is composed of an actin cytoskeletal network; lamel-

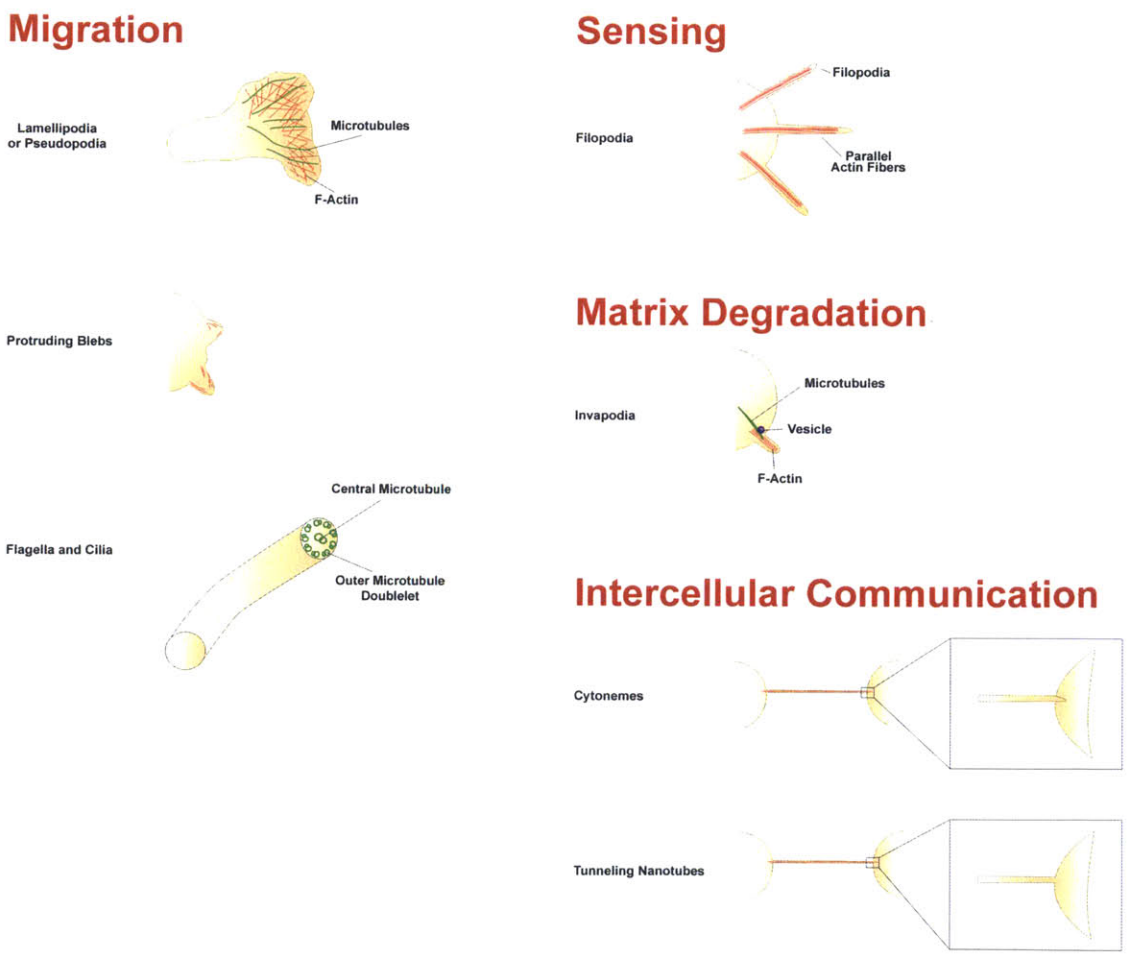

Figure 2-8: Cytoskeletal projections. Cells form diverse cytoskeletal projections that perform many critical cellular tasks including migration, environmental sensing, and cell-cell communication.

lipodia are formed by dendritic actin networks and filopodia are made of parallel actin bundles[88]. Exact mechanisms explaining the interactions between actin and microtubules to create diverse cytoskeletal projections are poorly defined and an active area of research. In lamellipodia, the dominant hypothesis is that microtubules are structurally linked to actin retrograde flow, which leads to net growth of microtubules toward the leading edge[88]. In filopodia, microtubule filaments grow alongside the actin bundles through a process called dynamic instability[94]. Microtubule-actin interactions are critical for directed motility where projections are targeted to specific locations. For example, recent studies on neuronal pathfinding have shown that actin bundles guide microtubules toward the leading edge, promoting extension of the projections toward the appropriate stimulus[88,94–97]. Membrane projections are initially devoid of actin and are formed at sites of local weakening of the plasma membrane[89,92]. They form when the plasma membrane transiently detaches at a focal position from the underlying actin cortex. This allows for hydrostatic pressure of the cytoplasmic contents to push the membrane out[89,92]. Invadopodia are actin-rich projections that also contain microtubules that likely function in transport of the protease filled vesicles[92]. The Rho family proteins are the primary regulators of protrusion formation, controlling actin remodeling. Rac, Cdc42, and RhoG are all required for lamellipodia and filopodia formation and function[91].

Recently, new forms of cytoskeletal projections have been described that function primarily in cell-cell communication. Cytonemes, or filopodial bridges, and tunneling nanotubes (TNTs) are thin cytoskeletal connections composed of actin that connect neighboring cell[98]. Cytonemes are closed end cellular projections, while tunneling nanotube are open-ended cellular projections. Cytonemes enable intercellular transfer of cell-surface associated cargo, for example membrane receptors or even pathogens. Tunneling nanotubes in contrast are open cellular connections that allow for the transport of both cell surface associated and intercellular cargo[98]. The dynamics of cytoskeletal formation of filopodial bridges and tunneling nanotubes is an active area of research.

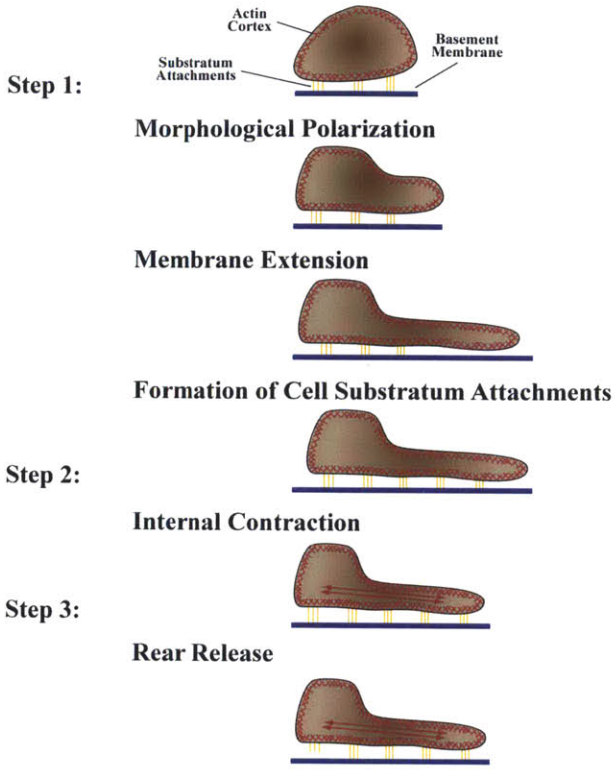

Figure 2-9: Cellular Migration. Cell migration can be described in three stages: (1) morphological polarization plus membrane extension and formation of cell-substratum attachments , (2) internal contraction, and (3) rear release.

Cell migration in 3D is complex involving interactions between chemical signaling pathways and mechanical mechanisms. Chemokines, which are chemotatic cytokines that bind G-protein coupled receptors, induce cell motility acting as potent stimulators of cell migration. Chemokines also induce infiltration of tumors by macrophages and lymphocytes, resulting in release of inflammatory stimuli and proteases. Matrix breakdown by matrix metalloproteinases (MMPs) proteolyticly degrade the ECM, leading to liberation of embedded growth factors and chemokines. These soluble factors act through signaling pathways such as PI3K, MAPK, FAK activating Rac and Rho signaling, which control actin polymerization.

Migration can be described in 3 distinct stages: (1) morphological polarization plus membrane extension and formation of cell-substratum attachments, (2) internal contraction, and (3) rear release[99,100] **(Figure 2-9)**. Dynamic interactions with the membrane leads to formation of protrusions that in response to a gradient of

soluble factors leads to directed growth of actin filaments and cytoskeletal structures[99].

Cells require polarization in order to migrate. This can be achieved through concentration gradients or spatial/temporal stimulus gradients that result from random fluctuations or microscopic non-uniformities in receptor-ligand binding[99] . Microscopic non-uniformities result from molecular rearrangements such as redistribution of chemosensory signaling receptors, integrin adhesion receptors, and integrin cytoskeletal linkages[99,100]. The consequence of polarization is extension of active membrane processes primarily at the cell front, giving cell locomotion a persistent random walk characteristic[100].

Membrane extension can be described using an elastic Brownian Ratchet model[101]. This model explains how polymerizing actin creates protrusive forces on the membrane without motor proteins[101]. Random thermal fluctuations in the membrane produce gaps between the actin polymer tip and the membrane, allowing for insertion of new monomers along the filament chain. Free energy released from the polymerization reaction alters the random thermal fluctuation of the membrane to create directed motion. An alternative mechanism called cortical expansion may also describe the formation of actin cytoskeletal protrusion[101]. In this mechanism, filament severing or favorable entropic driving forces due to filament-water interactions cause an increase in osmotic pressure. The increase in pressure triggers a local influx of water that causes the actin-filament gel to swell[101]. The Brownian Ratchet model may better describe filopodia formation while the cortical expansion model may provide insight into lamellipodia formation[101].

Speed of protrusion formation is dependent on the response time to a stimulus and the net polymerization of actin[91]. The Rho GTPase family is the primary molecular mediator of actin cytoskeletal dynamics that mediate formation of lamellipodia and filopodia protrusions[91]. In response to a stimulus, these molecules lead to increase in the number of actin polymerization sites. A net increase in the rate of addition of actin monomers results in a protrusion[91]. Protrusion formation is regulated by actin polymerization dynamics, which depend on ATP mediated

addition of actin monomers, depolymerization kinetics, and interactions of regulatory proteins. These proteins include profilin and ADF/cofilin, which function in depolymerization, cortactin, which stabilizes branches, and filamin A and α-actinin, which stabilizes the entire network by cross-linking filaments[91].

The net polymerization of actin is critical to the rate of protrusion formation; even with a specific stimulus, polymerization of actin will occur in random directions but only net growth in one specific direction will allow for cellular locomotion[99,100]. The speed of protrusion formation is primarily determined by actin polymerization speed and not signaling pathway kinetics, since signal transduction occurs very quickly, on the order of milliseconds[99,100].

Formation and stabilization of attachments is the final phenomenon to consider[99]. Evidence suggests that attachments to the substratum preferentially form at the leading edge of cells. New adhesions appear as small aggregates that increase in size as the cell migrates over them; these adhesions remained fixed until they reach the rear or edge of the cell[99]. Molecular mediators initiating this process are unknown. One potential hypothesis is that there may be pre-existing cytoskeletal complexes to which adhesion molecules incorporate; however, FAK, paxilin, tensin, and integrins are known constituents in adhesion complexes and are believed to play a big role in attachment to the substratum[99]. These adhesion bonds are reversible; proteins are recycled back to the leading edge to replenish those lost to existing adhesion complexes[99].

The second step of migration is internal contraction[99]. There are two primary forces that are generated by a moving cell: (1) protrusion force to extend membrane processes and (2) contractile forces that move the cell body forward. Generation of contractile forces depends on active myosin based motors. Contraction of filaments connecting cell-substratum adhesion complexes with intracellular structures results in relative motion of adhesion complexes across cortical actin filament tracks[99,100]. The substratum exerts an equal and opposite traction force on the cell via adhesion complexes. The magnitude of contractile forces do not alone directly explain migration speed; instead the ratio of contractile force to cell substratum

adhesion correlates to the rate of migration in a biphasic manner. Maximal migration speed is associated with an intermediate ratio of adhesive forces. If the ratio of adhesive forces becomes too large, the cells may be unable to move, however, if the ratio is too small, the cells may not be able to attach.

The final step is rear release[99]. The rate-limiting step is not formation of adhesion but disruption of adhesions[99]. The rate of disruption is proportional to the adhesion force to the substratum. This process is accelerated by myosin-mediate actin filaments pulling on adhesion complexes[99]. Rates of protrusion and rear release both contribute to overall migration speed but evidence suggests that rear release kinetics dominate in many cells[99]. Mechanisms of rear release combine mechanical contributions, signaling pathways regulating adhesion receptors, and ATP driven motor processes. Rear release results from optimal balance of adhesive forces and traction; however, forward attachments remain, creating asymmetry between the front and rear[99].

Summary of Development of the Primary Tumor Cancer arises from a series of genetic alterations that disrupt multiple physiological processes. In **Section 2.2.1.1**, I discuss the six key characteristic features of cancer progression, (1) unlimited replication potential, (2) self-sufficiency in growth signals, (3) insensitivity to anti-growth signals, (4) escape of apoptosis signals, (5) angiogenesis, and (6) tissue invasion summarized by **Figure 2-10**. Now I begin a discussion of the subsequent step in the metastatic cascade, interactions with the endothelium. Once a tumor cell develops an invasive phenotype, the endothelium provides a conduit of escape to the systemic circulation, exposing the cells to foreign organs and tissues.

2.2.1.2 Interactions with the endothelium

Interactions with the endothelium are critical to tumor progression occurring during multiple stages in the metastatic cascade and are pre-requisite for establishing secondary metastatic lesions. In addition to the essential role endothelial cells play in cancer progression through angiogenesis, it also provides the primary escape

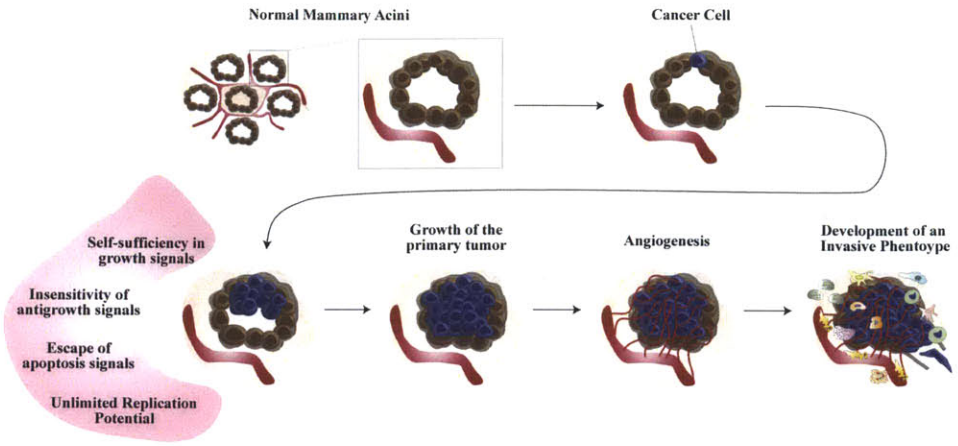

Figure 2-10: Schematic Summary of Primary Tumor Development. Tumor formation starts with development of a tumorigenic phenotype in a single cell. Development of a tumor requires multiple genetic and physiological changes. These changes lead to frank tumor formation characterized by the six hallmark features of tumor cells: (1) unlimited replication potential, (2) self-sufficiency in growth signals, (3) insensitivity to antigrowth signals, (4) escape of apoptosis signals, (5) angiogenesis, and (6) tissue invasion.

routes tumor cells must take to form secondary lesions[44]. Tumor cells can enter the circulation directly or indirectly. Hematogenous dissemination represent the direct entry of tumor cells in the circulation. Alternatively, tumor cells may also enter the circulation through the lymphatic system. The lymphatic system empties into the lymphatic ducts, which drain into the subclavian veins at the junction of the subclavian and internal jugular veins **(Figure 2-11)**.

Entry and exit of tumor cells from a blood or lymphatic vessel is referred to as intravastion and extravasation, respectively. The mechanisms underlying these physical interactions are not well-characterized, primarily due to the lack of models that allow for isolation of these interactions[102]. Successful intravasation and extravasation in metastasis requires coordination between mechanical and chemical signaling pathways that coordinate alterations in the cytoskeleton to allow for transmigration in response to chemical stimuli that lead to migration. Much of the insight gained on tumor cell intravasation and extravasation have come from an understanding of leukocyte entry and exit from the vessel[102]. Similar to leukocytes during an inflammatory response, tumor cells undergo diapedesis to enter the en-

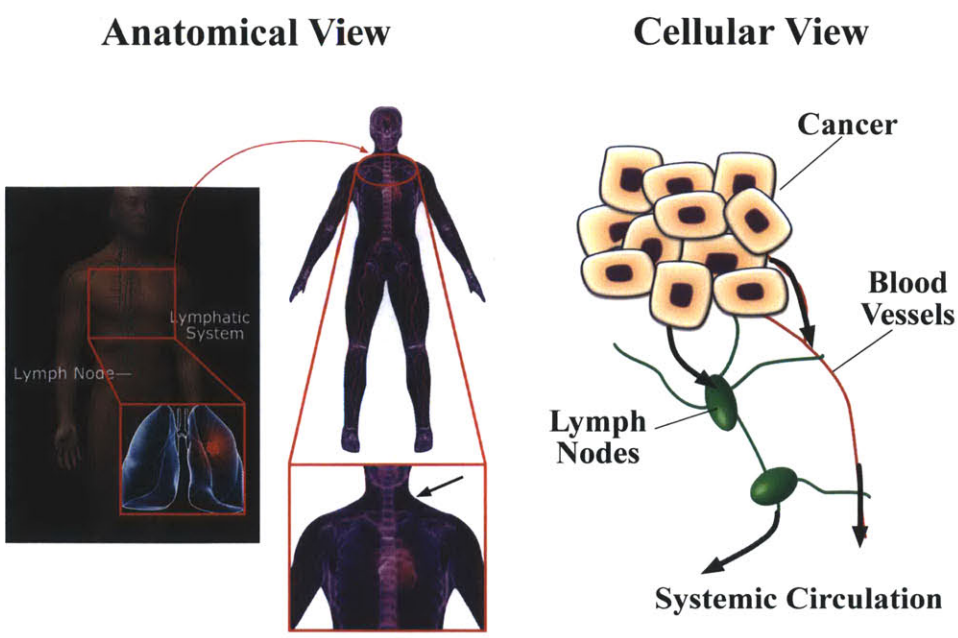

Figure 2-11: Anatomical versus cellular view of metastasis. Tumor cells can enter the circulation directly, referred to as hematogenous dissemination, or indirectly through the lymphatic circulation.

dothelium. Diapedesis refers to the process of extending psudopodia projections disrupting intercellular junctions in the endothelium. This process leads to remodeling of the cytoskeleton allowing the metastatic cells to penetrate the endothelial layer[1]. Metastatic cells are 80% softer than benign cells. The decrease in cell stiffness may enhance the ability of these cells to successfully cross the endothelial cell barrier[103,104] Diapedesis is also facilitated by actin rearrangement in the endothelial cell population. However, the mediators of this process have not been elucidated, but it's clear that reciprocal interactions between the two cell types is critical for invasion[102]. For example, tumor cells lead to up-regulation of IL-8 and Gro-β chemokines in the endothelium[105]. In response to increased secretion of these chemokines tumor cells expressed higher levels of CXCR2, the receptor for IL-8 and Gro-β. The combination of increased secretion of IL-8 and Gro-β in endothelial cells and increased expression of CXCR2 in the metastatic cancer cells resulted in enhanced tumor cell transmigration[105]. There has been work to suggest that metastasis in lung cancer model were initiated predominantly by attachment

to the endothelium rather than by extravasated tumor cells[106]. However, these results remain controversial and have been contradicted by other reports[107]. Nevertheless, emphasizing the dynamic role of endothelial cells in metastasis.

Tumor cells extravasate by inducing endothelial cell retraction. However, the mechanism by which this occurs has not been elucidated. Cdc42, a member of the Rho GTPases family of proteins has been linked to endothelial cell retraction and in mediating interactions between metastatic cancer cells and the endothelium[108]. Cdc42 was shown to be required for spreading, protrusion extension, and colonization in an *in vivo* mouse lung model. However, the mechanism by which expression of a Rho GTPase protein in the metastatic *epithelial* cells results in changes in an *endothelial* cell, remains to be elucidated.

Although cancer cells do not require adhesion to the endothelium to arrest, transmigration is strongly dependent on the expression of adhesion molecules such as integrins and other cell-surface glycoproteins. For example, in breast cancer, transmigration through endothelium was enhanced by CD44 and expression of $\beta 1$-integrins[102]. Similarly, $\beta 1$ intgrins acting through cdc42 have been shown to promote transendothelial migration of metastatic cancer cell[108] . In addition, endothelial cell expression of certain adhesion molecules has been linked to organ-specific metastasis. Lectins and selectins are two classes of cell adhesion molecules involved in metastasis. Lectins are carbohydrate binding proteins and selectins are glycoproteins that function as cell adhesion molecules. The mechanism of organ-specific dissemination can in part be explained by adherence of tumor cells to tissue specific endothelium, which has been demonstrated both *in vivo* and *in vitro*[102]. This may partly explain seeding difference for different metastatic cancers[8,102]. For example carbohydrates sLe_a and sLe_x have been shown to play a role in organ-specific spreading in several tumors including colon, gastric, and breast cancers[109].

Integrin associated ligands have been identified as key regulators of metastatic progression in several tumor types, including colon, skin, and breast, linked directly to the roles integrins play in mediating interactions with the endothelium during intravasation and extravasation[109]. For example, in breast tumors, integrin-

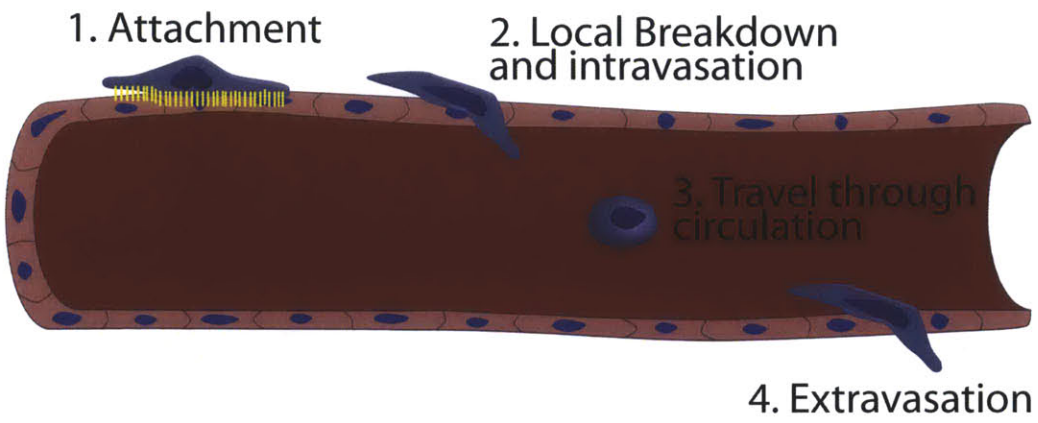

Figure 2-12: Interactions with the endothelium. Interactions with the endothelium is an essential step in the metastatic cascade, beginning with attachment to the vessel, local breakdown of endothelial cell tight junctions and intravasation, travel through the circulation, and finally extravasation from the vessel.

β3 and 4 have been linked to lung cancer metastasis, while only integrin-β3 is linked to metastasis to the bone[109]. The steps underlying interactions with the endothelium are given by **Figure 2-12**.

Survival in the Circulation Following intravasation, cells which have escaped from the primary tumor must travel through blood circulation to reach secondary sites. Unlike white blood cells which utilize adhesive interactions mediated by selectins and integrins, arrest of cancer cells is due primarily to size restrictions in small capillaries in the new organs[110]. However, in certain circumstances cancer cells can undergo adhesive arrest. For example, in the liver activation of the endothelium by interleukin (IL)-1α leads to tumor cell adhesion[110]. A similar phenotype has been seen in colon cancer metastases within the lung[111].

In order to metastasize, cancer cells must be able to withstand the harsh environment of blood[8]. While in the circulation, tumor cells are detached from the substratum exposed to high shear forces and immune cells **(Figure 2-13)**. In normal cells, detachment from the substratum should lead to cell death through a process called anoikis[8]. Metastatic cells which cannot avoid anoikis die in the circulation, possibly contributing to the high number of cell deaths in the circulation[8].

The trajectory taken by a tumor cell depends on several factors including the

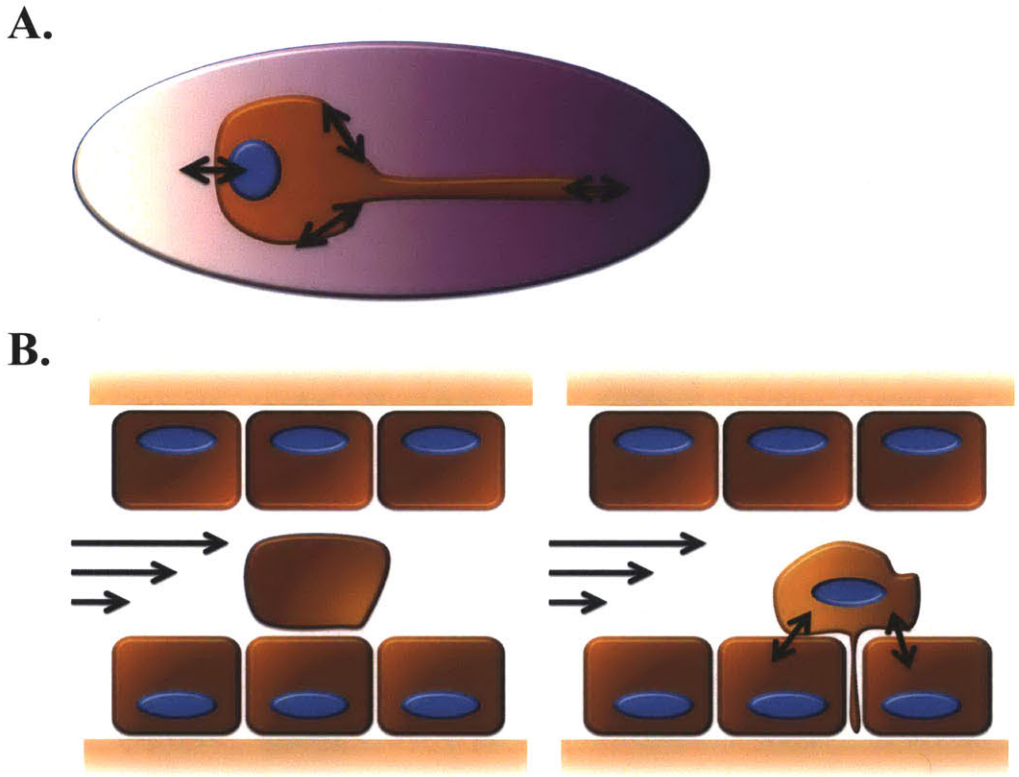

Figure 2-13: Survival in the Circulation. In order to metastasize, tumor cells must be able to withstand the harsh environment within the bloodstream. (A) Tumor cells that are detached still exchange mechanical forces with the environment. (B) Shear forces from fluid flow activate cytoskeletal remodeling and cell-cell adhesion genes. Diapedesis requires new mechanical interactions between tumor cells and endothelial cells. (Adapted from Kumar et. al., 2009)[1]

pattern of blood flow, the capillary diameter, and the balance between sheer forces and adhesive forces with the endothelium[15]. Metastatic cancer cells must be able to withstand shear forces in order to successfully form a secondary lesion. Deformation of the cells in the new organ system is dependent on blood pressure. Difference in deformation patterns can be seen in high-pressure (e.g. muscle) versus low-pressure systems (e.g. liver)[110]. Cells sense forces using mechanochemical systems which includes adhesion receptors like integrins, focal adhesion complexes, cytoskeletal networks, and molecular motors[1]. The shear forces experienced while in the circulation activate the mechnobiological regulatory systems. These pathways interact with signaling pathways that lead to reorganization of the cytoskeleton and changes in adhesion molecule expression[1].

Tumor cell arrest can occur through three mechanisms: adhesion to the endothelium, size restriction in the capillaries, or by binding coagulation factors to form a tumor embolus[8]. As mentioned previously, tumor cell arrest is not primarily mediated by adhesive forces, instead physical constraints in the capillary play a larger role[112]. Formation of tumor emboli involve coagulation factors such as tissue factor, fibrinogen, fibrin, and thrombin, but also involve adhesion molecules present on the endothelium such as P-selectin[113].

There are two possible initial fates for cells in a secondary site, as solitary cells or small pre-angiogenic micrometastases[110]. The majority of these cell populations are clinically undetectable and will remain as occult lesions falling into a state of dormancy or undergoing apoptosis. Dormancy for a single cell refers to a state where neither proliferation or apoptosis is occurring while a dormant micrometastases refers to a cell population where both apoptosis and proliferation occur at the same rate, resulting in no net increase in tumor mass[110].

Tumor cells interact with the endothelium in a variety of ways including recruitment of angiogenic vessels and as a means of escape from the primary tumor. Despite the important role that physical interactions between metastatic cells and the endothelium play in cancer metastasis, it remains a poorly understood aspect of cancer progression, underlying the need to better understand endothelial-

epithelial interactions. The final stage of the metastatic cascade is colonization, which is likely the most complex segments of metastasis and the next subject of discussion.

2.2.1.3 Metastatic colonization

Understanding the organ-specific pattern underlying cancer metastasis may likely present the most challenging aspect in unraveling the mysteries underlying cancer metastasis[110]. Many tumor types exhibit a predictable pattern of metastasis, for example breast cancer metastasizes commonly to liver, brain, bones, and lungs, prostate cancer preferentially metastasize to bone, while colorectal cancer commonly leads to liver metastasis[110].

Stephen Paget in an 1889 article in The Lancet explained the organ-specific pattern of metastasis using the concept of the tumor cells as Seed and the host environment as the Soil[114]. In this theory, the formation of secondary metastases is dependent on complex interplay between the biology of the primary tumor and the microenvironment. However, an opposing theory presented by James Ewing in the 1920s postulates that formation of a secondary tumor site is not dependent on tumor-stromal interplay, but instead is largely dependent on anatomical circulation routes[110]. Therefore the site of metastases is dictated by blood flow patterns.

There is scientific evidence to support both theories and it's likely that elements of each theory are necessary to predict the tissues where a secondary tumor will be formed. For example, in breast and prostate cancer, there are higher numbers of bone metastases then would be predicted by blood flow patterns alone[110]. A similar trend is seen in stomach and testicular cancers where blood flow routes explain only approximately 66% of metastatic lesions[110]. It's likely that once a tumor cell has arrested in a particular organ, molecular interactions with the surrounding stroma largely dictate whether a metastatic lesion will be formed[110].

Overall, the formation of a secondary metastatic lesion is an inefficient process. Less than 0.1% of tumor cells are viable 24 hours post entry into the circulation and only 0.01% of these cells will go on to form frank metastases[115]. To further add

to the complexity, metastases may occur years following treatment due to tumor dormancy[110]. Lastly, endothelium in tissues differs, explaining the inefficiencies in seeding efficiency in different organs[110].

Commonly metastatic lesions occur in the bone, liver, brain, and lung. The bone is common site of metastatic colonization for many tumor types including breast, prostate, lung, kidney, thyroid, and Multiple Myeloma[8]. There are two classes of metastatic lesions found in bone, osteoblastic, or bone forming metastases, and osteoclastic, or bone degrading metastases. Formation of these lesions involves aberrations in BMP/IGF signaling[8]. Osteoblastic bone metastases are commonly found in prostate cancer, while osteoclastic metastases occur more frequently in breast cancer and Multiple Myeloma[8] and have been linked to PTHrp/RANKL signaling[8]. Colonization of the liver is commonly seen in colon cancer primarily due to the circulatory pattern in the digestive system. Colon cancer cells enter the hepatic-portal system and first encounter the capillary beds of the liver[8]. Colonization of the brain occurs frequently in lung, breast, and melanoma. Drug therapies have also been linked to increased brain metastases. For example, treatment with HER2 inhibitors in breast cancer, or EGFRi inhibiters in lung cancer, have been linked to increased incidence of brain metastases[8]. Finally, colonization of the lung has been linked to signaling pathways involved in cell survival and resistance to apoptosis regulated by the TGF-β, NF-κB, and apoptotic signaling pathways.

2.3 Genetics of cancer metastasis

There are genes that positively and negatively regulate metastasis but these are not the same genes responsible for positive and negative regulation of primary tumor growth[116]. Metastasis suppressor genes work at multiple stages in the metastatic process. However, several of them have been demonstrated to directly suppress the colonization. Metastasis suppressor genes may act at several stages along the metastatic cascade in cancer and studies have shown that restoring metastasis suppressor functions may be a viable therapeutic strategy. Some metastasis suppres-

sor genes regulate cytoskeletal rearrangement. For example, DLC1 and Rho GDI2 regulates Rho GTPase signaling[116]. However, some metastatic suppressor proteins function directly on receptor pathways. For example, KAL1 leads to inhibition of EGFR signaling and the induction of senescence[116].

2.4 Tumor Microenvironment

A tumor is not composed of a singular cell type but instead is a complex tissue of multiple, diverse and important cells types that participate in heterotypic interactions to promote tumor progression[117–119] **(Figure 2-14)**. An understanding of tumor biology requires that cancer be studied in the context of physiologically relevant cell-cell and cell-matrix interactions[117,118]. Stromal cells that were once thought to be passive participants in cancer progression are now known to be vital contributors to the tumor niche[117,119]. Studies have shown that tumor stroma, particularly tumor endothelium, is genetically different than the stroma of normal epithelial tissue[120–122] and that pathological stroma can encourage tumor progression[117]. An understanding of the role of the stroma in cancer progression presents unique therapeutic opportunities.

In metastasis, understanding the role of tumor stroma requires additional considerations because metastatic progression is affected by the microenvironment of the primary tumor, in addition to the microenvironment of the secondary metastatic site[123]. In order for metastasis to successfully occur, a tumor cell must be able to take residency in foreign, potentially inhospitable environment. Although tumor cells can be present in multiple organs, metastatic lesions form in only a fraction of these tissues; thousands of cancer cells enter the circulation, however, only 0.01%, produce clinically detectable metastases[123]. Cancer cells can lie dormant for years before clinically detectable metastases are formed. The inefficiency of the metastatic process comes from the inability of cells to successfully navigate each of the steps required for progression, with a significant number of cells lost once they enter the circulation or undergo apoptosis due to inability to grow in a

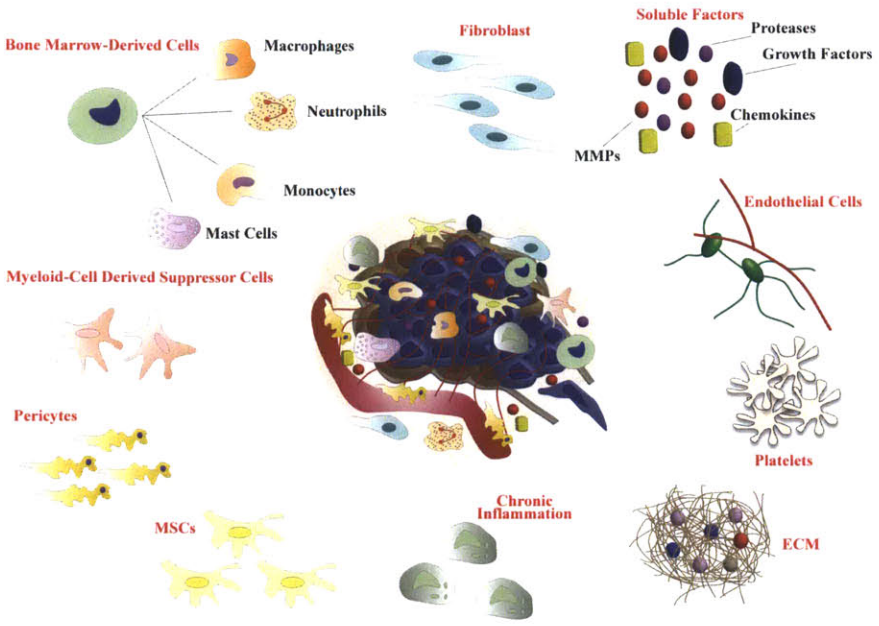

Figure 2-14: Tumor Microenvironment. The tumor microenvironment is a dynamic regulator of tumor biology. Tumor stroma has both cellular and acellular components that together contribute to a tumor's invasive potential.

foreign microenvironment. Formation of a metastatic lesion is an intricate dance between the biology of the metastasizing cell and its new stromal home. Successful metastatic cells must demonstrate significant plasticity in adapting to the diverse environments they will encounter during systemic invasion: primary tumor, blood circulation, and secondary tumor sites.

2.4.1 Tumor Stroma

There are two distinct components to the stroma, a cellular component and a matrix component. The non-cellular component is referred to as the ECM which provides the scaffolding on which tissues are built. The cellular stroma includes a wide range of cell types, namely fibroblasts, endothelial cells, mesenchymal stem cells, inflammatory cells, etc., each serving diverse and unique roles in normal physiology and tumor pathogenesis.

2.4.1.1 Extracellular Matrix

The ECM is a rich protein network composed of diverse macromolecules that creates a highly regulated structure on which cells attach to build complex tissue architectures. The composition of the ECM depends on the tissue type and location of the matrix. For example, interstitial ECM is rich in fibrillar collagens, glycoproteins, and proteoglycans, while basement membrane is a specialized ECM with a defined matrix of laminin, fibronectin, and type IV collagen[124]. The primary function of the ECM is to function as a physical scaffold on which cells attach and organize. However, the ECM also provides critical growth and development signals. It acts as a reservoir for growth factors that can be released by proteolytic cleavage[123]. Aberrant release of these growth factors can lead to disease pathology, for example, by metalloproteinases in cancer[124].

The extracellular matrix plays critical roles in regulating normal physiology and disease pathology. Disruption of its highly regulated biomechanical and biochemical behavior is strongly correlated to disease progression and potentially, disease initiation. For example, increased stiffness properties of ECM can initiate an oncogenic phenotype in normal mammary breast epithelial cells[125]. The breast epithelial cells lose their organized mammosphere morphology and instead adopt a tumor-like phenotype characterized by loss of a defined central lumen and decreased cell-cell and cell-ECM adhesion proteins.

Abnormal ECM is a hallmark feature of cancer pathology characterized by perturbations in composition, density, stiffness, and topography. For example, in breast tumors the ECM fibers are oriented in linear patterns, contrasting the criss-crossed orientation of normal ECM fibers[124]. Matrix degrading enzymes, such as heparanases and MMPs, play a large role in the abnormal features of the ECM in cancer[124].

The ECM acts as a natural barrier to cancer progression due to its role in separating tissue structures from one another. Disruption of the basement membrane in cancer by matrix digesting enzymes compromises its intrinsic barrier function, re-

ducing the ECM's ability to inhibit escape and migration from the tissue of origin. The ECM can also indirectly affect cancer cells by regulating the behavior of other stromal cells, such as endothelial cells or fibroblasts, to create a pro-tumorigenic environment.

The ECM is filled with pro- and anti-angiogenic factors that are critical for angiogenesis regulation. It is also important for endothelial cell survival, proliferation, and migration during angiogenesis. The ECM forms a protective barrier around endothelial cells that helps to prevent leakage of material from vessels. However, in tumors, the basement membrane around endothelial cells is defective and leaky allowing exudate, including metastatic cells, to easily exit the vessel.

The ECM has also been shown to regulate the stem cell niche[124]. Matrix fibers provide anchorage points for stem cells to remain in the stem cell niche, which is essential for the maintenance of paracrine signals that regulate stem cell function. The ECM can also directly regulate stem cell differentiation through mechanisms being actively explored[124]. Due to its regulation of stem cell biology, it's no surprise that the ECM may promote cancer by acting directly on stem cell populations. Abnormal ECM has been linked to expansion of cancer stem cell populations[124].

2.4.1.2 Tumor Fibroblasts

Fibroblasts are the dominant cell type found in tumor stroma and have been shown to be potent modulators of malignant progression in cancer. There are two types of fibroblast commonly found in tumors: cancer-associated fibroblast analogous to the fibroblasts found in normal tissue and myofibroblasts[14]. Myofibroblasts are not typically found in normal tissue; these cells are associated with chronic inflammation and are linked to the development of pathological fibrosis in many tissue types[14].

Tumor associated fibroblasts enhance a wide range of tumor cell traits including increased proliferation, angiogenesis, and invasion[14]. They are activated by inflammation associated growth factors such as IL-1, TGF-β, and PDGF. In contrast, normal healthy fibroblasts may be tumor protective. For example, in prostate

epithelial cells, normal fibroblasts were able to prevent, and even reverse, the development of a malignant phenotype[123].

One of the primary mechanisms tumor fibroblasts contribute to cancer progression is through the secretion of aberrant ECM protein components. As previously discussed, a displastic ECM is a potent mediator of cancer tumor invasiveness[20]. For example, in breast cancer, activated fibroblasts trigger a linear alignment of collagen fibers that promote cancer migration[20].

2.4.1.3 Mesenchymal Stem Cells

Mesenchymal stem cells (MSCs) are the precursor cells that form osteoblasts, condrocytes, and adipocytes. They are recruited to tumors and have been linked to increase metastasis[123]. For example, when co-cultured with metastatic breast cancer cells with weak metastatic capability, MSCs increased dissemination of cancer cells to the lung[123]. The enhancement of metastasis by MSCs seems to be dependent on the CCL5-CCR5 pathway. CCL5 has been known to simulate invasive behavior in tumorigenic cells[123]. Binding of CCL5 is linked to stimulation of this invasive behavior. However the effects of MSCs on development of metastatic lesions may be transient. MSCs did increase the number of metastases, however, in the long term there were no increases in metastatic cell outgrowth[123]. The transient nature of this effect illustrates the dynamic role of the microenvironment. Some cell populations might affect tumorigenesis in a transient manner, while other cell populations affect tumorigenesis more longitudinally. For example, endothelial cells regulate both early and late stage cancer progression.

2.4.1.4 Cancer Stem Cells

Dysregulation of stem cell self-renewal is a likely requirement for the development of cancer. Cancer may arise from a fully differentiated cell that has regained the ability to self-renew or from a mutation in a cell already with self-renewing potential. The self-renewing nature of cancer suggests that tumors may be derived from

mutations in cells that already exhibit a self-renewal mechanism. A cancer stem cell (CSC) refers to a cancer cell that is able to self-renew giving rise to the development of a tumor mass. These cells may have originated from mutations in the quiescent stem cells or the highly proliferative progenitor cells. Cancer stem cells are believe to play critical roles in cancer progression and may also be responsible for drug resistance in tumors.

2.4.1.5 Inflammatory Cells

The role of chronic inflammation as a potent enhancer of cancer progression has recently been recognized in the last decade. Described as wounds that never heal,[126] evidence of infiltration of immune cells can be found in almost all tumor tissue types[14] . Previously, immune cells were believed to be a natural defense mechanism against cancer. However, paradoxically the same cells that are designed to protect the body may at the same time be potent enhancers of cancer progression.

Inflammatory cells promote cancer primarily through the secretion of biological macromolecules into the ECM[123]. For example, inflammatory cells secrete growth factors that induce cellular proliferation (e.g. EGF, VEGF, FGF2) and matrix digesting enzymes (e.g. MMPs, hepranases, cysteine cathepsin proteases) which promote angiogenesis and metastasis. Inflammatory cells also release reactive oxygen species that cause genetic transformation in populations of cells that are inherently unstable.

Cancer cells have developed sophisticated mechanisms for evading immune-mediated rejection. For example, cancer cells can release TGF-β, which inhibits function of cytotoxic T cells and natural killer cells that target tumors[123]. Cancer cells also recruit immunosuppressive immune cells such as regulatory T cells or myeloid derived suppressor cells that inhibit the function of cancer targeting immune cells[123]. Tumor cells also directly promote recruitment of immune cells that are cancer promoting rather than cancer inhibiting. Bone marrow-derived cells (BMDC), notably macrophages, neutrophils, mast cells, and myeloid progenitor cells, gather at the margins of tumor lesions and initiate various cancer promoting

processes including the angiogenic switch, tumor cell invasion, and protection of the vasculature from drug therapies[14]. "Vascular progenitor cells" derived from the bone marrow have been found to incorporate within the neovasculature in place of endothelial cells or pericytes[14]. They have been linked to increased angiogenesis and metastasis[123].

The role of inflammatory cells in cancer is both tissue and context dependent with several cell types, CD4+ T cells, macrophages, and natural killer (NK) T cells, having both pro- and anti-tumorigenic properties[123]. For example, CD8+ T cells and mature dendritic cells are correlated with improved prognosis in both head and neck cancer and colorectal cancer[123]. In contrast, macrophage infiltration is strongly associated with poor disease outcome in several tumor types, such as breast, thyroid, and bladder cancer[123].

Tumor Associated Macrophages (TAMs) Tumor associated macrophages (TAMs) are the BMDCs with the most pro-tumorigenic characteristics, leading to increased angiogenesis, invasion and metastasis[123]. Activated by IL-4 producing cancer cells, macrophages encourage local invasion through secretion of matrix degrading enzymes[14]. Little is known about the overall mechanisms underlying the pro- and anti-tumorigenic characteristics of TAMs[14,123]. However, in breast cancer, TAMs activate EGFR signaling through the secretion of its receptor ligand, EGF. The tumor cells in return secrete CSF1, a chemoattractant for TAMS[14,123]. Immature myeloid cells with poorly differentiated macrophage features facilitate the spread of colorectal cells through MMP2 and MMP9 secretion[123].

An interesting theory has been developed to try to understand the role of macrophages in creating an "invasive niche."[123] The combination of endothelium, macrophage cells, and tumor cells seem to create an environment rich in metastasis promoting factors that function through paracrine signaling loops to promote invasion. In human breast cancer, the density of these three cell types together has been linked to increased metastasis[123].

Myeloid cell-derived suppressor cells (MDSCs) Similar to tumor-associated macrophages, myeloid cell-derived suppressor cells (MDSCs) have a primarily pro-tumorigenic function[123]. MDSCs are immature cells of the myeloid linage at different stages of differentiation that suppress T-cell mediated tumor cell death. MDSCs block CD4+ T cells and CD8+ T cells through three distinct mechanisms: secretion of arginase and nitric oxide, increasing regulatory T cells, and inhibition of NK cell activation[123]. These MDSCs promote tumors by inhibiting immune cell surveillance of tumor cells, creating a localized immunosuppressive state that favors metastasis[123].

2.4.1.6 Platelets

Although not normally considered part of the tumor microenvironment, platelets function in protecting tumor cells in the circulation[123]. In a wide range of cancers including breast, colorectal and lung, high platelet counts are associated with decreased survival[123]. Tumor cells bind to platelets using them as a shield to increase survival while in the circulation. Tumor cells express tissue factor which is the receptor for coagulation factors VIIA and X,[123] the main initiators of the coagulation pathway. This interaction allows for thrombomediated proteolysis, enabling the tumor cells to effectively form microthrombi and bind to the platelets[123]. Binding to platelets protects the tumor cells from cell mediated lysis by natural killer cells, and also through an additional mechanism of utilizing circulating prothrombin[127]. Formation of thrombi can also function to reduce shear forces in the vessels that can damage the circulating tumor cells[123]. Platelets can also enhance adhesion of cancer cells to blood vessels, encouraging subsequent extravasation at the secondary sites[123]. Furthermore, treatment with anticoagulants have shown to decrease metastasis in experimental models[123].

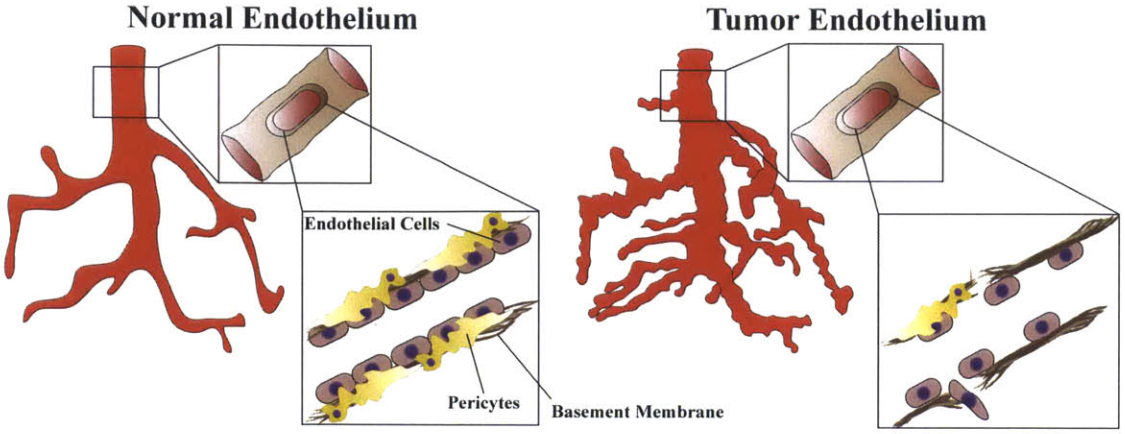

Figure 2-15: Endothelium in tumors is physiologically abnormal. Tumor endothelium is abnormal with large, leaky distorted vessels, excessive branching, disrupted basement membrane, and loss of support cells.

2.4.2 Tumor Endothelium

The endothelium can act as an enhancer of invasive phenotypes directly increasing metastatic capacity of tumor cells[105,120]. The endothelium of a tumor is dramatically different than normal physiological endothelium. Tumor endothelium is characterized by an abnormal morphology, with large distorted vessels, convoluted and excessive branching, precocious capillary sprouting, erratic blood flow, microhemorraging, leakiness, and abnormal cell proliferation and apoptosis[42,44] **(Figure 2-15)**. In normal adult tissue, there are few examples of continuous physiological angiogenesis in healthy adults, such as tissue injury or in the female reproductive system[42]. In healthy adults, endothelial cells are quiescent and are second longest lived cells in the body second to neurons[42].

Tumors have poorly defined venules, arterioles, and capillaries that are prone to leakage and hemorrhage. Blood vessels in tumors, are very heterogeneous, there are 6 distinct vessel types that are commonly found in tumors: mother vessels, capillaries, glomeruloid microvascular proliferations, vascular malformations, feeding arteries, and draining vessels[128]. Mother vessels are transient structures that arise from pre-existing venules[48]. They are large, thin-walled vessel structures,

with a serpentine architecture, characterized by loss of pericytes and high VEGFR receptor expression[48]. Blood flow through these vessels is disrupted, which increases risk of thrombosis. Mother vessels are transient structures from which different types of daughter vessel structures arise[48]. Glomeruloid microvascular proliferations are poorly organized structures that resemble renal glumeruli, characterized by tiny lumens and serpentine microvessels[48]. They have twice the amount of basement membrane that is normally present in vessels and are highly cellular due to increased replication of both endothelial cells and pericytes within these vessels[48]. The capillaries found in tumors are characteristic of vessels found in normal tissue[48]. In contrast, vascular malformations are characterized by asymmetry[48]. Smooth muscle cells initiate formation of vessel malformations[128]. Mother vessels which have acquired a coat of smooth muscle cells are apt to form vascular malformation[128]. You can distinguish vascular malformations from normal arteries and veins due to their unusually large size, and their thin and asymmetric coating of smooth muscle cells[128]. Vascular malformations are not permeable to macromolecules, and they can persist independent of VEGF-A signaling, unlike mother vessels and glomeruloid proliferations described previously[128]. This might be due to the fact that the smooth muscle cells that are in close proximity to these vessel structures actually secrete VEGF-A locally, which is able to maintain these structures[48,128]. This has important implications in the fact that vascular malformations will not be targeted by VEGFR inhibitors commonly used to treat cancer[48,128].

The last two types of vessels, feeding arteries and draining vessels are generated through arteriovenogenesis that occurs simultaneously with angiogenesis; however the exact mechanism by which this occurs is unknown[128]. Inhibition of feeding arteries and draining veins could be interesting therapeutical targets because these vessels lie upstream and downstream of tumor structures[128], therefore cutting off their blood supply would reduce the tumor blood supply both upstream and downstream, which may be more efficient than targeting the blood supply within just the tumor structure the approach taken by traditional anti-angiogenesis drugs[128]. Feeding arteries and draining vessels are formed through

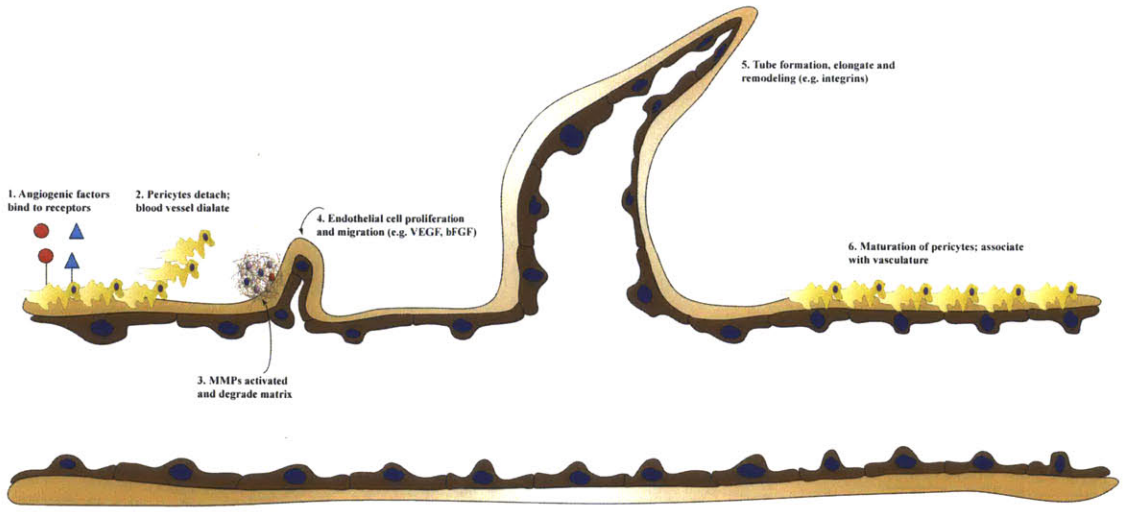

Figure 2-16: Schematic of angiogenesis. Angiogenesis is a tightly regulated process. However, in cancer, tight regulation is lost.

remodeling of existing vessel structures[128].

During embryonic vasculogenesis, vessels are formed de novo, from endothelial precursor cells called angioblasts[42]. These cells organize to form primary capillary plexus. The cells subsequently differentiate to form new blood sprouts that branch from pre-existing vessels in a process called angiogenesis. In tumors this process is altered.

Most tumor endothelium is formed through angiogenesis; however some tumors utilize vasculogenesis in recruitment of endothelial cell precursor cells in order to form the appropriate vasculature[42]. The steps of tumor angiogenesis or pathological angiogenesis can roughly be defined as follows **(Figure 2-16)**: The first step is vessel dilation and increasing vascular permeability of pre existing capillaries, or post capillary venules, in response to VEGF signaling[42]. This leads to extravasation, or flow out of the vessel, of plasma proteins. These plasma proteins form the provisional matrix on which the vessels will form[42]. The activated endothelial cells use matrix to migrate and form the vessel structure. Cell-cell adhesions between pericytes and endothelial cells are weakend in tumor endothelium. Loosing of pericytes on endothelial vessels occurs through the binding of ANG-2 to TIE-2, a tyrosine kinase receptor selectively expressed on endothelial cells[42].

Endothelial cells migrate into the peri-vascular space undergoing proliferation to form a migration column. Formation of the migration column signals for differentiation, creating a differentiation zone where the endothelial cells change shape and adhere to one another to form a lumen. The cells continue to proliferate along the vascular wall increasing the diameter of the vessel structures, and finally, there is recruitment of peri-vascular cells and formation of the vascular basal lamina[42].

There is speculation about the mechanism leading to pathological angiogenesis[120,122] including the role of microRNAs[106,129,130]. However, the molecular details on how this transformation occurs have yet to be elucidated.

Studies have shown that tumor associated endothelium is genetically abnormal, showing upregulation of many tumor and cancer promoting genes, such as the VEGFR receptors. Studies by Hida et. al. show that tumor endothelial cells have genetically abnormal centrosomes and demonstrate aneuploidy[131]. These findings were seen in multiple human cancers, such as human renal cell carcinoma, and also in mouse endothelial cells isolated from tumor xenografts of human melanoma and liposarcoma tumors[131]. The tumor endothelial cells are believed to acquire these genetic abnormalities from the tumor microenvironment, however the mechanism as to how these genetic abnormalities occur is still yet to be elucidated[132,133].

2.4.2.1 Pericytes

Pericytes are specialized mesenchymal cells that are related to smooth muscle cells[14]. They provide both mechanical and physiological support to the endothelium through projections that enclose endothelial tube blood vessels[14]. Pericytes typically communicate with the endothelium through paracrine signaling helping to maintain quiescence in the endothelial cells though the ANG1-Tie2 receptor pathways[14]. Pericytes aid endothelial cells in synthesis of the vascular basement membrane that help to keep vessel structures intact, anchoring both pericytes and endothelial cells and strengthening the vessel wall to withstand the hydrostatic pressure of blood flow. Abnormalities in pericyte function are strongly correlated

with the development of pathological angiogenic vessels. Loss of pericytes leads to increased instability of the tumor endothelial cell vessels and also enhances the ability of cancer cells to intravasation/extravasation into the circulatory system for hematologic dissemination[14].

2.5 The role of intercellular communication in the development of an invasive cancer phenotype

Cell-cell communication is an important part of maintaining cellular homeostasis, playing dynamic roles in cellular, organ, and organism function[3,134–136]. Evolution of multicellular organisms, embryonic development, adaptation to the external environment, and defense against pathogens would not be possible without local and systemic delivery of signaling molecules[3,134–136]. Despite the fundamental role of cell-cell communication in normal cellular physiology, inappropriate or deranged pathways of cell-cell communication play powerful roles in almost every human disease[136]. For example, in cardiovascular disease, derangements in growth factor, cytokine, or hormone signaling leads to myocyte hypertrophy contributing to cardiac dysfunction and eventually heart failure[137]. In a similar way, in the immune system, inappropriate intercellular communication is linked to immune dysfunction[138] and the spread of pathogens[136,139]. Neurological disorders such as Parkinsons disease and Alzheimers disease have also been linked to aberrant modes of intercellular communication[136]. Lastly, there is overwhelming evidence showing that disruption of classical modes of intercellular communication, such as cytokine and growth factor signaling pathways[140], in addition to alternate modes of intercellular communication, such as exosomes, play important roles in cancer pathology regulating primary tumor biology and promoting a pro-metastatic microenvironment[141–144]. Interestingly, intercellular transport of RNAs has been recently elucidated as a potent mediator of cellular transformation and disease progression in cancer and other diseases[145].

2.5.1 How do cells communicate?

Cell-cell communication can be grouped into indirect and direct modes. Indirect modes of communication are typically classified as receptor-ligand interactions involved in paracrine and endocrine signaling,[3,117,146,147] while direct modes of cell-cell communication involve physical interactions between cells that allow for transfer of intercellular contents[148]. Mechanisms of cell-cell communication are complex and varied, with many overlapping characteristics, making strict adherence to this classification system difficult. For example, under one classification, extracellular vesicles can be considered as a form of carrier-mediated chemokine signaling, activating receptor-ligand signaling pathways in a similar way to soluble factors[136,142]. However, extracellular vesicles also share similarities with modes of direct cell-cell communication. For example, like gap junctions and membrane bridges, exosomes allow for the transfer of genetic material such as functional mRNAs, miRNA, and DNA.

Roughly speaking, autocrine, paracrine and endocrine signaling fall into the category of indirect modes of communication, along with more recently discovered forms of indirect modes of cell-cell communication, such as exosomes, ectosomes, and apoptotic bodies. In contrast, direct modes of cell-cell communication include membrane bridges, gap junctions, fungal septa, and plasmodesmata **(Figure 2-17)**. Multicellular organisms have developed sophisticated machinery for utilizing many if not all of these mechanisms[149]. The number of varied mechanisms that exist underlies the evolutionary advantage provided to a cell which can effectively communicate with itself, neighboring cells, or cells far away – in other tissues, organs, or organ systems[149,150].

2.5.1.1 Modes of indirect cell-cell communication

The role of soluble factors Classical descriptions of cell-cell communication focused on the role of soluble factors in mediating biological functions. Cytokines, chemokines, growth factors, hormones, and neurotransmitters are examples of me-

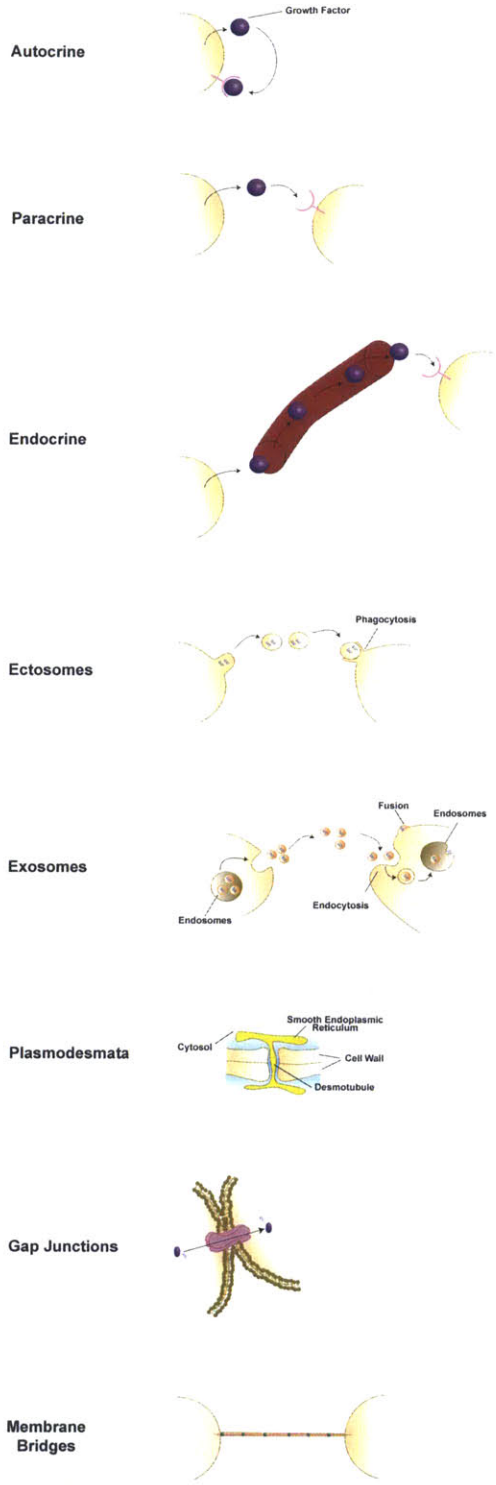

Figure 2-17: Modes of Intercellular Communication. Cells have adapted diverse mechanisms to communicate with the external environment. Each of these mechanisms have distinct and overlapping functions, but collectively function to regulate many aspects of cellular physiology. Modes of intercellular communication can be divided into direct and indirect modes of communication.

diators of this class of communication. There are three classically defined mechanisms of extracellular communication: autocrine signaling, paracrine signaling, and endocrine signaling. In autocrine signaling, cells secrete soluble factors that they themselves respond to. For example, autocrine signaling has been shown to allow for constitutive Wnt pathway activation in a significant number of human breast and ovarian cancers[151].

The second mechanism, paracrine signaling, involves the release of signaling molecules by a cell that unlike autocrine self-signaling, targets cells in close proximity. For example, activation of epidermal growth factor receptor (EGFR) by its ligands (e.g. epidermal growth factor and TGF-α) occurs through paracrine signaling. Paracrine signaling has also been demonstrated to be a mechanism of hedgehog pathway activation in cancer. Overexpression of Hh ligands in tumor cells leads to pathway activation of Shh in neighboring stromal cells through a paracrine signaling mechanism[152]. Furthermore, it was found that inhibition of the Hh pathway in the stromal microenvironment in turn results in suppression of tumor growth. This interaction is an example of the complex interplay in cell signaling, where changes in signal pathway activation in one cell type can affect neighboring cell populations through a paracrine signaling mechanism[152].

Endocrine signaling is the final classically defined mechanism of intercellular communication. It involves the systemic delivery of signaling molecules. The signaling molecules in endocrine signaling are usually referred to as hormones. Hormones are carried throughout the body in the systemic circulation, playing critical roles in maintaining homeostasis and in regulating physiologically processes in multi-cellular organisms. For example, hormones like angiotensin and aldosterone are critical for the regulation of cardiovascular function. Deregulation or inappropriate expression of these hormones leads to hemostatic instabilities and difficulties maintaining appropriate blood pressure both of which are large contributors to the development of cardiovascular disease[137].

To further add to the complexity several of these pathways act through many, if not all, of these mechanisms. One example is the EGFR pathway. Acting as a

hormone, EGF is secreted by the maternal mammary gland, regulating neonatal development[153]. However, EGFR activation can also occur through autocrine and juxtacrine mechanisms[153]. Juxtacrine signaling is unique because it combines aspects of traditional signaling by soluble factors with the requirement of physical contact, analogous to direct modes of intercellular communication. Juxtacrine signaling is a type of contact dependent signaling induced by cell-cell or cell-ECM interactions. The best example of juxtacrine signaling is the canonical Notch signaling pathway[154,155]. Notch is a transmembrane receptor protein that is activated by its ligands which are typically members of the Delta and Jagged family of cell membrane proteins[154,155]. Notch signaling requires that cells be in close physical contact as a consequence of its activation by cell membrane ligands. Contrast this requirement of close contact to other forms of direct modes of communication like membrane nanotubes that allow for directed cell-cell communication over long distances of separation[156].

Extracellular vesicles: A form of carrier-mediated signaling Carrier-mediated signaling provides an alternative mechanism for cells to communicate via autocrine[157], paracrine[143], endocrine signaling[143,158,159], as well as providing a conduit for transfer of biomolecules that until recently were less commonly associated as mediators of intercellular communication, such as cytoplasmic RNAs[135,136]. Carrier-mediated signaling is accomplished by cell-derived vesicles covered by membrane lipid bilayers[135,136]. Since the original description of extracellular vesicle release from rat and sheep reticulocytes,[160,161] membrane vesicles have been described in almost every body fluid such as urine, blood, sweat, serum, and plasma[162]. They have been described in both eukaryotic and prokaryotic cell types and have been shown to carry a wide array of cargo including proteins, lipids, and nucleic acids[136].

There are three main extracellular vesicles involved in chemokine signaling, exosomes, microvesicles, and apoptotic bodies. Exosomes are small intraluminal vesicles (ILVs) (30-100nm) formed inside late endosomes called multivesicular bodies (MVBs)[135,163]. They are released from cells when multivesicular bodies

fuse with the membrane. Exosomes have a distinct membrane composition that reflects their endosomal origin[135,163]. There are characteristic proteins associated with exosomes that have varied functions such as membrane fusion proteins, cytoskeletal proteins, signal transduction proteins, anti-apoptotic proteins, adhesion molecules, and cell specific proteins[163].

Ectosomes and apoptotic bodies represent the two other commonly studied extracellular vesicles. Ectosomes, are larger than exosomes (100nm-1μm), resulting directly from membrane blebbing and are believed to serve similar functions as exosomes[135]. Apoptotic bodies are the largest extracellular vesicles at >1μm[135]. They are commonly released by tumor cells but not other cell types. They are characterized by phosphatidylserine externalization and commonly contain fragmented DNA[135].

2.5.1.2 Modes of direct cell-cell communication

Direct modes of cell-cell communication require physical contact between two cell types. These modes of communication can range from short-range communication, for example via gap junctions, to long-range communication as is seen with membrane bridges. These modes of communication are unique in contrast to modes of indirect cell-cell communication because they allow for specificity in targeting an individual cell or a particular cell population. Examples of this mode of communication include membrane bridges, gap junctions, and plasmodesmata.

Plasmodesmata Plasmodesmata are plasma membrane lined channels within the cell wall of plants that allow for regulated transport of cellular contents between adjacent cells[164]. These structures can form between mature cells or during cellular division from components of the endoplasmic reticulum. Transport of molecules through plasmodesmata occurs between the plasma membrane and the endoplasmic reticulum central core called a desmotubule and is regulated by callose found at both ends of the pore[164].

Plasmodesmata have long been identified as a mode of intercellular communi-

cation in plants allowing for the transport of a wide range of biomacromolecules. They are an important mechanism for regulating plant cellular physiology and development and can also contribute to cellular pathology for example when exploited by pathogens[164]. One very interesting feature of communication through plasmodesmata is the ability to transport RNA silencing signals.

The discovery of mobile RNA sequences was first made in plant species. One early study demonstrated that silencing signals inserted in the stalk resulted in silencing of grafted scions derived from non-silenced plants. Silencing in this model occurred at 100% efficiency and transport was determined to be unidirectional from stalk to scion[165]. Transport of these signals has the potential to affect important physiological processes such as host genome defense against pathogens and response to external environmental stimuli. For example, transport of transgenes derived from sRNA and endogenous sRNA was shown to result in epigenetic modifications in the genome of the recipient cells potentially altering host responses to physiological stresses and insults[166].

Gap Junctions Gap junctions are a form of short-range direct cellular communication. Gap junctions are formed by the connexin family of proteins[167] and similar to previously described modes of cellular communication, gap junctions mediate important physiological process, such as T cell activation in the immunological synapse during antigen presentation by dendritic cells[168], and are involved in disease pathology. Gap junctions have a unique structure forming open channels between two adjacent cells that allow for intercellular connectivity and free diffusion of macromolecules and ions.

A single gap junction does not allow for intercellular contact between distant cells. However, gap junctional communication can still allow for intercellular communication between a population of cells because similar to plasmodesmata, gap junctions form a network of intercellular connectivity connecting each cell to its adjacent neighbors. Therefore this mode of communication too can enable rapid dissemination of intercellular signals within a population. Gap junctions can trans-

port miRNA and small interfering RNA (siRNA) silencing signals[169,170] that regulate gene expression for example in mammalian heart cells[170]. Furthermore, gap junctional communication has been shown to enhance a metastatic phenotype in breast cancer[171].

Membrane connections The final class of direct cell-cell communication mechanisms are the membrane bridges, which include, fungal septa, cytonemes, and tunneling nanotubes. Fungal septa are cross walls that divide individual fungal cells. In some ways they resemble plasmodesmata, functioning as pores that transport cytoplasm and organelles between neighboring cells[149]. Tunneling nanotubes and cytonemes have similar structures and overlapping, yet distinct, functions. Cytonemes and tunneling nanotubes are thin membrane bridges composed of cytoskeletal proteins, primarily F-actin. The primary distinction is that cytonemes are non-tubular bridges with no cytoplasmic connectivity, while tunneling nanotubes are open tubular structures that connect the cytoplasm of adjacent cells[98]. As a consequence, intercellular contents such as endolysosomal cargo can be transported within TNT structures, while cytonemes can only transport membrane bound macromolecules or pathogens[98]. Membrane projections have been implicated in a wide range of disease pathologies including cancer[172], autoimmune diseases[?], and infectious diseases[173]. For the purposes of this discussion, I will focus on the modes of communication relevant to mammalian cell biology giving specific emphasis to tunneling nanotubes.

Original description of Tunneling Nanotubes Tunneling nanotubes are a recently discovered, novel form of cellular communication wherein direct transfer of intercellular contents occurs through thin, nanotubular projections[2]. Since the initial observation of TNTs in rat pheochromocytoma cells (PC12)[2], TNT and TNT-like structure have been observed in prokaryotic[174] and diverse eukaryotic cell types such as neuronal, immune, and epithelial cells[2,3,117,175]. These structures provide a conduit for a dynamic mode of cell-cell communication that allows for the

exchange of cellular contents over hundreds of microns of physical separation[3,175]. Across cell types, there is a fair degree of heterogeneity in TNT length (major axis), width (minor axis), and cytoskeletal composition, so no single definition can be used to classify all TNTs[117,156,175]. The unifying feature among all TNTs is cytoplasmic continuity between cells; also unlike other cellular protrusions, such as lamellipodia and filopodia, TNTs are found to hover above the substratum[2,117]. TNTs carry a diverse array of cargo including cytoplasmic fluorophores, proteins, and organelles[117,156,175]; they are also mediators of bacterial[176,177] and viral pathogenesis[177,178] and present novel routes of disease transmission. TNTs may serve important roles in disease pathology, highlighting the motivation to understand their physical properties and biological characteristics[11,14,156].

TNT projections found in PC12 cells had unique physical dimensions with a average diameters ranging between 50 and 200nm and lengths greater than several cell diameters[2]. TNTs in this model system were fragile structures, rupturing from exposure to light, mechanical stress, and chemical fixation. Interestingly, exposure to trypsin-EDTA did not lead to disruption of structures[2]. TNTs were also observed in human embryonic kidney (HEK) and normal rat kidney (NRK) cells, implying that these structures may be evolutionarily conserved and present in many tissue types[2].

The authors speculate that TNTs were formed from growing filopodial protrusions that make contact with neighboring cells and emphasize that these structures are not remnants of incomplete cytokinesis. In this model system, TNTs appeared as single structures, rarely displaying branching characteristics; however occasionally existing as complex networks connecting many neighboring cells[2]. TNTs formed by PC12 cell types were composed of F-actin cytoskeletal components and not microtubules[2]. Future studies, however, have shown that TNT and TNT-like structures in other cell types contain microtubules, and the inclusion of microtubules may be dependent on the dimensions of the minor axis of the projection[176].

The primary reported function of TNTs has been intercellular communication.

Live cell video microscopy was used to capture transport of intercellular cargo within these projections. In PC12 cells, two hours post co-culture, TNTs allowed for unidirectional and selective transport of organelles with 74% of TNT+ve cells showing evidence of transfer. Furthermore, Myosin Va co-localized with the synaptophysin, the endosomal marker used to track the organelles, suggesting a possible actin-mediated active transport mechanism. TNT structures could be disrupted with inhibitors of actin polymerization, emphasizing the role of the actin cytoskeleton in formation of these structures. Only plasma membrane proteins and not cytoplasmic molecules such as green fluorescent protein or calcein, a small molecule dye, could be transported through these structures suggesting that passive diffusion of soluble cytoplasmic molecules did not occur through TNT structures observed in PC12 cells. However, subsequent studies have demonstrated that cytoplasmic molecules can indeed be transported through TNT projections, again emphasizing the variability of these structures among different cell types.

Tunneling Nanotubes in Normal Cell Physiology After the initial demonstration of TNTs in PC12, there has been a flurry of investigations into the role of TNTs in other cell types, particularly in the immune system. TNTs have been implicated in both normal and disease pathology of the immune system. Membrane nanotube structures have been shown to connect a wide range of immune cells such as Epstein-Barr virus transformed cells, primary macrophages, and NK cells[179].

In the immune system, TNTs display varied functions ranging from intercellular calcium signaling to pathogen transmission. Chemically or mechanically stimulated dendritic cells and monocytes quickly transmit calcium signals to neighboring cells through TNT structures[180]. Transport of calcium signals through TNTs is believed to be analogous to calcium signaling through gap junctions. Membrane nanotubes transport a second messenger inositol 1,4,5-trisphosphate (IP3). This second messenger induces calcium release from the endoplasmic reticulum. In addition, calcium may also be directly transferred within the TNTs, further enhancing

calcium signals in the second population[180]. In dendritic cells, transport of calcium signals within TNTs is believed to function in antigen recognition. In these cells, calcium signals received via TNTs promoted changes in cellular morphology that enhanced the ability of these immune cells to respond at an antigenic site. TNTs have also been identified as a mechanism for exchange of MHC class I molecules, potentially highlighting the role of these structures in antigen presentation[181]. In HeLa cells, membrane bound HLA-A2-EGFP was transported along the nanotube; however, soluble HLA-G2-EGFP protein was not[181]. Overexpression of LST1, an inducer of nanotube formation, could promote HLA molecule transfer[181]. LST1 has been previously identified as an inducer of functional nanotube formation in leukocytes[182]. LST1 is a transmembrane MHC class III protein, which functions through interactions with the small GTPase RalA and the exocyst complex[182].

Nanotubes function in both mechanisms of innate and adaptive immunity[183,184]. For example, in the innate immune system, these structures regulate interactions between NK cells and their target cells[183]. Nanotubes promote the cytotoxic function of natural killer cells through two distinct mechanisms. First, nanotubes create direct contact between the NK cell and its target, improving efficiency of cell lysis. Second, nanotubes move target cells closer to NK cells for lysis via formation of a conventional immune synapse[183]. Cytotoxic T cells also utilize membrane nanotubes in order to enhance killing of their targets in a similar manner as NK cells[184]. TNTs also enhance the antigen recognition in immune cells by creating what is referred to as a submicron synapse. This allows the NK cells to stay in contact with a previous target cell conferring antigens of interest that promote improved identification of other infected cells to target for destruction[183]. Similarly, in B-cells, antigen receptors can be transported between activated and bystander B cells leading to more efficient expansion of antigen binding B cells[185].

TNTs also play a protective role in the immune system by preventing development of autoimmunity[138]. In normal cellular physiology, healthy T cells destroy autoreactive T cells through Fas-FasL binding. However, a new mechanism utilizing TNTs has recently been identified, where transport of caspases between T

cells also contributes to destruction of autoreactive cells[138]. The TNT projections are themselves directly induced by secretion of Fas by autoreactive T cells. This mechanism, referred to as social apoptosis, appears to be critical in preventing autoimmune disease[138]. For example, defects in this pathway has been linked to development of autoimmune lymphoproliferative syndrome, characterized by the inability to completely eliminate autoreactive T cells[138].

Beyond the immune system, tunneling nanotubes have been described in a whole host of cell types including retinal pigment epithelial cells[186], vascular smooth muscle cells[187], cardiomyocytes and cardiofibroblasts[188], renal proximal tubular epithelial cells[146], and astrocytes[189]. There have been no unifying theories regarding the role of TNTs in normal cellular physiology. However, these structures seem to regulate a wide range of cellular activities and have been linked to disease pathogenesis.

2.5.2 Cell-cell communication in disease progression

Cell-cell communication plays critical roles in normal cellular physiology. Therefore it's unsurprising that aberrations in cellular communication are implicated in varied diseases including spread of pathogens[136], cardiovascular disease[137], neurodegeneration,[136] and cancer progression[136]. For example, gap junctional intercellular communication between breast cancer cells and bone marrow stroma have been implicated in cancer metastasis[167], highlighting that aberrations in ligand-receptor signaling is a fundamental element in cancer pathogenesis. In the cardiovascular system, microvesicle transport of miR-150 from THP-1 monocytes to microvascular endothelial cells promotes atherosclerosis through c-MYB[190]. As a final demonstration, exosomes released by diseased neurons may be linked to the transport of pathogenic proteins through neuronal tissue[191].

Membrane bridges and membrane vesicles are the two most recently discovered mechanisms of cell-cell communication. Unique to these modes of communication is the capability to transport genetic material, such as cytoplasmic

RNAs, making them dynamic and powerful modes of cell-cell communication. The unique nature of these communication mechanisms makes them interesting candidates of disease progression. Indeed, these mechanisms may represent two extremes of a single mode of communication where cargo is protected by the plasma membrane. As such, exosomes enable a long-range, low specificity form of this communication, and membrane bridges promote short range, high specificity communication. Each of these mechanisms has been linked to a wide range of disease pathologies; however, the largest body of evidence for the function of these modes of intercellular communication are in the fields of infectious diseases and cancer pathogenesis.

2.5.2.1 Infectious Diseases

There has been a great deal of interest in the role of TNTs in disease progression due to the specificity and signal-amplifying quality of communication through nanotube connections[192]. Membrane nanotubes present a potent mechanism of disease pathogenesis where one infected cell can simultaneously communicate with multiple neighboring uninfected cells, making nanotubes an efficient tool for exploitation by pathogens. There have been several studies demonstrating exploitation of TNT structures by both bacterial and viral pathogens[193]. For example, TNTs have been shown to be a mechanism of human immunodeficiency virus (HIV)-1 transfer[178,194]. HIV-1 can be transferred from infected T cells trough membrane nanotubes in a receptor dependent fashion[178]. Transmission of HIV through nanotubes was 100-1000 times more efficient than cell-free HIV transmission[178]. A similar study in macrophages showed that HIV-1 could directly induce formation of TNT structures to increase efficiency of infection[194]. In these studies, the authors describe the ability of HIV to "hijack" TNT communication in order to facilitate pathogenesis. The mechanism of HIV induced TNTs involves interactions between the exocyst complex and HIV-1 Nef[195].

The ability of pathogens to induce formation of cytoskeletal projections is not a new concept. Over a decade ago, *Listeria monocytogenes* was found to induce

protrusion of finger like projections from infected macrophages allowing for bacteria transport to neighboring cells[176]. Pathogens were able to induce formation of projections by directly promoting actin polymerization. These viruses (e.g. alpha herpes virus family and pseudo rabies virus family) utilized these projections to facilitate immune silent spread through entire cell populations, avoiding immune detection by reducing their exposure to the extracellular environment[176].

Microvesicles are also potent mediators of viral transmission[139]. For example, the chemokine receptor, CCR5, is transferred via membrane-derived microparticles released from the surface of peripheral blood mononuclear cells. CCR5 is a critical co-receptor used by macrophage tropic strains of HIV-1 to infect host cells. Transfer of CCR5 confers sensitivity to HIV-1 infection in previously resistant CCR5 deficient mononuclear cells. Furthermore, microvesicle transfer of CCR5 to endothelial cells enabled HIV-1 infection of these cells, demonstrating that exogenous CCR5 transported via microvesicles can make cells normally resistant to HIV, susceptible to infection[139]. There is also evidence to suggest that mature DCs can also transfer HIV to neighboring CD8+ and CD4+ cells through secreted exosomes[196].

Exploitation of these modes of communication to promote pathogen infectivity is not limited to viruses[192]. In macrophage cells, bacteria can utilize membrane nanotubes to infect healthy cells[176]. Two different classes of TNT structures have been described in macrophage cells; large projections containing F-actin and microtubules and smaller structures containing only F-actin. Bacteria can only be transported along the thin nanotube projections, while the thicker projections transport intercellular vesicles such as endosomes and lysosomes. Transport through both classes of projections was inhibited by azide treatment, suggesting that TNT formation is an energy-intensive process. However, disruption of TNTs with microtubule destabilizing agents, such as colchicine and nocodazole, resulted in only inhibition of organelle transport and not disruption of bacteria transport. These results emphasize the distinctly different role of the large and small TNT connections in these cell types[176]. TNTs formed from dendritic cells to primary

neurons have also been demonstrated as a mechanism of prion spreading from the peripheral nervous system to the central nervous system[173].

Pathogens have the unique ability to exploit normal cellular physiological processes to achieve ever increasingly efficient mechanisms of transmission, which in many ways characterizes the nature of malignant cells[197]. Similar to HIV, other pathogens are able to directly induce formation of disease-promoting membrane projections. For example, *Rice Dwarf Virus* (RDV), through a viral protein called PNS10 was able to induce formation of membrane projections between infected insect cells and non-infected mammalian cells[198]. The intercellular virus exploited these tubular structures to move into healthy neighboring animal cells[198].

2.5.2.2 Cancer

Membrane bridges and vesicles present exciting mechanisms for tumorigenesis, metastasis, and drug resistance[136,199]. Using these modes of communication, a tumor cell may be able to perturb, potentially even transform, surrounding epithelial and stromal cell populations. These modes of communication serve three primary roles: to promote tumorigenesis, to inhibit tumorigenesis, or as a means of communication between tumor cells and the stroma[75]. One example of the role played by membrane vesicles in cancer pathogenesis involves release of mRNA, miRNA, and protein filled microvesicles by Glioblastma cells. These microvesicles were taken up by surrounding tumor and microvascular endothelial cells, leading to increased tumor proliferation and enhanced angiogenesis[200]. The oncogenic receptor EGFRvIII was transferred between cells through microvesicles termed "oncosomes" that allowed for horizontal propagation of oncogenes and presented a potential mechanism of cellular transformation[201]. In another example, EMPPRIN, a transmembrane glycoprotein, was also transported via microvesicles between tumor cells and the surrounding microenvironement. EMPRINN is expressed at high levels by tumor cells leading to stimulation of matrix metalloproteinase expression in fibroblast to facilitate tumor invasion and metastasis[202]. In pleural mesothelioma cells, TNTs were demonstrated to transfer vesicles, proteins, and mitochondria be-

tween malignant cells[203].

Exosomes secreted by cancer cells also have immune modulating activity. For example, oral squamous cancer cells secrete microvesicles carrying Fas ligand that induces apoptosis of activated T cells and Jurkat cells. Tumors also release exosomes which promote expansion of regulatory T-cell populations that target tumor recognizing CD8+ T cells for destruction[204]. These mechanisms likely promote immune evasion by cancer cells[205]. In contrast, tumor derived exosomes can also enhance destruction of tumor cells by the immune system . For example, tumor-derived exosomes have been shown to induce antigen sensitization in dendritic cells[206].

Membrane bridges and vesicles may also be linked to drug resistance. For example, trastuzumab resistant breast cancer cells secrete HER-2+ve exosomes. Secretion of HER-2+ve exosomes has been previously linked to reduced drug toxicity. One possible mechanism to explain the reduced drug toxicity is that in these cells, internalized drug binds to exosome-bound Her-2 instead of intracellular Her-2. Therefore the drug is expelled from the cells during exosome release[207]. In MCF-7 breast epithelial cells, transfer of P-glycoprotein (pGp) resulted in a non-genetic multi-drug resistant phenotype[208,209].

These modes of communication may actually serve as the greatest roles in tumor stromal interactions. For example, tumor exosomes have been implicated in endothelial cell activation, angiogenesis[210], and metastasis[211141]. In melanomas, tumor-derived exosomes promoted metastasis through transformation of bone marrow progenitor cells, consequently leading to activation of an MET signaling pathway. Activation of the MET receptor created a pro-vascular phenotype that enhanced formation of a pre-metastatic niche[141]. In another study, transfer of tumor microvesicles containing oncogenic EGFR activated VEGF signaling in endothelial cells, promoting pathological angiogenesis[157]. Furthermore, transfer of mitochondria from tumor cells to endothelial cells through TNTs has been linked to chemoresistance[212]. Lastly, TNT-mediated exchange of pGp may also induce stromal cell transformation[213].

2.5.3 Transport of RNAs as potent mechanism of cellular transformation in cancer

Intercellular transfer of genetic material presents a powerful means of cellular communication, playing critical roles in both normal and disease pathology. Although transfer of genetic material in plants and other lower eukaryotic life forms has been well demonstrated, exchange of genetic information in mammalian cells is a relatively recent concept[135,136]. Horizontal transfer of DNA, mRNA, and small RNA (sRNAs) from one cell to neighboring cell populations have been described in many cell types including cancer cells, stem cells, and immune cells[135,136,214]. The nucleic acids can be encapsulated in extracellular vesicles, exist as free molecules, or bound to carrier proteins[214].

Early research examining intercellular communication in animals cells described the presence of mRNA and microRNAs in exosomes secreted from mouse and human mast cells[215]. The mRNA found in these vesicles was functional and expressed in recipient cell populations. The authors coined this mechanism of cellular communication as "exosomal shuttle RNA", a novel mechanism of cellular transformation[215]. The capability of genetic material to act as candidates for intercellular communication introduces new and dynamic mechanisms by which cells maintain homeostasis and interact with the surrounding environment. Horizontal transfer of genetic materials allow cells to directly manipulate the behavior of neighboring populations. For example, horizontal transfer of DNA through phagocytosis of apoptotic bodies has been implicated in viral pathogenesis and cancer progression. Co-culturing apoptotic bodies containing viral DNA derived from lymphoid cells infected with Epstein-Barr virus (EBV) led to expression of EBV genes in recipient cells[216]. Similarly, exosomes secreted by EBV positive B cells transferred functional miRNAs to uninfected monocytes[217].

Similar to DNA, circulating RNAs have been implicated in both normal and pathological disease states[136,214]. Once believed to be too fragile and susceptible to degradation by extracellular nucleases, RNAs have been detected in many body

fluids including serum, plasma, saliva, urine, and milk[214,218]. They have also been linked to pathological disease states such as diabetes, cancer, immune dysfunction, and tissue injury[214,219]. For example, antigen-dependent unidirectional transfer of microRNA+ve CD63+ exosomes from T cells to antigen presenting cells (APCs) functioned in immune synapse formation[220]. In the cardiovascular system, extracellular vesicles carrying miRNAs were found to be cardioprotective. Exosomes released by Kruppel-like factor 2 (KLF2) expressing endothelial cells or shear stress stimulated endothelial cells to transport miR-143/145 to smooth muscle cells leading to reduction of atherosclerosis in the aorta of $ApoE^{-/-}$ mice[221]. KLF2 is a regulator of endothelial cell genes in atheroprotective flow.

2.5.3.1 Initial identification of mobile RNA signals

The spread of mobile RNA sequences was first uncovered in plant species. Gene silencing signals were found to spread from cell-to-cell through specialized structures called plasmodesmata[134,135]. Although it would be several years until the identity of the mobile silencing signals was definitively identified as RNA[134], several studies demonstrated that the signals were found to spread over long distances and with high efficiency, lead to post-transcriptional silencing[134,135]. Local and systemic silencing caused by administration of double-stranded RNA (dsRNA) was also observed in *Caenorhabditis elegans*[222]. In this model system, dsRNA was more effective at signal interference than single-stranded RNA (ssRNA). Surprisingly, the authors observed silencing affects in both somatic and germline cells administration of dsRNA in the parent generation lead to silencing in the progeny[222]. The mobile systemic RNAi was believed to move through a transmembrane protein, Sid-1, possible acting like a channel for transport of dsRNA, siRNAs, or other yet to be discovered RNAi signaling molecules[223]. Hamilton et. al. found that RNA molecules could themselves be infectious agents producing symptoms analogous to viral infection in plants[224]. The viral RNAs were found to move between plant cells conferring systemic mosaicism in leaves[225]. However, the existence of endogenous silencing signals was still unknown[135].

In 2010 three groups described intercellular transfer of endogenous RNA species in plants. Using inhibitors to blocking small RNA (sRNA) biogenesis, movement of endogenous sRNA from donor shoots to recipient roots was demonstrated in *Arabidopsis thaliana*. The study illustrated the role sRNAs may play in epigenetic modifications providing resistance to pathogens and directing appropriate response to external stimuli through a mechanism that persists much longer than traditional soluble factors[166]. The sRNAs sequences themselves, and not the precursor sequences, were the mobile elements[226]. Movement of these mobile sequences were found to be a critical element in regulating physiological processes such as tissue pattern during organ development[227]. Furthermore, through the function of RNA polymerases IV (Pol IV) and RNA-dependent RNA polymerases (RDRs), the RNA signal could be amplified, resulting in potent downstream effects in neighboring recipient cells[134,135]. Signal amplification is a unique feature of RNA signals in plants and *C. elegans*

2.5.3.2 Circulating Nucleic Acids in Cancer

Intercellular communication of genetic materials may play important roles in cancer pathology. Transfer of mRNA and microRNAs have been implicated in many different tumor types, but microRNA communication holds particular promise because it allows for long-term regulation of biological function. MicroRNAs have been implicated in almost every type of cancer[218] and are potent mechanisms of biological regulation. A single miRNA can target several mRNA sequences giving miRNA signals a unique amplification effect. Therefore, aberrant miRNA expression can have widespread and diverse consequences.

Circulating RNAs have the potential to act as biomarkers to predict disease outcomes[218,228]. Specifically, circulating miRNA is a unique biomarker because unlike other biological macromolecules it does not undergo transcriptional or translational modifications[218]. Furthermore, microRNAs are robust and stable molecules compared to other RNAs, resistant to extreme pH and temperature conditions, and repeated freeze thaw cycles[229]. There is significant interest in the development

of cancer diagnostics based on circulating miRNA[230], as well as in other diseases and/or organ injury (e.g. brain, heart, kidney, and liver)[231].

Circulating RNAs are commonly found within lipids carriers (i.e. apoptotic bodies, microvesicles, or exosomes) that protect them from serum ribonucleases[135,214]. However, they can also exist as free molecules or bound to carrier proteins[214]. For example, they can be encapsulated in cholesterol rich lipid vesicles[214,232] or bound to carry proteins such as Argonute 2[233] and NPM1[234]. In actuality, the majority of circulating miRNAs are bound to proteins rather than vesicles[233].

Circulating microRNAs have been identified in almost every body fluid (e.g. plasma, urine, cerebrospinal fluid, pleural fluid, tears, breast milk, seminal fluid, amniotic fluid, saliva, peritoneal fluid, colostrum, and fluid from bronchial lavage)[235]. In cancer, many circulating RNAs have been linked to disease progression. One of the initial studies correlating serum miRNAs and disease found that high levels of miR-21 was linked to improved survival in B-cell lymphoma[236]. In prostate cancer, miR-141 serum levels distinguished healthy and diseased patients[218,230]. The presence of miR-141 also distinguished xenografted mice from control mice in an *in vivo* prostate cancer model[230]. Upregulation of circulating RNAs have been linked to several tumor types (e.g. breast cancer[237], lung cancer[238,239], ovarian cancer[240,241], pancreatic cancer[242,243], tongue squamous cell carcinoma[244], leukemia[245,246], colon[247,248], rhabdomyosarcoma[249], gastric[250], salivary cancer[251]). However, the functional role, if one exists, has yet to be elucidated.

The release of RNAs may be linked to cellular stresses. For example, following serum deprivation, cell secrete more miRNAs in an energy dependent process[234]. Therefore, not surprisingly, circulating RNAs are also associated with other diseases or states of cellular stresses. For example, detection of fetal nucleic acids circulating in the maternal plasma have the potential for non-invasive prenatal diagnosis, such as identification of chromosomal aneuploidies and single nucleotide mutations[252]. MicroRNAs are also increased in pregnancy[252] or other altered physiological conditions[253] such as liver injury[242].

The potential of Nucleic acids as cancer diagnostic markers is not limited to

RNA. Similar to observations with miRNA, soluble DNA can be found in the blood of healthy and diseased individuals[254]. The presence of circulating DNA has been described in a variety of cancers such as lung cancer[255,256], breast cancer[257], head and neck cancers[258], colon cancer[259], ovarian cancer[260] and prostate cancer[261]. Furthermore, mutations in circulating DNA are commonly observed in cancer patient[254,262,263]. For example mutated KRAS sequences can be found in the blood of patients with pancreatic cancer[254]. In prostate cancer, circulating DNA demonstrates loss of heterozygosity similar to tumor cells[257,262] and in melonoma patients mutant BRAF is often observed in plasma[263]. Mutant TP53 DNA is found in several cancers, such as stomach, colon and rectal cancers[264].

The amount of circulating DNA may provide insight into disease progression. Higher levels of DNA were found in the serum of patients with metastatic disease compared to patients with less advanced cancers[265]. Necrosis or apoptotic cell death may explain the high levels of circulating DNA in these patients[261]. Circulating DNA levels may also provide insight into a patient response to treatment. For example, radiation therapy led to decreased DNA levels in patient serum. The decrease in serum DNA was in general correlated with improved clinical outcomes?[266]. Circulating DNA is also present in diseased states such as hepatitis and rheumatoid arthritis[267]. However, there is still skepticism with regard to the utility of extracellular DNA as diagnostic tool[268].

The presence (correlation) of circulating nucleic acids with disease has long been established. However, only recently have the functional roles of circulating nucleic acids in cancer been identified. Intercellular transfer of mRNA, miRNA, and DNA serve important biological functions in tumor progression at all stages from primary tumor biology to interactions with the stroma, invasiveness, and metastasis.

Intercellular transport of nucleic acids has been linked to cancer progression in several tumor types, including glioblastoma, lung cancer[269] and heptocellular carcinoma[270]. In glioblastoma, microvesicles containing mRNA, miRNA, and proteins led to increased tumor proliferation and enhanced angiogenesis[200]. Furthermore,

serum from glioblastoma patients contained microvesicles with mutant mRNA sequences, reflecting mutations commonly found in gliomas[200]. Tumor promoting miRNA sequences can also be transported through gap junctions[271]. For example, miR-67 was transferred between glioma cells, regulating protein expression in neighboring tumor cells[271].

Intercellular communication of miRNAs regulate tumor biology in complex, sometimes, unpredictable ways. For example, transport of miRNAs have been shown to directly promote tumor growth by enhancing expression of proliferative pathways or indirectly by targeting tumor suppressors. For example, microvesicles released by gastric cancer cells contained members of the Let-7 family of microRNAs. These miRNAs are commonly regarded as tumor suppressors. Expulsion of the Let-7 family of miRNAsvia exosomes reduced expression of these miRNAs within tumor cells, indirectly promoting tumorigenesis within these cells[272]. In prostate cancer, genetic exchange between tumor cells has been shown increase the number of metastatic cells[273].

Intercellular communication of nucleic acids may potentially explain, at least in part, the genetic alterations commonly found in the tumor stroma. Genetic alterations found in tumor stromal cells may be critical regulators of cancer progression, and in some tumor types, such as mammary carcinoma, may even preceed frank tumor development[274]. Mechanisms leading to transformation of tumor stroma are likely multifactorial, with the transfer of genetic material playing a key role.

One of the early demonstrations of transfer of genetic material from tumor cells to stromal cells involved apoptotic bodies derived from rat fibrosarcoma cells. The apoptotic bodies secreted by these tumor cells contained DNA and were endocytosed by neighboring endothelial and fibroblast cells. Uptake of the vesicles resulted in transformation of these stromal cells in both *in vitro* and *in vivo* model systems[275,276]. Furthermore, stromal cells isolated from a fibrosarcoma murine *in vivo* model also demonstrated evidence of cellular transformation exhibiting immortalized cell growth when placed in culture. Horizontal transfer of mRNA containing

microvesicles also induced angiogenesis through a PI3K/AKT signaling mechanism[277]. Lastly, RNAs may themselves exert a pro-tumorigenic phenotype. For example, extracellular RNAs have been shown to induce VEGF release by binding directly to and activating the VEGFR receptor[278].

Intercellular transfer of nucleic acids not only regulates tumor endothelium, but also functions in immune system regulation. For example, tumor derived microvesicles can transfer mRNA and surface molecules to monocytes[279]. Exosomes released by lung cancer cells carry microRNAs (miR-16, miR-21, and miR-29a)[280]. These microvesicles bind to intracellular endosomal bound toll-like receptors (TLR8 in human and TLR7 in mice) in macrophages in the tumor microenvironment. These miRNA molecules act as paracrine agonists of TLRs; their release and subsequent binding to the TLRs causes a prometastatic inflammatory response, leading to upregulation of NFκB, TNFα, IL6, and CD69[280].

Inflammation is an important step in the formation of premetastatic niche[280]. Macrophages recruited to tumor cells in response to an elevation of inflammatory signals, play a significant role in tumor progression[123]. For example, microvesicles released by renal cancer stem cells that carry RNA that have been linked to angiogenesis and metastasis to lungs[281]. In these studies lung endothelial cells was found to overexpress markers of "pre-metastatic niche" such as MMP2, MMP9, PECAM, CD146, CD45, VEGFR1 and α6-integrin[281]. Studies show an extensive list of several miRNAs up- and down-regulated in pathological angiogenesis possibly secondary to microvesicle transport[281]. In pancreatic cancer, secretion of extracellular DNA in plasma and serum has been associated with invasiveness and metastasis[282]. This effect may result for up-reglation CXCL9 and other inflammatory chemokines in response to release of the extracellular DNA. Furthermore, treatment with DNAse I was shown to reduce invasive and metastatic characteristics[282].

Lastly, intercellular transfer of nucleic acids has been linked to tumor dormancy. In metastatic breast cancer, gap junctions enable intercellular transfer of miRNAs from bone marrow stromal cells to metastatic cells. This communication induces cell cycle arrest and quiescence in the tumor cells. However, these metas-

tases can reoccur years later with no history of primary tumor[283].

The mechanisms by which intercellular transfer of nucleic acids occurs is a subject of several research efforts. The role of exosomes in transport of nucleic acids has been well demonstrated[199]. However, our recent work has demonstrated that intercellular transfer of RNAs can also occur through membrane bridges and may be mechanism leading to pathological angiogenesis. Exosomes derived from tumors differ from exosomes released by normal cells; tumor exosomes are bigger and carry unique microRNAs and receptors[284]. Tumor derived vesicles also contain proteins which modulate miRNA activity[285]. These proteins are involved in assembly and breakdwon of RISC complexes that are believed to be important for miRNA loading into vesicles and may be important of miRNA target recognition in monocytes, HeLA cells, and dendritic cells[285]. Incorporation of miRNA in exosomes is believed to occur through a ceramide dependent pathway[145]

2.5.4 Comparative Review: Conclusions and implications

Functional microRNA and mRNA sequences can be transported from tumor cell to surrounding cellular populations, affecting each stage of the metastatic cascade from growth of the primary tumor to development of metastases. Transport of genetic material introduces a new role for cell-cell communication. Unlike the tradition concepts of intercellular communication which only elicit transient changes in cellular physiology, intercellular communication of genetic material may be a mechanism by which one cell can exert long term effects the surrounding environment.

Although cells are capable of transferring DNA, miRNA, mRNA molecules, transport of different classes of nucleic acids may not all be equivalent. For example, DNA transfer occurs almost exclusively through apoptotic bodies and unbound sequences. Contrast this to RNA transfer which appears to be tightly regulated, commonly packed in exosomes?. The distinction between how these two molecules are transported may provide insight into the physiological significance

of each. Release of DNA is unregulated and may be a result of cellular catastrophe occurring in cell death, and not a long term mechanism of cellular transformation. There may also be distinctions between RNA molecules involved in intercellular communication. MiRNAs may be better candidates for causing long-term changes in the recipient cell population than other cellular RNAs. MiRNAs have a long half-life and can exhibit profound effects on gene expression due to the ability of a single miRNA molecule to regulate multiple pathways.

MiRNAs are released from cells via three overall mechanisms passive leakage from cells, encapsulated within membrane vesicles, or bound to carrier proteins[214]. MicroRNAs delivered by each of these mechanisms may serve distinct physiological roles. For example, packaging of miRNAs within exosomes does not appear to occur randomly. The selectivity of exosomal miRNA packaging may be dictated by varying cellular responses to different stimuli[214].

Although, intercellular miRNA transport holds fascinating possibility, important questions remain to be addressed about its role *in vivo*. Currently, many studies have focussed only on phenomenological descriptions of RNA molecules in body fluids without any understanding of the role, if any, these nucleic acids are serving. There has been some promising work regarding understanding the role of intercellular communication of miRNA molecules in the microenvironemnt. Intercellular communication of miRNA may be a mechanism for local cell-cell communication and the function of these molecules may be found locally within the tumor microenvironment and not systemically within the body. MicroRNAs found freely in body fluids may just be by-products of cellular metabolism and only encapsulated miRNAs exhibit long-term effects on cell biology.

Communication of genetic material significantly alters traditional paradigms of cell-cell communication, introducing the possibility that intercellular communication can provide a mechanism of intercellular transformation. In other words, communication through membrane vesicles and membrane bridges may enable a single cell to genetically transform surrounding cellular populations. This prospect holds particular intrigue in the field of cancer biology where it has previously been

established that genetic mutations are present in both the tumor compartment as well as the stromal microenvironment[120–122]. Important similarities (i.e. mechanism of formation and transported cargo) and differences (i.e. biological function and specificity of transport) between these modes of communication exist, which presents opportunities for therapeutic interventions.

2.6 Conclusion: Why is cancer metastasis so difficult to treat?

Metastasis remains the number one cause of cancer deaths. Surgical interventions are ineffective for treating metastasis, and there are few alternative therapeutic options currently available. It is universally accepted that cancer, particularly advanced cancer, is a serious and sometimes life-threatening disease, however, its often unclear exactly how cancer leads to death. Approximately 50% of individuals with advanced cancer dies from complications due to invasion and compression of normal tissue by the malignant tumor. For example, invasion of tumor cells into a large blood vessel can result in hemorrhage. Alternatively, invading cells can compress healthy tissues, as is the case with cerebral metastases.

Organ dysfunction is also a common cause of death in cancer. Metastases can often lead to respiratory or hepatic failure or anuria from ureteric compression. Tumor cells can directly invade endocrine organs (e.g. adrenal and pituitary glands). Cancer may also compromises a patient's immune system either directly by suppressing bone marrow function or indirectly, through immune-suppressing chemotherapeutics. Patients with advance cancer often face severe recurrent infections commonly succumbing to disease such as pneumonia. Similarly, cancer patients experience cachexia (i.e. the progressive loss of body fat and lean body mass) and anorexia (i.e. reduced appetite), resulting in prolonged negative nitrogen balances. Paraneoplastic syndromes caused by secretion of humoral factors (e.g. hormones or cytokines) by tumor cells commonly lead to life-threatening

physiological disturbances. Finally, many cancer patients succumb to the adverse effects associated with treatment complications.

Most metastatic disease is not treated with surgery instead treatment typically involves a combination of chemotherapy, hormonal therapy, and radiation therapy. However, therapeutic options remain limited. The complexity of the metastatic cascade, coupled with the limited understanding of tumor pathogenesis, contributes to the lack of metastatic specific therapeutics. There is a diversity of mechanisms by which cancer kills; however, optimistically, there are also diverse untapped therapeutic opportunities in cancer metastasis treatment. For example, the development of more efficacious anti-angiogenesis therapies that specifically target the biology of tumor endothelium may function to prevent metastatic spread. Alternatively, metastasis suppressing therapies targeting genes or modes of cell-cell communication that promote metastasis may be effective. Treatment strategies targeting early metastases may focus on disrupting interactions with the endothelium that occur early in invasive spread, while therapies targeting late metastases may inhibit mechanisms controlling metastatic colonization. Nevertheless, despite the diversity of opportunities for intervention, one commonality among them all is that development of new therapies requires a better understanding of the mechanisms underlying cancer metastasis. To this end, the development of reliable, low-cost, and reproducible model systems of metastasis may be the first step in gaining the knowledge required for development of novel therapeutic approaches to address these unmet needs.

Chapter 3

Establishing an epithelial-endothelial co-culture model system

3.1 Introduction

As discussed extensively in **Chapter 2** the initiation, growth, and spread of a tumor is a complex and intricate process involving many separate, yet interconnected stages that together result in the multi-dimensional disease we refer to as cancer. Although each stage in cancer presents unique therapeutic opportunities, mechanisms underlying cancer metastasis remain the most underexplored, yet arguably, the most ripe for development of new therapeutic strategies. Beginning with formation of a primary tumor, the steps of metastatic invasion can be summarized into breakdown of the basement membrane and local tissue invasion, systemic dissemination through the vasculature, and finally seeding of a secondary tumor site. These steps are reviewed in **Figure 3-1**. Each of these stages presents an opportunity for intervention[12]. However, as described in **Chapter 2** our current insight into the mechanisms that control colonization are less well developed than our understanding of the initial stages of metastasis: formation of the primary tumor and interactions with the endothelium.

The majority of current drug therapies target the biology of the primary tumor.

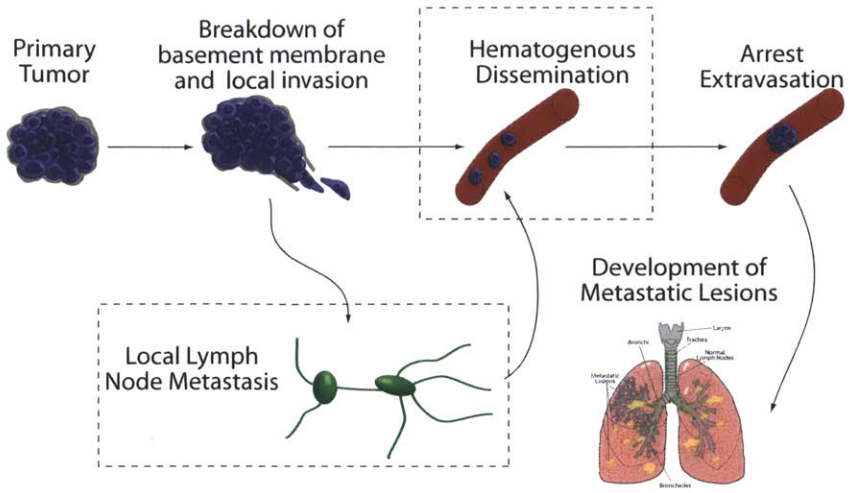

Figure 3-1: Overview of cancer progression. Cartoon schematic of the steps of metastatic progression. Interaction with the endothelium is prerequisite for the development of metastatic disease (dashed boxes). An invasive tumor cell can directly enter the systemic circulation in a process referred to as hematogenous dissemination. Alternatively, metastatic cells can invade neighboring lymph nodes. The lymphatic system in turn empties directly into the systemic circulation. Once in the systemic circulation a metastatic cell has access to surrounding tissues and organ systems.

However, arguably one of the most promising yet untapped opportunities for therapeutic intervention within the metastatic cascade is disruption of interactions between metastatic cells and the endothelium that are prerequisite for formation of secondary tumor sites **(Figure 3-1)**. Disruption of the events underlying these interactions may introduce new therapeutic strategies for both early and late stages of metastasis.

There is a diversity of biological mechanisms that enable metastatic cells to successfully interact with the endothelium **(Figure 3-2)**. These interactions can be classified in three categories: (1) biomechanical interactions, (2) chemokine mediated interactions, and (3) tumor-endothelial intercellular communication. One example of biomechanical interactions between tumor cells and the endothelium involves mechanisms underlying endothelial cell retraction. Metastatic breast epithelial cells change the biomechanical properties of the endothelium in order to promote metastatic invasion[120]. Previous studies have demonstrated a decrease

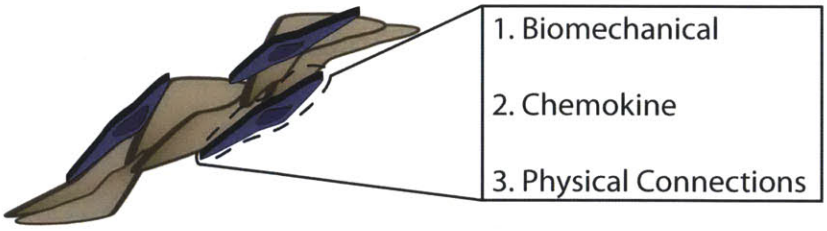

Figure 3-2: Epithelial-endothelial cell (EEC) interactions. There are diverse mechanisms of interaction between endothelial cells and epithelial cells, including biomechanical, chemokine, and physical connections.

in endothelial cell stiffness when the two cell types are co-cultured together. This decreased stiffness is believed to enhance epithelial cell transmigration[120].

The second mechanism of epithelial-endothelial cell (EEC) interactions utilizes chemokine signaling pathways. Secreted factors have long been established to be mediators of metastatic progression through recruitment of angiogenic vessels. For example, VEGF-A, the primary growth factor involved in pathological angiogenesis[286], has been extensively demonstrated to be a critical initiator of the "angiogenic switch". The development of a pathological angiogenic phenotype is required for invasive disease. In another example of chemokine-mediated EEC interactions, miR-126, a suppressor of metastatic cell invasion that inhibits endothelial cell recruitment, is regulated by the IGF signaling pathway[287]. Lastly, chemokine signaling can also regulate biomechanical interactions between metastatic cells and the endothelium. For example, secretion of IL-8 and Gro-β by endothelial cells increases transmigration of metastatic epithelial cells through the actions of the CXCR2 receptor[105].

The third, and final mechanism involves EEC interactions mediated by intercellular communication. In recent years, intercellular communication between cancer cells and the endothelium has gained research interest. For example, transfer of mitochondria from endothelial cells to cancer cells has been linked to development of chemoresistance in breast cancer[212]. In another example, microvesicles released by glioblastoma tumor cells were demonstrated to encourage a pro-angiogenic phenotype that enhances the invasive phenotype of the tumor[200].

The metastatic cascade is a chaotic, multi-system process underscoring the need to develop model systems that decouple the stages of metastasis into discrete segments. This chapter discusses the engineering of a 3D co-culture model system that combines epithelial cells and the endothelium in order to study EEC interactions essential for metastatic progression. It introduces evidence that demonstrates the utility of the model system in elucidating novel EEC interactions involving biomechanical, chemokine, and cell-cell communication mechanisms. This chapter illustrates the use of this model system to enable the discovery of important mediators of EEC interactions, providing a high-throughput platform for screening molecular targets and therapeutics. In addition, the model system enables the discovery of novel phenotypes by providing an observable platform that may be used as a first-order approach to shed light into the occult processes that underly metastasis.

3.1.1 Motivation

Due to the complexity of cancer pathology, one of the greatest obstacles in cancer research remains the development of physiologically relevant model systems that allow for accurate mimicry of tumor development *in vivo* and are also efficient, reproducible, and cost effective[18]. This need is even more pronounced for the development of model systems capturing elements of metastasis. *In vivo* model systems are the gold standard and an invaluable resource of biomedical research. However, these systems are complex, inefficient, and expensive. Cost-effective drug development ideally utilizes animal model systems predominately in the later stages of pre-clinical drug screening once a druggable target has been identified and candidate drugs have been optimized in more high-throughput platforms. Probing the role of pro- and anti-metastatic pathways utilizing only *in vivo* model systems often leads to confounding and uninterpretable results. For example, a protein target can be identified as a regulator of metastasis, but it's often difficult to isolate exactly where in the cascade this target is acting.

3.1.1.1 Metastatic cancer model systems

Much of the insight into cancer metastasis has been gained through the development of *in vivo* model systems or retrospective analysis of metastatic tissues removed from human patients[8,16]. Each of these approaches suffers from unique weaknesses. Xenograft studies in mice have become the mainstay of model systems used to probe the molecular players of metastasis[8,130,288]. Spontaneous assays are commonly used. These model systems require that the tumor be injected into a site, preferably the site of greatest physiological relevance (i.e. orthotopic location), and then to wait for the formation of metastatic lesions[130]. Such studies are often long, inconclusive, and difficult to quantify[8,130]. As a time saving alternative, tail vein injections are performed to directly inoculate metastatic cells into the systemic circulation, yielding higher numbers of metastatic lesions[8,130]. Although this method allows for reliable and consistent results in shorter times, it does not capture the pre-intravasation stages of metastasis[8]. Transgenic metastatic model systems have been created but these mouse models are expensive and time-consuming. The greatest limitation of all of the animal model systems is their inability to decouple the individual stages of metastasis.

Retrospective analyses of human metastatic tumors also suffer from a similar weakness due to the difficulty of determining *de novo* the site-specific role that the genetic anomaly may have served[16]. Appropriate *in vitro* model systems would create a platform for the direct observation and manipulation of cellular processes involved in metastasis that the other previous approaches would not allow **(Figure 3-3)**[16,17]. Current *in vitro* model systems for metastatic cancer generally only examine migratory or invasive phenotypes through chemoinvasion boyden chamber assays[288,289]. However, these approaches do not allow for the examination of cell-cell interactions, specifically epithelial-endothelial cell interactions that are pre-requisite for metastatic invasion.

The use of videomicroscopy studies have gained recent interest in the study of cancer metastasis and have elucidated roles of metastatic mediators previously

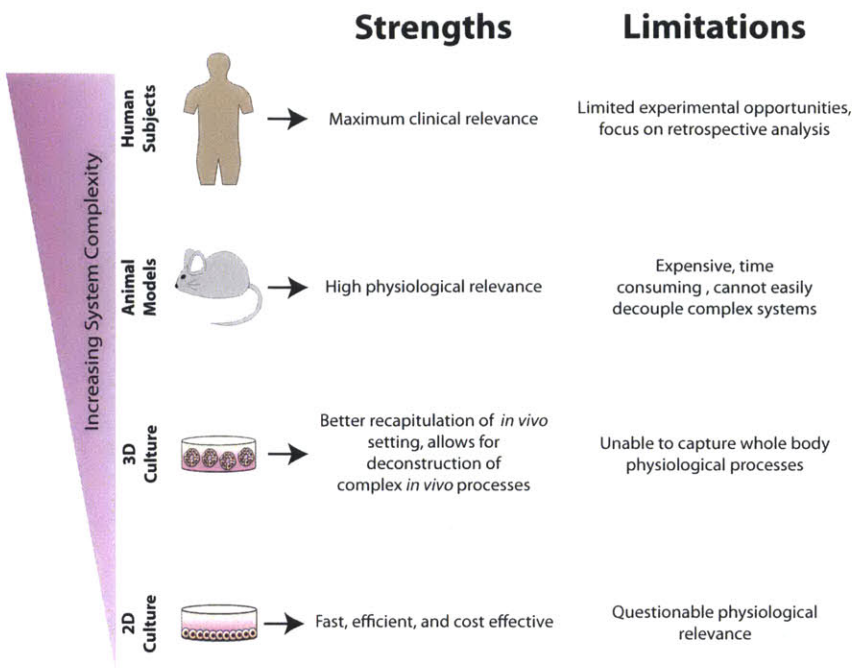

Figure 3-3: Model systems. Three-dimensional model systems may address unmet experimental needs not conveniently solved using current *in vivo* models and traditional 2D cultures.

unidentified[110]. For example, videomicroscopy has been used in elucidating the roles of MMPs in metastasis. Originally believed to function only in early stages of metastasis, videomicroscopy studies have shown that MMPs have many functions in metastasis including metastatic colonization[110].

Deconstruction of the critical events that lead to an invasive phenotype may enable the development of metastasis specific therapies. However, development of novel pharmacological interventions requires that individual metastasis promoting mechanisms and signaling pathways be identified and isolated to allow for experimental intervention. Without the capacity to probe the effects of drug therapies on a singular druggable target, development of metastasis preventing drugs will be stymied due to difficulty in determining how to effectively assess drug efficacy. For metastasis-specific therapeutics, this screening becomes increasingly cumbersome due to limitations of current model systems and the lack of reliable study endpoints and measurements of efficacy. Furthermore, since metastasis is a multi-cellular disease the ability to characterize cell-cell interactions is an essential

characteristic of an effective screening platform.

3.1.2 Three-dimensional model systems

The development of cancer is a complex process that involves genetic, mechanochemical, and environmental changes, which initially lead to amplification, and eventually to a complete disruption of normal physiological processes[290]. As a result of the complexity of this disease, a major obstacle in cancer research is the development of physiologically relevant platforms that allow for accurate mimicry of tumor development *in vivo*[18,291]. Appropriate model systems would serve two primary purposes: to allow for recapitulation of both the tissue architecture and physiological condition and to provide opportunities for experimental modifications to gain insight into development and pathogenesis[18,291].

Over the last several decades, the development of three-dimensional (3D) *in vitro* systems have been emphasized, based on the recognition that the 3D organization of a tumor underlies an important component of tumor progression[18,118,119,292–295]. A tumors interaction with neighboring cells and the extracellular matrix (ECM), response to growth factors, and activation of signaling pathways are dependent on the 3D context[16,18,290,291]. Monotypic 3D cell culture systems, established for a variety of cell types including liver, lung, skin, kidney and mammary epithelium[18] have been used to elucidate important pathways for cell adhesions such as integrins and focal adhesion kinase (FAK) pathways[17,296,297]; to probe oncogenic pathways such as PI3K and ERK/MAPK pathways[16,297,298]; and also as platforms for drug screening[298]. Organotypic co-cultures of various cell types have also been developed in order to capture cell-cell interactions, in addition to cell-ECM interactions[18].

3.1.2.1 Three-Dimensional Mammosphere Cultures

Much of the work on 3D *in vitro* culture systems has focused on the study of breast cancer pathogenesis. To establish these cultures, laminin-rich Matrigel® is used as

a substitute for ECM[18,297–299]. Physiologically, epithelial cells create a laminin-rich basement membrane, making Matrigel® an appropriate substitute for the ECM. However, it should be noted that Matrigel® is not a perfect representation of the ECM because it is composed of a poorly characterized mixture of ECM proteins derived from mouse sarcoma tumor cells[17,18,299,300].

3D mammosphere cultures have provided valuable insight into: (1) the development and maintenance of glandular lumens and disruption of these structures in cancer[18], (2) the role of cell-cell and cell-matrix adhesion pathways in mammary epithelial tumorigenesis[296,297], (3) regulation of mammary polarity and its disruption in cancer, and (4) the importance of adhesion forces in maintaining tissue architecture and promoting pathogenesis[17,296,297]. Three-dimensional model systems were used to demonstrate that cellular behavior of mammary epithelial cells is dependent on both the genetic and architectural phenotype. Furthermore, in breast cancer it has been shown that disruption of normal mammosphere architecture leads to the development of an oncogenic phenotype independent of the existence of genetic anomalies[297].

Current 3D mammosphere cultures provide a platform to study the development of normal and tumorigenic mammary structures, however they do not capture the interactions between tumor cells and the angiogenic component, an essential step in tumor progression[106]. The ability to closely examine epithelial cells interactions with endothelial vessels would provide an opportunity to elucidate mechanisms for metastatic cell invasion into the vasculature[106]. An understanding of this process may result in generation of possible metastasis specific therapies[106].

3.2 Development of an epithelial-endothelial co-culture model system

The development of a model system that can mimic features of EEC interactions in metastasis could potentially provide a valuable tool for identification of novel

druggable targets and for high-throughput screening. An appropriate model system must exhibit the following elements:

1. Decouple EEC interactions from other stages within the metastatic cascade
2. Allow for single point experimental interventions to probe the effects of individual molecular pathways
3. Be highly modular, enabling quick modifications in order to create model systems that range from simple to complex
4. Allow for multiple cell types to interact in a physiological and architecturally appropriate context
5. Reproducible
6. High-throughput
7. Quantifiable

To tackle this challenge, based on the criteria outlined above, we have engineered a 3D co-culture system that combines epithelial cells and the endothelium to study EEC interactions that are essential for metastatic progression. In engineering our model, we hypothesized that interactions between metastatic epithelial cells and the endothelium would be distinct from interactions of non-metastatic epithelial cells with the endothelium. In addition, a model system allowing for elucidation of these differences will aid in the the discovery of novel anti-metastasis targets. The power of our model system is the ability to isolate a single stage within the metastatic cascade: interactions between metastatic cells and the endothelium that may precede intravastion / extravasation within vessels.

3.2.1 Experimental design

We have established an organotypic co-culture model system combining endothelial cells with epithelial cells of varying grades of tumorigenicity, ranging from normal primary cells to highly metastatic cell populations. **Figure 3-4** is a schematic

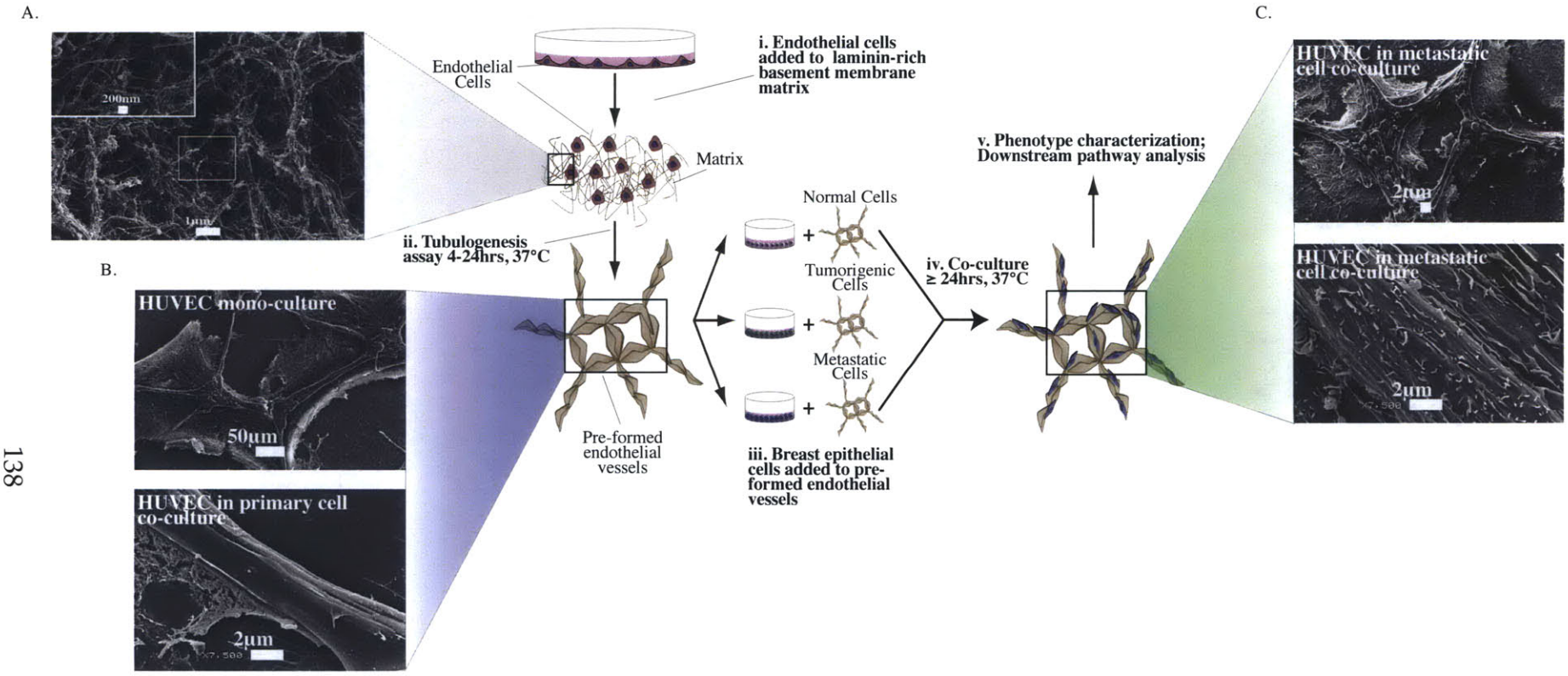

Figure 3-4: Schematic overview of epithelial-endothelial co-culture model system experimental design. Endothelial cells are added to a laminin-rich basement membrane matrix and undergo spontaneous tubulogenesis. Epithelial Cells are added to the endothelial vessels and the cells are co-cultured for $\geq 24hrs$. The phenotypes are characterized using microscopy and various molecular biology techniques. Differences between co-cultures with primary epithelial cells, tumorigenic non-metastatic epithelial cells, and metastatic epithelial cells are assessed. (A) SEM micrographs illustrate the matrix fibers, which form the scaffold for the three-dimensional structures. (B/C) Co-cultures with metastatic cells affect endothelial vessels leading to vessel widening and lengthening. (C) Projections can be seen on the cell surface of endothelial cells in metastatic co-cultures, (B) while the endothelial cell surface is smooth in co-cultures with primary epithelial cells. The projections may provide anchorage points for metastatic cell attachment to the endothelium.

overview of the co-culture model system experimental design. The model system was established using primary human umbilical vein endothelium cells (HUVEC) obtained from ATCC. To further validate observed phenotypes, selected cell populations were also co-cultured with primary human dermal microvascular blood and lymph endothelial cells **(Section 3.5.1)**. These cells are true untransformed primary cell populations isolated from fresh human plasma of a single patient. Analyzing co-culture phenotypes with primary endothelial cell populations further emphasizes the physiological relevance of the observed phenotypes.

To begin a co-culture, endothelial cells were plated in a laminin-rich basement membrane matrix (1:1 PBS : Matrigel®) for 4-24hrs, wherein the cells spontaneously formed vessel-like structures **(Figure 3-4)**. Growth factor enriched Matrigel® was used for all experiments unless otherwise noted. Following completion of tubulogenesis, epithelial cells are added to the culture and the cells are incubated together for 24hrs unless otherwise stated. Epithelial cells are labeled with carboxyfluorescein succinimidyl ester (CFSE) cell-impermeable dye to distinguish the two cell populations. CFSE is a widely used tracer that is retained within cells for long periods of time without leaching through the plasma membrane.

Following an incubation period, the cultures were analyzed with a variety of microscopy and cell biology techniques. To summarize, light microscopy was used to characterize overall morphology and phenotype, angiogenic parameters, and the degree of epithelial-endothelial cell interaction. In this analysis, epithelial-endothelial cell interaction is defined as physical alignment of the epithelial cells on the vessel surface. Quantification of these parameters is described in great detail in **Section 3.4.3**. Scanning electron microscopy (SEM) was used for closer examination of the culture phenotype and to detect evidence of metastatic invasion. The model system was also used to assess molecular mediators of adhesion and cell-cell interactions. The role of these pathways was probed using RNA interference (RNAi), neutralizing antibodies, or pharmacological inhibitors. Finally, the model system was used as a screening platform to test anti-angiogenic and anti-tumorigenic small molecule inhibitors to assess the drug effects on disruption of

EEC interactions. A detailed protocol of the co-culture study design can be found in **Appendix B**.

Figure 3-4A is a high-magnification SEM micrograph that illustrates the laminin-rich basement membrane matrix fibers in which the cells are embedded. The matrix provides the scaffold on which the cells can establish a three-dimensional conformation. In co-culture, the metastatic MDA-MB-231 breast epithelial cells can be seen aligning along the endothelial vessels **(Figure 3-4C)**. The vessel structures in co-culture appear visibly distinct compared to HUVEC monoculture **(Figure 3-4B)**, exhibiting visible widening, increased number of branches, and larger nodes. Interestingly, in high magnification micrographs of metastatic cell co-cultures, small projections can be seen on the surface of the endothelium **(Figure 3-4C)**, contrasting the smooth appearance of the endothelial cells in co-culture with primary epithelial cells **(Figure 3-4B)** in which there is little interaction between cell types. One can speculate as to how these projections form and the role they may play in mediating interactions between cell types. On possibility is that these structures form in response to soluble factors secreted by metastatic cells that are not present in HUVEC monocultures or co-cultures with primary epithelial cells. The projections may serve a biomechanical function providing points of anchorage for the metastatic cells to better adhere to the endothelial vessels. One could speculate on the invasive advantage that inducing these structures in the endothelium may provide the metastatic cells as they attach to the vessels. **Figure 3-5** further illustrates differences in endothelial vessels in primary, tumorigenic non-metastatic, and metastatic epithelial cell co-cultures.

3.2.2 Matrix

The selection of an appropriate matrix is a critical element for establishing 3D model systems. There are a variety of natural and synthetic matrices such as collagen, fibrin, Matrigel®, and hydrogels that have been used to engineer three-dimensional model systems[301]. We selected Matrigel®, a commercially available

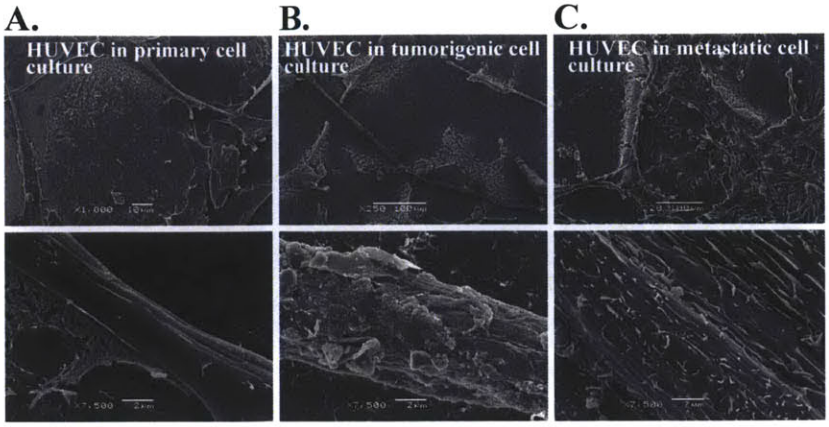

Figure 3-5: Endothelial cells appear distinct in co-cultures with epithelial cells exhibiting increased tumorigenicity. SEM micrographs show low- and high-magnification views of endothelial cells in co-culture with primary epithelial cells, tumorigenic non-metastatic epithelial cells, and metastatic epithelial cells. Endothelial cell morphology appears distinct in each culture model. In a metastatic cell co-culture platform the endothelium is significantly wider with small projections on the cell surface. Contrast this with the smooth narrow vessels seen in the primary cell co-culture platform.

tumor-derived laminin-rich basement membrane matrix from mouse sarcoma tumor cells as the appropriate basement membrane to establish the co-culture system **(Figure 3-6)**. Although, synthetic matrices are highly tunable allowing for manipulation of various matrix properties such as stiffness, pore sizes, and proteoglycan composition, Matrigel® remains the best characterized extracellular matrix and is well established in the use of mammosphere cultures[18,297–299]. Therefore in extending this work to include the endothelial cell compartment we decide to continue with the same matrix. Furthermore, cells *in vivo* normally produce a laminin-rich basement membrane, making Matrigel® a suitable substitute for the naturally produced ECM. However, it should be noted that Matrigel® is not a perfect representation of the ECM because it is composed of a poorly characterized mixture of ECM proteins[17,18,299,300]. Furthermore, Matrigel® often leads to batch-to-batch variations in cellular phenotypes that commonly lead to inconsistencies between experiments, potentially affecting the fidelity and reproducibility of the cultures.

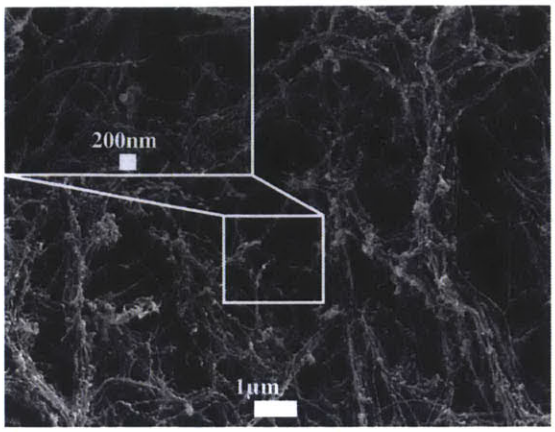

Figure 3-6: Laminin rich basement membrane matrix. SEM micrograph image illustrating matrix fibers. Cells use this scaffold to adopt 3D morphologies that mimic tissue structures *in vivo*.

The variabilities in batches of Matrigel® may alter vessel structures, which may in turn affect epithelial-endothelial interactions. However, this limitation can be minimized by maintaining consistent lot numbers and by increasing the number of experimental replicates. In future extensions of this work there is a possibility of extending the model system into alternative matrices that are better characterized to increase experimental reproducibility.

3.2.3 3D model system provide a more physiologically relevant platform to study cancer

By recapitulating the cells native orientation *in vivo*, 3D cultures are a better representation of a cells physiological responses, including (1) cell-cell and (2) cell-ECM interactions and (3) communication with, and in response to, the external environment. In a 3D matrix, the metastatic breast epithelial cells organize into mammary body structures, resulting in remarkably different cell-cell interactions than the

traditional 2D planar cultures. **Figure 3-7** illustrates the architectural differences present between 2D and 3D monoculture systems. In 2D both non-malignant and malignant breast epithelial cells adopt similar morphologies. However, in 3D the architectural differences between 2D and 3D cultures becomes evident[299]. Non-malignant epithelial cells adopt an organized morphology with a distinct central lumen, apical-basal polarity, cell-cell tight junctions, and an intact basement membrane. In 3D cultures, malignant epithelial cells lose this organized phenotype and adopt a disorganized and erratic morphology **(Figure 3-7)**[17]. Furthermore, in addition to differences in cellular architecture, culturing cells in 3D leads to changes in expression patterns of important oncogenic signaling pathways, such as the PI3K and ERK/MAPK pathways, that better correspond to expression levels present *in vivo*[16]. **Figure 3-7** illustrates the up-regulation of p-AKT(S473), p-ERK1/2 (T202/Y204), and p-FAK(Y925) expression in MDA-MB-231 cells both in 2D (inset) and 3D platforms. There is significant activation of these oncogenic pathways in the 3D culture that is not observed when the cells are plated in 2D. The activation of these oncogenic pathways is likely due to the enhanced cell-cell interactions that are present in 3D environments, but absent in 2D cultures.

Similarly, in epithelial-endothelial co-cultures, there are dramatic changes in both cellular architecture and in expression of oncogenic pathways. As an illustrative example, **Figure 3-8** provides representative images that highlight the architectural and phenotypic differences present in 2D and 3D cultures. The upper panels show metastatic breast cancer cells MDA-MD-231 monocultures in 2D and 3D platforms, while the lower panels illustrate MDA-MB-231 + Human Umbilical Vein Endothelial Cell (HUVEC) co-cultures also in 2D and 3D platforms.

Three-dimensional organotypic culture systems combining several cell types provide greater advantages compared to traditional systems. They can be used to capture cell-cell interactions that do not exist in 2D culture platforms **(Figure 3-8)**. Instead of forming the expected mammary structures, in the 3D co-culture platform the metastatic MDA-MB-231 breast cancer cells (EPI) interact directly with the endothelium (ENDO), elongating and aligning along the endothelial vessels

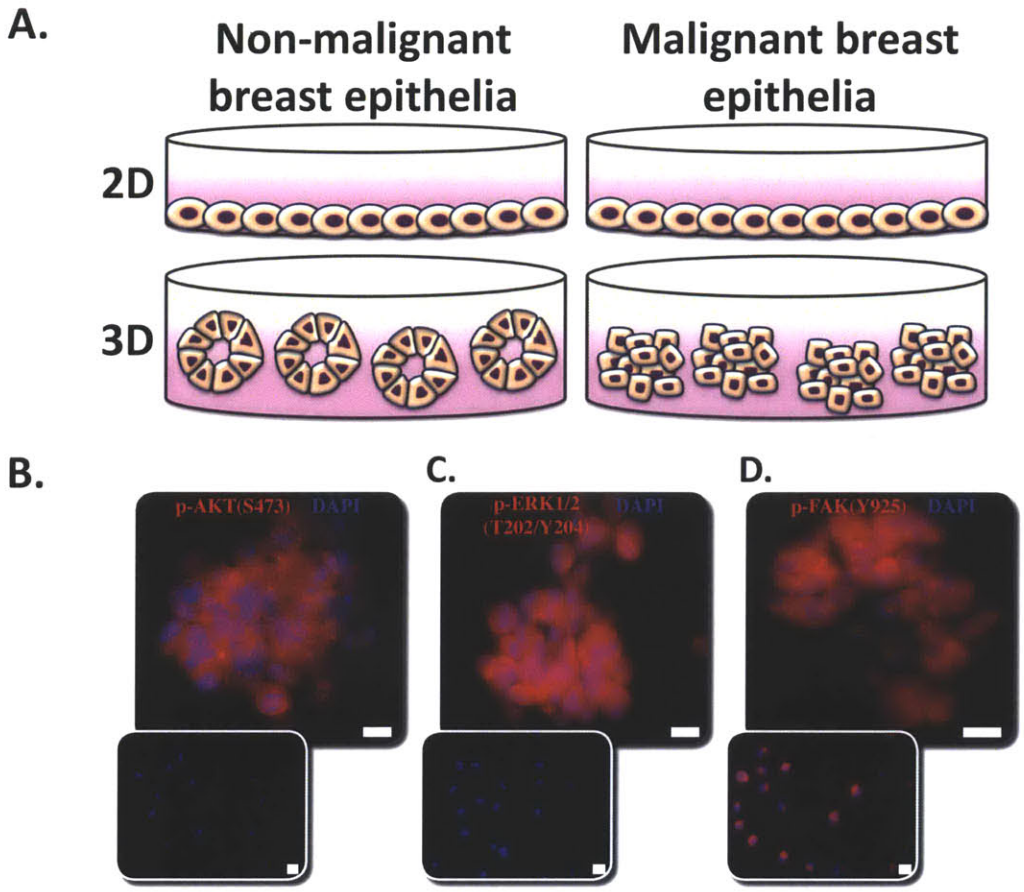

Figure 3-7: 3D model systems are physiologically relevant platforms for studying cancer. (A) When seeded in a basement membrane matrix, breast epithelial cells form mammospheres that significantly differ from the planar architecture present in 2D. In traditional 2D cultures there are limited differences in morphology between non-malignant and malignant breast epithelial cells. However, in 3D malignant cells adopt an architecture that is very different from the phenotype of non-malignant cells. Primary epithelial cells form organized spheroid structures with characteristics resembling mammary acini *in vivo*. Contrast this phenotype with the disorganized mammosphere structures formed by malignant cells, which lack a central lumen and organized morphology consistent with normal cellular morphology. (B) The difference between 2D and 3D cultures also extends to expression of oncogenic pathways. There is up-regulation of p-AKT (S473), p-ERK1/2 (T202/Y204), and p-FAK (Y925) expression in 3D cultures compared to 2D cultures (inset). Cells were immunostained with the aformentioned antibodies (Red) and counterstained with DAPI (Blue).

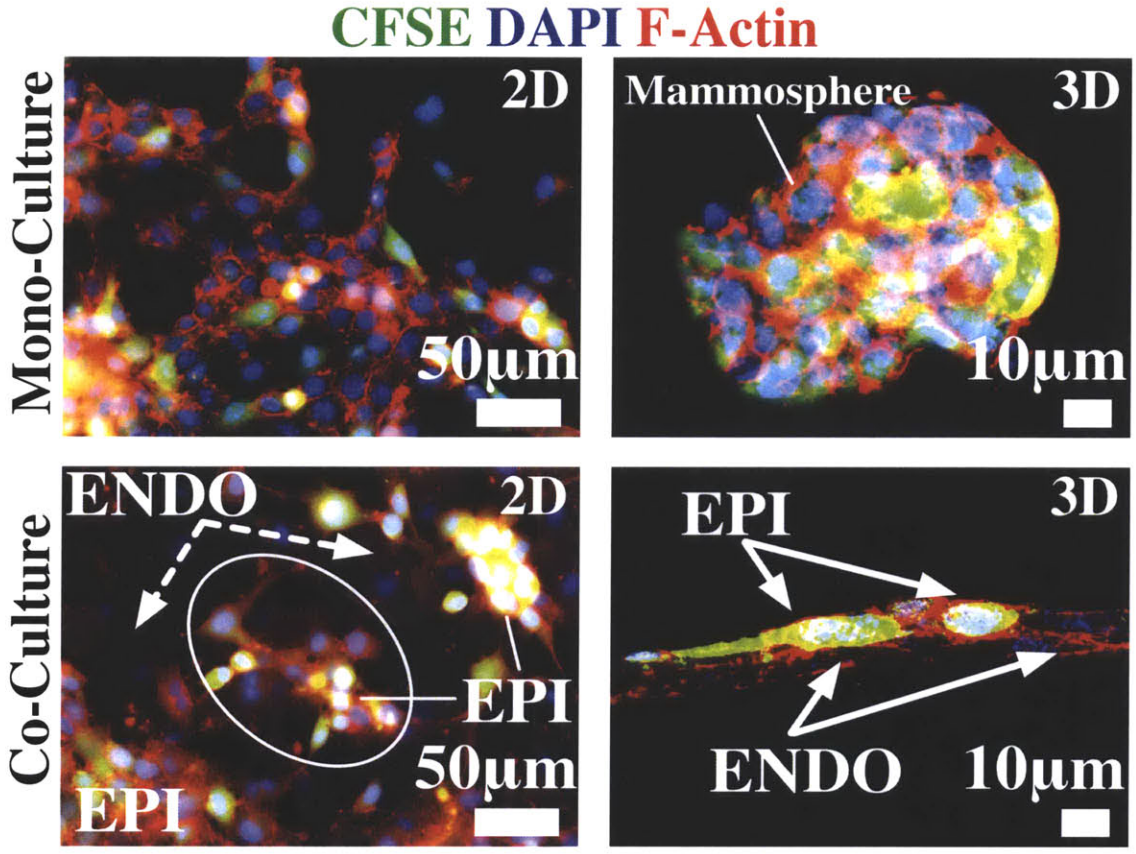

Figure 3-8: 3D model systems capture cell-cell interactions in tumorigenesis. Analogous to results seen with breast epithelial cell monocultures, our data highlights the advantages of 3D organotypic co-cultures to study epithelial-endothelial (ENDO/EPI) cell-cell interactions. The 2D co-culture is characterized by a segregation phenotype where the epithelial cells sit upon a bed of endothelial cells (dashed arrow) clustered in epithelial islands (circle). However, in 3D co-cultures there is a high degree of interaction between the cell types (solid arrow). All cultures were incubated for 24-hours followed by immunostaining with rhodamine phalloidin (Red) and counterstaining with DAPI (Blue).

(solid arrow). There are limited numbers of mammary spheroids formed in these cultures indicating preferential interactions of the MDA-MB-231 cells with the endothelium compared to other epithelial cells. Compare this phenotype with the 2D platform. In a 2D culture, the cells adopt no particular organizational structure. Furthermore, in contrast to the intimate interaction formed in 3D cultures, in the 2D cultures we observe segregation of cell types, characterized by the formation of epithelial islands (circle) that sit atop a platform of endothelial cells (dashed arrow) **(Figure 3-8)**.

Three-dimensional co-cultures also reveal alterations in expression of important signaling pathways. Similar to results seen in monocultures, in 3D co-cultures there was notable up-regulation of oncogenic pathways. This up-regulation seemed to be strongly associated with areas of interaction between epithelial cells and the endothelium. **Figure 3-9** illustrates immunostaining of MDA-MB-231 and HUVEC co-cultures with p-AKT (S473), p-ERK1/2 (T202/Y204), and p-FAK (Y925). In areas of EEC interactions, there is enhanced FAK phosphorylation, suggesting that the FAK-Integrin signaling axis is critical for epithelial-endothelial cell interactions **(Figure 3-9C, solid arrows)**. Compare this to phosphorylated FAK signaling in areas with minimal EEC interactions **(Figure 3-9C, dotted arrows)**. In these areas, there is lower expression of FAK signaling.

Upregulation of phosphorylated FAK in turn activates downstream targets of the PI3K and MAPK pathways **(Figure 3-9)**. Similar to p-FAK expression, p-AKT (S473) and p-ERK1/2 (T202/Y204) expression is also enhanced in areas of high EEC interactions **(Figure 3-9 A and B, solid arrows)** compared with areas of minimal interaction **(Figure 3-9 A and B, dotted arrows)**. Surprisingly, AKT activation seems to occur mostly in the endothelial cells **(Figure 3-9A)**, while ERK activation occurs predominantly in the tumor compartment **(Figure 3-9B)**. The differential activation of these pathways in the tumor and endothelial compartments may suggest a possible therapeutic strategy to target the endothelial cell compartment with a PI3K inhibitor and the tumor compartment with a MAPK inhibitor.

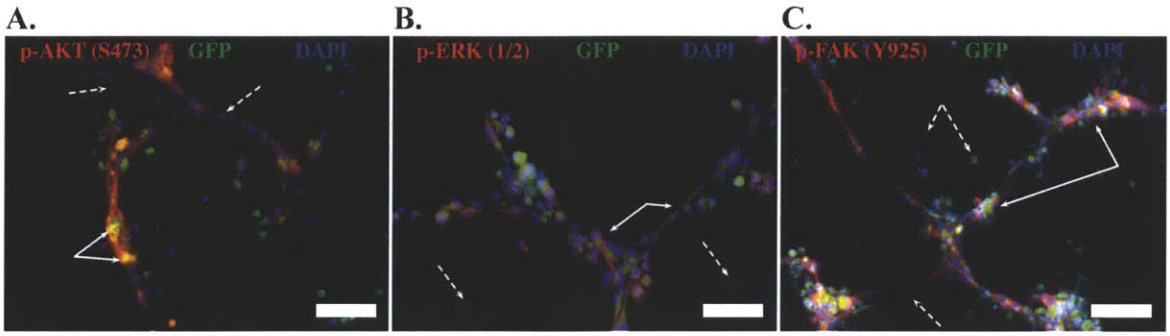

Figure 3-9: Activation of oncogenic pathways in co-culture model system. Co-culture model systems with GFP labeled metastatic breast epithelial cells (green) were immunostained with (A) p-AKT (S473), (B) p-ERK1/2 (T202/Y204), and (C) p-FAK (Y925) (Red) and counterstained with DAPI to identify nuclei. Activation was observed in areas of epithelial-endothelial interactions (solid arrows) versus areas with limited cell-cell interactions (dotted arrows). This data highlights the unique features that can be captured in model systems, combining multiple cell types that are not present when either cell type is cultured alone. A platform modeling cell-cell interactions is particularly important for complex, multicellular disease pathways such as metastasis.

3.3 The effect of the endothelium on oncogenic phenotypes

There are multiple mechanisms by which cells interact in the co-culture system. These mechanisms can be categorized as biomechanical, chemokine, and communication interactions. Each of these mechanisms may individually or collectively enhance metastatic capacity of the cells. Indeed, previous work has established that the endothelium increases the invasiveness of metastatic breast epithelial cells by enhancing transmigration through an endothelial layer[105]. To better understand the complex dynamics that occur within the co-cultures, we attempted to decouple these mechanisms. We first began by studying the role of chemokine signaling on EEC interactions that may regulate tumorigenicity and invasiveness of metastatic cells in co-culture. Specifically, we probed the effects of endothelial cell soluble factors on cellular proliferation **(Section 3.3.1)** and migration **(Section 3.3.2)** of MDA-MB-231 cells. The role of intercellular communication in mediating EEC interactions is extensively discussed in **Sections 4, 5, and 6**.

3.3.1 Endothelial cells increase metastatic cell proliferation

To assess cellular proliferation, we measured the expression of Ki67 in the MDA-MB-231 cells in co-cultures versus monocultures. Ki67 is a nuclear protein that is commonly used as a marker of cellular proliferation. It is present during the entire cell cycle, but is absent in non-dividing cells. **Figure 3-10** summarizes the results from this experiment. GFP labeled MDA-MB-231 cells were co-cultured with unlabeled endothelial tubes. The cultures were fixed and immunostained with Ki67 antibody 24hrs post co-culture. Compared to monoculture, in co-culture there is an increase in Ki67 staining in MDA-MB-231 cells **(Figure 3-10A)**. The increase in Ki67 in co-cultured MDA-MB-231 cells was confirmed via flow cytometry. In the flow cytometry experiments, GFP labeled MDA-MB-231 cells were added to DiL-Ac-LDL labeled endothelial cells. After 24 hours, cultures were stained with PECAM-1 antibody to identify endothelial cells. The dual-labeling protocol allows for easy separation of the two cell populations. The details of this analysis are extensively described in **Section 4.3.1**. The pink outline highlights the MDA-MB-231 population.

Histogram measurements of the MDA-MB-231 population shows a shift of the Ki67 peak in co-cultured endothelial cells signifying increased Ki67 expression compared to cells in monoculture (separate). Interestingly, at the 24hr time point there seem to be minimal changes in Ki67 expression in the endothelial cell population. However, at later time points, endothelial cells show an increase in proliferation markers in co-cultured in comparison to monocultured cells. Therefore, it is likely that 24 hours is too soon to observe the proliferative effect in the co-cultured endothelial cells. Co-cultured epithelial cells have higher expression of Ki67 compared to cells in monoculture. However, it is unclear as to what mechanisms lead to this increase in cellular proliferation.

We hypothesized that soluble factors secreted by the endothelium may contribute to the enhanced proliferation. To test our hypothesis, we performed a cell viability assay using an MTS (3-(4,5-dimethylthiazol-2-yl)-5-(3-carboxymethoxyphenyl)-

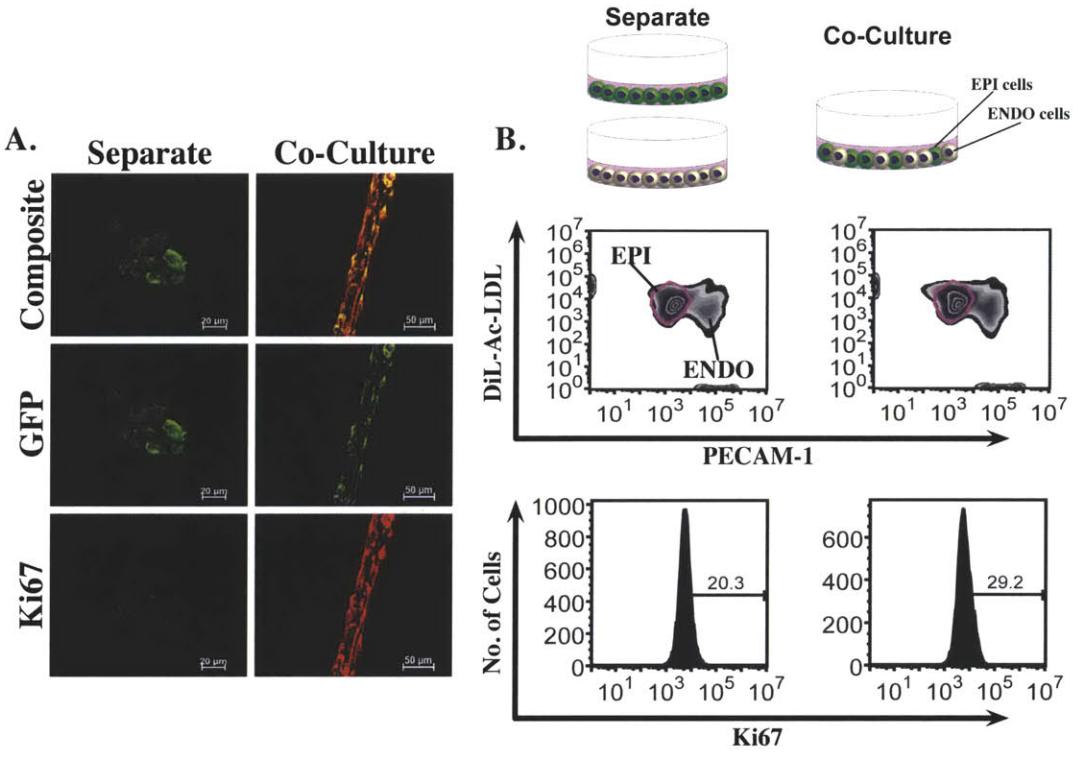

Figure 3-10: Co-cultured MDA-MB-231 cells show increased Ki67 expression. (A) Immunostaining with a Ki67 antibody in GFP+ve MDA-MB-231 epithelial cell and HUVEC endothelial cell co-culture shows enhancement of Ki67 expression in co-cultured epithelial cells. (B) This phenotype is confirmed via flow cytometry. In these studies, GFP+ve MDA-MB-231 cells are added to DiL-Ac-LDL labeled endothelial cells. After 24hrs, the cultures are fixed and stained with PECAM-1 and Ki67. PECAM-1 is used to stain the endothelial cells to allow for sufficient separation of the two populations. The MDA-MB-231 cells are gated (pink) and the Ki67 expression is measured. Co-cultured MDA-MB-231 cells have higher expression of Ki67 than cells in separate monocultures. The increased Ki67 expression may be a response to soluble factors released by the endothelium.

2-(4-sulfophenyl)-2H-tetrazolium) reagent on MDA-MB-231 cells exposed to conditioned media. This assay is described in detail in **Section 4.4.1**.

To summarize our protocol, conditioned media was collected after four days of incubation with HUVEC endothelial cells as well as other tumor stromal cells including mesenchymal stem cells (MSCs), fibroblasts, smooth muscle cells (SMCs), and embryonic stem cells (ESCs). Although ESCs are not found in the tumor environment, they may potentially provide a surrogate for poorly differentiated cells, commonly found in the tumor microenvironment, such as cancer stem cells. Media was collected from cells at 65-90% confluency to ensure viability and proliferative activity of the stromal cells. MDA-MB-231 cells were incubated in non-conditioned and conditioned media from each cell type. For both groups media optimized for each cell type was used. For exact media preparation refer to materials and methods in **(Appendix B)**. The study was performed in this manner to ensure that stromal cells received the appropriate media in order to minimize cellular stress that could potentially alter the composition of released soluble factors.

Three distinct treatment protocols were used in this study summarized in **Figure 3-11**. In the first protocol, labeled *conditioning*, the cells were pre-treated for 4 days in conditioned media and then incubated in non-conditioned control DMEM for 36hrs, 60hrs, 84hrs, and 5days. This group was included to observe the long-term effects of the secreted factors persisting after removal of the stimulus. In the second treatment strategy, referred to as *no pre-conditioning*, the cells were added to conditioned media without a 4 day pre-conditioning. This group allows for direct probing of immediate proliferative responses of cells to stromal growth factors. Similar to the *conditioning*, the cells were incubated for 36hrs, 60hrs, 84hrs, and 5days. In the final condition, the cells were pre-treated for 4 days and continued in conditioned media for the aforementioned time points. This group was referred to as *conditioned media throughout*, which allowed us to assess the effect of continued exposure to the secreted factors, analogous to continued exposure in the tumor microenvironment. Each data point was normalized to the DMEM non-conditioned control.

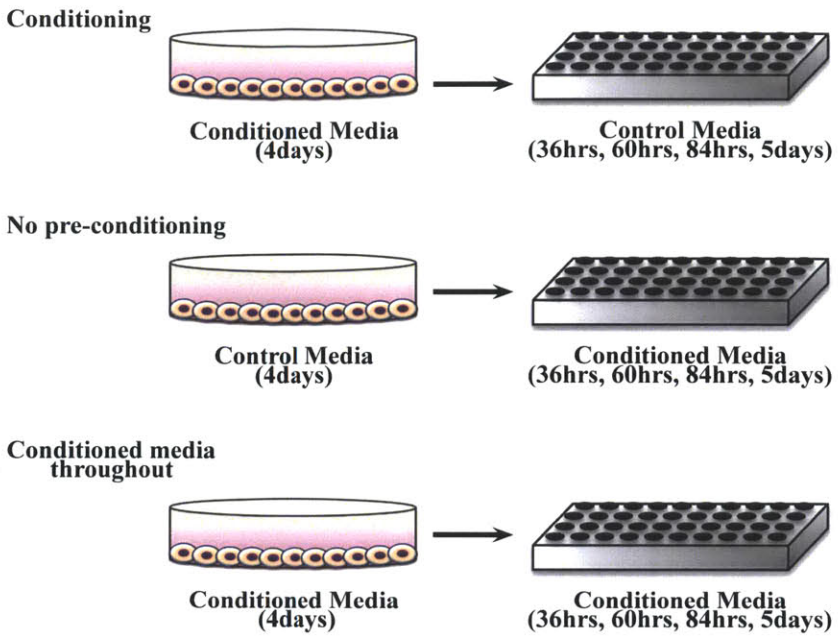

Figure 3-11: Schematic overview of proliferation assay protocol. Three treatment protocols were used to assess the role of soluble factors on proliferation of MDA-MB-231 and MCF-7 cells.

Figure 3-12A shows images of the MDA-MB-231 cells in conditioned media±ve groups, while **Figure 3-12B-D** summarizes the results of this analysis. Conditioned media from HUVEC endothelial cells increased cellular proliferation in all three treatment strategies. However, the proliferative response diminished after continued exposure to conditioned media, illustrated by only a modest increase in cellular proliferation in the conditioned media throughout treatment protocol **(Figure 3-12D)**. The decreased robustness of the response may be due to receptor down-regulation secondary to continuous receptor stimulation. Changes in receptor expression after continuous exposure to growth factors is commonly observed in many growth factor signaling pathways[302].

There was no statistically significant proliferative advantage conferred by conditioned media from fibroblast, MSCs, or SMCs. Indeed, conditioned media from these cell types actually inhibited growth of MDA-MB-231 cells. The only exception was the 60hr time point of the *no pre-conditioning* group **(Figure 3-12C)**. At this time point, conditioned media from fibroblast cells showed an increase in prolif-

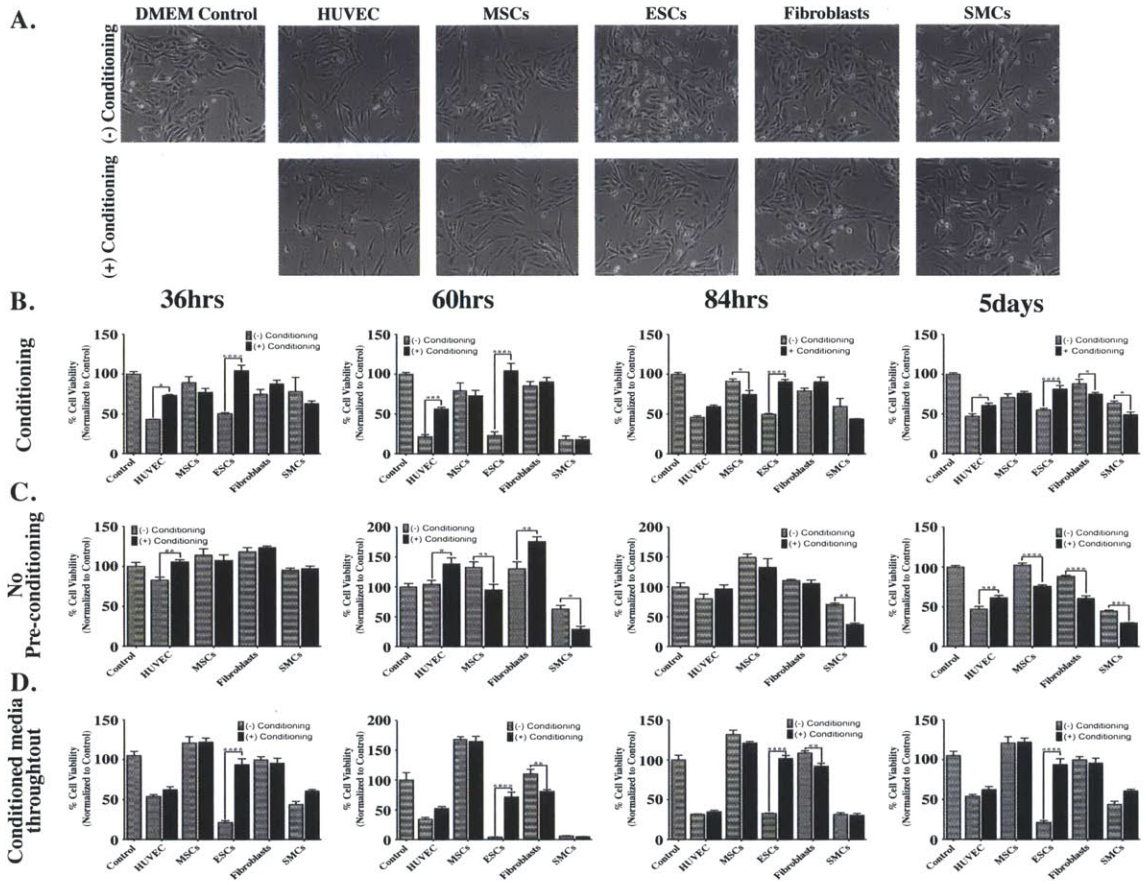

Figure 3-12: Effects of secreted growth factors on proliferation of MDA-MB-231 cells. (A) Bright field image showing MDA-MB-231 cells in conditioned+ve and conditioned-ve from each cell type. The effects of secreted growth factors isolated from HUVEC endothelial cells, mesenchymal stem cells, embryonic stem cells, fibroblasts, and smooth muscle cells were measured using a commercially available viability assay. The following three protocols were used: (B) *conditioning*: metastatic cells are pre-conditioned for 4 days and then transferred to DMEM; (C) *no pre-conditioning*: metastatic cells are not pre-conditioned and then transferred to conditioned media; (D) *conditioned media throughout*: metastatic cells are incubatd in conditioned media for 4 days and remain in conditioned media for the duration of the study. Measurements were taken at 36hrs, 60hrs, 84hrs, and 5days. Conditioned media collected from endothelial cells, and no other tumor stromal cells increased proliferation of MDA-MB-231 breast epithelial cells.

eration, the opposite effect from what was observed in every other measurement. However, this effect was only transient. At 84 hours there was no difference between conditioned±ve groups and even a reversal of the phenotype to an inhibition of cellular proliferation was observed by 5 days. The reversal of the phenotype may again be due to down-regulation of growth factor receptors on the surface of the cells after continued stimulation.

Interestingly, the only other cell type that increased proliferation of the MDA-MB-231 cells were embryonic stem cells. ESCs create a growth factor rich environment that is needed in development of tumors. The metastatic cells robustly responded to this stimulus. It is interesting to speculate if there are any similarities in the composition of growth factors secreted by ESCs and cancer stem cells. Cancer stem cells have been shown to enhance tumorigenic qualities of cancer cells.

It should be noted that there were some inherent toxicities associated with growing the MDA-MB-231 cells in stromal cell media. For example, non-conditioned media from some groups resulted in either increased or decreased proliferation compared to the DMEM control. MDA-MB-231 cells are generally grown in DMEM. However, each group was compared to a matched control, keeping the media constant, eliminating this consideration from analysis. It should also be noted that the stromal cells used here are normal cells, not tumor stromal cells. It is well established that stromal cells in tumors are transformed[274]; therefore the growth factors secreted by these cells are likely to be different from the growth factors secreted by normal cells. Nevertheless, secreted factors from endothelial cells did indeed enhance proliferation of MDA-MB-231 cells, while secreted factors from other cell types did not have a similar effect, thus highlighting the unique nature of epithelial-endothelial interactions.

In order to understand if the observed effects on cellular proliferation were unique to metastatic breast epithelial cells, we performed a similar study with MCF-7 breast epithelial cell lines. This data is summarized in **Figure 3-13**. The MCF-7 cell line is a tumorigenic non-metastatic breast epithelial cell line that is estrogen receptor positive, progesterone receptor positive, and HER2/neu nega-

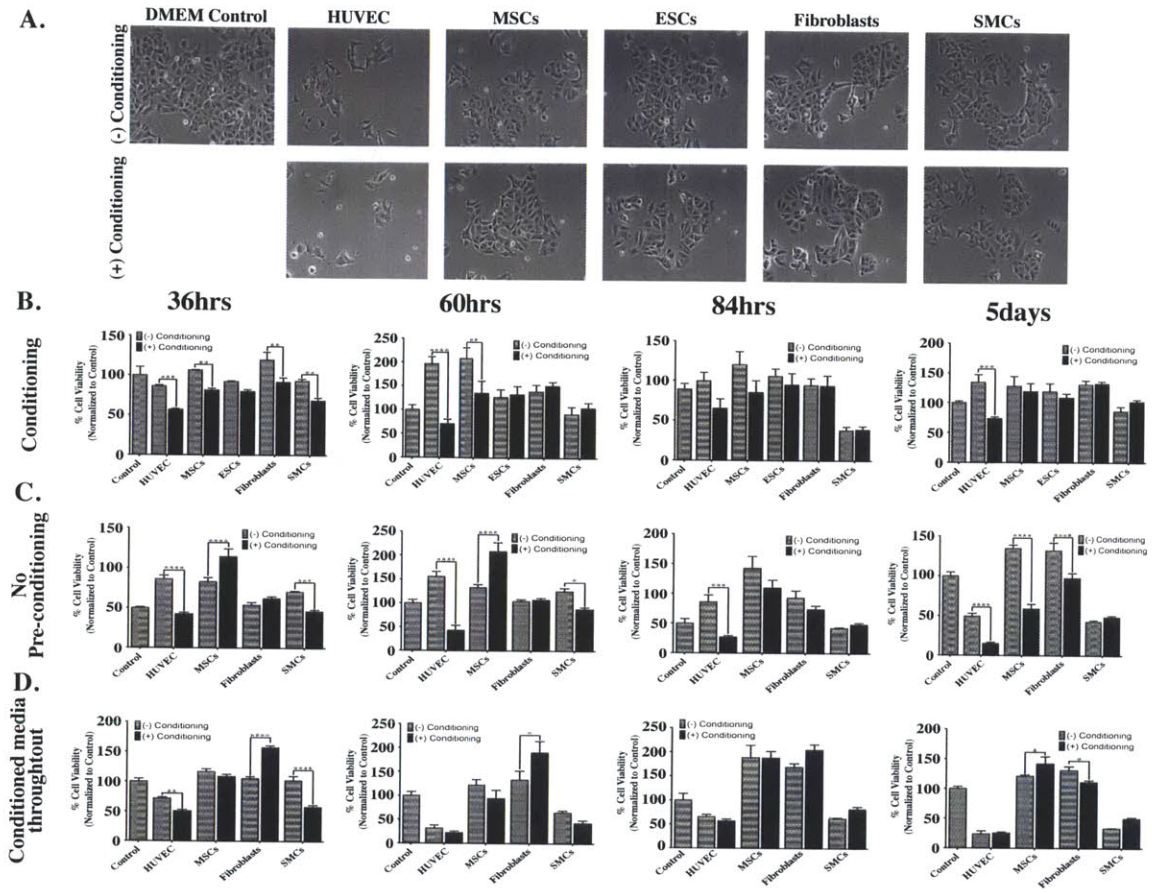

Figure 3-13: Effects of secreted growth factors on proliferation of MCF7. (A) Bright field image showing MCF7 cells in conditioned+ve and conditioned-ve from each cell type. The effects of secreted growth factors isolated from HUVEC endothelial cells, mesenchymal stem cells, embryonic stem cells, fibroblasts, and smooth muscle cells were measured using a commercially available viability assay. The following three protocols were used: (B) *conditioning*: tumorigenic cells are pre-conditioned for 4 days and then transferred to DMEM; (C) *no pre-conditioning*: tumorigenic cells are not pre-conditioned and then transferred to conditioned media; (D) *conditioned media throughout*: tumorigenic cells are conditioned for 4 days and remain in conditioned media for the duration of the study. Measurements were taken at 36hrs, 60hrs, 84hrs, and 5days. In contrast to results with MDA-MB-231 cells, soluble factors from endothelial cells suppress growth of MCF7 cells. These results suggest that tumorigenic cells respond differently to soluble factors secreted by endothelial cells than metastatic cells of the same tissue type.

tive. These cells offer an ideal comparison to the highly invasive, triple negative MDA-MB-231 cells, enabling examination of responses of metastatic cells and non-metastatic cells to soluble factors released by stromal cells.

Surprisingly, in contrast to results with MDA-MB-231 cells, conditioned media from the HUVEC endothelial cells inhibited growth of MCF7 cells, an effect that persisted for up to seven days of continued exposure to soluble factors **(Figure 3-13D)**. This effect even continued once growth factor had been removed for up to five days **(Figure 3-13B)**. Conditioned media from mesenchymal stem cells initially increased proliferation of MCF-7 cells for the first 60hrs of exposure **(Figure 3-13C)**. However, following this time period, this phenotype reversed dramatically to an inhibitory phenotype **(Figure 3-13B,C)**, which persisted for several days. Only after 9 days of exposure was there a slight change in phenotype to a pro-proliferative state **(Figure 3-13D)**. As described before, the altered response of cells from an anti-proliferative to a pro-proliferative state after continuous stimulation is likely due to transient changes in receptor expression.

Fibroblast and SMCs had only a minimal inhibitory effects on proliferation of MCF-7 cells **(Figure 3-13C)**. However, when exposed to growth factors derived from fibroblast cells, the inhibitory effect was slightly reversed after several days of exposure to the conditioned media **(Figure 3-13D)**. Unlike the MDA-MB-231 cells, proliferation of the MCF-7 cells was not affected by secreted factors from embryonic stem cells **(Figure 3-13A)**.

The results of this study are complex due to variability of receptor expression, leading to changes in stimulus response. This data also highlights that a singular time point measurement cannot completely capture the effects of the stromal environment on tumor growth. Furthermore, cell-cell interaction dynamics are complex with varying and hard to to predict responses that are difficult to capture with such simple experimental methods. However, in spite of these weaknesses, two trends were clear. The first was that growth factors secreted by the endothelial cells enhanced proliferation of metastatic cells while inhibiting growth of tumorigenic cells. In addition, tumorigenic cells did not show any proliferative

response to conditioned media from ESCs while metastatic cells showed a very robust response. These results highlight that metastatic cells respond differently to the endothelium than the non-metastatic cells. These differences may not be limited to the endothelium as suggested by differential responses of the tumorigenic and metastatic cell lines to soluble factors secreted by ESCs. Presumably, a cell's ability to respond to and interact with the endothelium in a certain manner may strongly indicate which cells will be able to continue to successfully progress through the multiple of steps of the metastatic cascade.

3.3.2 Endothelial cells increase metastatic cell migration

It has been clearly outlined in the literature that endothelial cells can directly stimulate transformation of metastatic cells[105]. Furthermore, in the co-culture model system, we observed preferential interaction and alignment of metastatic cells along the endothelial tubes that support these findings. We hypothesized that these observations may in part be due to the ability of metastatic cells to respond to secreted factors released by endothelial cells that enable the metastatic cells to specifically home to endothelial vessels. Presumably, the metastatic cells may be following a concentration gradient of growth factors secreted by endothelial cells. Migration can be described in 3 distinct stages: (1) morphological polarization plus membrane extension and formation of cell-substratum attachments, (2) internal contraction, and (3) rear release. Dynamic interactions with the membrane leads to formation of protrusions that, in response to a gradient of soluble factors, leads to directed growth of actin filaments and cytoskeletal structures.

Cells require polarization in order to migrate. Cellular polarization can be achieved directly via concentration gradients or indirectly via spatial/temporal stimulus gradients due to non-uniformities in receptor-ligand binding. The consequence of polarization is extension of active membrane processes primarily at the cell front, giving cell locomotion a persistent random walk characteristic. In order to determine if soluble factors secreted by endothelial cells increase the migratory

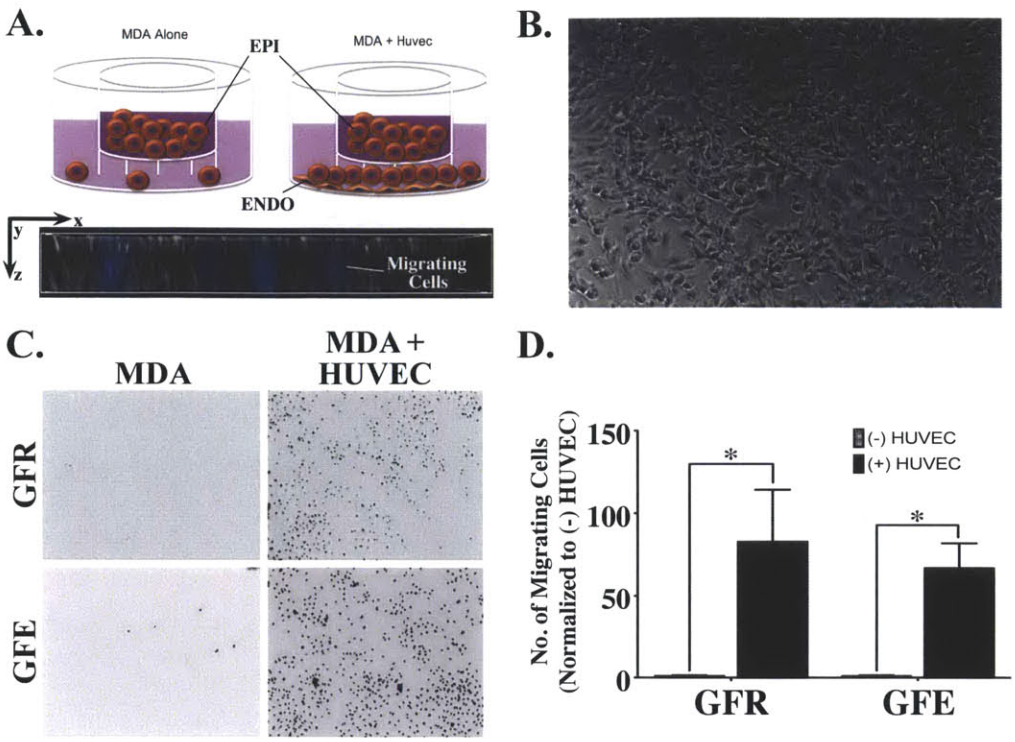

Figure 3-14: Endothelial cells increase migration of metastatic cells. (A) Schematic of Boyden chamber study design. Metastatic cells are seeded in the top chamber in matrix, while endothelial cells are plated on a layer of fibronectin in the bottom chamber. Metastatic cells can be seen migrating through the membrane pore. (B) Image of HUVEC monolayer on the bottom of each well. (C) Representative images of migrated cells through growth factor enriched and growth factor reduced matrix in HUVEC±ve groups. (D) Quantification of the number of migrated cells. In both growth factor reduced and growth factor enriched matrix groups, the presence of endothelial cells enhanced cellular migration.

and invasive capacity of MDA-MB-231 metastatic breast epithelial cells, a Boyden chamber assay was performed.

The study was designed as depicted in **Figure 3-14A**. MDA-MB-231 cells were plated in the top chamber coated with growth factor reduced (GFR) or growth factor enriched (GFE) Matrigel® in order to eliminate confounding results from growth factors within the matrix. In the bottom chamber endothelial cells were seeded in complete endothelial cell basal media on a fibronectin coating and incubated overnight until a monolayer was formed. An image of the endothelial cells is given in **Figure 3-14B**. An 8μm pore size transwell membrane was used that

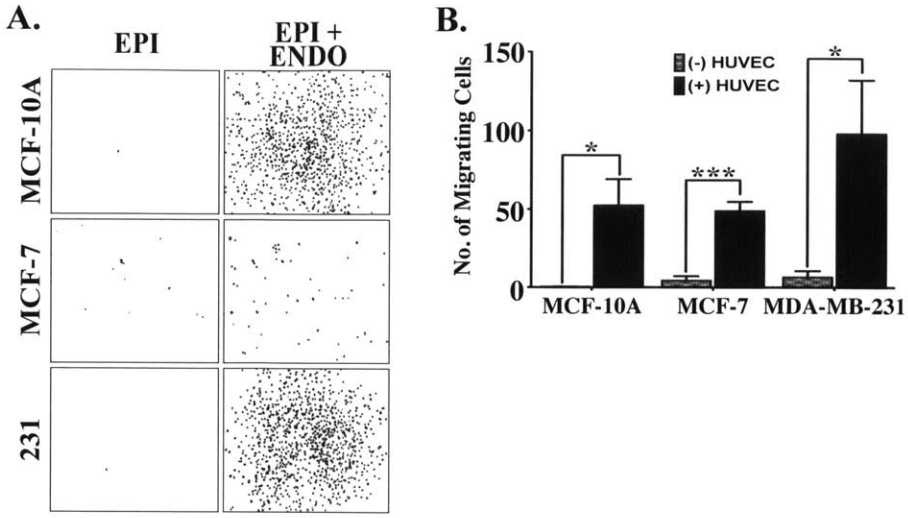

Figure 3-15: Endothelial cells increase migration of breast epithelial cells. The presence of endothelial cells enhance migration of fibrocystic MCF-10A, tumorigenic non-metastatic MCF-7, and metastatic MDA-MB-231 cells. (A) Representative images of migrated cells and (B) graph of quantification results illustrate the enhanced migration of cells due to the presence of the endothelium.

allowed cells to freely migrate from the top of the membrane to the bottom. **Figure 3-14A** provides an illustration of cells migrating through the pores. The cells were allowed to migrate for 6 days prior to quantification. The results of this analysis is given in **Figure 3-14C and D**. Addition of endothelial cells led to an increase of 82.837±31.360% and 66.736±14.973% in the number of migrated cells in GFR and GFE groups, respectively. Subsequently, this analysis was extended to include MCF-10A and MCF-7 breast epithelial cells. MCF-10A is a non-tumorigenic cell line isolated from a fibrocystic nodule. All three cell lines exhibit increased migration in the presence of endothelial cells **(Figure 3-15)**. Presumably endothelial cells secrete growth factors that increase epithelial cell migration with the greatest enhancement seen in the metastatic cell population.

This data is further supported by a matrix invasion assay performed with MDA-MB-231 cells, which confirms that growth factors secreted by the endothelial cells are responsible for the increased invasive potential. To establish this assay a criss-cross pattern of matrix was deposited in each well as shown in **Figure 3-16A**.

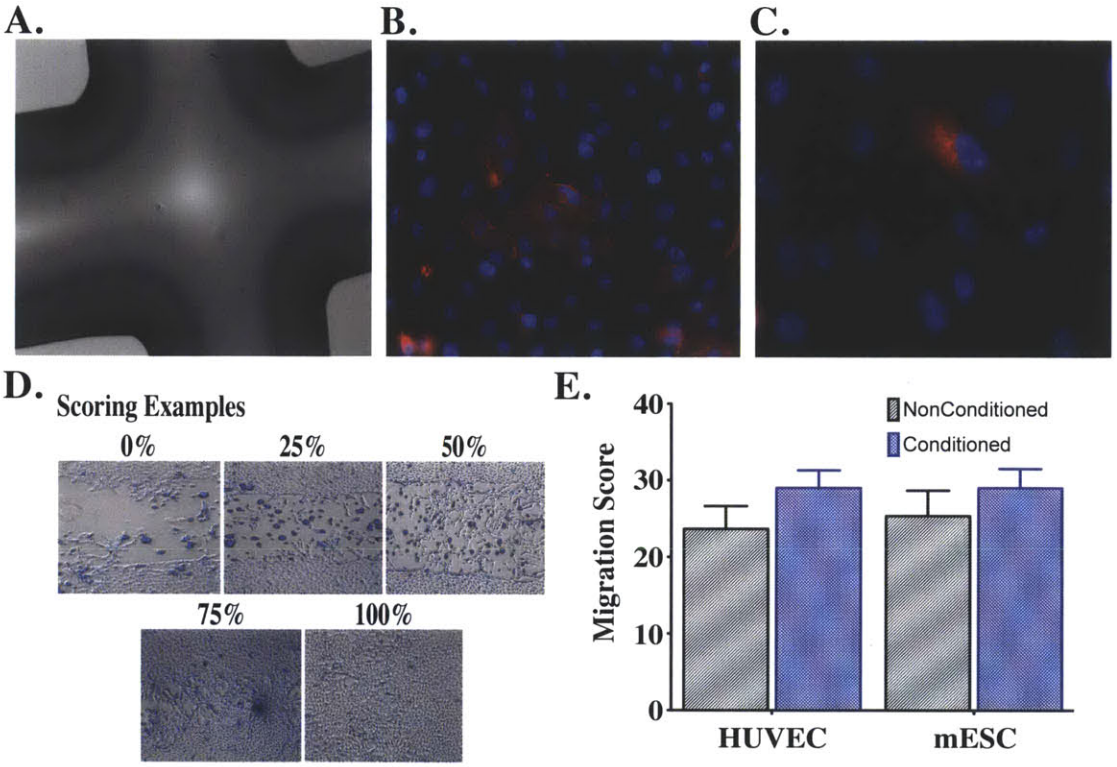

Figure 3-16: Growth factors secreted from HUVEC endothelial cells increase migration of MDA-MB-231 in a matrix invasion assay. (A) Illustration of criss-crossed pattern of matrix enriched with conditioned media from HUVEC endothelial cells and mouse ESCs. (B/C) MDA-MB-231 cells were stained with phallodin and counterstained with DAPI. (C) MDA-MB-231 cell can be seen migrating toward the growth factor enriched matrix. (D) Scoring examples used in quantifying the matrix invasion assay. (E) Graph summarizing results of the matrix invasion assay. Conditioned media increases migration of metastatic cells.

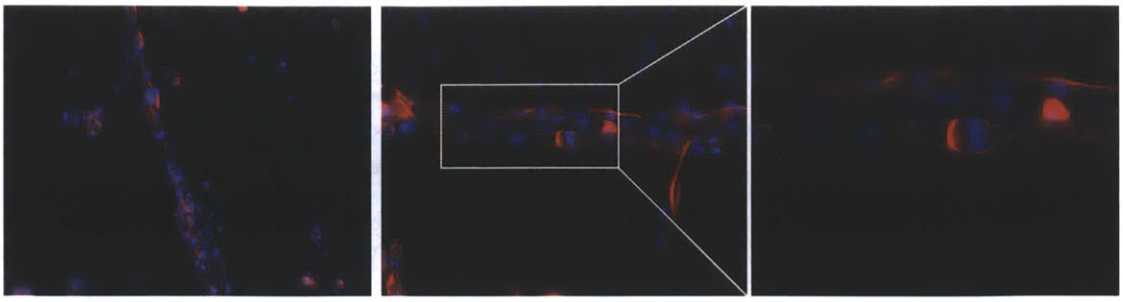

Figure 3-17: Metastatic cells align along the matrix. MDA-MB-231 cells can be seen aligning along the matrix analogous to alignment along endothelial vessels.

MDA-MB-231 cells were added to the wells and invasion into the matrix was quantified. The matrix was supplemented with concentrated growth factors from conditioned media collected from HUVEC endothelial cells and mouse ESCs (mESCs). MDA-MB-231 cells migrating into the matrix were captured in **Figure 3-16B and C**. MDA-MB-231 cells were stained with phalloidin to identify actin filaments and counterstained with DAPI **(Figure 3-16B and C)**. Only a fraction of the population seems to be pre-disposed to migration as highlighted by positive phalloidin staining of F-Actin fibers **(Figure 3-16B)**. A cell can been seen with migrational polarity in the direction of the growth factor enriched matrix **(Figure 3-16C)**.

The invasion assay was quantified as outlined in **Figure 3-16D**. There was an increase in migration for Matrigel® enriched with conditioned media from HUVEC endothelial cells and mESCs. This data correlates with previous observations showing an increase in cellular proliferation of MDA-MB-231 cells when exposed to conditioned media from these cell types **(Figure 3-12)**.

Interestingly, analogous to the phenotype obtained in the co-culture model system, the metastatic cells can be seen aligning and elongating along the growth factor enriched matrix lattice as shown in **Figure 3-17**. The ability to re-create this phenotype suggests that both chemical and biomechanical forces are necessary for EEC interactions. Similar to techniques used for tissue patterning, when presented with a structure approximating the physical properties of a endothelial tubes, the

MDA-MB-231 cells adopt the elongated morphology seen in the co-culture model **(Figure 3-17)**. Potentially, artificial recreations of this phenotype may offer additional insight into the critical elements underlying the EEC interactions. For example, the matrix could be seeded with a single growth factor, or a combination of growth factors to probe which soluble factors are responsible for attracting the metastatic cells. Alternatively, physical properties of the matrix (e.g. stiffness) can also be altered in order to investigate the biomechanics of EEC interactions.

3.4 Expansion of the co-culture model system to a panel of breast epithelial cells

Our studies and others have demonstrated that endothelial cells alter the biology of metastatic breast epithelial cells resulting in increased cellular proliferation and migration. The response of the metastatic cells to soluble factors secreted by the endothelium may in part dictate the observed EEC phenotype seen in co-culture, which in turn may provide insight into invasive mechanisms *in vivo*. We next turned our attention to elucidation of biomechanical and physical cell-cell interactions that may further enhance our understanding of EEC interactions in metastasis.

The model system was expanded to include a panel of breast epithelial cells of varying grades of tumorigenicity ranging from normal to highly metastatic. These cells types offer a basis of comparison necessary to determine features unique to metastatic cells.

3.4.1 Breast cancer

In the US, breast carcinoma is the most prevalent cancer in women[10,17]. The mammary gland is an intricate network of ductal structures lined by epithelium[17]. It is composed of a double-layer of epithelium; an inner sheet of polarized luminal epithelial cells surrounded by an outer layer of myoepithelial cells. Crosstalk

between the cell types are important for maintenance of mammary gland homeostasis and normal and carcinogenic physiologies.

The most common forms of breast cancer arise from carcinogenesis of the luminal epithelial cells. In breast tissue, as with many tissue types, the *in vivo* 3D architecture is critical to the maintenance of normal physiological processes[17,303] and 3D mammary recapitulation has also been shown to highlight tumorigenic changes and responses to experimental intervention that could not be gleaned from 2D cultures alone[16–18,303].

Like metastasis in other tissues, breast cancer metastasis involves a variety of physical and biochemical changes to both the metastasizing cells and the surrounding environment. Breast cancer metastasis occurs primarily through lymphatic endothelium, however, metastasis can also occur through vascular endothelium. The primary sites of breast cancer metastasis are lung, liver, and bone. The tumor biology underlying the development of primary breast cancer is relatively well understood making it an ideal platform to study subsequent stages along the metastatic cascade.

3.4.2 Co-culture model with breast epithelial cell lines of varying grades of tumorigenicity

The HUVEC endothelial co-culture model system was expanded to include a panel of breast epithelial cells lines ranging from normal primary epithelial cells to highly metastatic cell lines. Representative images of 2D and 3D monocultures and co-cultures for each of the cell types can be seen in **Figure 3-18**. The cell lines included in the panel are given below: Human Mammary Epithelial Cells (HMEC), a primary breast epithelial cell line, MCF-10A, a non-tumorigenic, fibrocystic cell line, MCF7 and SKBR3, tumorigenic/non-metastatic breast epithelial cell lines, MDA-MB-468, tumorigenic, low metastatic breast epithelial cell line, MDA-MB-231, tumorigenic, highly metastatic breast epithelial cell line, and 4T1 highly metastatic breast epithelial cell line of mouse origin engineered to mimic human metastatic

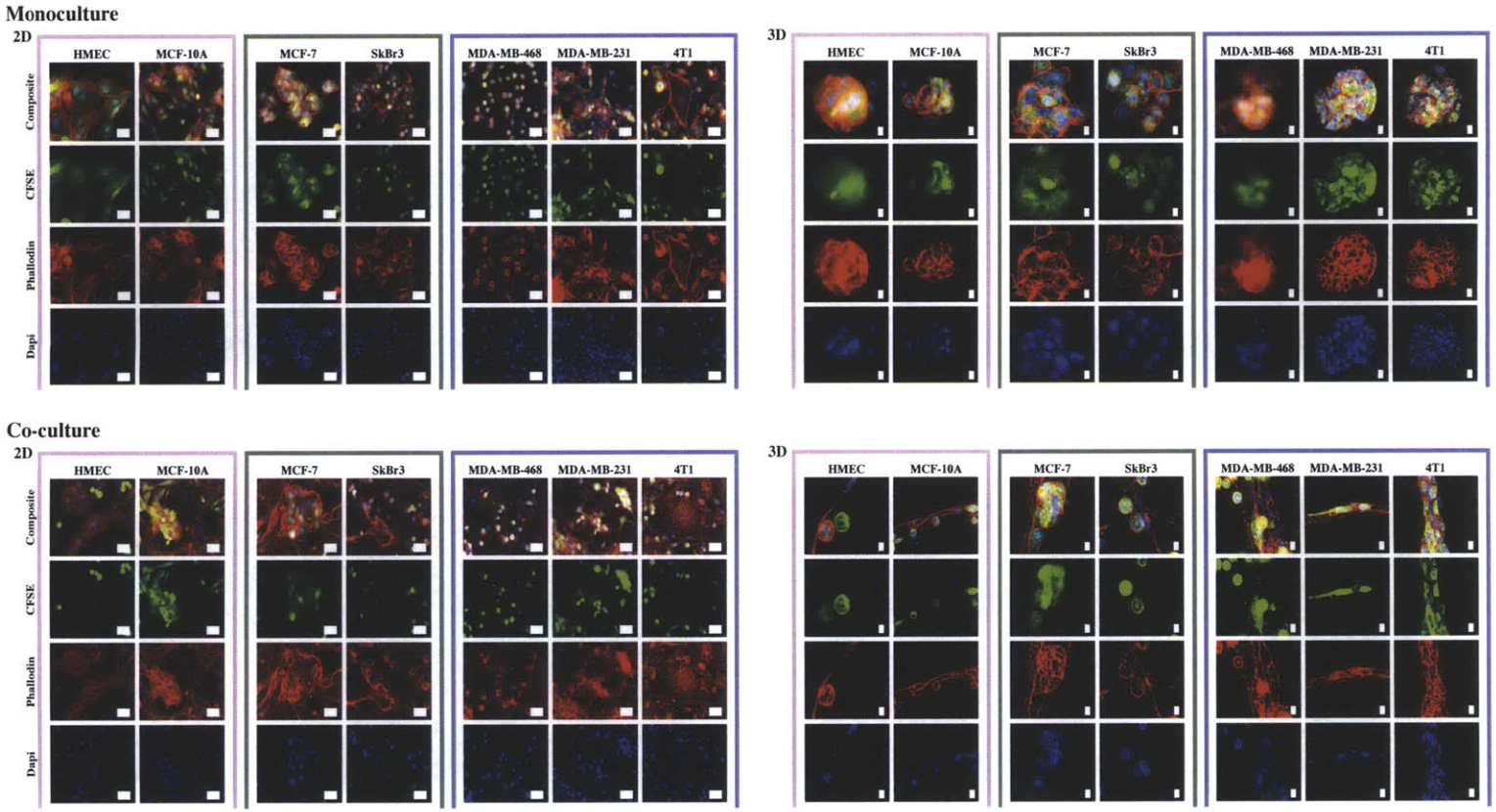

Figure 3-18: Representative 2D and 3D monoculture and co-culture images for a panel of breast epithelial cells. HUVEC endothelial cell co-cultures with breast epithelial cells of varying grades of tumorigenicity. Epithelial cells are labeled with CFSE prior to addition to unstained endothelial tubes. Samples are fixed after 24 hour co-culture and counterstained with phallodin and DAPI. Three-dimensional co-cultures reveal striking differences between EEC interaction phenotypes that correspond to tumorigenicity of the cell types.

breast cancer. As in previous studies, the epithelial cells are labeled with CFSE and therefore appear green in the images.

Similar to the phenotype observed with MDA-MB-231 cells, in 3D monocultures the breast epithelial cells adopt a characteristic mammosphere structure analogous to mammary acini *in vivo*. This phenotype dramatically differs from the 2D conformation. Further, in 2D co-cultures the breast epithelial cells segregate from the endothelium, revealing few difference between normal and metastatic cells. However, this phenotype is dramatically altered in 3D, showing striking differences between the cell types. Similar to the phenotype observed with the MDA-MB-231 cells, the other metastatic cells lines preferentially interact with the endothelium, aligning and incorporating within the vessel structure. In contrast to this phenotype, co-cultures with primary and tumorigenic epithelial cell lines exhibit low to moderate interaction with the endothelium, respectively. Throughout this analysis primary cells are highlighted in pink, tumorigenic cells are highlighted in green, and metastatic cells are highlighted in purple.

A kinetics study examining the co-cultures over a 24hr period further highlights these differences **(Figure 3-19)**. Epithelial-endothelial co-cultures with MCF-10A, MCF-7, MDA-MB-231, and 4T1 were imaged at 0min, 5min, 15min, 30min, 2hr, 6hr, 12hr, 16hr, 20hr, and 24hr time points. At early time points the cells can be seen just after seeding into the matrix. As time progresses, the phenotypes begin to diverge. Co-cultures with metastatic epithelial cells show a high degree of interaction between the cell types exhibiting intact robust vasculature for the entire 24hr time period. In contrast, in the MCF-10A and MCF-7 co-cultures, the endothelial tubes begin to regress, exhibiting more fragile and thinner branches. There is also limited interaction between the non-metastatic cells and the endothelium.

These observations are confirmed via time lapse imaging of MDA-MB-231 co-cultures. Time lapse imaging captured the dynamic and rapidly changing nature of the model system phenotype over a 12 hour period. Metastatic cells are observed actively integrating within the vessels, as well as directly remodeling vessel structures (i.e. fusing neighboring branches into a larger single branch). This

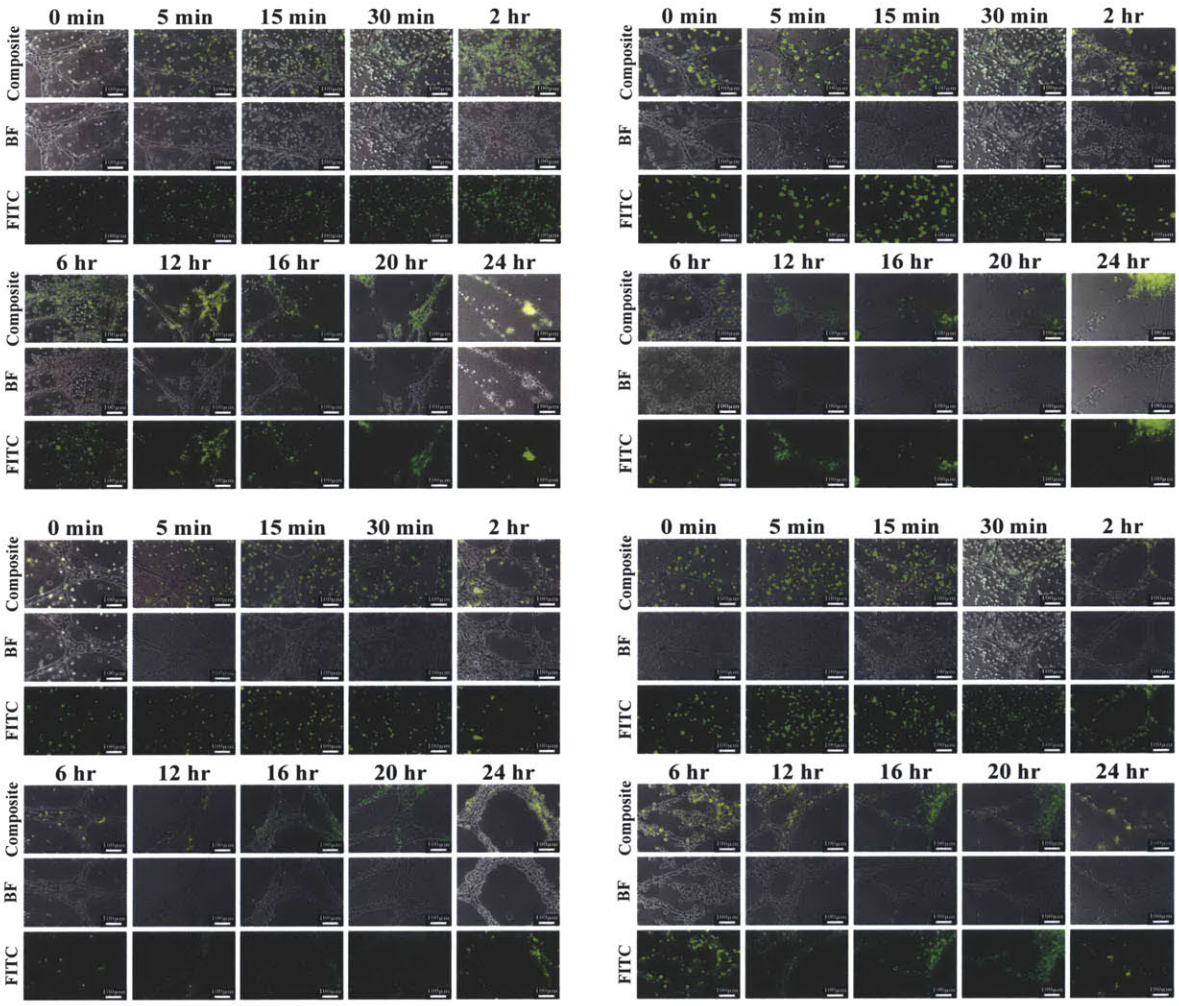

Figure 3-19: Kinetics of formation of co-culture phenotypes. HUVEC endothelial co-cultures with MCF-10A, MCF-7, MDA-MB-231, and 4T1 cells were monitored over a 24hr period.

remodeling contributes to the wide and robust vessel structures observed in these co-cultures.

SEM micrographs show high magnification views of the co-culture model system with primary **(Figure 3-20A, pink)**, tumorigenic **(Figure 3-20B, green)**, and metastatic **(Figure 3-20C, purple)** breast epithelial cell lines. Epithelial cells are indicated with the abbreviation EPI and endothelial cells are indicated with the abbreviation ENDO. A dotted line is used to outline the endothelium. On the left of each panel are mammosphere images taken in monocultures and on the right are co-culture images. The SEM micrographs show clear differences in EEC interaction phenotypes in primary, tumorigenic, and metastatic cell co-cultures.

Primary epithelial cell lines **(Figure 3-20A)** preferentially interact with other epithelial cells, exhibiting minimal interactions with the endothelium. At points of interaction the cells can be seen sitting discretely on the endothelial cell tubes. There are clear boundaries between the cell types with no evidence of intravasation into the endothelial tube lumen. Co-cultures with tumorigenic cell lines exhibit similar phenotypes as the primary cells **(Figure 3-20B)**. The tumorigenic cell lines are commonly seen forming large tumor spheroids near the vasculature, however, with limited interaction with the endothelium. In co-cultures with metastatic epithelial cells, this phenotype is dramatically altered **(Figure 3-20C)**. Here the cells align along the vessel, elongate, and potentially invade the endothelium. There are no clear boundaries between the cell types due to incorporation of metastatic epithelial cells within the vessel structures. The dramatic alteration in phenotype seen in metastatic cell co-cultures may suggest that this specific mechanism of interaction with the endothelium may be unique to metastatic cells. Indeed a cell must potentially be able to interact with the endothelium in a similar manner as captured in these images before it can progress along the metastatic cascade, successfully intravasating into and extravasating from the vasculature.

To capture invasion of the metastatic cells into the co-cultured endothelial vessels, the co-cultures were cryosectioned. Cryosectioning of vessel structures show a clear lumenal structure **(Figure 3-21A)**. Epithelial cells can be seen surround-

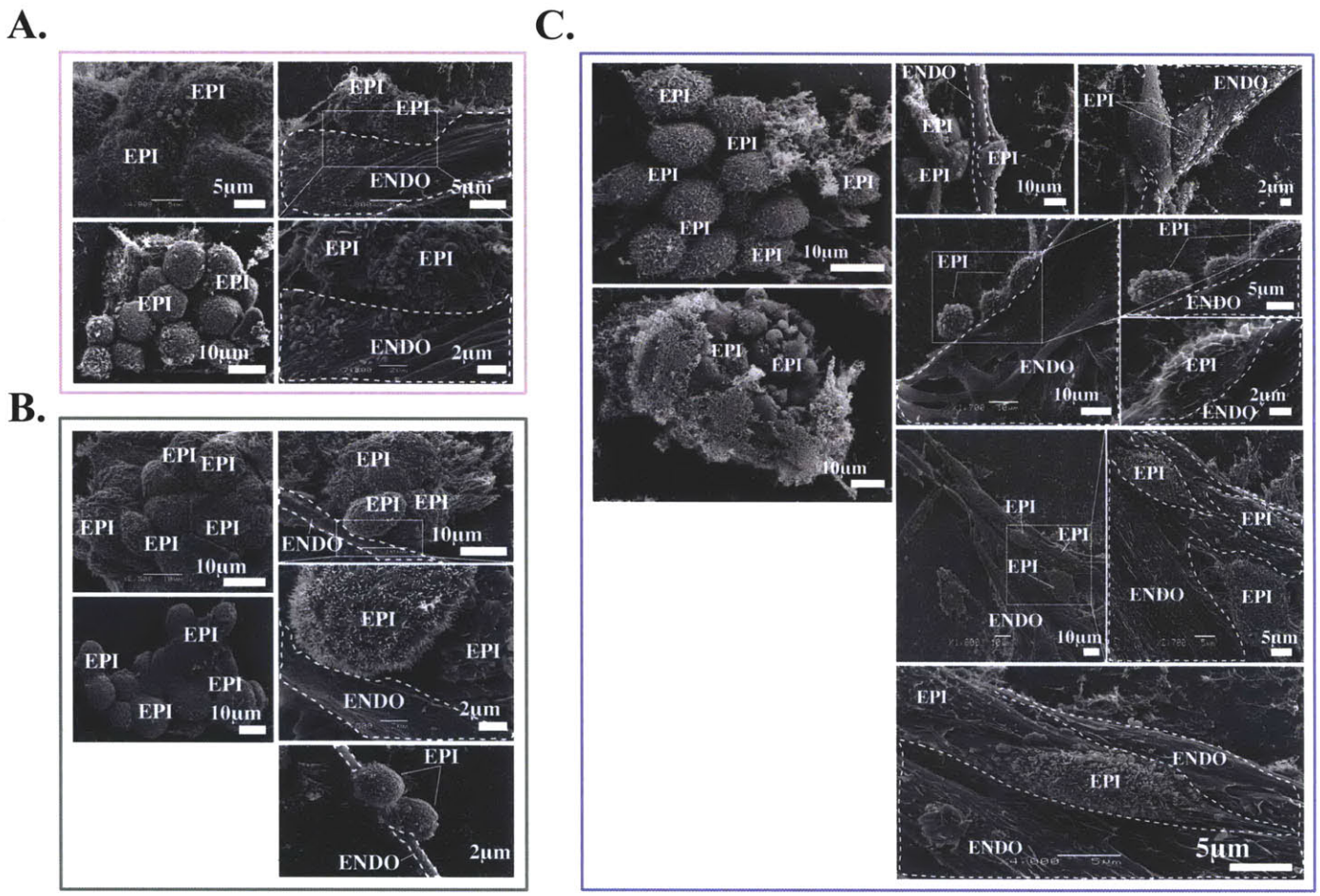

Figure 3-20: SEM images of epithelial-endothelial co-cultures. SEM micrographs show EEC interaction phenotypes in HUVEC endothelial co-cultures with (A) primary, (B) tumorigenic non-metastatic, and (C) metastatic cells lines. Epithelial cells are indicated by EPI and endothelial cells are given by the abbreviation ENDO. Vessel structures are outlined with dotted lines. Monoculture and co-culture images for each class of cells are given on the left and right of each panel, respectively.

ing the endothelial tubes. **Figure 3-21B** shows an epithelial cell penetrating the endothelial cell layers, passing through intercellular junctions to enter into the endothelial lumen. The ability of this model system to potentially capture elements of intravasation expands its utility as a mechanism for not only examining EEC interactions preceeding intravasation/extravasation, but also the actual process itself. This finding highlights the utility of this model system and emphasizes the ability of simplistic artificial systems to capture elements of complex cellular interactions.

3.4.3 Quantification of epithelial-endothelial co-culture model system

The above descriptions have only qualitatively described differences been endothelial cell co-cultures with primary, tumorigenic, and metastatic cell lines. However, to fully understand the differences in phenotypes, we have developed an algorithm for quantifying the different co-culture phenotypes. **Figure 3-22** shows representative examples of bright field images used to quantify the co-culture model system. The breast epithelial cells were labeled green, while the endothelial cells were left unlabeled. Again, these images highlight the dramatic differences between primary, tumorigenic, and metastatic co-culture phenotypes.

There were two main classes of quantification parameters analyzed, angiogenic parameters and interaction parameters. Angiogenic parameters focus on changes in the endothelium, while interaction parameters attempt to quantify EEC interactions. **Figure 3-23** is a schematic illustration of the quantified parameters, showing both a cartoon representation and an example of an actual image used for quantification. The angiogenic parameters quantified were vessel length, vessel width, and nodal area. These are parameters commonly quantified in endothelial cell tubulogenesis studies. However, since we were also interested in quantifying the degree of interaction between the two cell types we developed two novel quantification parameters, namely an epithelial-endothelial dissociation index (EEDI) and an elongation index (EI).

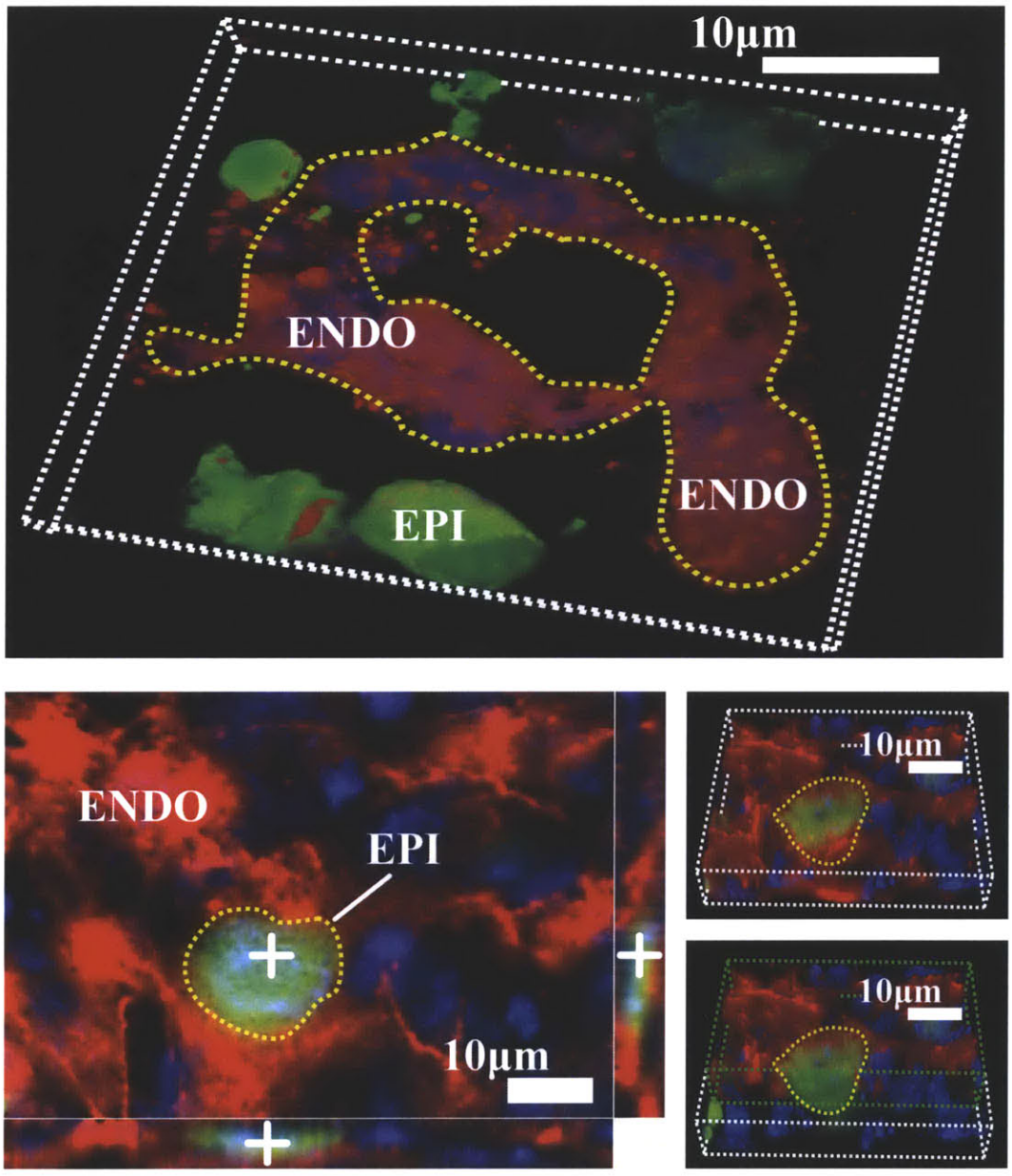

Figure 3-21: Cryosectioning of co-culture model with metastatic epithelial cells. (A) Cryosectioning of vessel structures in co-culture show an open vessel lumen. The vessel is surrounding by metastatic cells (green). (B) Metastatic cells can be seen penetrating the endothelial cell boundary. Endothelial cells are labeled with DiL-Ac-LDL (red) and metastatic cells are labeled with CFSE (green). The cultures are fixed and counterstained with DAPI.

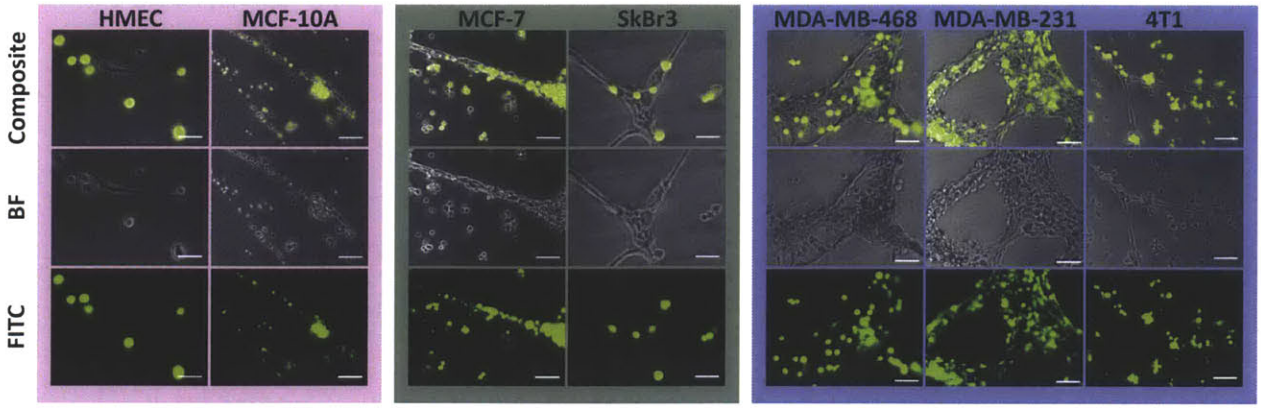

Figure 3-22: Bright field images of co-culture model systems with primary, tumorigenic, and metastatic cells. Angiogenic and interaction parameters were quantified using bright field images. Primary cells, tumorigenic non-metastatic cells, and metastatic cells are outlined in pink, green, and purple, respectively.

For each cell line analyzed approximately ~300-400 4x images were taken over 2-3 independent experimental setups with a minimum of 4 replicates each. The images were taken across the entire well capturing the diversity of phenotypes present in the co-culture system. Thousands of vessel structures were analyzed for each epithelial cell line in co-culture. Strict metrics were developed and applied to maintain consistency of the analysis over several cell lines and experiments. The rules applied in this analysis are summarized below; however, for a more detailed description of the methods used in quantifying the co-cultures refer to **Appendix B**.

Quantification of angiogenic parameters The following rules were applied for quantification of angiogenic parameters:

1. Vessel structures were identified as a network of endothelial tubes in bright field images

2. Vessel length was measured from the outer edge of one node to the outer edge of an adjacent node

3. A node is defined as an intersection of two branches. A node attached to less than two branches is not quantified. A node is approximated as a circular

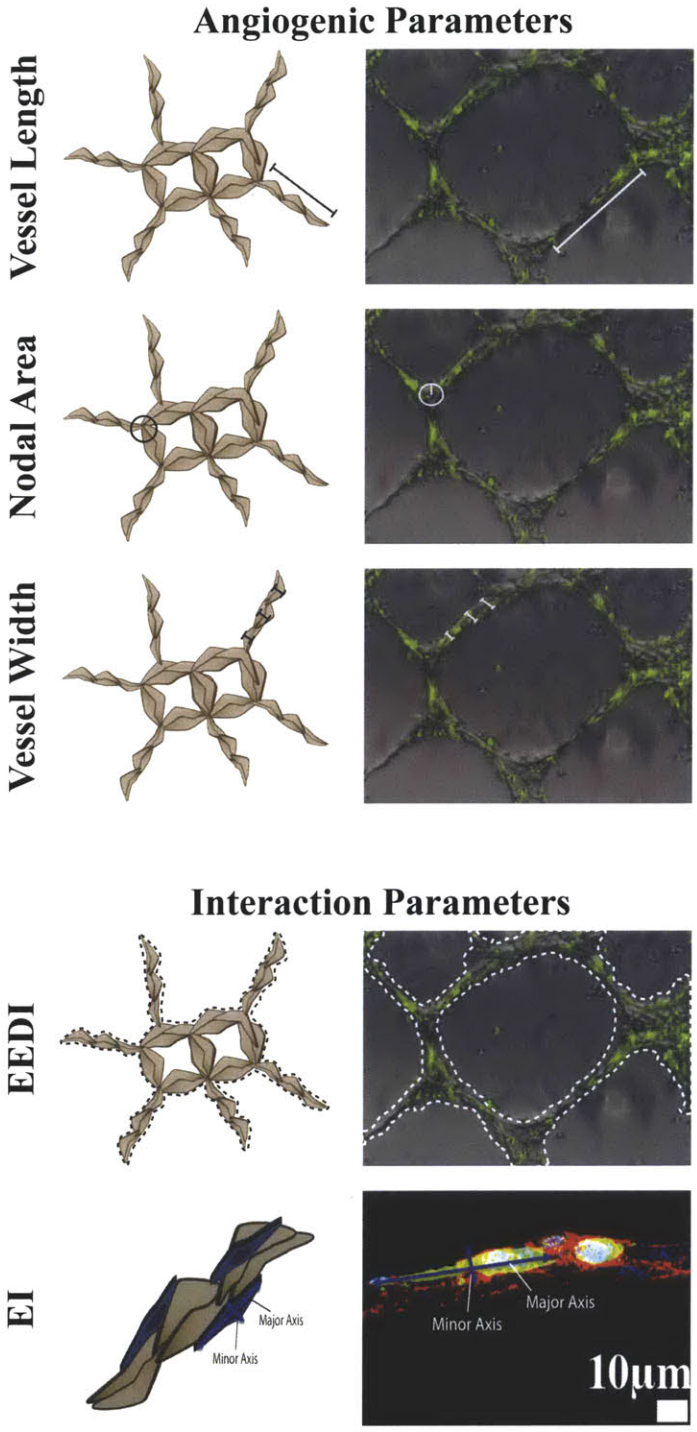

Figure 3-23: Example of quantification parameters. Images demonstrating how the quantification of angiogenic and interaction parameters were performed. The angiogenic parameters quantified were length, width, and nodal area and the interaction parameters quantified are EEDI and the elongation index.

region and the nodal area is defined as the area of the circle.

4. Vessel width measures the short-axis of the vessel structure. Given that the vessels are very heterogenous structures with varying widths, three width measurements are taken for each branch and then averaged to obtain an average width.

Quantification results from the angiogenic parameter are summarized in **Figure 3-24**. Vessel length **(Figure 3-24A)**, vessel width **(Figure 3-24B)**, and nodal area **(Figure 3-24C)** results have been normalized to quantification results for endothelial cell monocultures (black bar). Epithelial-endothelial co-cultures with normal cells (pink bars) showed no enhancement of angiogenic parameters. Moreover, co-cultures showed regression of the endothelial tubes as given by a decrease in vessel width ($p<0.0001$) and nodal area ($p<0.0001$). This data suggest that the primary epithelial cells are not able to support the vasculature and may be even enhance endothelial cell death. Angiogenesis is regulated by a dynamic balance of pro- and anti-angiogenic factors. These cell types may create a more anti-angiogenic environment. This phenotype contrasts quantification results with both tumorigenic (green) and metastatic (purple) cell lines. There is increased vessel width and nodal area in tumorigenic co-cultures compared to HUVEC only control and primary epithelial cell co-culture model systems. The increase in these parameters highlights both the ability of the tumorigenic cells to support the vasculature and the resulting vessel widening and enlargement of the nodes due to increased EEC interactions. As expected quantification results with the metastatic cell lines show the greatest enhancement of angiogenic parameters with statistically significant increases in vessel length ($p<0.001$), vessel width ($p<0.001$), and nodal area ($p<0.001$) compared to both HUVEC endothelium alone and primary epithelial cell co-cultures.

Quantification of interaction parameters Not surprisingly, both tumorigenic and metastatic cells supported the vasculature to a greater extent then the primary epithelial cells, likely as a result of secretion of pro-angiogenic factors. However, the

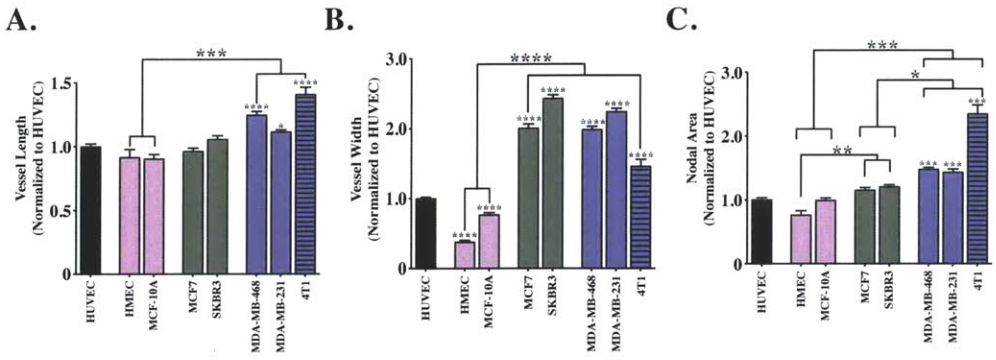

Figure 3-24: Summary of results of quantification of angiogenic parameters. Quantification of (A) vessel length, (B) vessel width, and (C) nodal radius area show that metastatic cells increase angiogenic parameters. Primary cells are indicated with pink, tumorigenic non-metastatic cells are indicated with green, and metastatic cells are indicated in purple. Results are normalized to HUVEC monoculture cells (black bar graph). Cell lines of non-human origin are indicated with stripped bars.

most interesting differences between these two cell types was found when characterizing EEC interaction phenotypes. The epithelial-endothelial dissociation index provides a measure of the degree of interaction between the cell types by indirectly quantifying the percentage of the cell population physically interacting with the endothelium and the percentage of the cells not in physical contact with the endothelial cell tubes.

The following assumptions were made and rules were applied to quantify the epithelial-endothelial dissociation index:

1. An epithelial cell physically on the endothelial tube is considered an interacting cell, or as being "on" the vessel, while an epithelial cell not in physical contact with the endothelium is considered "off" the vessel.

2. Fluorescence intensity was assumed to be an estimate of cell number so that a higher intensity implies a greater number of cells.

3. The vessels are outlined as illustrated in **(Figure 3-23D)**. The fluorescence intensity is measured within the outlined region. This measured value represents the fluorescence intensity on the vessel and is a measure of the number

of interacting cells.

4. Total fluorescence is an approximate measure of the total number of epithelial cells present in the image. Total fluorescence is equal to the fluorescence "on" plus the fluorescence "off" the vessel.

The epithelial-endothelial dissociation index (EEDI) is defined by the following expression:

$$EEDI = \frac{Fluorescence_{total} - Fluorescence_{on}}{Flourescence_{total}},$$

where $Fluorescence_{total}$ is a measure of the total number of epithelial cells and $Fluorescence_{on}$ is a measure of the number of epithelial cells on the vessel.

Figure 3-25A summarizes quantification results for the EEDI parameter. This metric provides a measure of the percentage of cells not interacting with the endothelium. Therefore, cells with a high EEDI index have little interaction (i.e. primary epithelial cells), while cells with a low EEDI index exhibit a high degree of interaction with the endothelium (i.e. metastatic cells). The EEDI score for all cells lines was normalized to HMEC, the primary epithelial cell line, which serves as the control in this analysis.

As discussed previously, primary cells show minimal interaction with the endothelium. MCF-10A show a higher degree of interaction than the true primary cells (i.e. HMECs). This difference in phenotype highlights that although a cell type might not be tumorigenic it does not necessarily behave exactly as a normal cell might. The highly metastatic MDA-MB-231 cells showed the highest degree of interaction with the endothelium, which was statistically significant compared to both primary ($p<0.0001$) and tumorigenic cell lines ($p<0.0001$). The moderately metastatic cell line, MDA-MB-468, showed slightly less interaction with the endothelium compared to the highly metastatic MDA-MB-231 cells, suggesting that increased interaction with the endothelium may correlate with increased invasive capacity. Surprisingly the 4T1 showed less interaction with the endothelium than the MDA-MB-468 cells despite being highly metastatic **(Figure 3-25A, purple stripped bar)**. However, this may be due to species-to-species differences that may

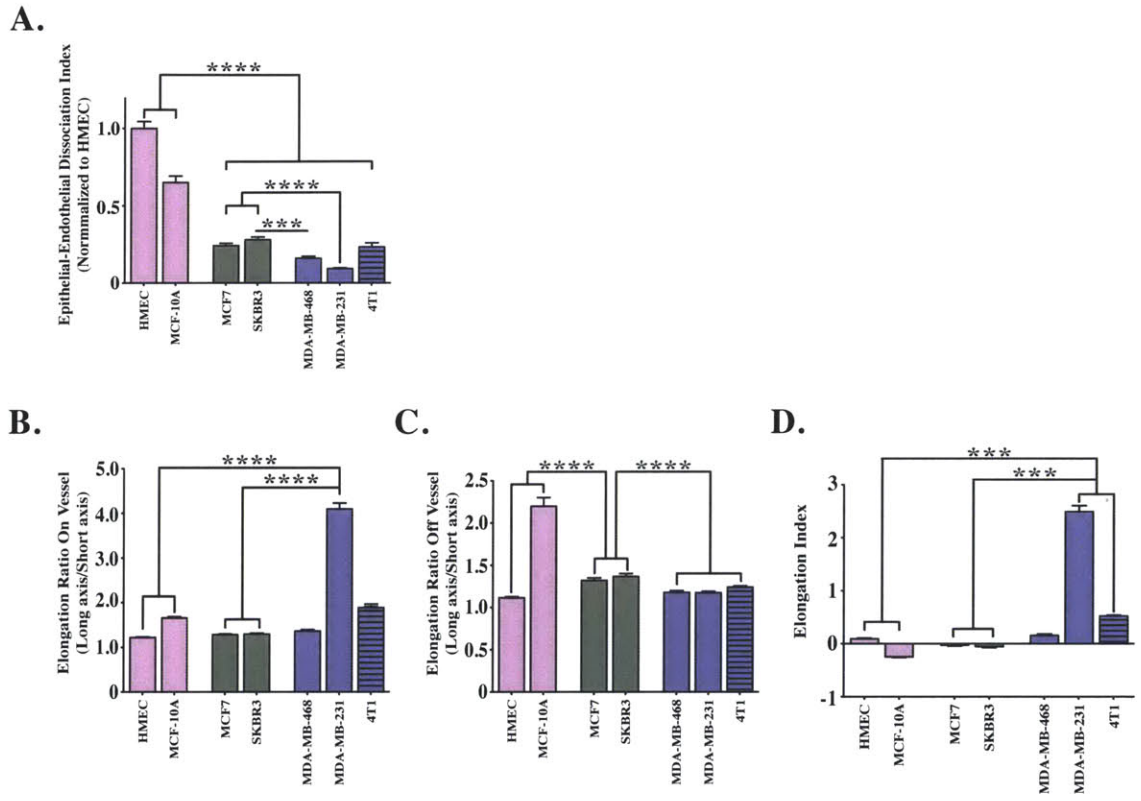

Figure 3-25: Summary of quantification results of interaction parameters. (A) Quantification results of the EEDI. Metastatic cells exhibit increased interaction with the endothelium compared to other cell types. (B) Elongation ratio on the vessel, (C) elongation ratio off the vessel, and (D) elongation index are presented. Metastatic cells undergo a large deformation when in contact with the endothelium as indicated by the elongation index $>>1$. Primary cells, tumorigenic non-metastatic cells, and metastatic cells are indicated by pink, green, and purple, respectively. Cell lines of non-human origin are indicated with stripped bars.

affect the cells' ability to interact. Therefore the human and non-human cell lines cannot be directly compared. Nevertheless, these results support a trend indicating that metastatic cells lines greatly interact with the endothelium. Furthermore, unlike the angiogenic parameters, the EEDI metric easily distinguishes the tumorigenic and metastatic cell populations. Could measurement of the EEDI shed light on to the invasive potential of a population of cells?

A second feature unique to metastatic cells is the ability of these cells to undergo large deformations when in contact with the endothelium, resulting in dramatic changes in cellular morphology from rounded structures to flat fibroblast like structures. Indeed, studies have shown that the adoption of a flat, spindle-like fibroblasts morphology aids cells during metastatic invasion[120]. The elongation index is used to quantify the deformation that occurs when the epithelial cells come in contact with the endothelium.

The following assumptions and rules were used in calculating the elongation index:

1. An epithelial cell physically on the endothelial tube is considered an interacting cell or "on" the vessel, while an epithelial cell that is not in physical contact with the endothelium the cell is considered "off" the vessel.

2. The long axis (length) to short axis (width) of cells "on" and "off" the vessel were measured as depicted in **Figure 3-23**.

3. The elongation ratio (ER) for each cell is calculated by relating the long axis to the short axis:

$$ER = \frac{longaxis}{shortaxis}$$

4. The final elongation index is determined using the following expression:

$$EI = \frac{ER_{On} - \overline{ER_{Off}}}{\overline{ER_{Off}}}$$

5. ER_{Off} is measure of the normal baseline cellular morphology prior to defor-

mations resulting from interactions with the endothelium

The elongation index quantifies the change in shape of epithelial cells due to interaction with the endothelium. When "off" the endothelium, the breast epithelial cells appear rounded with no distinct cellular polarity. This result is supported by the calculated elongation ratio of the endothelium approximately equaling 1 for each of the cell lines **(Figure 3-25C)**. When interacting with the vessel, normal and tumorigenic cells maintain this morphology or actually become more rounded as indicated by a negative EI **(Figure 3-25D)**. The cells may become more rounded because these cell types likely organize into tumor spheroid structures when in contact with the vessel as seen in the SEM micrographs **(Figure 3-20)**. Unlike the other cell types, metastatic cells undergo a significant deformation from rounded to spindle shaped when in contact with the endothelium as indicated by an EI>1 compared to normal ($p<0.001$) and tumorigenic ($p<0.001$) **(Figure 3-25D)**. This linear deformation may be required for successful intravisation and may be a unique property of metastatic cells.

The observed cellular deformation results from dynamic remodeling of the cytoskeleton that occurs when the two cell types interact. Alterations in cellular morphology is an energy intensive process requiring mobilization of signaling pathways and cytoskeletal regulatory pathways. These alterations may potentially lead to changes in cell biomechanical properties (i.e. stiffness) that may enable a normally immobile and stiff cell to squeeze through tight endothelial cell-cell junctions.

This observation introduces several interesting questions on the biological significance of the EI. What enables a cell to undergo these deformations? Do these changes in cellular shape enhance the cells' ability to adhere to the endothelium or intravasate into /extravasate from the vessel? Does elongation of the cells change the biomechanical properties of metastatic cells to promote invasion?

3.4.4 2-parameter metastatic index

Quantification of interaction phenotypes introduces two features unique to metastatic cells, namely the EEDI and EI. Metastatic cells lead to significant changes in the endothelium. However, examining interaction phenotypes provides the best criteria to distinguish between metastatic and non-metastatic phenotypes. The results of the epithelial-endothelial co-culture quantification is summarized in **Figure 3-26A**.

Using the results from our quantification parameters, we derived a 2-parameter metastatic index. The graph in **Figure 3-26B** correlates EEDI and EI parameters from each cell line. The EEDI is plotted on the x-axis and the EI is plotted on the y-axis. From these correlations emerge three regions that can be used to differentiate normal, tumorigenic, and metastatic cell population (shaded regions). The elongation and interaction phenotype observed *in vitro* corresponds with observations of metastatic cells within mouse lung endothelium *in vivo*.

The 2-parameter index may potentially provide a predictive model to identify cells with a higher metastatic capacity from a population of tumorigenic cells. By measuring the EEDI and EI unique regions on the plot begin to emerge distinguishing normal, tumorigenic, and metastatic cells. Future studies can focus on validating the use of the metastatic index using cells of unknown metastatic capacity.

3.5 Expansion of the co-culture model system

3.5.1 Co-culture model system with primary blood and lymph endothelial cells

Metastatic breast cancer cells may invade the systemic circulation directly, haematogenous dissemination, or indirectly through the lymphatic circulation. However, once in the lymph nodes the cells must travel into the systemic circulation to access the common organs of metastasis (e.g. bone, liver, brain, and lung) because there are no direct lymphatic routes to these sites. Entering the systemic circu-

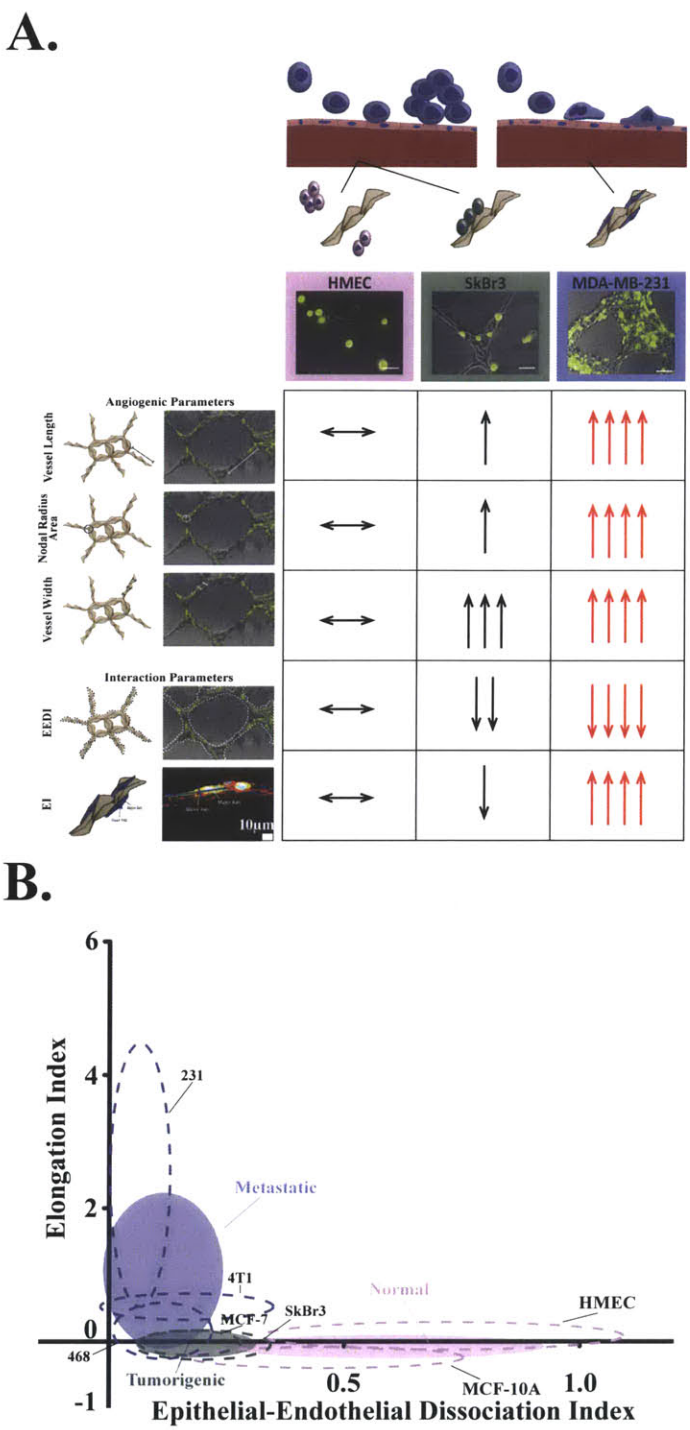

Figure 3-26: 2-parameter metastatic index. (A) Summary of quantification results of angiogenic and interaction parameters. (B) The 2-parameter index may be a predictive model for identifying metastatic capacity based on the behaviors of cells in co-culture.

lation could occur directly through growing blood vessels feeding lymph node metastases or indirectly through emptying of efferent lymphatic vessels into the venous system. Lymph node metastasis is a negative prognostic factor for many cancers, however, it's unclear if metastasis to other sites occurs as a result of lymphatic spread or if lymphatic dissemination occurs concurrently with haematogenous dissemination.

In consideration for both the haematogenous and lymphatic routes of dissemination, the model system was expanded to evaluate interactions between metastatic MDA-MB-231 cells with primary human microvascular blood endothelial cells and primary lymph endothelial cells. **Figure 3-27** illustrates co-culture phenotypes with primary endothelial cells. Interactions between metastatic cels and primary epithelial cells are analogous to observations with HUVEC endothelial. Cells can be seen elongating and aligning along both blood and lymph endothelial vessels **(Figure 3-27B and C)**. Analogous to the *in vivo* phenotype, lymph endothelial cells form less defined vessel structures with looser cell-cell junctions and disorganized vessel structures **(Figure 3-27A)**.

Quantification of these co-cultures further confirm observations with HUVEC endothelial cells. Results are summarized in **(Figure 3-28B)**. There is a significant increase in nodal area ($p<0.0001$) **(Figure 3-28B)** and vessel width ($p<0.0001$) **(Figure 3-28C)** in metastatic cell co-culture compared to monocultures. Furthermore, there is a high degree of interaction between the metastatic cells and the endothelial cells that does not occur with other stromal cells **(Figure 3-28D)**. Metastatic cell co-cultures with SMCs show minimal interaction between the two cell types, providing additional evidence that metastatic cell interactions with the endothelium are unique and distinct from interactions with other cell types commonly found in the tumor stroma.

Metastatic epithelial cells show the highest degree of interaction with blood endothelial cells when compared to lymph endothelium with no significant difference in interaction with HUVEC. It's unclear why this difference in phenotype between the blood and lymph endothelium is present. It may be due to differential

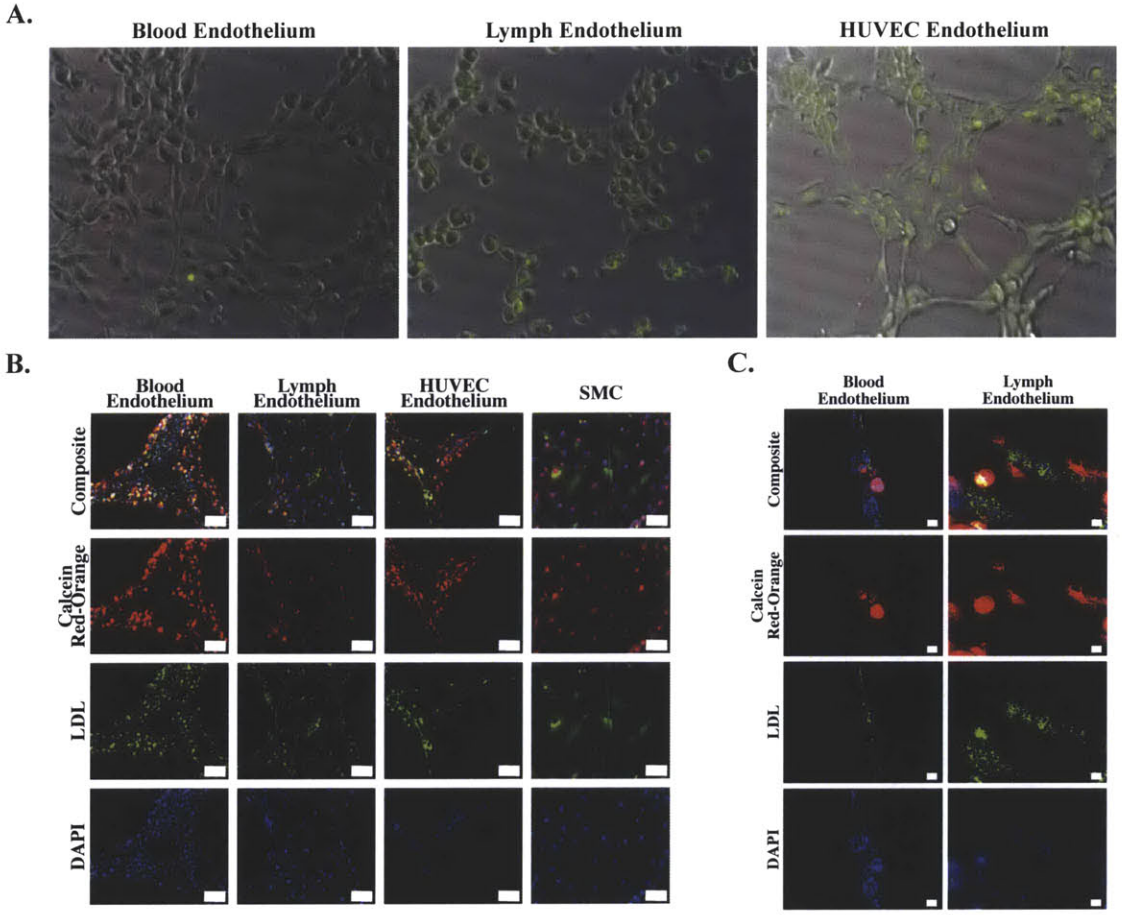

Figure 3-27: Co-culture model with primary epithelial cells. Co-cultures with MDA-MB-231 cells established with primary blood and lymph endothelial cells. (A) 10x bright field images show formation of the co-culture phenotype with primary endothelial cells that support observations with HUVECs. (B) 10x and (C) 40x fluorescence images of co-cultures. Endothelial cells are stained with LDL (green), MDA-MB-231 cells are labeled with Calcein Red-Orange (red), and samples are counterstained with DAPI.

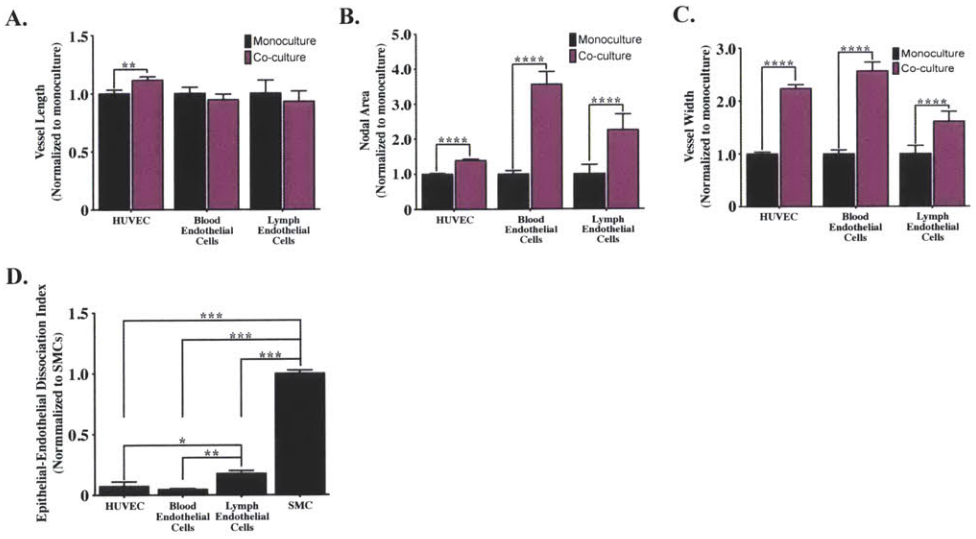

Figure 3-28: Quantification of metastatic cell co-cultures with primary blood and lymph endothelial cells. (A) Vessel length, (B) nodal area, (C) vessel width, and (D) EEDI were quantified in co-cultures with primary blood and lymph endothelial cells and compared to quantification results in HUVEC co-culture. Co-cultures with SMCs were used as a negative control to identify if interactions with endothelial cells were unique compared to other stromal cells.

secretion of soluble factors that attract metastatic cells to the endothelium. Alternatively, the differences may emerge due to differential expression of adhesion molecules.

3.5.2 Expansion of co-culture model to other tumor types

Breast, colorectal, lung and prostate cancers represent the four most prevalent cancers. However, in less than 10% of breast and prostate cancer patients, 20% of colorectal cancer patients, and 40% of lung cancer patients are distant metastases found at diagnosis[8]. This finding presents a therapeutic opportunity and indicates that for many cancer patients, interruption of the metastatic process at diagnosis could result in improved clinical outcomes. Therefore, the co-culture model system was expanded to several tumor types to determine if the observations found in breast cancer extended to other tumor types.

We have successfully established co-cultures with epithelial cells of breast, lung,

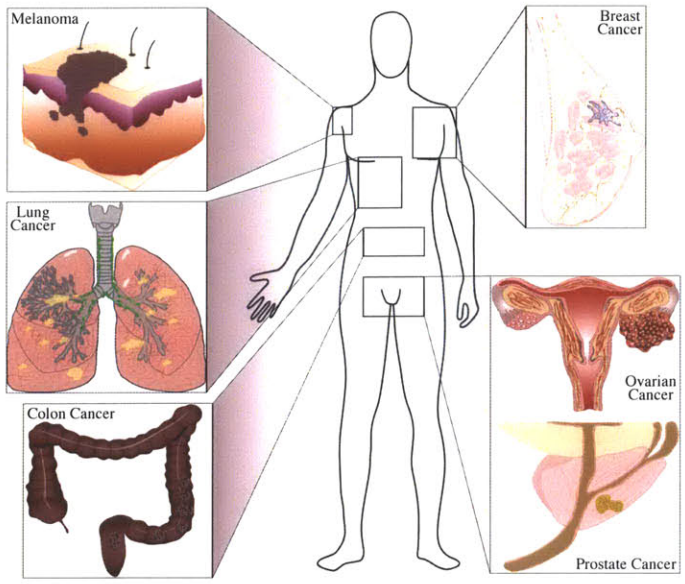

Figure 3-29: Schematic of the cancer types included in the co-culture model system. The co-culture model was established with epithelial cells from a wide range of tissue types to determine if the phenotypes observed with breast epithelial cells were translatable to other tumor types.

ovarian, prostate, colon, and skin origin. These tissue types were selected because they represent the majority of human cancers, which all have a high propensity for metastatic invasion. **Figure 3-29** illustrates the most commonly occurring cancers, which we have included in our co-culture model.

Figure 3-30A summarizes quantification results from a panel of prostate cancer cell lines derived from human and rat origin. Again in this data analysis primary, tumorigenic, and metastatic epithelial cells are indicated with pink, green, and purple bars, respectively. Similar to results obtained with breast epithelial cells, the metastatic cells showed an increase in angiogenic parameters. Cell lines of nonhuman origin are indicated with stripped bars. The increase in vessel length, vessel width, and nodal area correlates with the metastatic behavior of the cells. These results are further supported when examining the interaction indices. The metastatic prostate cancer cell lines have low EEDI values indicating a high level of interaction with the endothelium. Similarly, the metastatic cells showed a high

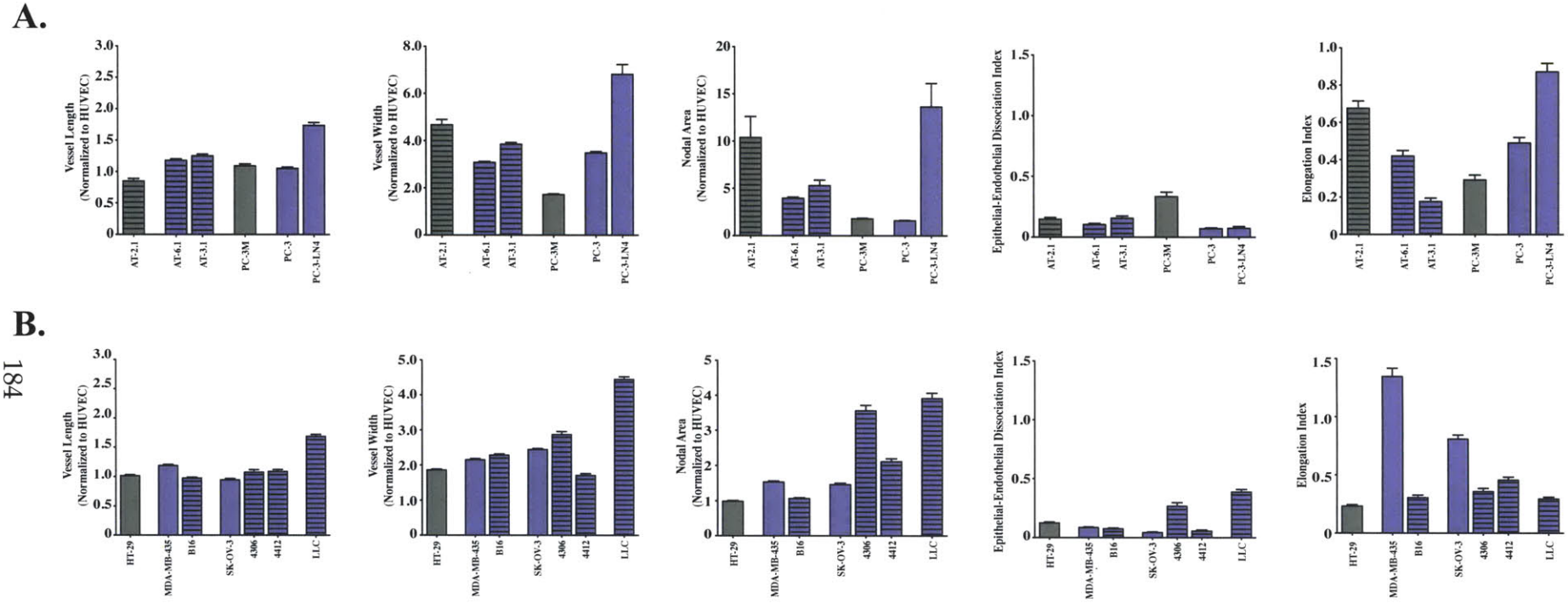

Figure 3-30: Schematic of the cancer types included in the co-culture model system. Quantification results from (A) prostate cancer epithelial cell lines and (B) epithelial cells from other tissue types. Primary, tumorigenic non-metastatic epithelial cells are indicated with pink, green, and purple bars, respectively. Cell lines of non-human origin are indicated with stripped bars. Quantification results in other tissue types are similar to results observed with breast epithelial cells.

elongation index, indicating large deformations when in contact with the endothelial tubes. However, these observations are seen consistently in the prostate cancer cells derived from human origin. Similar to results seen in 4T1 cells, the prostate cancer cells of nonhuman origin exhibited erratic interaction phenotypes with the human endothelium that may be due to species-species incompatibilities.

Interestingly, the prostate cancer cell lines caused very dramatic increases in vessel width and nodal area. These cells have distinct morphologies in co-culture characterized by a high degree of interaction, aligning, and elongating along vessel structures, similar to metastatic co-cultures with breast epithelial cells. Furthermore, these cell lines also exhibit unique features in co-culture. The prostate cancer cells can be seen completely encapsulating vessel structures. Metastatic cell lines derived from lung cancer, ovarian cancer, and melanoma further confirm these quantification results, emphasizing the physiological significance of these observations **(Figure 3-30B)**.

3.6 Disruption of co-culture phenotype

The previous sections describe our characterization of the co-culture model system. Through this analysis novel metrics of measuring cell-cell interactions were introduced, highlighting unique methods for studying interaction phenotypes between metastatic cells and the endothelium. However, these findings do not provide evidence on how this model system can be used used to directly probe pathways responsible for these cell-cell interactions.

As a proof of concept, we investigated the role of the FAK-integrin signaling axis in mediating EEC interactions between metastatic cells and the endothelium. Integrins are important for cell-ECM interactions and have been implicated in endothelial cell transmigration[108]. Integrins act through FAK, which in turn activate cellular signaling pathways. As illustrated in **Figure 3-31A**, attachment to the endothelium is a critical step in metastatic cell dissemination likely involving adhesion mechanisms utilizing integrins. We hypothesized that metastatic cells use

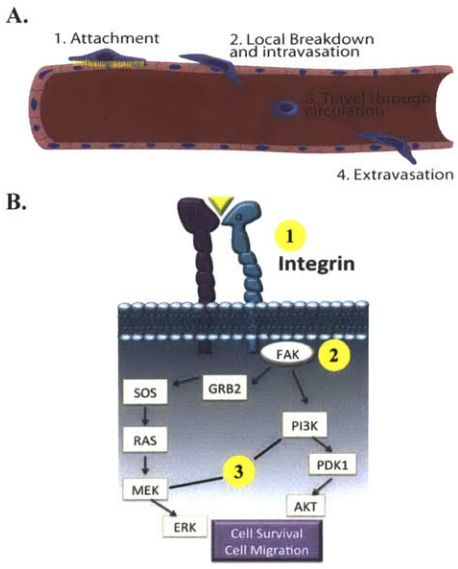

Figure 3-31: Co-culture model can be used to examine molecular mediators of EEC interaction phenotypes. (A) Adhesion to the endothelium is a critical precursor to metastatic dissemination. (B) The role of the FAK-integrin signaling axis in mediating the metastatic co-culture phenotype was probed at three points along the pathway.

integrins to bind to endothelial vessels, which in turns activates FAK and other downstream signaling pathways. To test this hypothesis, we probed this mechanism by independently targeting each point along the pathway as illustrated in **Figure 3-31B**, beginning first with integrins.

β-1 integrins have been implicated in metastatic phenotypes in breast cancer cells[298,304]. Furthermore, there is increased expression of β-1 integrins in metastatic MDA-MB-231 cells compare to MCF-7 cells in both a 2D and 3D platform **(Figure 3-32A)**. Furthermore, areas of interaction between the cells types show a punctate staining signature pattern **(Figure 3-32B)**.

To test the role of β-1 integrins in EEC phenotypes, β-1 integrins were knocked down in MDA-MB-231 cells using siRNA prior to addition of these cells to co-cultures. siRNA knockdown of β-1 integrins completely disrupted the interaction phenotype, typically observed in metastatic cell co-cultures **(Figure 3-33A)**. The breast epithelial cells (green) are scattered throughout the image with few cells aligning along the vessels as is seen in control cultures **(Figure 3-33A)**. However,

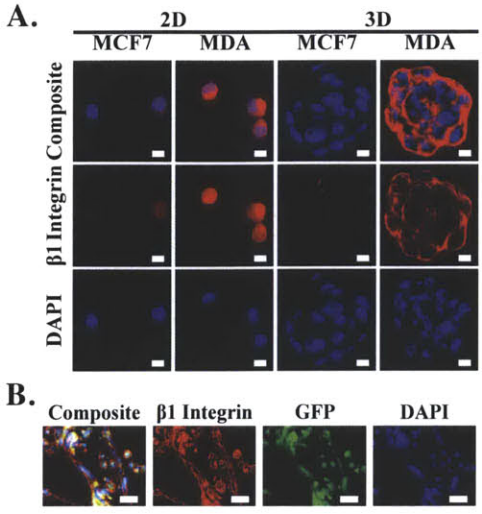

Figure 3-32: β-1 integrins are implicated in cancer metastasis. (A) Immunostaining with β-1 integrin antibody (Red) showed increased expression of the protein in metastatic cells. (B) Areas of EEC interaction show a punctate β-1 signature in co-cultures with GFP-labeled metastatic breast cancer cells (green). Cultures were counterstained with DAPI (blue).

interestingly, knockdown of the β-1 did not indiscriminately reduce cell-cell adhesion. Surprisingly, there were no significant differences observed in monoculture between control and β-1 siRNA groups. KD of β-1 integrins seemed to disproportionally affect epithelial-endothelial adhesion, rather than cell-cell adhesion in general. The EEDI was calculated to quantify the change in the EEC interaction phenotype due to knockdown of β-1 integrins. The EEDI shows that knockdown of β-1 integrins resulted in an 8.6 ± 1.225 ($p<0.001$) fold change in epithelial-endothelial interactions compared to control **(Figure 3-33C)**.

These results were confirmed using a β-1 integrin blocking antibody. β-1 integrins are important for both endothelial vessel formation **(Figure 3-34A)** and interactions between the two cell types **(Figure 3-34B)**. Treatment of endothelial cells with a blocking antibody reduced the ability of the endothelial cells to form vessel structures. Therefore, pre-treatment of the endothelial cells with blocking antibody completely disrupted the metastatic cell co-culture phenotype due to improper vessel formation **(Figure 3-34B, top panel)**. Pre-treatment of breast epithe-

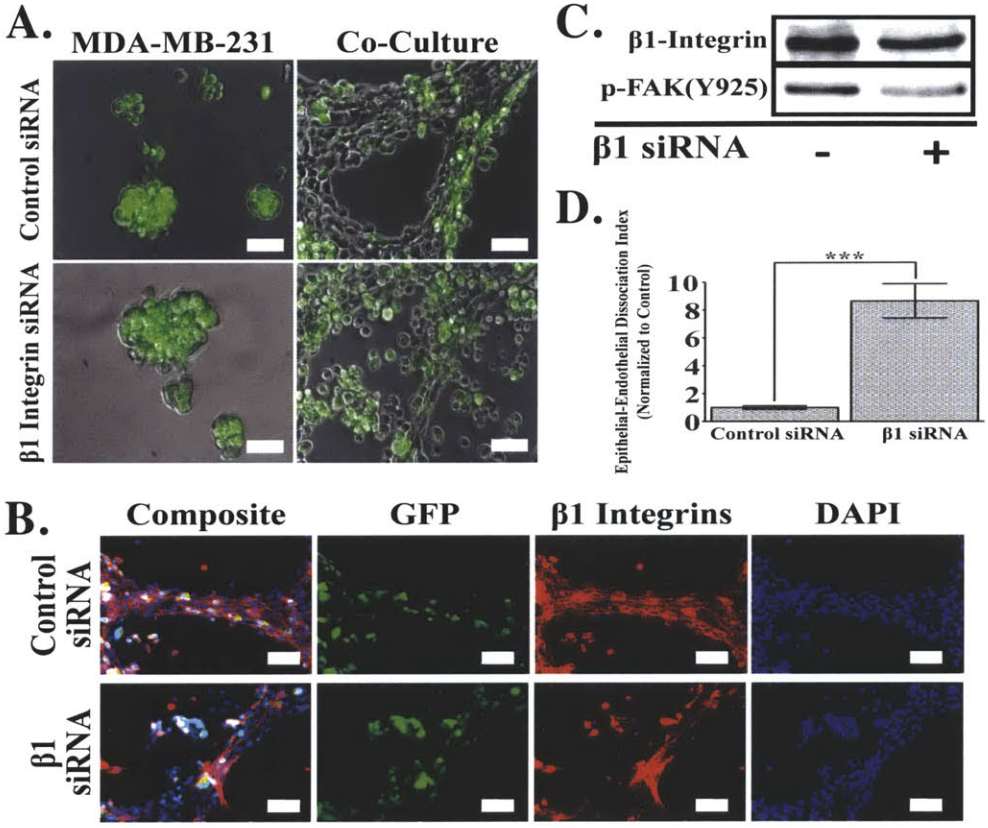

Figure 3-33: SiRNA knockdown of β-1 integrins led to disruption of the co-culture phenotype. (A) SiRNA knockdown of β-1 integrins disrupted the ability of metastatic cells to interact with the endothelium. (B) Western blots show knockdown results. (C) Calculation of EEDI metric quantified the increased dissociation resulting from inhibition of β-1 integrins.

lial cells with blocking antibody produced similar results as seen with RNAi. The metastatic cells were unable to effectively migrate toward or adhere to the endothelial tubes **(Figure 3-34B, middle row)** . Pre-treatment of both cell types with blocking antibody again led to disruption of the co-culture phenotype **(Figure 3-34B, bottom row)**.

Focal adhesion kinases lie downstream of β-1 integrins in FAK β-1 integrin pathway. Therefore, we next probed the pathway at the level of FAK phosphorylation. FAK is a critical regulator of cell-cell adhesion. It regulates a variety of cellular functions including cell spreading, migration, and proliferation. FAK can be phosphorylated at several different sites, each implicated in regulating separate downstream pathways **(Figure 3-35A)**.

SiRNA knockdown of FAK showed similar results as knockdown of β-1 integrins except the effects were slightly more muted **(Figure 3-35D)**. The result of this analysis is summarized in **Figure 3-35**. There was a 3.42 ± 0.162 fold increase in metastatic cell dissociation from the endothelium following knockdown of FAK. FAK signaling is activated in areas of high EEC interactions **(Figure 3-35B)**. Therefore, it follows that inhibition of FAK expression resulted in loss of the ordered phenotype typically seen in metastatic cell co-cultures. Loss of FAK results in erratic co-cultures, characterized by reduced interaction between the two cell types. Quantification of the EEDI confirmed the increased dissociation resulting from loss of FAK **(Figure 3-35D)**. Furthermore, FAK knockdown resulted in decreased phosphorylation of several FAK targets including pAKT and pERK, as well as other molecules within these pathways **(Figure 3-35E)**. The effects of FAK knockdown on the EEC interaction phenotype were much less dramatic than loss of β-1 integrins. β-1 integrins are upstream of FAK and may mediate cell-cell adhesion through FAK independent mechanisms. Therefore, it may be a more effective strategy to target the most upstream regulators of a pathway.

Since FAK plays varied roles in cellular physiology, it's likely that inhibition of FAK may reduce EEC interactions through several mechanisms. However, the two primary ways are likely through a reduction in the ability of metastatic cells to ad-

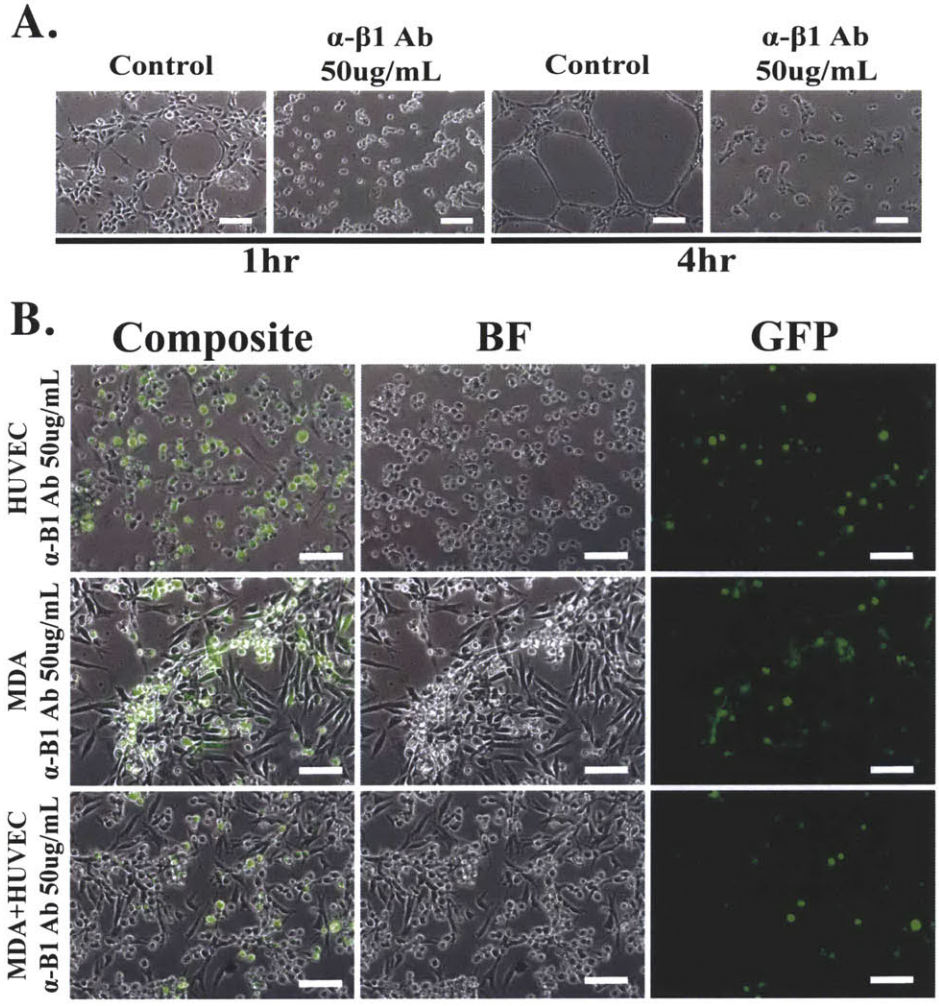

Figure 3-34: Inhibiting β-1 integrins with a neutralizing antibody disrupts the metastatic co-culture phenotype. β-1 integrins are important for (A) endothelial vessel formation and (B) adhesion between metastatic cells and the endothelium in co-culture. These interactions can be blocked with a neutralizing antibody.

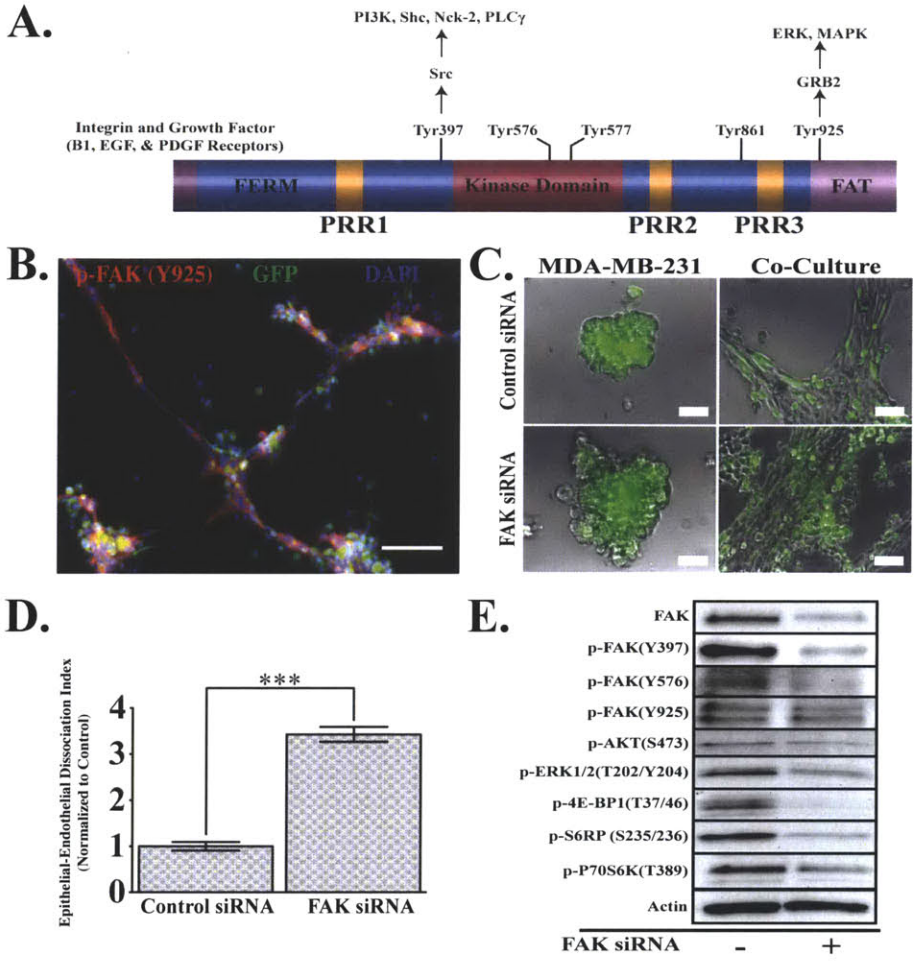

Figure 3-35: FAK knockdown disrupts the co-culture phenotype. (A) FAK can be phosphorylated at several sites, affecting signaling to several important regulator pathways. (B) FAK phosphorylation is increased in areas of high EEC interactions (C) that can be disrupted by siRNA knockdown of FAK. (D) Quantification results show an increase in EEDI after FAK knockdown consistent with the observed decline in epithelial-endothelial interactions. (E) Knockdown of FAK decreases signaling in several downstream pathways.

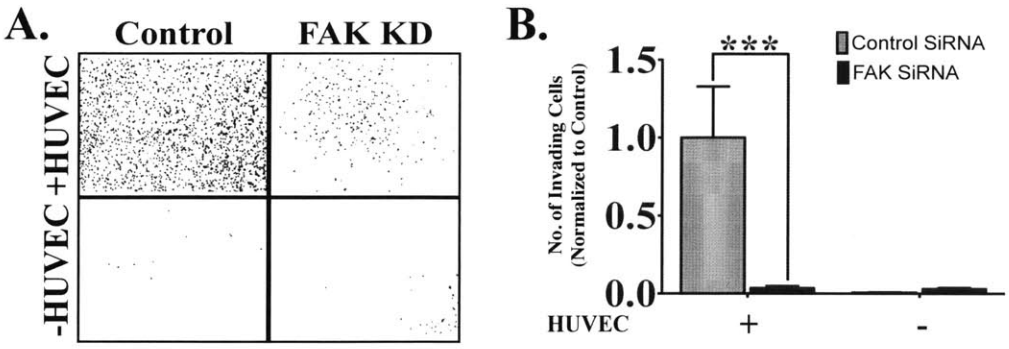

Figure 3-36: FAK KD decreases migration of metastatic breast cancer cells. Knockdown of FAK expression leads to defects in cell migration. (A) Images and (B) quantification results showing a decline in cell migration. The decrease in migration likely contributes to the disrupted EEC interaction phenotype seen in co-culture.

here to the endothelium or defects in the ability of the metastatic cells to effectively migrate toward the endothelial tubes. To distinguish these contributions, we examined the effect of FAK inhibition on migration. **Figure 3-36** shows the result of a Boyden chamber invasion assay examining migration of metastatic cells after FAK knockdown. Loss of FAK seems to affect both the ability of the cells to adhere to one another, as well as the migratory capability of the metastatic cells. FAK knockdown inhibited the ability of these cells to migrate towards the endothelial cells. Loss of FAK expression leads to migrational defects which may in part explain the disrupted EEC interaction phenotype.

Recruitment of angiogenic vessels by tumor spheroids is a PI3K dependent pathway. Recruitment of vessel structures was captured over 100 minutes. The vessel structures do not form randomly, but instead are directly recruited by the tumor spheroids. This experimental design differs from the traditional co-culture setup because endothelial cells are added to pre-existing tumor spheroids, therefore instead of capturing EEC interaction phenotypes, this experiment captures angiogenesis. Increasing concentrations of the PI3K inhibitor, LY294002, disrupted formation of endothelial vessel structures **(Figure 3-37B)** leading to an increased expression of apoptotic markers **(Figure 3-37C)**.

Ours results illustrate that RNAi inhibition of FAK and β-1 integrins can dis-

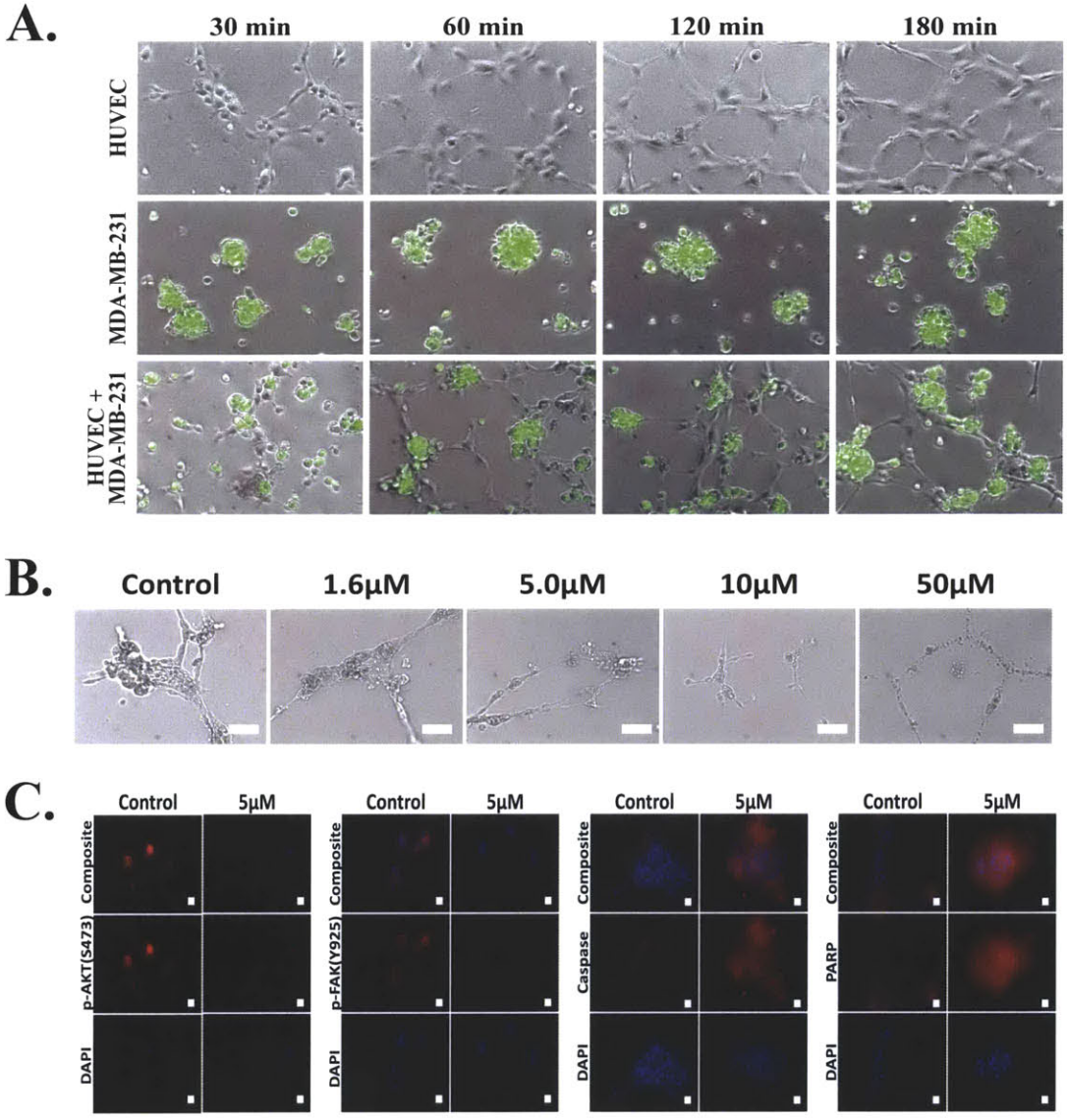

Figure 3-37: PI3K pathway is critical for endothelial cell biology. (A) Recruitment of angiogenic vessels by tumor spheroids is dependent on PI3K. Vessel recruitment assay shows recruitment of endothelial vessels by tumor spheroids. (B) Endothelial vessels can be disrupted by the PI3K inhibitor LY294002. (C) Treatment with the PI3Ki led to a decrease pAKT expression and an increase in apoptotic markers (e.g. caspase-9 and pARP). Interestingly, there was also inhibition of p-FAK after treatment with PI3Ki. This may be due to a feedback loop.

rupt the co-culture phenotype. However, can small molecule inhibitors of their downstream targets also disrupt EEC interactions? Using small molecule inhibitors to disrupt interactions between metastatic cells and the endothelium expands the utility of the model system into a tool for screening therapeutics.

To test this hypothesis, we used commercially available inhibitors of the PI3K and MAPK pathways. These pathways were targeted for two primary reasons. The first is because they are downstream of the integrin-FAK signaling axis and enable testing of targets further downstream of these pathways. The second is due to differential activation of the AKT and ERK signaling pathways in the endothelial and tumor compartment, respectively.

A dose titration was performed using the PI3K inhibitor, LY294002, and the mitogen activated protein kinase (MAPK) inhibitor, PD98059, in the MDA-MB-231 cells to determine the dose of drug that inhibited signal but did not lead to toxicity **(Figure 3-38A)**. Once appropriate drug doses were determined, the effects of the drugs on proliferation and migration of the MDA-MB-231 cells was tested using both free drug and a hybrid nanoparticle conjugated with both inhibitors **(Figure 3-38B,C)**. Inhibition of these pathways lead to defects in both proliferation and migration of the MDA-MB-231 cells, suggesting that the combination of these inhibitors would be an effective strategy for targeting EEC interactions.

Treatment of co-cultures with a combination of these inhibitors disrupted the co-culture phenotype similarly to results obtained with RNAi of FAK and β-1 integrins. Furthermore, drug treatment increased the susceptibility of the cultured cells to doxorubicin treatment **(Figure 3-39A,B)**. Combination of the three inhibitors resulted in complete disruption of the EEC phenotype. Fragmented vessel structures are seen after drug treatment. There is minimal interaction between the cell types. In fact, there is very little cellularity after drug treatment indicative of cell death in response to treatment. These results are further confirmed by examining apoptosis markers. There is an increase of PARP signaling following treatment, further supporting the decreased cellularity present in the representative images **(Figure 3-39C)**. Lastly, quantification of the EEDI showed increased dissociation

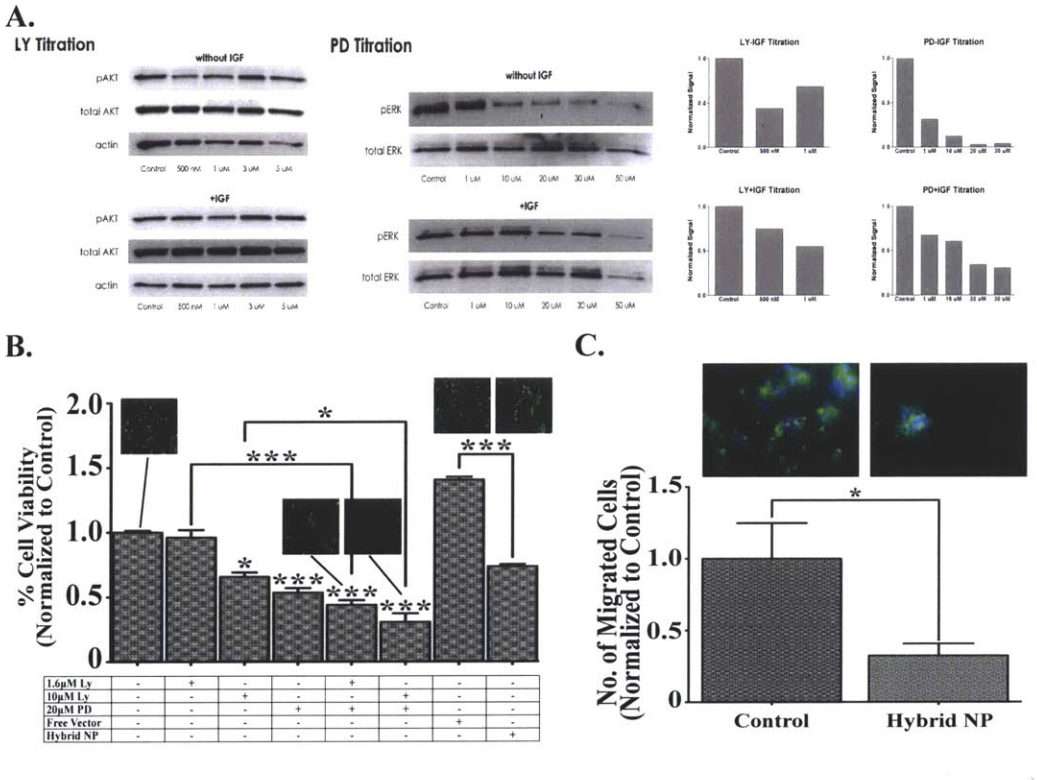

Figure 3-38: Inhibiting the PI3K and MAPK pathways affects migration and proliferation of MDA-MB-231 cells. (A) Dose titration was performed to determine appropriate drug concentrations. Combination of PI3Ki and MAPKi leads to defects in (B) proliferation and (C) migration of MDA-MB-231 cells. These defects likely both contribute to reduced EEC interactions.

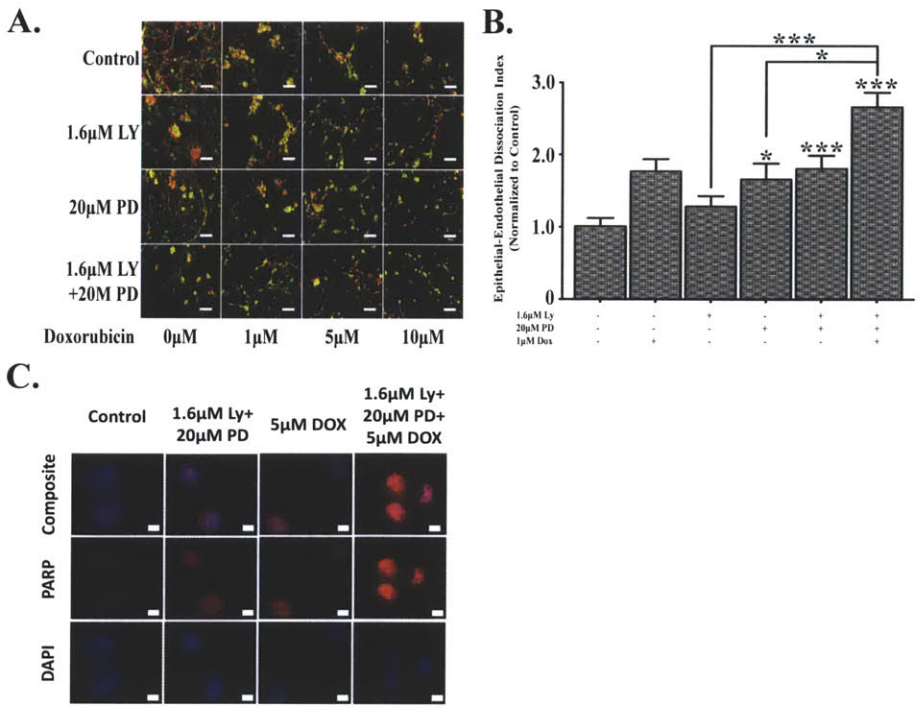

Figure 3-39: Combination of PI3Ki and MAPKi reduce EEC interaction phenotypes. (A) Images and (B) quantification of co-cultures following treatment with a combination of inhibitors targeting the PI3K and MAPK pathways. (C) Drug treatment results in increased apoptosis markers.

characteristic of the decreased cell-cell interaction observed after knockdown of FAK and β-1 integrins. Nevertheless, inhibition of PI3K and MAPK pathways was not as potent as inhibition of FAK or β-1 integrins. These results further support the conclusion that targeting mediators further downstream in the pathways may be less effective in disrupting EEC interactions. To probe this observation, we next targeted an upstream regulator of PI3K and MAPK that could be inhibited with drug.

Similarly to the FAK integrin signaling axis, EGFR also acts through the PI3K and MAPK pathways **(Figure 3-40A)**. Abberations in EGFR signaling have been strongly linked to cancer of the breast. Furthermore, there are several commercially available inhibitors to target this receptor. Therefore, we tested the effects of EGFRi on the metastatic co-culture phenotype. Similar to previous results, treatment with EGFRi led to defects in cellular proliferation **(Figure 3-40F)**, migration

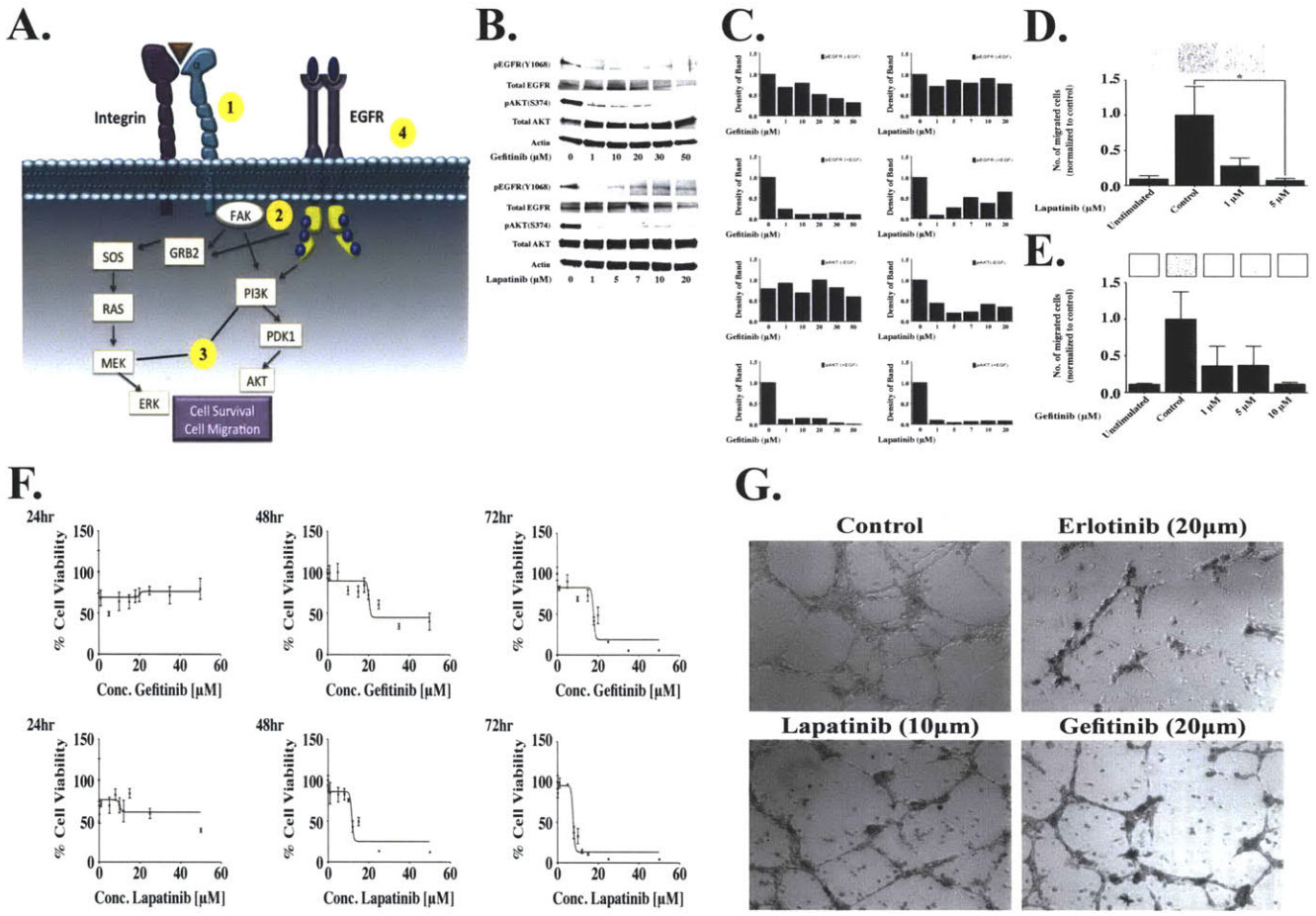

Figure 3-40: Inhibition of EGFR signaling disrupts the co-culture phenotype. (A) EGFR pathways acts through PI3K and MAPK pathways. (B/C) Dose titration using increasing concentrations of EGFRi leads to pathway inhibition. Inhibition of EGFR signaling results in decreased cellular (D/E) migration, (F) proliferation, and EEC interactions.

(Figure 3-40D), and disruption of the EEC interaction phenotypes **(Figure 3-40G)**. Future work may investigate further the role of the EGFR pathway in EEC interaction phenotypes.

3.6.1 Conclusion of drug studies

We demonstrated that FAK and β-1 integrin signaling are important mediators of the observed phenotypes. Inhibiting FAK-β-1 signaling disrupted the architecture, reducing the ability of the MDA-MB-231 cells to migrate and adhere to preformed vessels. Furthermore, treatment with small molecule inhibitors of phosphatidylinositol 3 kinase, LY294002 1.6uM, and mitogen activated protein kinase (MAPK), PD98059 20uM, also perturbed this architecture, indicating that these signaling pathways play a key role in controlling the observed phenotype. Furthermore, the inhibition of the PI3K and MAPK pathways destroyed the tumor vasculature and inhibited progression and invasion of the MDA-MB-231 by 86% ($p<0.001$) while enhancing the cells susceptibility to the cytotoxic agent doxorubicin. We also showed that inhibitors of EGFR signaling can also disrupt EEC interactions, further emphasizing the utility of the model. Our studies show that a three-dimensional co-culture system provides a powerful *in vitro* model system to study the mechanisms underlying tumor metastasis and is a powerful tool to screen combination therapies.

3.7 Summary of co-culture model system data

This chapter outlines the development of a co-culture model system to study unique interaction phenotypes between epithelial cells and the endothelium. Understanding these interactions may provide insight into mechanisms underlying cancer metastasis, which could in turn offer new therapeutic strategies for the treatment of cancer. The data demonstrates that soluble factors released by endothelial cells enhance the proliferation and invasion of metastatic cells that presumably enable the

cells to effectively home to the endothelium **(Figure 3-41A)**. Once in contact with the endothelium, the cells undergo cytoskeletal deformation, flattening, and elongation along the vessel **(Figure 3-41B and C)**. Surprisingly, the co-culture model system could even capture intravasation of the epithelial cells into the endothelial tubes. Confocal images show that the epithelial cells begin to intravasate into the endothelial lumens **(Figure 3-41D)**, finally appearing completely within the endothelial cell lumen **(Figure 3-41E)**. Furthermore, the data demonstrates that these interaction phenotypes could be targeted by disrupting pathways implicated in cell-cell adhesion. This suggests that the model system may provide a platform to screen pharmacological therapies targeting both the tumor and the endothelial compartments.

This data furthers understanding of the biomechanical and chemokine signaling mechanisms critical to defining EEC interaction phenotypes. However, it does not address the role of intercellular communication in EEC interactions. The following chapters discuss the identification of a novel form of intercellular communication that enables direct communication between tumor cells and the endothelium. Communication through thin cytoskeletal projections that connect the two cell types may underly potential mechanisms of pathological angiogenesis.

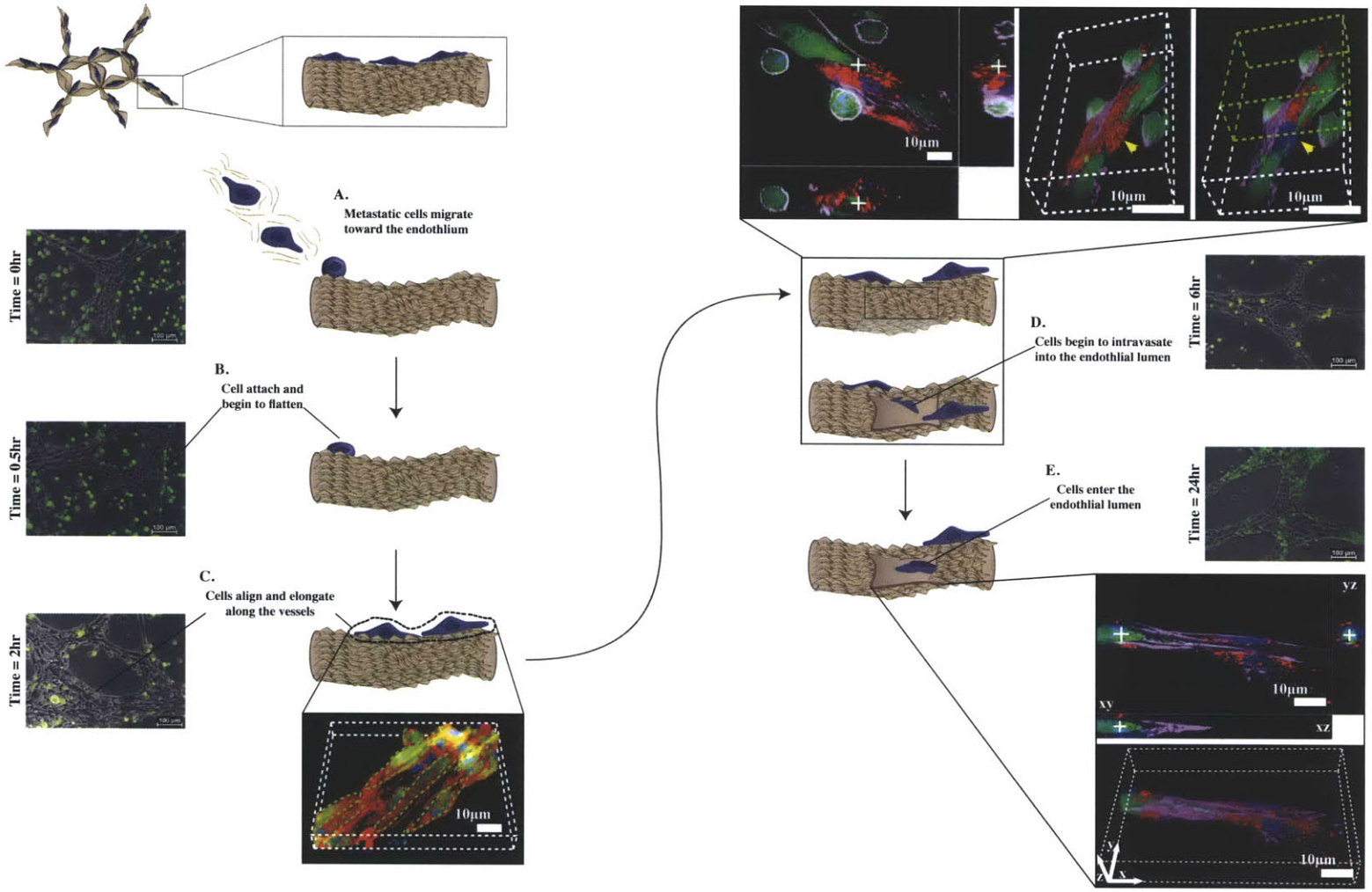

Figure 3-41: Overview schematic of steps captured by the co-culture model. CFSE (green) labeled metastatic breast epithelial cells are added to the matrix containing DiL-Ac-LDL (red) labeled endothelial tubes. The figure depicts the distinct stages captured in the co-culture model.

Chapter 4

NanoChannel-mediated communication between metastatic breast cancer cells and the endothelium

4.1 Introduction

Uncovering molecular mechanisms underlying metastasis is the final-frontier in cancer biology[7–9]. Currently, therapeutic options for advanced invasive disease are limited, resulting in dismal 5-year survival rates[8]. Cancer metastasis is difficult to study due to dynamic and reciprocal system-wide interactions that define the advanced stages of cancer[20]. Metastasis is a complex process with many discrete stages: development of the primary tumor, progression to invasive disease, intravasation, transport and survival in the systemic circulation, extravasation at distant sites, colonization of secondary tumor sites, and induction of neovasculature by the micrometastatic colony[7,8]. While there has been much research on the seed (metastatic tumor cells) and the soil (colonized host tissue) hypothesis, limited knowledge exists on the interaction between metastatic cells and vascular en-

dothelial cells, which leads to attachment and extravasation. Metastatic cell interactions with the endothelium is a pre-requisite for the development of metastatic disease and presents a key point of therapeutic intervention[7,102,105,106].

Intercellular communication between cancer cells and the endothelium is a key element in metastasis[287]. For example, early studies implicated traditional chemokine signaling (e.g. secreted soluble factors) in mediating the retraction of endothelial cells and the subsequent attachment and transmigration of tumor cells through the endothelial monolayers[105]. More recent studies indicate that physical interactions between cells can also mediate intercellular communication promoting cancer progression. For example, heterocellular gap junctional intercellular communication was reported to be involved in breast cancer diapedeses through the endothelium[305]. Similarly, intercellular membrane exchange was recently implicated in cell-to-cell p-glycoprotein transfer resulting in multidrug resistance in breast cancer cells[209]. Taken together these results suggest that better understanding of tumor-endothelial intercellular communication can offer attractive therapeutic opportunities in the management of metastatic cancer[142,209,287,305,306].

An emerging mechanism of intercellular communication is through the formation of physical nanoscale structures. Recently, a novel form of cellular communication was discovered wherein direct transfer of intercellular contents occurs through thin, nanotubular projections called tunneling nanotubes (TNTs)[2]. Since the initial observation of TNTs in rat pheochromocytoma cells (PC12)[2], TNT and TNT-like structure have been observed in prokaryotic[174] and diverse eukaryotic cell types, such as neuronal, immune, and epithelial cells[2,3,117,175]. TNTs form continuous connections between cells, serving as a conduit for dynamic cell-cell exchange of contents over hundreds of microns of physical separation[117,193]. These structures mediate the transfer of a diverse array of cellular contents, including organelles, proteins, and pathogens[117,176,178,193]. TNTs may serve important roles in disease pathology, highlighting the motivation to understand their physical properties and biological characteristics[178,193,195]. For example, in a recent study the formation of tunneling nanotubes (TNTs) was shown to mediate bacterial com-

munication resulting in the transfer of non-hereditary resistance. Similar structures have been shown to facilitate HIV-1 transmission between T cells[178], traffic organelles[2], and enable the spread of calcium-mediated signal between connected cells[180]. TNTs have been implicated in cancer promoting mechanisms in breast cancer cells and malignant plueral mesothelioma[203,209]; however, the role of physical intercellular communication between tumor cells and endothelium during metastasis is yet underexplored. Transport of intercellular cargo through TNT or TNT-like structures may mediate pathological transformation of tumor stromal cells that is commonly seen in cancer[20,203].

In this chapter, I describe a novel form of intercellular communication between metastatic cells and the endothelium. Formation of nanoscale tubular structures, or *nanoChannels* (nCs), mediates early intercellular communication between tumor epithelial cells and the endothelium *in vitro* and *in vivo*. The ability to form such nanoChannels correlates with metastatic potential of the tumor cells and enables direct trafficking of both synthetic materials (chemicals and nanoparticles) and bioorganic macromolecules (proteins and miRNAs).

These structures were examined in a 3D *in vitro* co-culture model system capturing molecular and physical interactions between metastatic cells and the endothelium. NanoChannel (nC) connections are structurally unique compared to other TNT projections in both composition and transported cargo. We make the functional distinction between nCs and TNTs because nCs contain actin and tubulin cytoskeletal components, while only a fraction of the TNTs described have both. Furthermore, nCs seem to indiscriminately transport small molecules, and particles, including proteins, small fluorescent dyes, organelles, nanoparticles, and cytoplasmic RNAs through active and passive mechanisms. As one specific example, we show that miR-132, which is implicated in pathological angiogenesis[129], can translocate from tumor cells to the endothelial cells through the nanoChannels, resulting in decreased p120RasGAP and activation of AKT in the recipient endothelial cells. Furthermore, in the endothelium, nanoChannel-mediated communication resulted in the upregulation of markers of pathological angiogenesis, such

as CD137 and CD276[307]. The increase in these pathological angiogenesis markers could be reduced by pharmacological inhibition of nanoChannel formation. We refer to this phenomenon as *metastatic parasitism* which describes the transformation of a normal endothelial cell into a pathological phenotype induced by intercellular communication received from metastatic cancer cells through nanoChannels. Targeting the formation of these nanoChannels and the resulting *metastatic parasitism* may potentially emerge as a new therapeutic opportunity in the management of metastatic cancer.

4.2 NanoChannels form visible connections between metastatic cells and the endothelium

4.2.1 Experimental Design

To study nanoChannel-mediated communication between metastatic cells and the endothelium, we utilized our previously described 3D co-culture model system **(Chapter 3)**. The engineered 3D co-culture model creates an ecosystem that closely mimics tumor pathophysiology, where endothelial tubulogenesis was enabled on a laminin-rich basement membrane tumor-derived matrix prior to the addition of tumor cells. In contrast to the characteristic tumor spheroids (mammospheres) that are formed in 3D monocultures[16] **(Figure 4-1)**, the metastatic MDA-MB-231 breast cancer cells preferentially interacted with the endothelium (ENDO), aligning on and incorporating into the vascular network **(Figure 4-1, solid arrow)**. This phenotype differs from that present in 2D cultures, where there is limited interaction between epithelial cells (EPI) and the endothelium. Instead, in 2D co-cultures the epithelial cells segregate into epithelial islands **(Figure 4-1, circle)**, which sit upon a layer of endothelium **(Figure 4-1, dotted arrow)**. This phenotype had been previously described in a lung epithelial-endothelial 2D co-culture model[147].

The co-culture phenotype was validated using scanning electron microscopy (SEM) **(Figure 4-2A1,A2)**. Interestingly, inspection of the model system using SEM

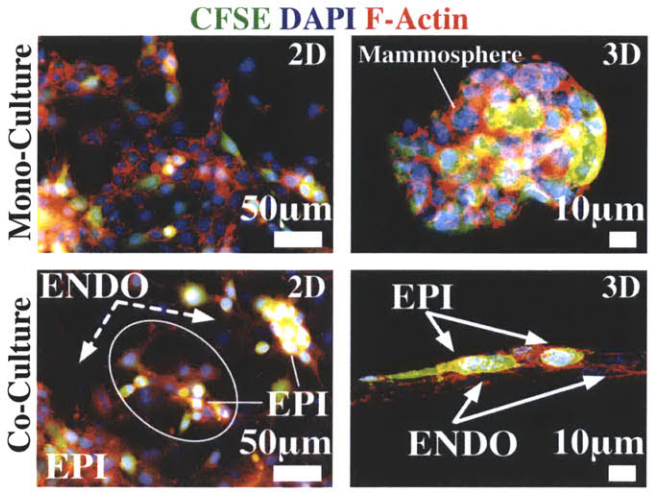

Figure 4-1: Three-dimensional co-cultures provide a physiologically relevant platform to study interactions between metastatic cancer cells and the endothelium. Epifluorescence imaging of 2D and 3D monocultures and co-cultures of metastatic cancer cells (EPI) and the endothelium (ENDO). CFSE (green) loaded MDA-MB-231 tumor cells were incubated with pre-formed HUVEC endothelial tubes in a 3D matrigel® matrix followed by immunostaining with rhodamine phalloidin and counterstaining with DAPI. In the 3D platform, the metastatic breast cancer cells interact directly with the endothelium, elongating and aligning along the endothelial vessels (solid arrow). This phenotype contrasts with the mammospheres observed in traditional 3D monotypic cultures. In 2D co-cultures, there is segregation of cell types where epithelial cells cluster together in epithelial islands (circle) atop a bed of endothelial cells (dashed arrows).

revealed nanoscale tethers connecting the tumor and endothelial cells **(Figure 4-2B)**. The change in phenotype from round to elongated in co-culture was consistent with observations in previous studies of tumor cells adopting elongated, spindle-shaped morphologies as a consequence of interaction and migration through endothelial layers[105]. Interestingly, long filopodial extensions were also observed in these cells, reminiscent of nanoscale membrane projections seen in our system[105].

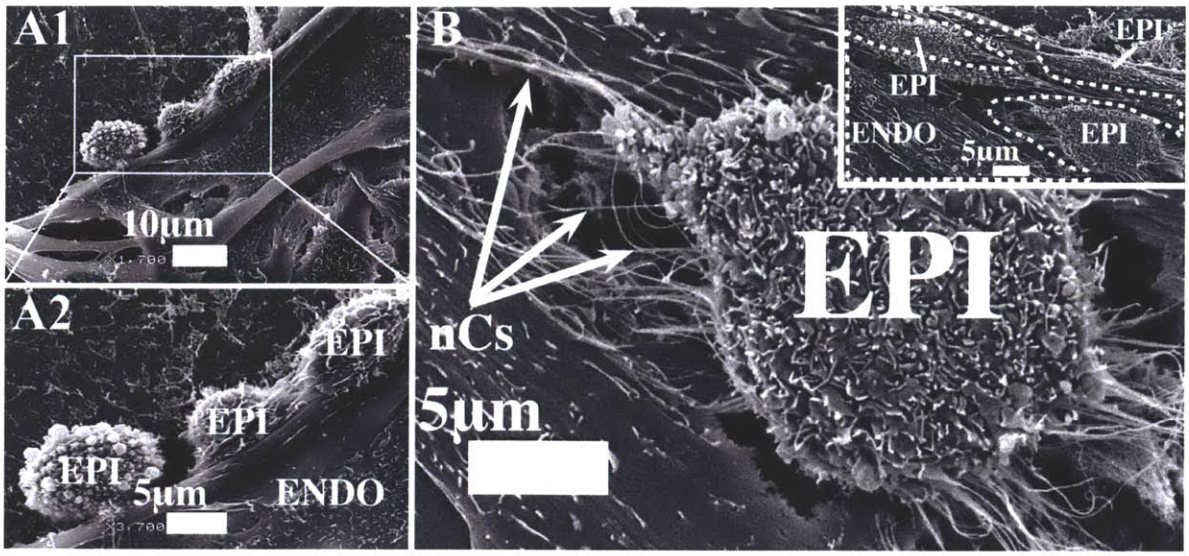

Figure 4-2: SEM images of co-cultures model reveal intimate interactions between metastatic cells and the endothelium. (A1/A2) Metastatic breast epithelial cells MDA-MB-231 (EPI) align along endothelial tubes (ENDO). Metastatic cells preferentially interact with the endothelium compared to normal and tumorigenic, non-metastatic cell lines. (A2) Higher magnification view of the intimate interactions between the cell types. (B) NanoChannels (nCs) form connections between metastatic breast epithelial cells and endothelial tubes (arrow). NanoChannel structures project from the surface of the metastatic epithelial cell to the surface of the endothelium. Inset shows lower magnification view.

4.2.2 Characterization of nanoChannel structures

In an attempt to better understand the unique properties of nanoChannel projections, the physical dimensions, the kinetics of formation and the composition of nanoChannel structures were characterized. Whenever possible, attempts were made to provide quantitative, as well as qualitative descriptions of the structures. From the results of this quantification emerged a definition of what structures are considered nanoChannels, providing clear distinctions from other cytoskeletal projections, such as lamellipodia and filopodia.

4.2.2.1 NanoChannels contain actin and tubulin cytoskeletal proteins

To understand the physical properties of nanoChannels, the cytoskeletal compositions of the structures were determined. Immunocytochemistry staining with

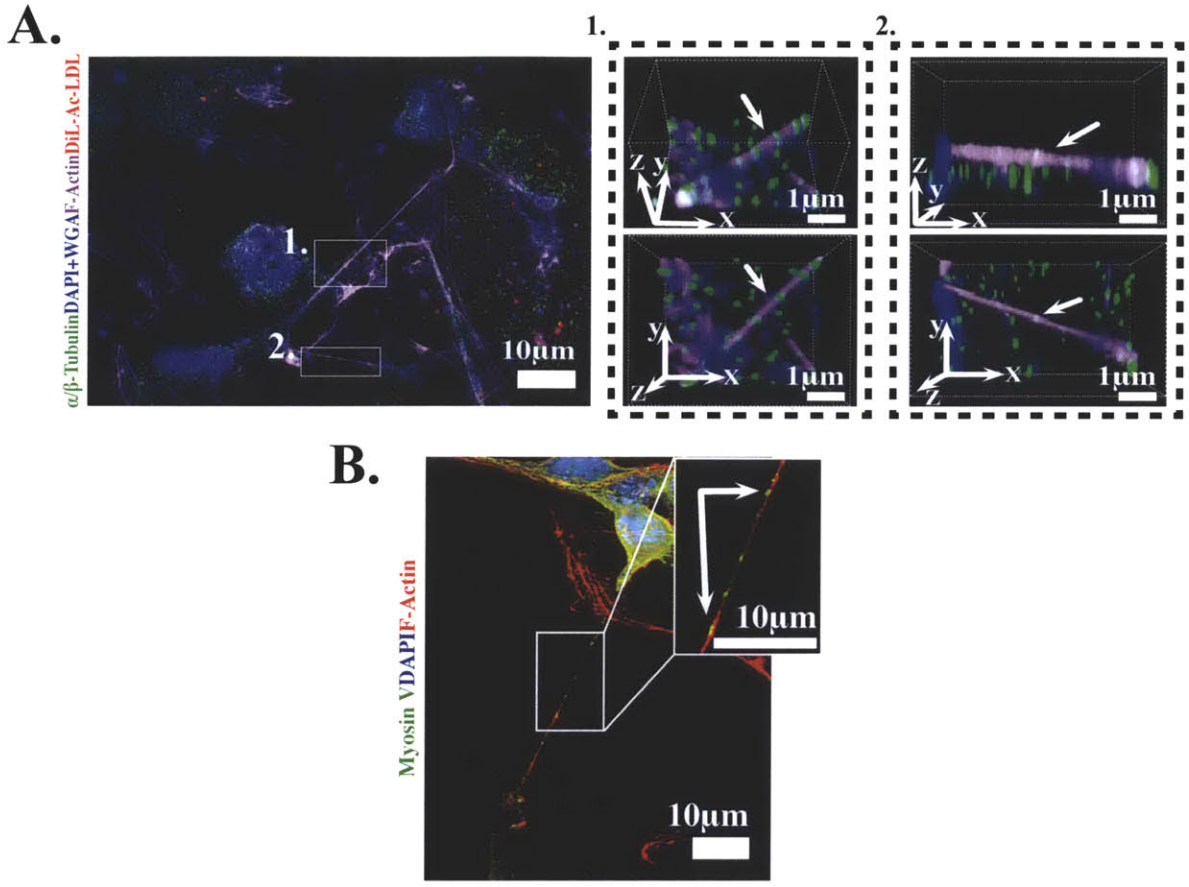

Figure 4-3: NanoChannels contain both actin and tubulin cytoskeletal components. Unlike TNTs, which are typically formed from actin fibers[2,3], the nanostructures observed in this study included both F-actin and α/β-tubulin cytoskeletal components. (A) Representative epifluorescence images reveal F-Actin and α/β-tubulin cytoskeletal components within nC structures. Co-cultures were stained with α/β-tubulin antibody (green) and phalloidin (purple) and counterstained with DAPI (nuclear) + WGA (plasma membrane) (blue). Endothelial cells were labeled with DiL-Ac-LDL (red). (B) Immunocytochemistry revealed the presence of myosin V (green) within the nCs. The presence of myosin V motor proteins suggests a possible active transport mechanism in intercellular transfer of cargo within nCs. Samples were counterstained with phalloidin (red) and DAPI (blue).

α/β-tubulin and phalloidin identified tubulin and actin cytoskeletal components, respectively, within the nanoChannel structures **(Figure 4-3A)**. This was a unique finding because previous observations of similar structures (i.e. TNTs) in other cell types describe these projections as containing only F-actin cytoskeletal components[2,3]. However, examination of TNT structures in macrophages did identify tubulin cytoskeletal components in larger TNTs ($\geq 0.7\mu$m), suggesting that the incorporation of tubulin cytoskeletal components may alter the physical properties of the structures[176]. Additionally, immunocytochemistry with a myosin V antibody revealed a punctate expression signature within the nanostructures, suggesting an active transport system may exist within nCs **(Figure 4-3B)**. The myosin family is a group of actin motor proteins that function in many diverse and important cellular properties. Specifically, myosin V has been implicated in transport of RNAs, membrane trafficking, and establishing cellular polarity[308]. Identification of myosin V motor proteins holds interesting prospects for the possibility of an active transport based mechanisms within nCs.

4.2.2.2 Measurement of physical dimensions of nanoChannels

Experimental design To better understand the physical properties of nanoChannels and to clearly distinguish nanoChannels from other projections, the dimensions of these structures were quantified in the MDA-MB-231 cell line. This quantification was performed on greater than 300 cells from a minimum of 5-6 culture replicates for 2D and 3D cultures in both monoculture (culture with only epithelial cells) and co-culture (culture with epithelial cells and HUVEC endothelial cells) formats. Quantification of length (long axis) and width (short axis) of nanoChannel structures was determined using either fluorescence microscopy or SEM. Structures were grouped into the following categories:

1. nCs from 2D monocultures imaged with SEM
2. nCs from 3D monocultures imaged with SEM
3. nCs from 2D monocultures imaged with Fluorescence Microscopy

4. Other projections (non-nC) from 2D monocultures imaged with SEM

5. nCs from 2D co-cultures imaged with SEM

6. nCs from 3D co-cultures imaged with SEM

7. nCs from 2D co-cultures imaged with Fluorescence Microscopy

8. Other projections (non-nC) from 2D co-cultures imaged with SEM

Figure 4-4 shows representative illustrations of nanoChannels versus *other projections*. In our quantification schema, the category of *other projections*, in general, includes lamellipodia and filopodia, the most common cellular projections[88]. **Figure 4-4 A and B** compare the structures of filopodia, lamellipodia, and nanoChannel projections. Filopodia contain parallel actin bundles while lamellipodia and nCs are composed of both actin and tubulin cytoskeletal components. Lamellipodia are typically wide and flat containing a meshwork of actin at the leading edge supported by a zone of microtubules and function primarily for migration[88]. In contrast, filopodia are much smaller projections (similar in size to nCs), functioning primarily for environmental sensing. Although filopodia and lamellipodia are structurally distinct, for the purposes of this quantification, they are grouped together in the category *"other projections"*.

The following constraints were applied when classifying these structures:

1. The structure must extend from one cell (donor) and physically come in contact with another cell (recipient) **(Figure 4-5A)**. Incomplete or broken projections were not considered to be nanoChannels **(Figure 4-5D)**. Small hair-like structures **(Figure 4-5B)** were also not considered to be nanoChannels and were instead considered to be filopodia and fell into the category of *other projections (non-nC)*. The only exception to these rules was quantification performed at time points $\leq 6hrs$ or quantification performed after pharmacological inhibition of nCs. NanoChannel formation was found to peak approximately 5-6hrs after plating of cells. At early time points (i.e. before mature

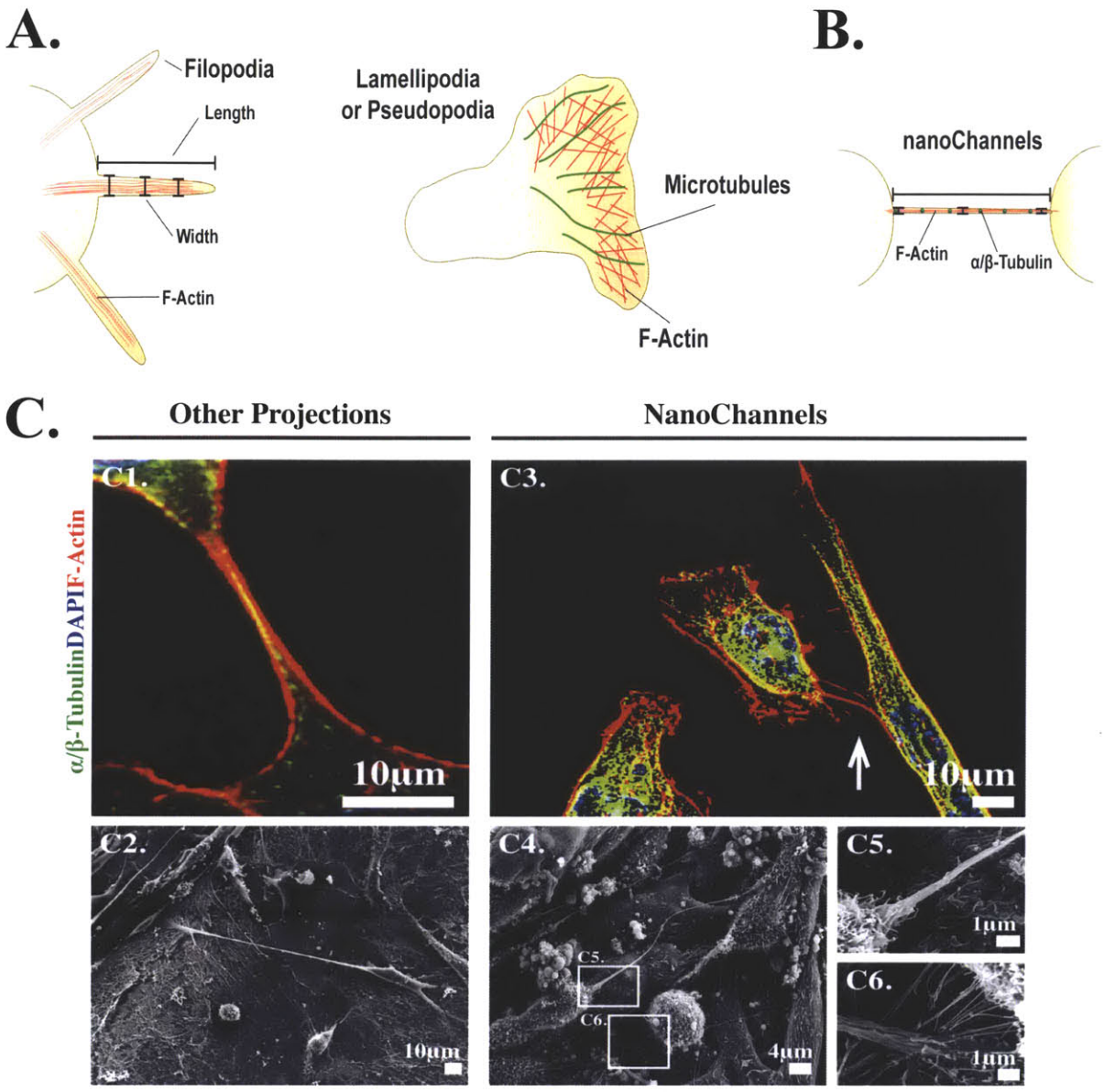

Figure 4-4: Schematic of nCs versus other cytoskeletal projections. (A) Filopodia are composed of parallel actin bundles, while lamellipodia contain a meshwork of actin filaments supported by a zone of microtubules. (B) nCs are structurally unique. They are approximately the same physical dimensions as filopodia but contain both actin and tubulin cytoskeletal components. (C) Images illustrating other projections versus nC structures. NanoChannels are thinner structures, while many of the other projections quantified in the culture are typically much wider. (C4-6) nCs are very structurally diverse, ranging from linear projections to structures with large curvatures.

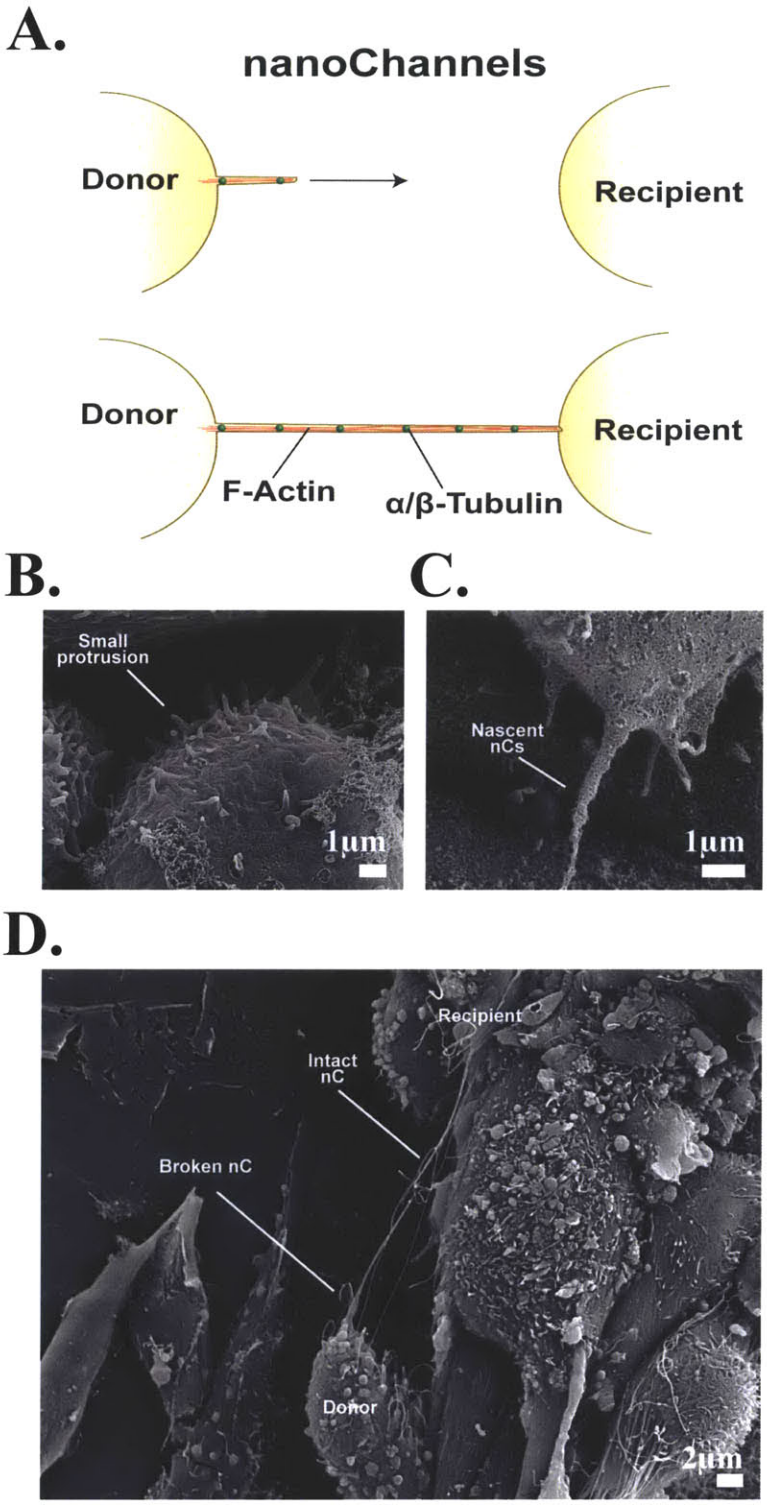

Figure 4-5: Rules for defining nC structures. (A) Schematic illustration of nC growth. A structure must extend from a donor cell, an epithelial cell, to a recipient cell, typically an endothelial cell, in order to be considered an nC. SEM images show examples of (B) small protrusions, (C) nascent nCs, or (D) broken nCs.

nanoChannels are formed) or after pharmacological inhibition of nCs, filopodia **(Figure 4-5B)**, disrupted (broken) nCs **(Figure 4-5D)**, and nascent nCs **(Figure 4-5C)** appear indistinguishable. In these limited circumstances, small hair-like projections were also included as potential nCs or disrupted nCs for the purpose of quantifying nC structure formation kinetics **(Section 4.2.2.4)** or nC formation disruption by pharmacological inhibitors (cytoskeletal polymerization inhibitors) **(Section 4.4)**, respectively. Except for the above mentioned circumstances, quantification was performed 24hrs post culture, and only intact nC structures were considered. Any deviations from the descriptions above are noted on a case-by-case basis.

2. The length (long axis) of the nC projection was measured from the point of origin to the point of termination **(Figure 4-6)**.

3. Due to size variabilities in length of nC projections, three width (short axis) measurements were taken at distinct positions along the length of the nC structure. The three width measurements were used to obtain an average width **(Figure 4-6)**.

4. The length of non-linear nC structures were quantified by summing the lengths of shorter linear segments **(Figure 4-6)**.

5. NanoChannel structures were classified as intercellular connections, approximately ≤ 1 μm in width.

NanoChannel structures have unique physical characteristics The nanostructures observed in our model system have unique physical dimensions. These projections are thinner (short axis: $0.31\pm0.01\mu$m)($p < 0.0001$) and longer (long axis: $36.58\pm2.07\mu$m) ($p < 0.0001$) than other cytoskeletal projections such as lamellipodia and filopodia (short axis: $4.99\pm0.23\mu$m; long axis: $12.90\pm1.79\mu$m) that primarily function in cellular migration and chemotactic sensing **(Figure 4-7A)**. These averages were obtained by measuring nC structures present in MDA-MB-231 and

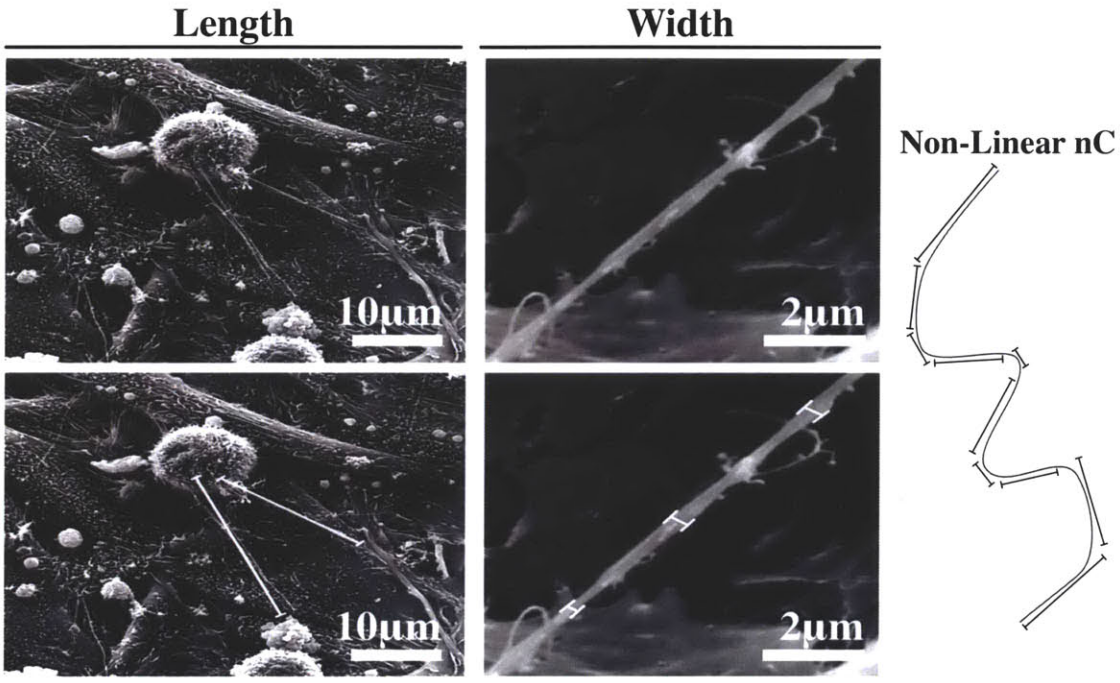

Figure 4-6: Demonstration of nanoChannel length and width measurements. This schematic provides an illustration of how length (long axis) and width (short axis) measurements were performed. The long axis (length) of the structures were considered from the point of origin (donor cell) to the point of termination (recipient cell). Due to size variabilities along the length of the structures, measurements of the short axis were taken at three distinct positions along the length of the structure and then averaged together to obtain an average width measurement. Non-linear nC structures were quantified by summing the lengths of shorter linear segments.

HUVEC epithelial-endothelial co-cultures. To determine if nCs structures were unique to the 3D culture format nCs measurements from both 2D and 3D cultures were compared **(Figure 4-7B)**. There were no statistical differences between the widths of nCs in either culture format. However on average, the length of nCs in 3D co-cultures is slightly shorter than the average length of structures in 2D. This reflects the close proximity of the cell types in 3D epithelial-endothelial co-cultures. In contrast to the intimate interactions formed in 3D cultures, in the 2D cultures we observe segregation of cells types **(Figure 4-1)**. Because the cells are spatially separated (farther away) in 2D, on average, nCs are slightly longer in these cultures. However, in all other comparisons (e.g. composition, cargo transported) nC structures in 2D and 3D cultures are similar. Therefore, we concluded that this difference likely arises as an artifact of the culture and that the structures in 2D and 3D cultures are identical in composition and function.

We also assessed which imaging modality, SEM or fluorescence microscopy, would allow for more precise identification of nC projections **(Figure 4-7B)**. There are strengths and limitations to both techniques. For example, correlative microscopy (i.e. the ability to determine relationships between structure and function) is significantly more straight forward using fluorescence microscopy than with traditional electron microscopy (EM). Furthermore, EM suffers from complex sample preparation requirements that are both cumbersome and mechanically stressful on the samples, often disrupting delicate structures. On the other hand, EM allows for powerful resolving capacity that could never be achieved with fluorescence microscopy.

We performed a side-by-side comparison of the projection length and width quantification measurements using SEM and fluorescence microscopy. As hypothesized, thinner structures could be observed using SEM, yielding an average width of $0.32\pm0.02\mu$m compared to $1.53\pm0.13\mu$m ($p < 0.0001$) for 2D co-culture samples imaged with fluorescence microscopy. Interestingly, nCs imaged with fluorescence microscopy were also slightly longer ($60.15\pm6.24\mu$m) than nCs in analogous cultures imaged with SEM ($42.46\pm3.26\mu$m) ($p < 0.0001$). There is a degree of error

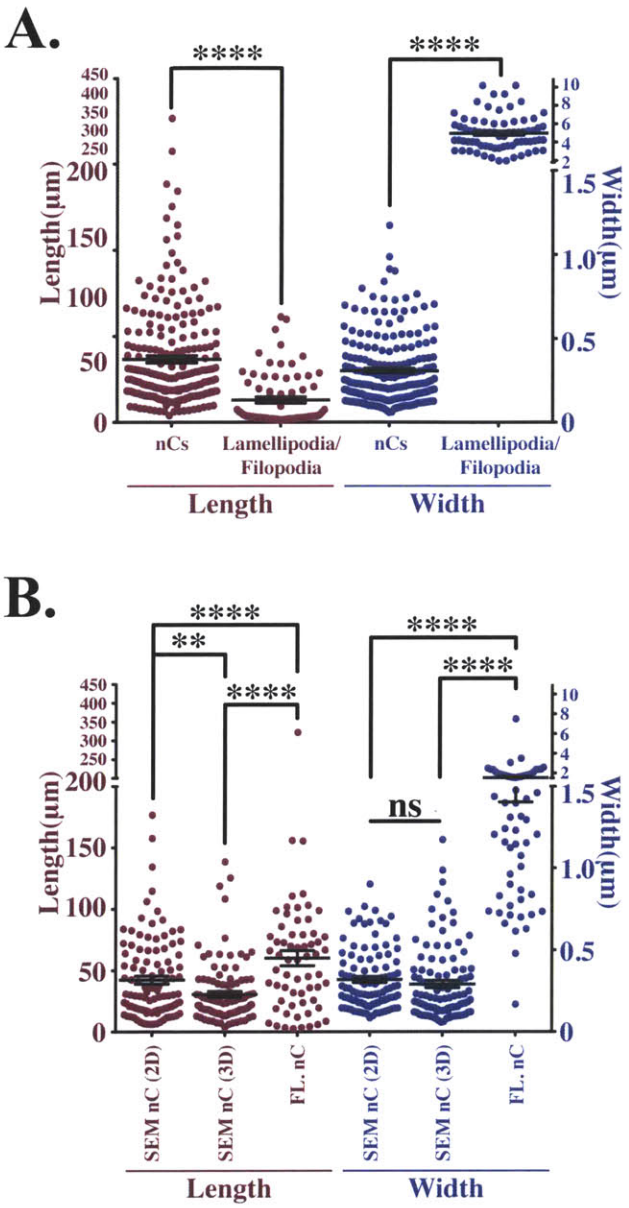

Figure 4-7: Physical dimensions of nanoChannel projections. (A) Length and width of nanoChannels (nCs) and larger cytoskeletal projections, such as lamellipodia and filopodia were quantified using SEM. NanoChannels have unique physical properties. They are much thinner and longer then other cytoskeletal projections found in co-cultures ($p < 0.0001$). (B) Length and width of cytoskeletal projections in 2D versus 3D cultures. nCs have the same width dimension in both 2D and 3D. However, nCs are slightly longer in 2D likely due to the spatial separation of the cells. SEM captures smaller projections that are not easily visible with fluorescence microscopy.

associated with length scale measurements made on SEM micrographs due to foreshortening effects. Efforts were made to minimize this error; however, since our measurements were conducted on biological samples for the purposes of distinguishing nCs from different classes of cellular projections and because we were dealing with relatively large length scales, greater error was tolerated. However, this error may explain the differences between length measurements made using fluorescence microscopy versus SEM. An additional explanation may be that due to the mechanical stress of SEM sample preparation the larger projections may have broken. Nevertheless, projections larger than 200μm can be observed in SEM micrographs **(Figure 4-8)**.

Identification of a characteristic length A characteristic size descriptor, defined as the width:length ratio of the projections, can be used to distinguish nCs (0.0134$\pm$0.001) from other cytoskeletal projections (1.254$\pm$0.140) ($p < 0.0001$). Plotting the characteristic size of the structures against width shows a visible difference between nCs and other projections. **(Figure 4-9B)**. On a plot of width versus length **(Figure 4-9A)**, nCs cluster distinctly from other projections ($n > 300$). Defining appropriate lengths scales may provide insight into future work examining transport dynamics within nC structures.

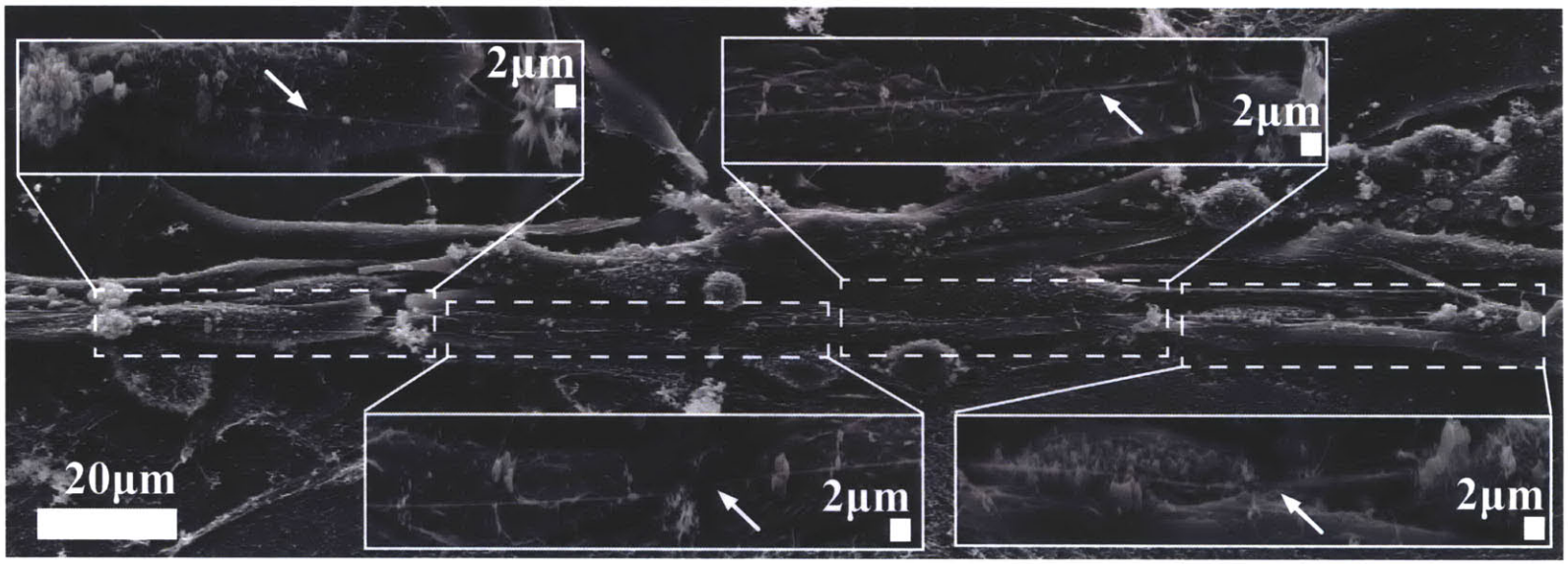

Figure 4-8: nC structures can span hundreds of microns of distance.

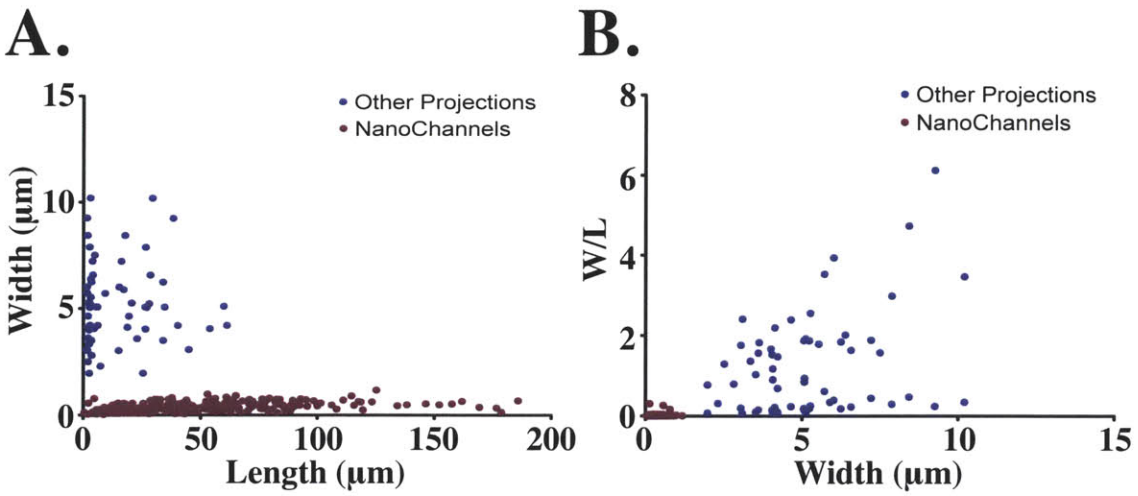

Figure 4-9: NanoChannel characteristic size descriptor (A) Length and width dimensions of nCs and other projections were plotted, demonstrating unique length scales of nCs. (B) A characteristic length scale was defined by taking a ratio of the width:length of the projections. This parameter was plotted against width. nCs tightly cluster at W/L ratio less than 0.3036.

Comparison of nCs in co-cultures versus monocultures In order to assess whether nC structures were unique to co-culture model systems, we compared nC projections in MDA-MB-231 epithelial-epithelial cultures with MDA-MB-231 and HUVEC co-cultures. We assessed the physical characteristics of the projections, as well as the percentage of the population expressing nCs and the average number of nCs per cell. There were no measurable differences in the physical dimensions of nCs in co-culture and monoculture **(Figure 4-10A, Table 4.1)**, indicating that the same structures are present in both culture platforms. Interestingly, the presence of endothelial cells induced increased expression of nC structures. In both the 2D and 3D platforms, a higher percentage of the metastatic epithelial cells were nC+ve compared to the same cells in monoculture. In 2D and 3D co-cultures, 56.10±3.90% and 69.93±5.91% of the breast epithelial cells, respectively, were nC+ve compared to 24.15±1.64% and 32.98±1.45% of cells in 2D and 3D monocultures, respectively **(Figure 4-10B)**. In addition, the average number of nCs expressed by cells in co-culture were also higher **(Figure 4-10C,D)**. There was a 1.5 fold ($p < 0.001$) and 1.8 fold ($p < 0.0001$) increase in nCs per cell in 2D and 3D co-cultures compared

	EPI-EPI			
	2D	**3D**	**FL**	
Width (μm)	0.31±0.02	0.29±0.02	1.05±0.05	
Length (μm)	31.55±5.67	45.62±4.29	6.75±0.41	
	EPI-ENDO			
	2D	**3D**	**FL**	**Other**
Width (μm)	0.32±0.02	0.29±0.022	1.53±0.13	4.99±0.23
Length (μm)	42.46±3.26	30.69±2.43	60.15±6.24	12.90±1.79

Table 4.1: Summary of nanoChannel projection length and width measurements.

to analogous monocultures, respectively **(Figure 4-10C)**. This difference in nCs per cell is further emphasized when averaging in the nC-ve cells **(Figure 4-10D)**. Including nC-ve cells, there is a 3.5 ($p < 0.0001$) and 4.2 ($p < 0.0001$) fold increase in nCs per cell in 2D and 3D co-cultures compared to monoculture, respectively. Taken together, this data indicates that the presence of endothelial cells induces nC formation in metastatic breast epithelial cells, increasing both the number of cells expressing nCs and the number of nC structures per cell. Surprisingly, the percentage of nC+ve cells was also dependent on the culture format. There is a 37% and 25% increase in percentage of nC+ve in 3D platforms compared to 2D in monoculture and co-culture formats, respectively. This difference further highlights that adopting a 3D conformation in culture leads to significant biological differences that are otherwise lost in cells cultured on 2D substrates.

4.2.2.3 Speculation on the unique arrangement of cytoskeletal fibers within nanoChannels

The unique physical properties of these structures may provide insight into why tubulin cytoskeletal components are incorporated within nC structures. **Figure 4-11B** provides a schematic of idealized cytoskeletal arrangements within nCs. Extending the arguments made by Atilgan et al. in describing filopodial projections,

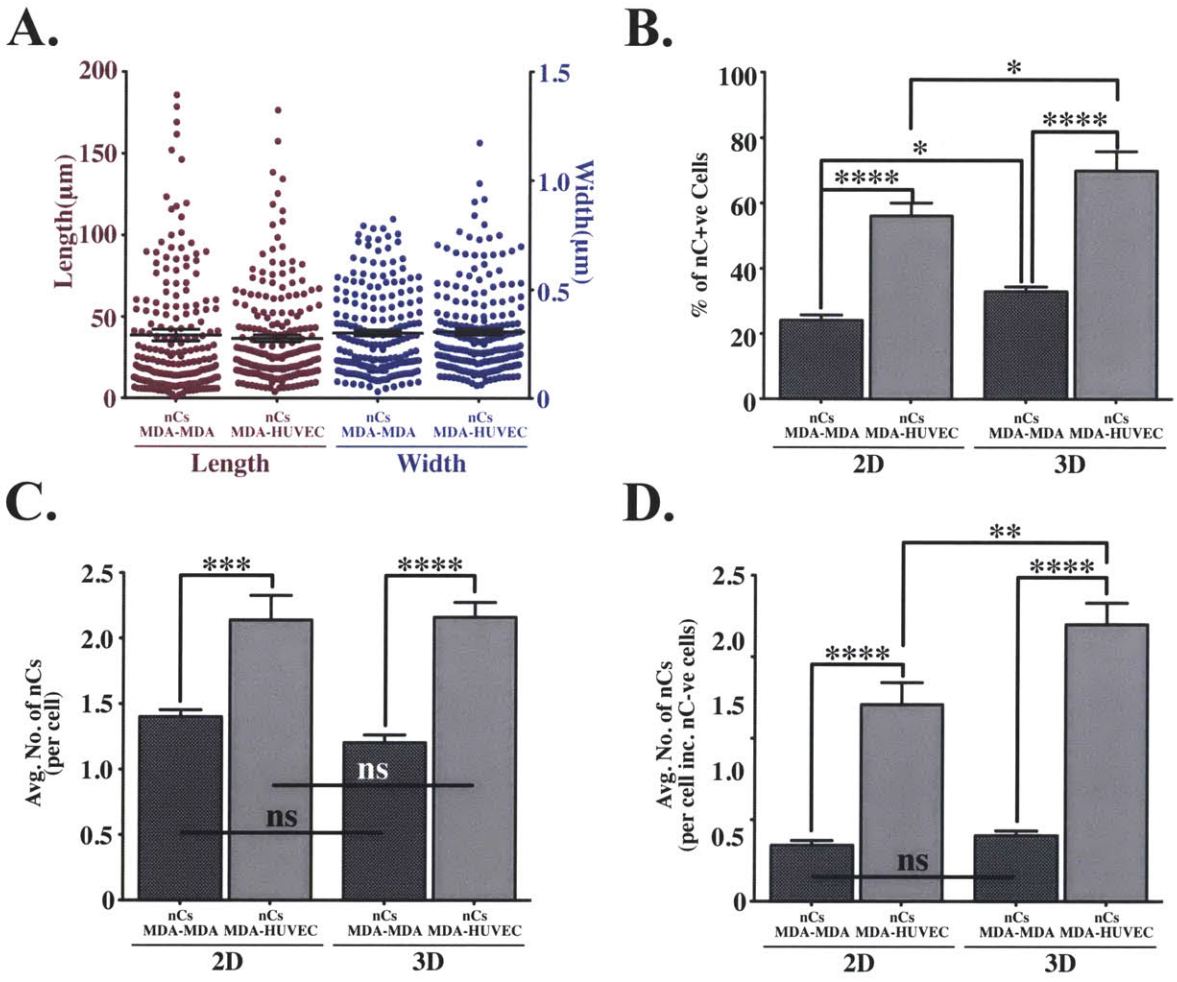

Figure 4-10: Comparison of nanoChannel structures in monoculture versus co-culture. (A) Length and width measurements of nCs in monoculture and co-culture. The physical dimensions of the structures are the same in both mono and co-culture indicating that the structures in both culture platforms are the same. (B) Percentage of nC+ve cells in monoculture versus co-culture. (C/D) Average number of nCs per cell excluding nC-ve cells (C) and including nC-ve cells (D).

it is possible to estimate the theoretical number of actin cytoskeletal bundles required to achieve the length scales observed in nanoChannels[309] **(Figure 4-7)**. This model incorporates properties of cell membrane elasticity and fluctuation dynamics with actin polymerization kinetics to describe protrusion speed of filopodia as a function of the number of filaments in a bundle[309]. In this model, the authors describe that one filament alone is not sufficient to cause a protrusion longer then several hundred nanometers even though the chemical energy derived from polymerization can lead to protrusion; a filopodia will not form without sufficient stiffness to create a projection[309]. They define the buckling force of a filopodia to be $f_b = \frac{\pi^2}{4}\frac{l_p k_b T}{l^2} I$, where l_p is filopodia persistence length, l is actual filopodia length, I is a dimensionless quantity for bundle stiffness, k_b is the Boltzmann constant, and T is temperature[101,309]. Using this model, a nanoChannel with an average length of approximately 50μm would require ≥ 410 actin filament bundles, creating a projection with a minimum diameter 1.5μm, 5x greater than the average measured nC diameter. This model would predict that nC projections should buckle at lengths on the order of several microns[309]. However, our studies have shown that nCs in nature are significantly longer (several hundred microns). We hypothesize that these descriptions fail to define structural characteristics of nCs because they do not account for actin-tubulin interactions **(Figure 4-11A)**. NanoChannels seem to be formed from an actin core supported by a punctate β-Tubulin signature **(Figure 4-11C)**. Microtubules are roughly two orders of magnitude more rigid than microfilament bundles. The presence of microtubules may be critical in providing the structural support required to achieve the length scales observed in nC structures **(Figure 4-7)**.

Figure 4-11B illustrates the possible arrangement of cytoskeletal fibers within nCs. Two extremes are possible: a hollow cylinder with cytoskeletal fibers arranged along the periphery of the channel or a solid pipe with cytoskeletal fibers packed at a high density throughout the structures. The reality likely exists somewhere in between these two extremes.

The cytoskeletal arrangement within nC structures may play a critical role in

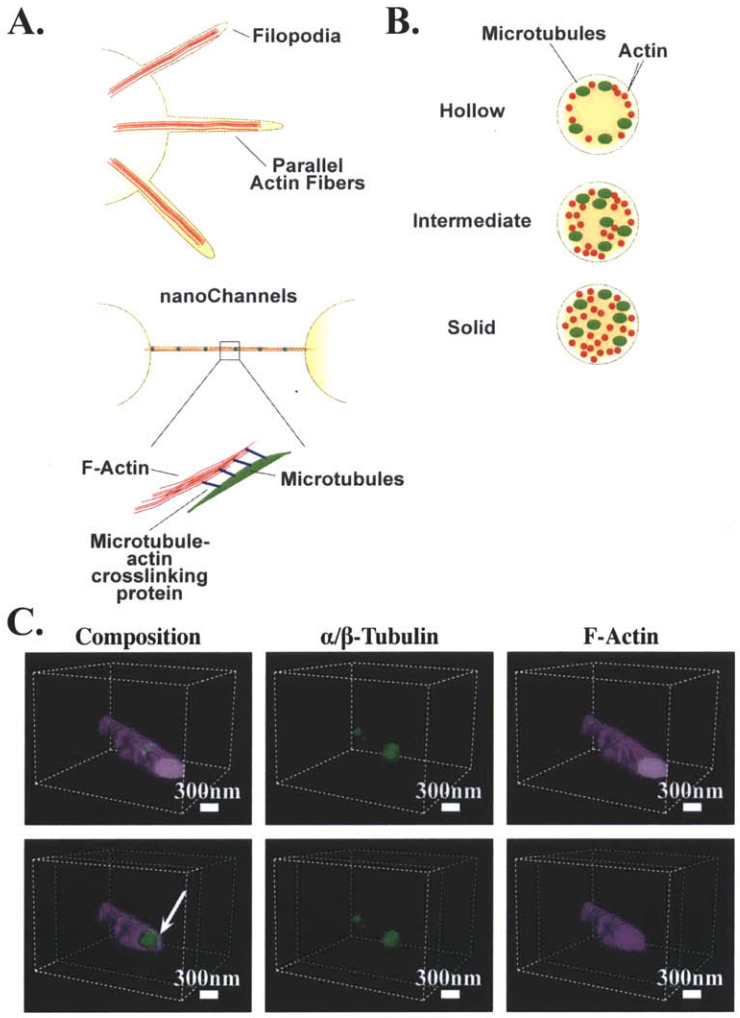

Figure 4-11: Cytoskeletal arrangement inside nCs. (A) Unlike filopodial cellular projections, nanoChannels are composed of both actin and tubulin cytoskeletal fibers. Filopodia contain parallel actin fibers and few microtubules. Interactions between actin and tubulin may be critical in achieving the unique length scales seen in nCs. Models used to describe mechanical properties of filopodia are not appropriate to use in describing nCs. These models may fail to define structural characteristics of nCs because they do not consider actin tubulin interactions. Microtubules are roughly two orders of magnitude more rigid than microfilament bundles. The presence of microtubules may be critical in providing the structural support required to achieve the length scales observed in nC structures. (B) Schematic of idealized cytoskeletal arrangement inside nCs represents the two extremes: hollow cylinder and solid pipe. The reality may likely exist somewhere in between. (C) 3D cross-section of an nC projection with labeled α/β-Tubulin and F-Actin cytoskeletal proteins. nCs seem to be formed from an actin core supported by a punctate β-tubulin signature. Tubulin may provide structural support as the nC elongates, potentially serving as a protein cap for the elongating actin filaments (solid arrow).

the transport mechanisms that dominate within nanoChannels. A more hollow configuration may indicate that diffusive mechanisms dominate. In contrast, a more dense configuration might suggest an active transport mechanism. A high density of cytoskeletal fibers may inhibit passive diffusion (within the time scales of interest) of large molecules due to spatial constraints. Actin motor proteins (i.e. myosins) and microtubule motor proteins (i.e. kinesins and dyneins) may predominate in a diffusion limited context.

4.2.2.4 Kinetics of formation of nanoChannel structures

We next examined the kinetics of nanoChannel formation over a 24 hour time period **(Figure 4-12)**. Cultures were fixed at the indicated time points and visualized using SEM **(Figure 4-12A)**.The length of nC structures **(Figure 4-12B)** and the average number of nCs were quantified at each time point **(Figure 4-13A)**. At 1.0hr after addition of MDA-MB-231 cells to the culture, the epithelial cells appeared rounded with a smooth surface. However, within 1.5hrs, visible projections were seen forming from MDA-MB-231 cells with directional polarity **(arrow, Figure 4-12A)**. NanoChannels were found to arise from the surface in closest proximity to the endothelial vessel, while limited projections were observed on the opposing side (arrowhead), suggesting that nanoChannel formation is a highly directed and non-stochastic process. At 2.0hrs, the structures continue to lengthen toward the endothelium to form complete nCs (arrow). By 3.0hrs intact projections were observed but did not appear to be fused with the endothelial membrane, indicating non-functionality (solid arrow). An epithelial cell can be seen invading the endothelial structure (dotted arrow). By 5.0hrs intact projections were present, which persisted over 24hrs. At 24hrs the structures appear to be fused with the membrane correlating with functional studies examining intercellular transport through nCs **(Section 4.3)**. The growth of nanoChannel structures was measured over time supporting these qualitative observations **(Figure 4-12B)**. Elongation of nCs occurs slowly until approximately 2hrs, at which point structures quickly elongate until approximately 16hrs when nC growth plateaus **(Figure 4-12B)**.

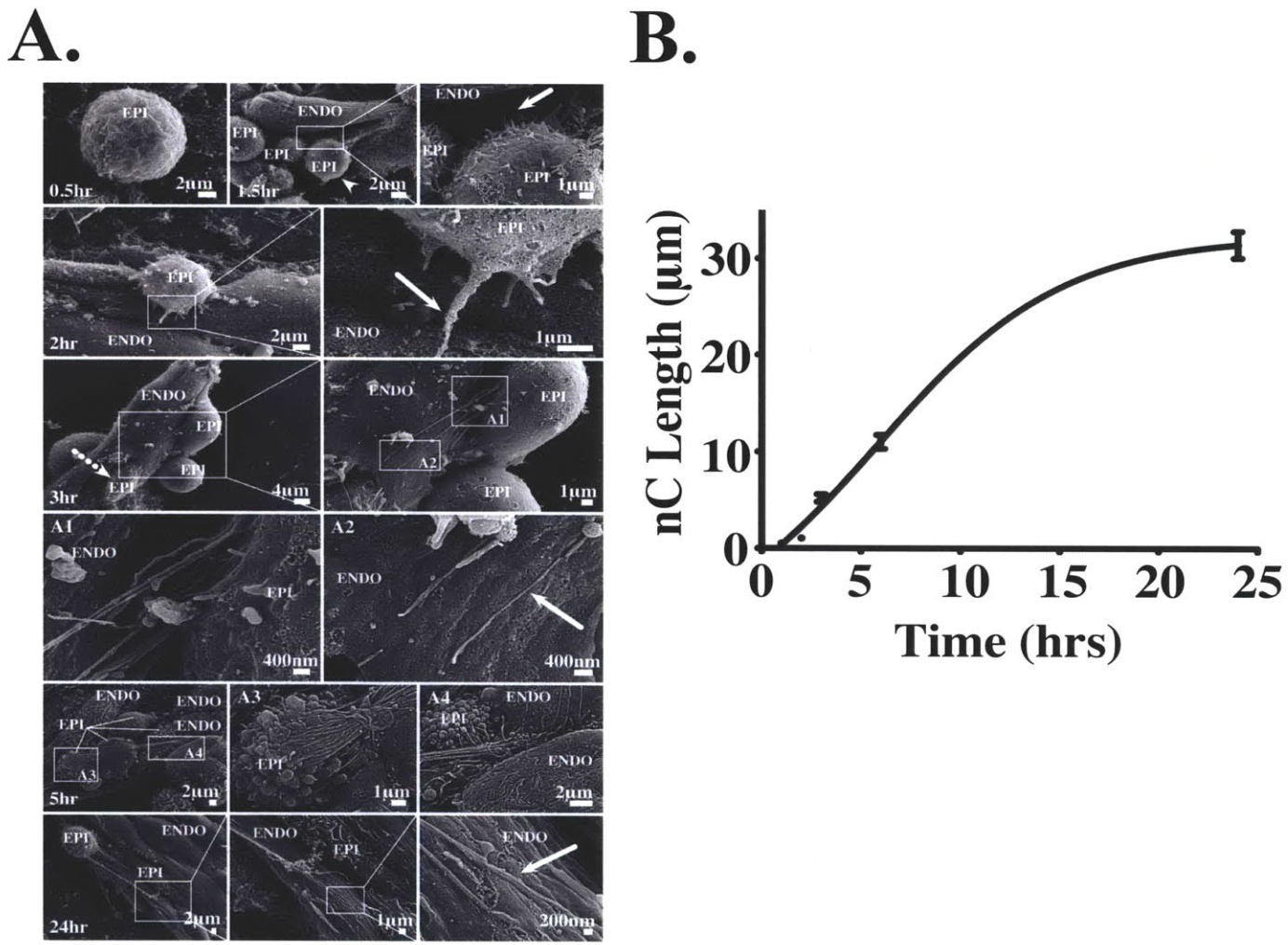

Figure 4-12: Kinetics of formation of nC structures over 24hrs. (A) SEM micrographs show representative nC structures at a selected subset of time points (0.5hr, 1.5hr, 2.0hrs, 3.0hrs, 5.0hrs, and 24hrs). NanoChannel formation appears to be a directed process with structures forming with directional polarity toward endothelial cells. (B) Growth of nC projections was quantified over time. Lengthening of nC structures begins slowly, followed by a burst of nC growth from 2-16hrs with a plateau of length after 16hrs. These results correlate with studies examining intercellular transport through nC structures over time.

Next, the average number of nC structures per cell was quantified over time **(Figure 4-13A)**. NanoChannels were classified into two groups nascent nCs or complete nCs. Nascent nCs refer to the small hair-like projections that can be seen forming from cells at early time points **(Figure 4-5C)**, while complete nCs extend from donor epithelial cells to the recipient cells without disruption **(Figure 4-5A,D)**. The average number of complete (green) and nascent (pink) nCs was quantified over a 24hr period **(Figure 4-13A)**. Total projections (black) represents the sum of nascent nCs and complete nCs at each individual time point. At early time points the majority of projections are nascent nCs with very few complete nCs present. This phenotype reverses at later time points. Interestingly, the number of projections is greatest at low time points. This data suggests that at very early time points metastatic breast epithelial cells form several small projections on their surface. At slightly later times, a fraction of these projections, maybe in response to a soluble factors released by endothelial cells, go on to form complete nC structures. Nascent nCs may have receptors that respond to factors secreted by neighboring cells. The nascent nCs that efficiently respond to nanoChannel growth signals go on to form complete nCs, while the remaining nCs regress, possibly due to an inability to sense the appropriate growth signal. The number of complete nC structures peaks at approximately 5hrs and declines quickly by 6hrs and remains fairly constant until 24hrs. The number of complete nCs is likely proportional to nC growth signals released by neighboring cells. The sudden decline in nCs structures between 5 and 6 hours is likely due to equilibration of nC projections with the concentration of nC growth signals. The number of projections present at 5hrs may not be maintained by the level of nC growth signals released at 6hrs. **Figure 4-13C** illustrates the proposed mechanism of growth of nCs over time.

To further understand how nCs form over time, we quantified the percentage of nC+ve cells **(Figure 4-14B)**. We assessed the percentage of cells with nascent nCs, complete nCs, and both nascent and complete nCs **(Figure 4-14B)**. At early time points, almost 100% of the cells were nC+Ve. However, the percentage of the population declined slightly by 24hrs. As illustrated in **Figures 4-13A and 4-14B**,

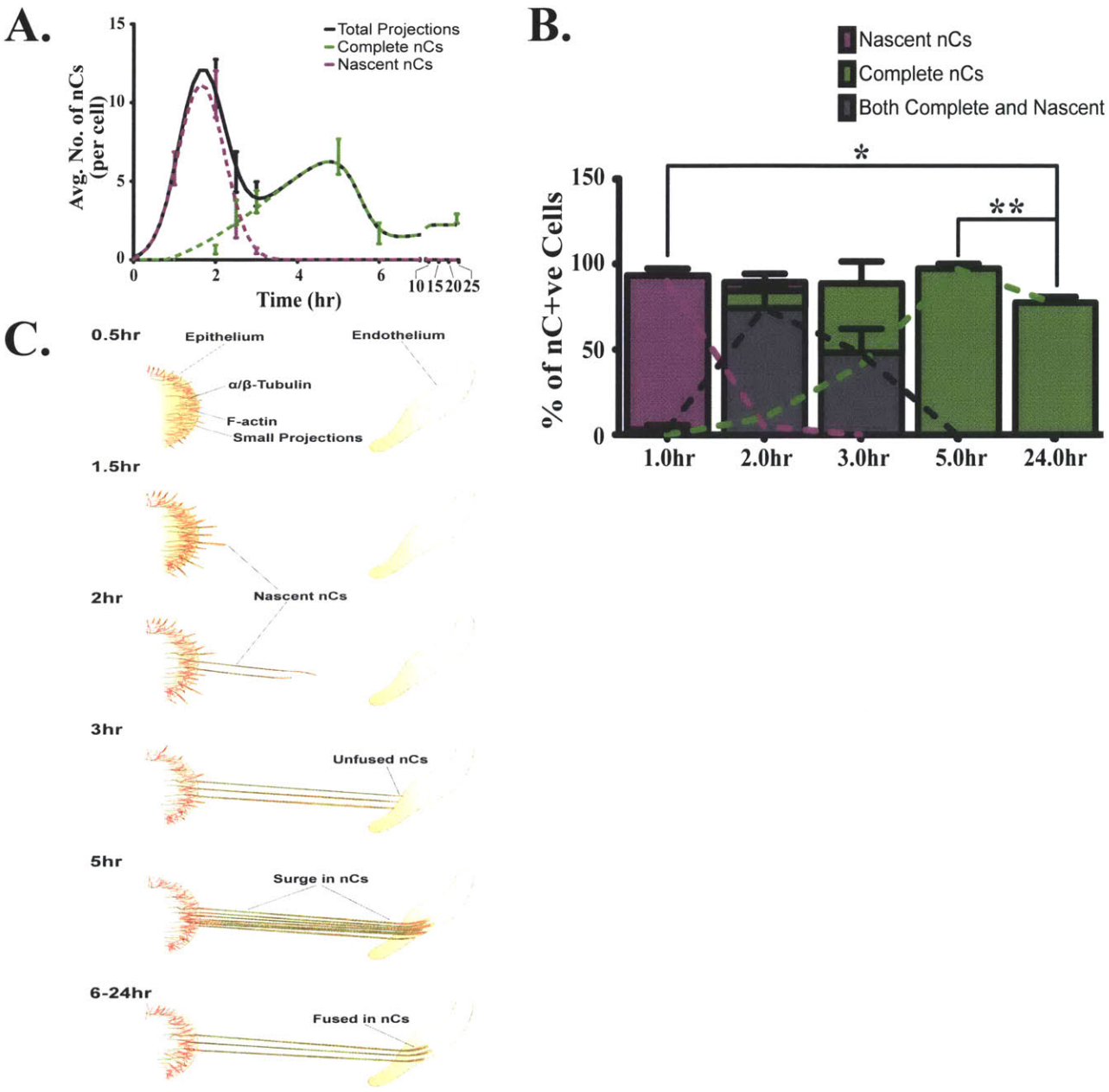

Figure 4-13: Quantification of nascent versus mature nCs over time. (A) NanoChannel projections were quantified over time. NanoChannels were quantified as complete nCs (green) or nascent nCs (pink). Total projections (black) is the sum of complete nCs and nascent nCs. At early time points the majority of projections are nascent nCs, while at later time points mature nCs dominate. (B) The percentage of nascent nC+ve cells, complete nC+ve cells, and both nascent and complete nC+ve cells was quantified over time. (C) Schematic illustration of nC growth over time. At early time points, small projections emerge on the cell surface. A fraction of these nascent nCs go on to form complete nCs, while the remaining nCs regress. At 5hrs, the number of complete nCs peaks, quickly declining by 6hrs and staying fairly constant up to 24hrs.

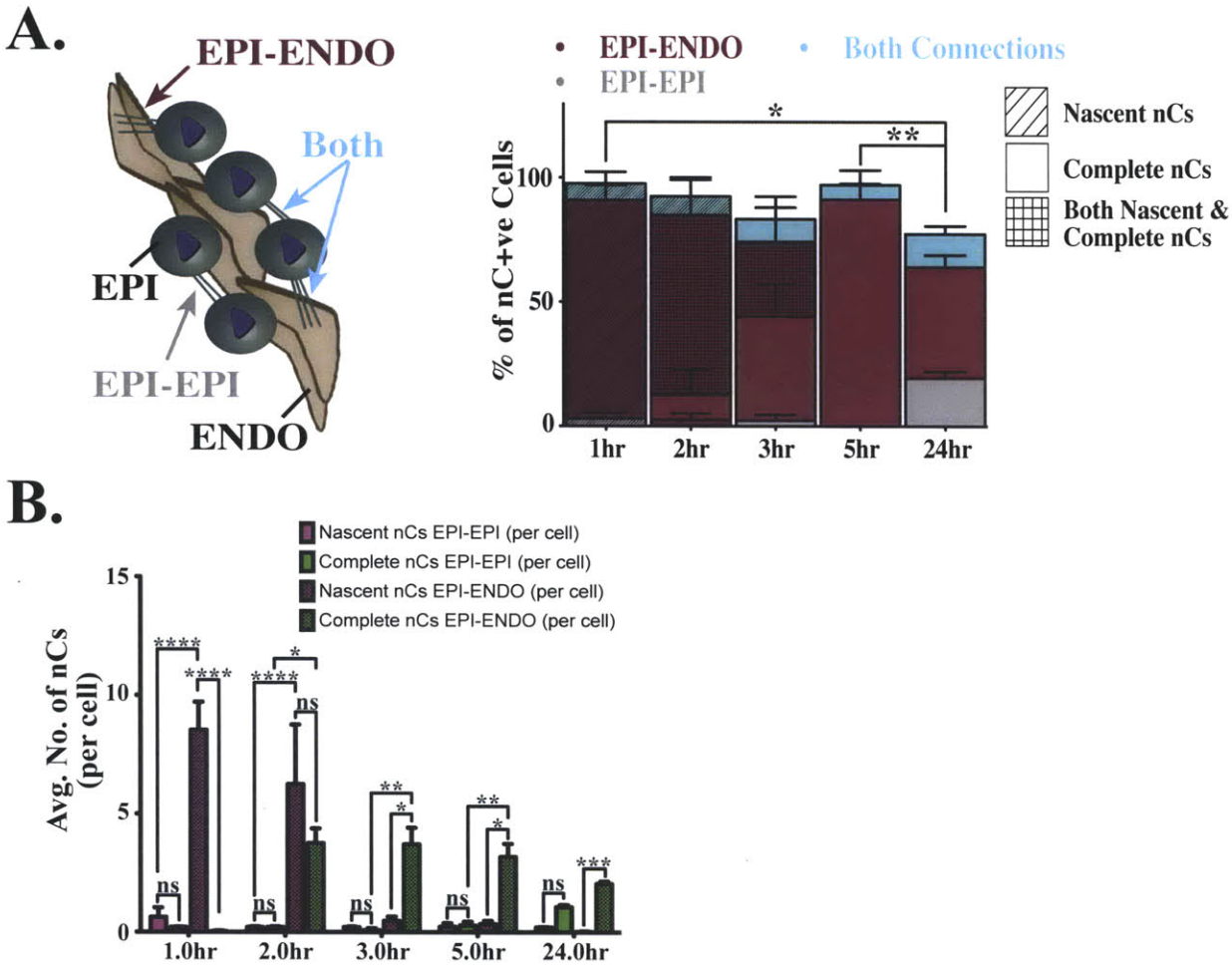

Figure 4-14: Percentage of nC+ve cells over time. (A) The nC+ve population was further subdivided into cells with epithelial-epithelial connections (EPI-EPI) (grey), epithelial-endothelial connections (EPI-ENDO) (maroon), and both connections (light blue). A majority of metastatic cells form connections with the endothelium. (B) Average number of nCs per cell were quantified and classified according to the type of nC projection (mature vs. nascent) and the recipient (EPI, ENDO, or Both). Cells which form EPI-ENDO connections also express a higher number of nC structures per cell.

at early time points most of the nC+ve cells have nascent nC projections, while at later times the nC+ve cells express exclusively mature nCs. From approximately 2-5hrs, nC structures transition from nascent to mature projections with the majority of cells expressing both complete and nascent nCs.

We further stratified the quantification into epithelial-epithelial connections (EPI-EPI) (grey), epithelial-endothelial connections (EPI-ENDO) (maroon), and both connections (light blue). In **Graph 4-14A**, nC+ve cells were grouped by both the type of nCs formed (nascent vs complete) and by the recipient cells (endothelial, epithelial, or both epithelial and endothelial cells). A majority of nCs structures formed are toward the endothelium with very few cells forming connections with other epithelial cells **(Figure 4-13A)**. In addition, at each time point cells that form connections with the endothelium exhibit a higher number of both nascent and complete nCs per cell than the same cell type forming connections with other epithelial cells **(Figure 4-13B)**. Taken together these data show that the endothelium may be producing a signal that induces formation of nC structures.

4.2.3 NanoChannels preferentially form between metastatic cells and the endothelium

From our analysis of nC structures in MDA-MB-231, we were able to characterize the cytoskeletal composition, physical dimensions, and kinetics of formation of nC structures. However, to investigate the correlation between the ability to form nanoChannels and metastasis, we co-cultured epithelial cells of increasing tumor grades with the endothelial networks. Developing these model systems allowed for analysis of nC structures in other epithelial cell lines.

NanoChannels were analyzed in co-cultures of primary human mammary epithelial cells (HMEC), tumorigenic non-metastatic breast epithelial cell lines (SkBr3, MCF-7), or metastatic epithelial cell lines (MDA-MB-468, MDA-MB-231, and MDA-MB-435). Again, the nCs quantified were grouped into three types of connections: epithelial-epithelial (EPI-EPI) connections, epithelial-endothelial (EPI-ENDO) con-

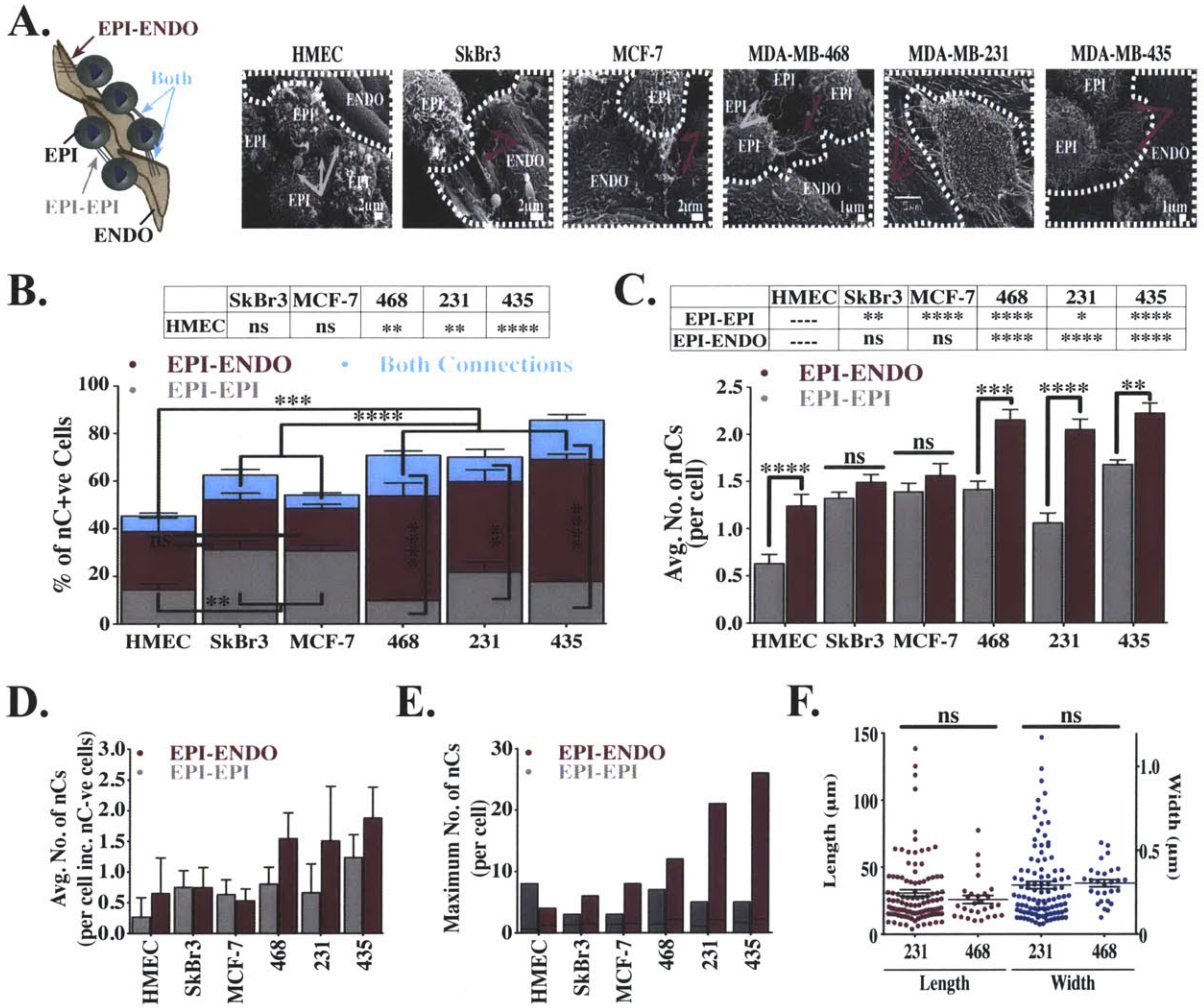

Figure 4-15: NanoChannel structures in primary, tumorigenic, and metastatic cells (A) SEM images show nanoChannels formed by primary breast epithelial cells (HMEC), tumorigenic breast epithelial cell lines (SkBr3, MCF-7), and metastatic breast epithelial cell lines (MDA-MB-468, MDA-MB-435). (B) Graphs show the percentage of nC+ve cells and (C) average number of nCs per cell quantified in each culture. (D) Average number of nCs per cell including nC-ve cells. (E) Maximum and mean number of nCs (per cell) for each analyzed epithelial cell line. Averages are indicated by the black band on each bar. (F) nC structures formed by different cell lines have similar length scales. Quantification was performed on >300 cells of each cell type.

nections, or both connections **(Figure 4-15A)**. Over 70% of the metastatic cell populations were nC+ve, which was 1.73±0.12 fold ($p<0.01$) greater than the percentage of nC+ve cells in the case of normal epithelial cells **(Figure 4-15B)**. Metastatic cells preferentially formed EPI-ENDO to EPI-EPI connections, at a ratio of approximately 2:1 ($p<0.01$). Compared to normal epithelial cells, tumorigenic non-metastatic populations contained 1.34±0.10 fold ($p<0.05$) higher percentage of nC+ve cells. However, contrary to the phenotype observed in the metastatic cell lines, these connections were primarily EPI-EPI type, with similar levels of EPI-ENDO connections in tumorigenic cell lines compared to normal **(Figure 4-15B)**. We next quantified the number of nanoChannels formed per cell. Interestingly, the metastatic cells which formed nC connections with the endothelium expressed 1.59±0.18 times ($p<0.05$) the number of nanostructures per cell than the same cell type forming EPI-EPI connections **(Figure 4-15C)**. Furthermore, compared to the normal breast epithelial cells, both tumorigenic and metastatic populations formed more EPI-EPI nC connections per cell; however, only the metastatic cells expressed higher EPI-ENDO nC connections **(Figure 4-15C)**. The average number of nCs per cell including nC-ve cells is given in **Figure 4-15D**. Taken together these data suggest that a higher percentage of metastatic cells are nC+ve, and metastatic cells preferentially form connections with the endothelium compared to normal ($p<0.001$) and tumorigenic cell lines ($p<0.0001$), which preferentially form monotypic intercellular connections. Indeed, the ability of a cell to form nCs may provide important insight into its metastatic potential. **Figure 4-15E** graphs the maximum and mean number of nCs (per cell) observed for each analyzed epithelial cell line. In accordance with the previous data, cells with ten or more nCs were commonly found in the metastatic cells lines.

To confirm that the structures analyzed in each of the co-cultures are similar, we quantified the physical dimensions of nC projections in MDA-MB-468 co-cultures **(Figure 4-15F)**. There is no statistical difference between the length and width of nC structures formed by MDA-MB-231 and MDA-MB-468 cells when in co-culture, confirming that nCs formed by different cell lines have similar length scales. There-

fore, this data provides confidence that the same structures are being analyzed in each of these model systems.

4.3 Communication of intercellular contents occurs through nanoChannels

The aforementioned data highlights important characteristics of nC structures. Formation of nanoChannel structures occurs in a regulated fashion with a high degree of correlation with a metastatic phenotype. Furthermore, nanoChannels formed by metastatic cells are induced by endothelial cells. Normal breast epithelial cells preferentially form monotypic nC connections (EPI-EPI), while metastatic cells predominately form epithelial-endothelial (EPI-ENDO) nC connections. Formation of nanoChannels requires polymerization of the actin-tubulin cytoskeleton and is therefore likely a high energy process. To understand why cells have evolved the ability to form nC structures, we sought to investigate their biological function, specifically the role of nCs in intercellular communication.

4.3.1 Experimental Design

We first assessed the ability of nanoChannel structures to transport cytoplasmic contents. To perform these studies MDA-MB-231 cells were loaded with carboxyfluorescein succinimidyl ester (CFSE) cell-impermeable dye prior to their addition to DiL-Ac-LDL labeled endothelial cells tubes. CFSE is a small, fluorescently labeled, non-membrane permeabilizing, cytoplasmic dye that can be used as a non-specific maker of cytoplasmic contents. CFSE was chosen as an appropriate reagent to use in these experiments due to its minimal cytotoxicity and its inability to cross the plasma membrane once it has been internalized by cells. CFSE is formed from carboxyfluorescein diacetate succinimidyl ester (CFDA-SE) after the removal of acetate groups by intercellular esterases. CFDA-SE is highly cell permeable due to the presence of acetate groups, while CFSE is highly membrane impermeable.

CFSE can be retained in cells through many cell division, making it an excellent marker for non-specific intercellular contents.

Figure 4-17 provides a general overview of the experimental design used to evaluate nC-mediated intercellular transfer. Epithelial cells were pre-treated with cytoskeletal inhibitors for 24hrs to disrupt formation of nanoChannel structures prior to loading with fluorescently labeled synthetic materials (CFSE, quantum dots) or labeling of endogenous cytoplasmic contents (GFP). Co-cultures were incubated for 24hrs after which nC-mediated intercellular transfer was analyzed via FACS. Endothelial cells were isolated, the percentage of cells receiving intercellular contents was quantified, and the effects of drug treatment were determined. These methods were used to evaluate changes with drug inhibition and phenotypic differences in endothelial cells receiving intercellular communication verses endothelial cells receiving no intercellular communication. Specifically, the adoption of a pathological phenotype due to intercellular transport received via nanoChannels was assessed.

Flow cytometry was used as the primary method for quantifying intercellular transport through nC structures. Optimization of the flow cytometry protocol required determination of the appropriate concentration of CFSE to load in the epithelial cells and the development of a robust mechanism for identifying each of the cell populations.

The first requirement was optimization of the concentration of CFSE to load into the epithelial cells. Endothelial cells naturally autofluoresce producing an autofluorescent background. As a result, it was critical to choose a concentration of CFSE that would allow for an optimal signal to noise ratio. In order to determine this concentration, we performed a dose titration of CFSE to assess the minimum concentration required to achieve a concentration-independent measure of intercellular transport.

Figure 4-16 illustrates the results of this dose titration. The percentage of intercellular transfer in the recipient population was quantified as illustrated in **Figure 4-16A**. At low concentrations of CFSE only a small percentage of the recipient

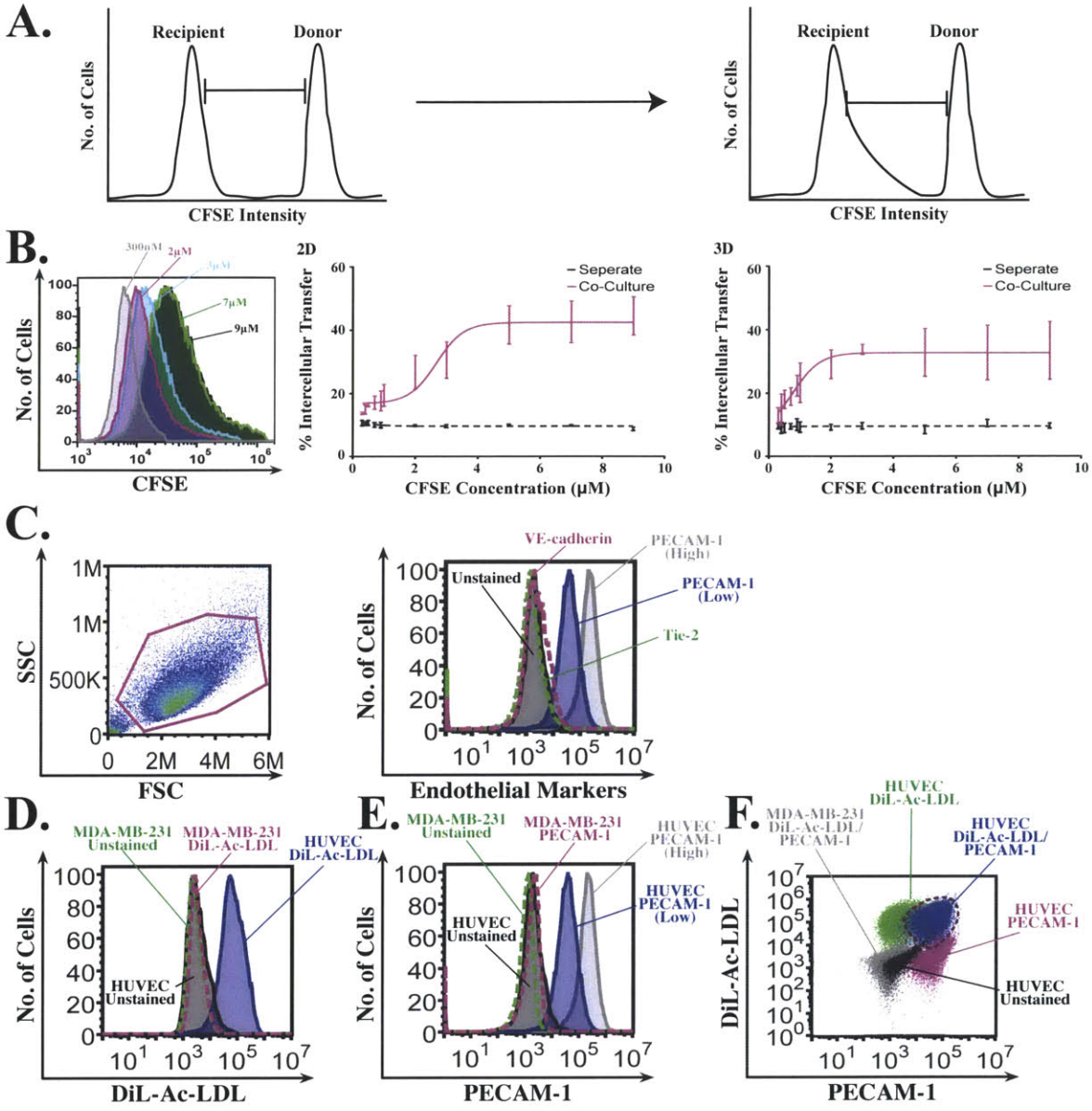

Figure 4-16: Optimization of flow cytometry experiments to detect intercellular transfer. (A/B) Optimization of CFSE concentration for loading MDA-MB-231 cells. (C-F) Optimization of endothelial cell labeling. Endothelial cells are dual labeled with Dil-Ac-LDL and PECAM-1.

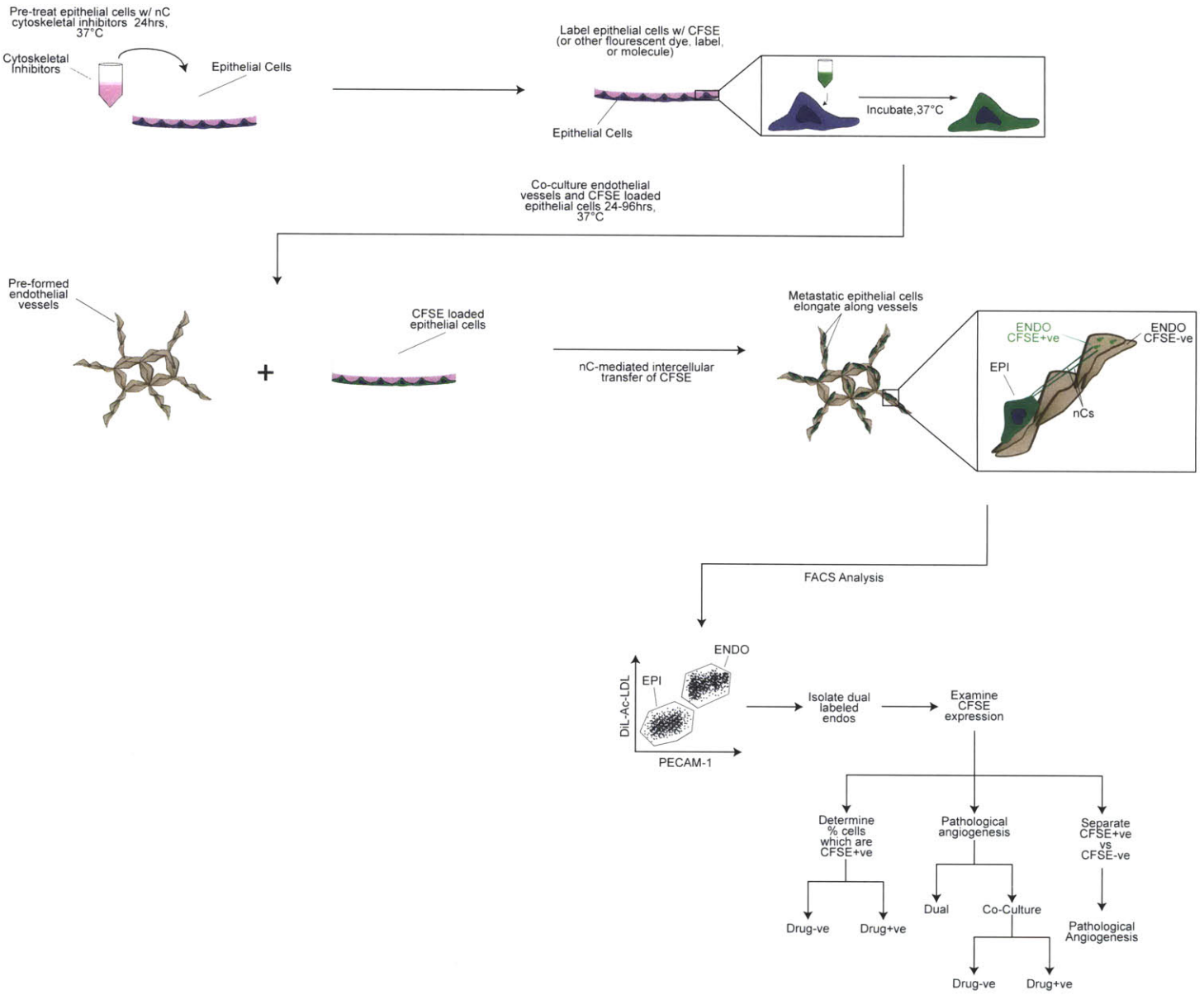

Figure 4-17: Experimental overview of studies examining nC-mediated intercellular transport of cytoplasmic contents.

cell population receives intercellular transfer **(Figure 4-16B)**. The percentage of recipient cells increases with CFSE concentration until approximately 2μM. In the range of 5-9μM the percentage of cells receiving intercellular contents is constant, indicating that this range is appropriate to achieve a concentration-independent measure of intercellular transfer **(Figure 4-16B)**.

The second requirement was to optimize the staining protocols used to differentiate each of the cell types. HUVEC endothelial cells were stained with VE-cadherin (pink), two concentrations of PECAM-1, PECAM-1 low (blue) and PECAM-1 high (grey), and Tie-2 (green) **(Figure 4-16C)**. Immunostaining with PECAM-1 offered the best separation of the stained population from unstained cells (black). However, MDA-MB-231 breast epithelial cells express low levels of PECAM-1 (pink) **(Figure 4-16E)**. Therefore, in order to achieve complete separation of the populations, HUVEC endothelial cells were also stained with DiL-Ac-LDL. Staining with DiL-Ac-LDL was beneficial for two primary reasons. First, DiL-Ac-LDL staining could be done on live cells allowing for staining of endothelial cells prior to co-culturing. Staining the endothelial cells independently of epithelial cells better ensured specificity of the staining. Second, MDA-MB-231 cells (pink) did not stain positive for DiL-Ac-LDL even when directly incubated with the dye due to the absence of LDL receptors on the surface of breast epithelial cells **(Figure 4-16D)**. Dual labeling with DiL-Ac-LDL and PECAM-1 provided optimal separation of two cell populations. **Figure 4-16D** illustrates the double stained endothelial cell population (blue) providing significant separation from MDA-MB-231 cells in co-culture (grey).

4.3.2 NanoChannels provide continuous conduits for intercellular transfer

To analyze the role of nanoChannels in intercellular communication, cross-sections of MDA-MB-231 (EPI) and endothelial (ENDO) cell co-cultures were analyzed using transmission electron microscopy (TEM). In **Figure 4-18A** a nanoChannel

(white arrow) is seen connecting an epithelial cell to and endothelial cell. TEM micrograph shows intercellular connectivity between the cell types. Intercellular connectivity further differentiates nanoChannels from other cellular projections. NanoChannels are open conduits of communication between two cells. Protrusions with similar physical dimensions but closed ends are referred to as cytonemes or filopodial bridges **(Figure 4-18B)**.

To examine transfer of intercellular contents through nanoChannels and correlate the kinetics of nanoChannel formation with acquisition of functionality, MDA-MB-231 cells were loaded with CFSE and then added to DiL-Ac-LDL labeled endothelial cell tubes **(Figure 4-18C)**. The co-cultures were counterstained with phalloidin and wheat germ agglutinin (WGA) to label the actin cytoskeleton and plasma membrane boundaries, respectively. De-convolved volume rendering provided a 3D view of the co-cultures **(Figure 4-18C)**, revealing trafficking of CFSE via nanoChannels formed between the cancer cells and endothelial cells in both 2D **(Figure 4-18B1-B3)** and 3D **(Figure 4-18B4-B7)** settings. nC projections can be seen penetrating neighboring endothelial cells (white arrow) **(Figure 4-18B1,2)**. **Figure 4-18B2** is a 3D reconstruction of **Figure 4-18B1**. The nanoChannel burrows through the endothelial cell boundaries, entering the cytoplasmic compartment of a neighboring endothelial cell. The nanoChannel can be seen depositing CFSE into the endothelial cell cytoplasmic compartment (yellow arrow heads) **(Figure 4-18B3)**.

In a 3D co-culture, a metastatic epithelial cell can be seen invading within the lumen of the endothelial tube (dotted white arrow) **(Figure 4-18B4,5)**. A nanoChannel projection can be seen extending to the surrounding endothelial cells **(Figure 4-18B7)**, depositing intercellular contents (yellow arrow heads). These data confirm that nanoChannels are able to transfer intercellular contents from metastatic breast epithelial cells to the endothelium. To provide insight into the frequency of nanoChannel-mediated intercellular communication, we next sought to quantify the percentage of the endothelial cell population receiving intercellular transfer through nCs.

Endothelial cells were dual-labeled with DiL-Ac-LDL and PECAM-1 antibody,

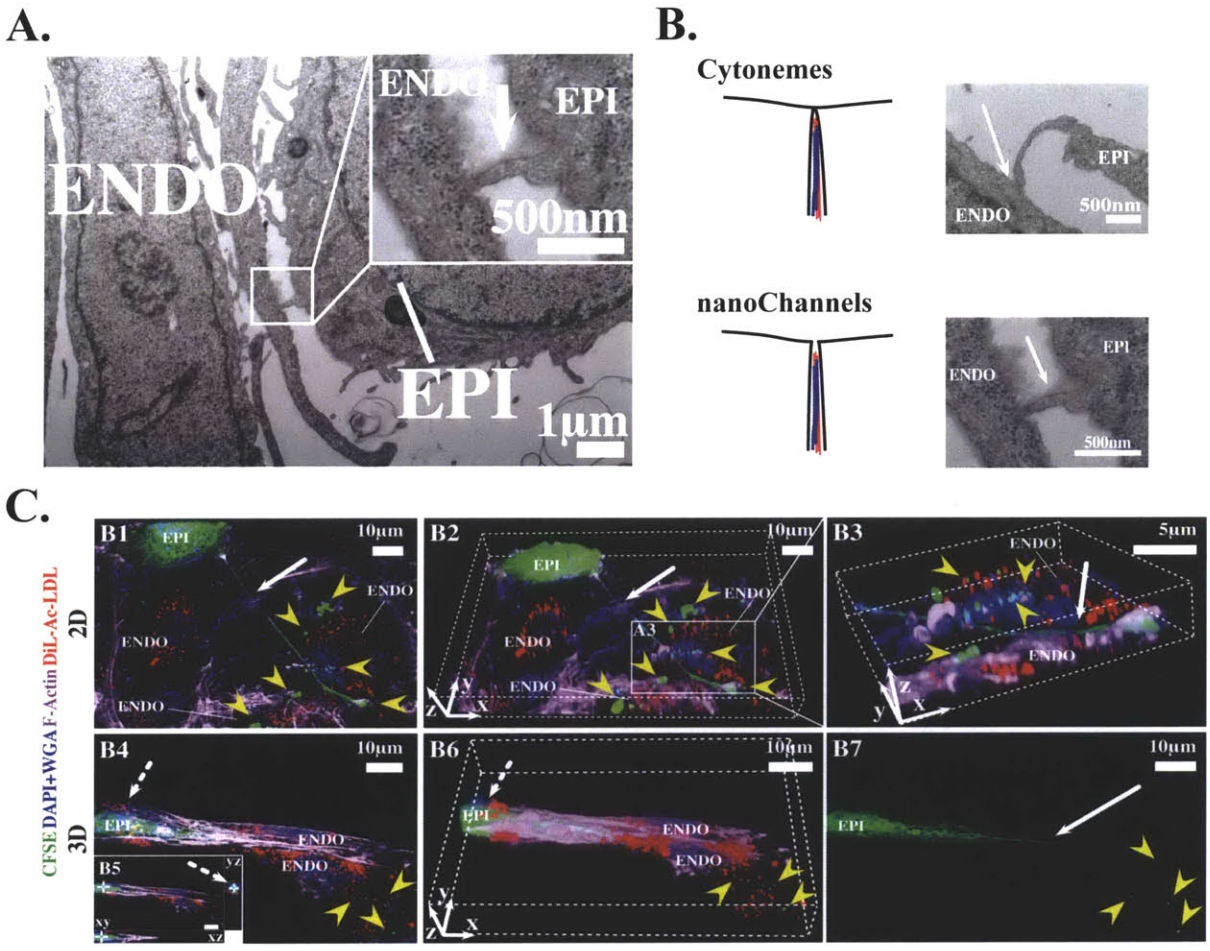

Figure 4-18: NanoChannels provide intercellular connectivity between cells. (A) TEM micrograph shows intercellular connectivity between an MDA-MB-231 epithelial cell (EPI) and a HUVEC endothelial cell (ENDO). (B) Cytonemes versus nanoChannels. (C) Confocal microscopy images capture nanoChannel-mediated transfer of cytoplasmic contents. CFSE loaded MDA-MB-231 (EPI) cells (green) were co-cultured with HUVEC endothelium (ENDO). Transfer of the CFSE dye was observed after 24-hr co-culture through nCs (solid white arrow). CFSE dye can be seen within the DiL-Ac-LDL (red) labeled HUVEC cells (yellow arrowheads). Metastatic breast epithelial cells can be seen invading endothelial vessels (white dashed arrow).

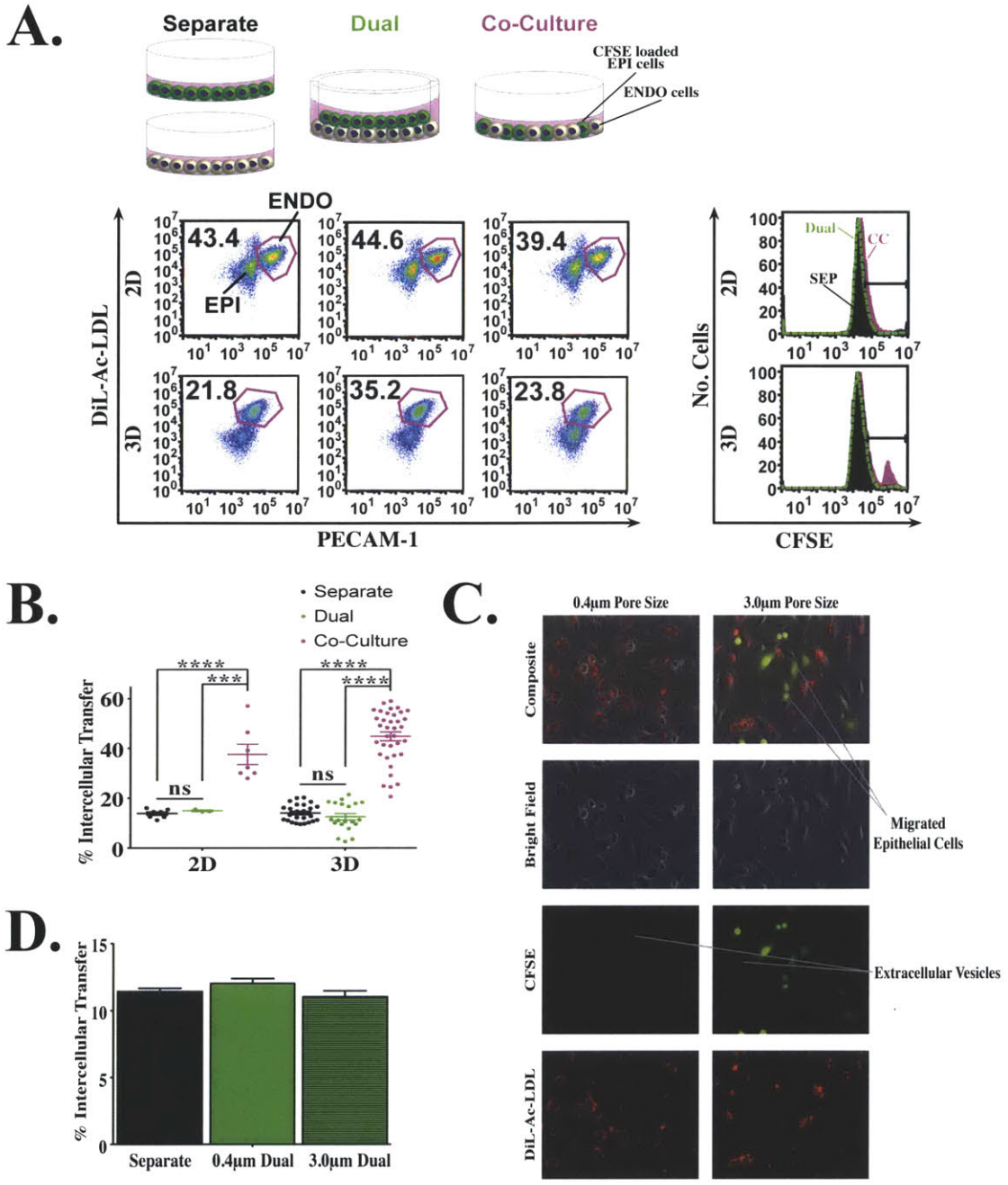

Figure 4-19: Quantification of transport of intercellular contents through nanoChannels. (A) Schematic and (B) graph summarize flow cytometry results examining intercellular transfer of CFSE from metastatic cells into the endothelium through nCs. Dual cultures control for endocytosis/exocytosis-mediated intercellular transfer. Separate cultures control for background autofluorescence of endothelial cells. (C) Images illustrate bottom chamber of 0.4μm and 3μm dual chamber assay. Both pore sizes allow for transport of extracellular vesicles. (D) The percent intercellular transfer in both chambers was equivalent to background, illustrating that extracellular vesicles are not mediating the observed intercellular transfer in co-culture.

and the percentage of CFSE+ve endothelial cells was measured using flow cytometry **(Figure 4-19A)**. The cells were grown in three different configurations, separate, dual, and co-cultures **(Figure 4-19A)**. In separate cultures the cells are grown in two separate wells and then combined together during sample collection and run on the flow cytometer. Separate cultures were used to control for background autofluorescence of the endothelial cells because at no time do they come into contact with the CFSE labeled MDA-MB-231 cells. As a control for potential endocytic/exocytic mechanisms of intercellular transfer, the two cell types were grown in separate compartments in Boyden chambers (dual cultures) that allow for media contact but do not allow for physical contact between the cells. Expression of CFSE in the dual-labeled endothelial cells is compared across the three culture types. **Figure 4-19B** is a graph summarizing the percentage of the endothelial cell population receiving intercellular communication. In co-cultures, 43.30±2.35% ($p<0.0001$) of the endothelial cell population was found to be CFSE+ve, compared to 14.09±0.69% and 15.47±1.46% in the separate cultures and dual cultures, respectively.

To ensure that the dual chambers were an appropriate control for endocytotic-exocytotic mechanisms both 0.4μm and 3μm pores-size Boyden chambers were used. Extracellular vesicles may aggregate making it difficult to fit through smaller pore sizes. In order to determine if 0.4μm dual chambers allowed for sufficient diffusion of extracellular vesicles, such as exosomes, a comparison of percent intercellular transfer was performed with both 0.4μm and 3μm dual chambers. **Figure 4-19C** shows a representative image of the bottom well of a Boyden chamber assay. Endothelial cells are DiL-Ac-LDL labeled and MDA-MB-231 cells are loaded with CFSE. Endothelial cells are grown in the lower chamber while MDA-MB-231 cells are seeded in the upper chamber.

Both pore sizes allow for the exchange of extracellular vesicles. In the 3.0μm pore chambers, migrated cells and extracellular vesicles can be seen in the bottom chamber. However, these migrated vesicles do not lead to transfer of CFSE compared to background autofluorescence measured in endothelial cells grown in separate chambers. These results confirm that the observed transfer is not occurring

through endocytotic or exocytotic mechanisms. The background autofluorescence values observed in 0.4μm and 3.0μm pore chambers are equivalent. Both pore sizes exhibited similar results, demonstrating that exososomes can cross the pores and that this mode of communication is not the source of the observed intercellular communication.

4.3.3 Kinetics of nanoChannel-mediated intercellular transfer

The analysis of nanoChannel growth kinetics in **Section 4.2.2.4** examined formation of nanoChannel projections over a 24-hour period. However, a full understanding of nC kinetics requires correlating both form and function. To better understand nC dynamics, we next sought to correlate nanoChannel development with acquisition of functionality **(Figure 4-20)**. This analysis was performed by assessing intercellular transport through nanoChannels at multiple time points ranging from 0hrs to 96hrs. Data was collected at thirty minute intervals for the first hour, at hour intervals from 1-2hrs, two hour intervals from 2-12hrs, four hour intervals from 12-24hr, and at twenty-four hour intervals from 24-96hrs. At each time point, percent of the endothelial cell population receiving intercellular transfer was plotted with time **(Figure 4-20B)**.

Temporal quantification of CFSE transfer directly correlated with the kinetics of nanoChannel formation **(Figure 4-20B)**. Intercellular transfer begins approximately 4hrs after initiation of co-cultures, coinciding with initial formation of intact nC projections around 3-5hrs **(Figure 4-12)**. Transfer of intercellular contents occurs primarily between 4-20hrs and remains fairly stable until 72hrs **(Figure 4-20B)**.

These results provide insight into initiation of nanoChannel-mediated intercellular communication. However, a critical question that remains unanswered is whether nC transport occurs through active transport, passive transport, or combination of both mechanisms. In addition, another confounding factor in transport dynamics through nCs is the cytoskeletal arrangement within nC structures. As

previously described in **Section 4.2.2.3**, the cytoskeletal arrangement within nCs may dictate which transport mechanisms dominate: a hollow configuration may indicate that diffusive mechanisms dominate, while a solid configuration might suggest an active transport mechanism. To address these questions required modeling of CFSE transport.

CFSE is a small molecule that is foreign to the cellular environment and therefore with almost complete certainty is transported through a diffusion based mechanism. Therefore, we were able to compare a theoretical diffusion model based on physical properties of CFSE with the experimental data of CFSE transport in order to get a first order approximation of transport dynamics within nCs.

To begin this analysis, we derived a concentration versus time plot from our experimental data **(Figure 4-20E)**. This graph was derived by correlating fluorescence intensity with concentration over a 24-hr period. The following assumptions were made to derive the concentration curve:

1. Concentration of intercellular CFSE is directly proportional to fluorescence intensity.

2. The intercellular concentration of CFSE is equivalent to the initial concentration of CFDA-SE in which the cells are incubated.

3. Intercellular CFSE is not significantly degraded over the time scales of interest.

4. There is negligible change in CFSE concentration in the MDA-MB-231 cells in separate cultures over time. Therefore, the initial concentration is equal to to the final concentration.

5. The intercellular concentration of CFSE in MDA-MB-231 is $>>$ than the concentration of CFSE transferred to the endothelium. Therefore, MDA-MB-231 cells act as an infinite source of CFSE.

With these assumptions, at each time point we estimated the average concentration

of CFSE in the HUVEC populations isolated from both separate cultures and co-cultures. Utilizing the expression

$$\frac{X}{MedianFl._{HUVEC}} = \frac{Concentration_{SeparateMDA}}{MedianFl._{MDA}},$$

where X represents the average CFSE concentration of the HUVEC population, $Concentration_{SeparateMDA}$ represents the initial intercellular concentration of CFSE inside the MDA-MB-231 cells in separate cultures, and $MedianFl._{SeparateMDA}$ and $MedianFl._{HUVEC}$ represent the median intensity value of the $MDA_{separate}$ and HUVEC peaks, respectively, the average CFSE concentration within HUVEC cells was calculated at each time point **(Figure 4-20A)**.

Figure 4-20C shows the percent difference in intercellular CFSE concentration between MDA-MB-231 cells in co-culture compared to separate cultures at each time point (pink bars). There was $\leq 10\%$ difference between intercellular CFSE concentration in MDA-MB-231 cells isolated from separate and co-culture groups validating the assumption that the MDA-MB-231 cells act as an infinite source of CFSE and that the intercellular CFSE concentration in the MDA-MB-231 cells is not changed as a result of transfer. The black region denotes the range of percent difference between the cultures over time. With this validation we were able to obtain a relationship between CFSE concentration versus time in the co-cultured HUVEC cells. The results are given by the graphs **Figure 4-20E**. The data was corrected to account for background autofluorescence and experimental variability by subtracting the separate curve **(black curve, Figure 4-20D)** from the co-culture **(pink curve, Figure 4-20D)** curve producing the final relationship illustrated in **Figure 4-20E**. This concentration curve derived from experimental data could then be compared to a theoretical model of diffusion.

4.3.3.1 CFSE diffusion model

Fick's laws provide a general mathematic description of diffusive transport dynamics. The second law of diffusion describes the change in concentration over

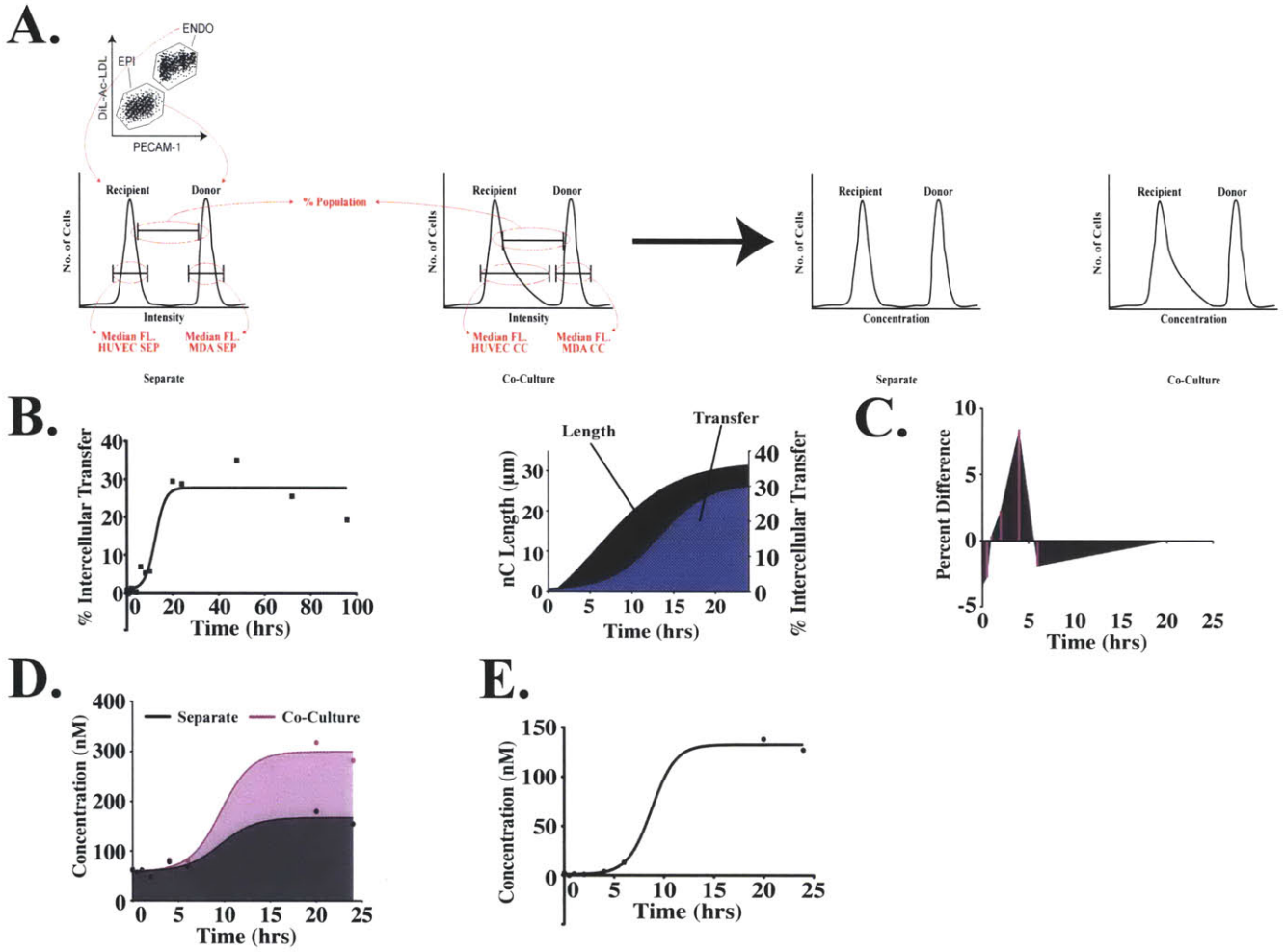

Figure 4-20: Kinetics of intercellular transport through nanoChannels. (A) Schematic of how quantification of intercellular transfer was performed in co-culture. (B) Intercellular transport was quantified over time. Plot of nC projection length growth and intercellular transfer are overlayed. Intercellular transfer lags projection formation by a few hours. (C) Percent difference of intercellular CFSE concentration in MDA-MB-231 cells in separate cultures and co-culture. There is less than $\leq 10\%$ difference between groups indicating that MDA-MB-231 cells act as an infinite source of CFSE and the concentration of CFSE does not change significantly in co-culture. (D) A concentration versus time curve was plotted for separate and co-cultures based on fluorescence intensity values. However, to obtain the actual concentration plot requires correcting for background autofluorescence.

time and is given by the following expression,

$$\frac{\partial C}{\partial t} + \nabla \cdot (C\vec{v} - D\nabla C) = R(C),$$

where **C** is the concentration scalar field in *Molar* units, **t** is time in units of *seconds*, **D** is diffusion constant in units of m^2/s, $\vec{v}$ is the velocity vector field in units of *m/s*, and **R** is a generation/consumption term (scalar field) of the molecule of interest in units of *Molar/s*. Fick's second law will be used as the basis of modeling CFSE transport through nanoChannels.

Diffusion through a nanoChannel can be modeled as one-dimensional axial transport as illustrated in **Figure 4-21A**. In constructing this model, we made the following assumptions:

1. MDA-MB-231 cells act as the singular CFSE source so at $t = 0, x = 0, C = C_0$
2. NanoChannel walls are impermeable so CFSE can not diffuse radial or circumferentially, and can only travel in the axial direction. Therefore, diffusion through the nanoChannel can be considered as one-dimensional axial transport.
3. $C_{recipient} << C_0$, therefore MDA-MB-231 cells can be modeled as an infinite source, and MDA-MB-231 cell concentration change with time is negligible.
4. At time zero, CFSE is only in the intercellular compartment of MDA-MB-231 cells, and not in nanoChannels or endothelial cells, so that $t = 0, x > 0, C = 0$.
5. At infinite lengths the CFSE concentration is zero, so that $t > 0, x = \infty, C = 0$.
6. CFSE is not consumed or generated in nanoChannels therefore the generation term (R) is zero.
7. There are no convective forces presents making the $\vec{v}$ equal to zero.

Molecule	Diffusion Coefficients
Small Molecule in water	1000-1500$\mu m^2/s$
Carboxyflourescein in water	487$\pm$22$\mu m^2/s$
Carboxyflourescein in cytoplasm	162$\mu m^2/s$
Small Protein in water	100$\mu m^2/s$
Protein in cytoplasm	10$\mu m^2/s$
miRNA in water	100$\mu m^2/s$
miRNA in cytoplasm	10$\mu m^2/s$

Table 4.2: Diffusion coefficients for different classes of molecules[4–6].

8. NanoChannels are presumably filled with cytoplasmic contents which are composed of 80% water. At low velocities, water, and therefore cytoplasm, can be considered incompressible flow.

9. CFSE can freely diffuse from MDA-MB-231 to HUVEC endothelium as unbound free molecules.

Applying these assumptions in the limited case of one-dimensional diffusion with a singular source into the more common form of Fick's second law,

$$\frac{\partial C}{\partial t} = -D\frac{\partial^2 C}{\partial x^2},$$

where C is the concentration in *molar* units, t is time in *seconds*, D is diffusion constant in units of μm^2/*sec*, and x is length in units of μm gives the final expression:

$$C = C_o(1 - \text{erf}\frac{x}{2\sqrt{Dt}}),$$

where C_o is the initial CFSE concentration loaded in the MDA-MB-231 cells.

Figure 4-21 presents the results of this analysis compared to theoretical data. Estimation of diffusion constants were taken from the literature and presented in **Table 4.2**. CFSE was considered to be analogous to a carboxyfluorescein molecule in cytoplasm. NanoChannel length was used as the value of x and diffusion was modeled over a 24hr period. **Graph 4-21B** is a plot of predicted CFSE concentration

versus length at varying times. An average nanoChannel length of 31μm given in **Table 4.1** was used to generate this graph. At early times, CFSE has only diffused a small fraction of the length of nanoChannels. At approximately 5hrs, similar to the behavior of the experimental data, the CFSE molecules have traveled down the entire length of the nanoChannel and have begun to diffuse into the endothelium.

To probe the dynamics of CFSE diffusion, we next varied the input parameters of this model. In all plots experimental data is given by the black curve. **Figure 4-21C and D** plot changes in diffusion dynamics of CFSE with changing nanoChannel length. Setting the diffusion constant at D=0.005μm^2/sec, we varied nanoChannel length over the range of nCs. Intuitively, and supported by the theoretical results given in **Figure 4-21C and D**, CFSE diffuses to the endothelium more quickly through shorter nCs. **Figure 4-21D** is a blow up of **Figure 4-21C**, focusing only on the longer nCs. The experimental data **(black curve, Figure 4-21C,D)** of CFSE transfer represents a statistical average over a population of structures, with a range of length scales. However, two trends emerge from the plots. The first trend shows that theoretical data predicting diffusion through longer nanoChannel structures better correlates with experimental data. This observation is supported by length scale measurements given in **Figure 4-7** which show that the majority of nCs tend to be long. The second trend is that the diffusion constants used to fit this data are several orders of magnitude smaller than the values given in the literature. This trend is further highlighted in **Figure 4-21E**, which probes the affects of varying diffusion constants on transport. **Figure 4-21E** presents results of diffusion constant varied over a constant nanoChannel length. Increasing the diffusion constant, enhanced the speed of diffusion and also increased the maximum concentration achieved in the endothelium by 24hrs. The apparent diffusion constant that best fits the experimental data is much smaller than values predicted in the literature. This could imply that CFSE does not freely diffuse or that diffusion is impeded within the nanoChannel. The reasons for this impediment may be linked to the cytoskeletal composition of the nC. This analysis suggests that nanoChannels may have a more solid configuration, characterized by densely packed cytoskeletal

proteins that impedes free diffusion.

A densely packed configuration of cytoskeletal proteins within nanoChannels is further supported when comparing experimental and theoretical CFSE concentrations at 24hrs. At early time points, the gray curve given in **Figure 4-21E** closely models experimental data . However, at later time points the graph significantly overshoots the maximum CFSE concentration measured experimentally. The experimental data plateaus at a concentration of 127nM while the theoretical plot predicts a concentration of 679nM. The vast difference between these two values likely arises due to an incorrect assumption made when creating this model. We initially assumed that CFSE was able to freely diffuse through nanoChannels, however this may not be the case. Instead diffusion through nanoChannels may be more analogous to diffusion through a porous medium. An effective diffusion coefficient describes the actual diffusive transport accounting for restrictions placed on free diffusion.

An effective diffusion coefficient is given by the following expression:

$$D_e = \frac{D\epsilon_t\delta}{\tau},$$

where **D** is the free diffusion coefficient in units of m^2/s, ϵ_t is the porosity, δ is the constrictivity, and τ represents the tortuosity. Porosity is the measure of empty space in a material given by the fraction of the volume of voids over total volume. **Figure 4-21G** illustrates a cross-section of a nanoChannel with a dense cytoskeletal network. There is limited void space in this type of structure making free diffusion very difficult due to a low porosity. Constrictivity accounts for spatial constraints affecting diffusion and is calculated by taking a ratio of the diameter of a diffusing particle to the pore diameter. Tortuosity is a measure of curve being tortuous. Constrictivity likely has a negligible effect due to the small particle diameter of CFSE. However, tortuosity and porosity may significantly contribute to the low effective diffusion coefficient compared to theoretical diffusions coefficients initially used for this analysis. For example nanoChannels adopt a varied, often curved, config-

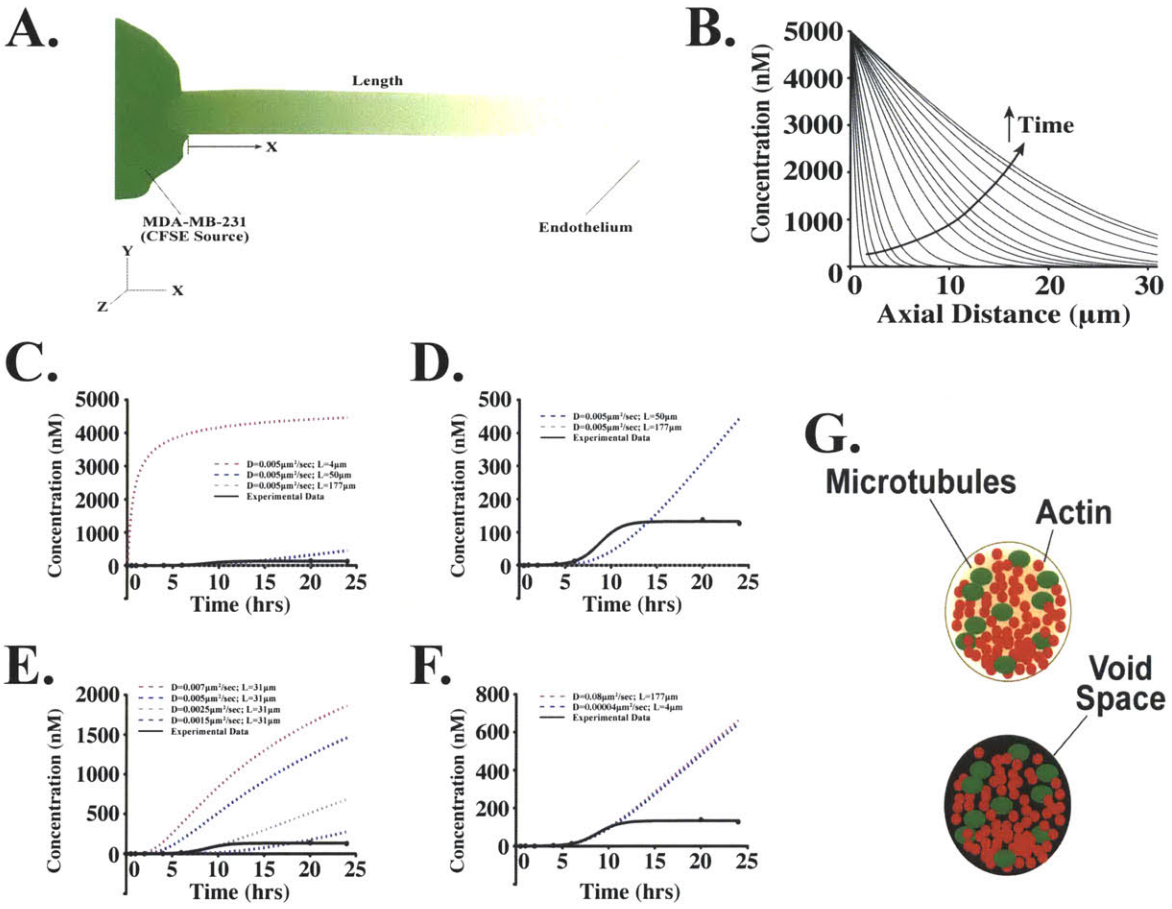

Figure 4-21: Modeling diffusive transport through nanoChannels (A) Diffusion through nanoChannels can be modeled as one dimensional axial transport. (B) CFSE concentration versus length plot in endothelial cells. Intuitively, increasing nanoChannel length increases time required for CFSE to diffuse through the entire length of the projection. (C/D) Examines concentration of CFSE in endothelial cells versus time with changing nanoChannel length or (E) diffusion constant. (F) Concentration versus time over the range of possible diffusion constants determined by fitting the experimental data over the entire range of nanoChannel length. (G) Based on results of the diffusion model, it can be concluded that nanoChannels are likely solid structures with limited empty space. The lack of void space significantly retards diffusion possibly implying the existence of an active transport mechanism within nCs.

uration that results in a high tortuosity. A combination of low porosity and high tortuosity may contribute significantly to restricted diffusion within nanoChannels. Finally, **Graph 4-21F** fits the model for the two extremes of nC length scales to find the possible range of diffusion constants. The effective diffusion constant may lie within the range from $0.00004\mu m^2/s$ - $0.08\mu m^2/s$. How can we explain this large deviation from theoretical values of CFSE diffusion coefficients in water?

First diffusion coefficients in the cytoplasm are typically one order of magnitude lower than diffusion coefficients due to macromolecular crowding caused by steric restrictions and weak intermolecular interactions[6]. CFSE is a small molecule with an atomic radius of approximately $\tilde{9}.4\mathring{A}$ so steric constraints are unlikely. A second contributor to this large deviation results from the large inaccuracy of the assumption that CFSE freely diffuses when transported through nCs. Due to a succinimidyl group, CFSE covalently couples to intercellular molecules. Therefore, bound CFSE does not have the same transport dynamics of free CFSE. For example, if CFSE were covalently bond to a protein the diffusion coefficient would be two-orders of magnitude less than free CFSE. However, the effective diffusion coefficient is 4 to 7 orders of magnitude smaller than would be predicted by transport of bound CFSE. Therefore, covalent bonding of CFSE to intercellular proteins can not completely account for the dramatic difference in theoretical vs effective diffusion coefficients.

Other limitations not accounted for by the model is that CFSE may be degrading in the endothelium. However, this is highly unlikely to occur within the time scales of interest. In addition, fluorescence intensity may not be directly correlated with concentration, leading to errors in determining a concentration versus time plot from experimental data. Also, experimental data represents a statistical average of a diverse population of nCs, while the ideal model is narrowly constrained considering only a single projection at a time. Therefore it is unlikely to be a complete representation of diffusion through nCs. To address this limitation, transport through a single nC must be studied. Lastly, the model does not include the kinetics of cytoskeletal rearrangement required for nC projection formation. A more

robust model would integrate transport membranes with cytoskeletal dynamics.

4.3.4 Transport of synthetic materials and bioorganic macromolecules through nanoChannels

NanoChannels are a complex mode of intercellular communication with unique properties. In order to understand the physiological role of nanoChannels, we sought to understand the range of intercellular contents that could be transported through these structures. NanoChannels facilitated the trafficking of nanostructures (quantum dots) **(Figure 4-22)**, intercellular proteins (GFP) **(Figure 4-23)**, cytoplasmic organelles (lysosomes) **(Figure 4-24)**, and miRNAs. MicroRNA transport will be discussed in **Chapter 5**.

The ability of nCs to transport quantom dots (Qdots), GFP, and lysosomes holds interesting implications on the physiological roles of these structures and also introduces a mechanism to exploit these structures for therapeutic benefit. Analogous to studies done with CFSE, the MDA-MB-231 cells were loaded with either Qdots or GFP (through transfection) prior to incubation with DiL-LDL labeled endothelial cells (red). In **Figure 4-22A and Figure 4-23**, transported intercellular contents are indicated with yellow arrows in 3D reconstructions of de-convolved fluorescence images. **Figure 4-22A and Figure 4-23** reveal fluorescent cargo within the endothelial cell bodies. **Figure 4-22 schematic (A) and graph (B)** quantify intercellular transport of Qdots which supports imaging data.

Transport of GFP highlights that active proteins can be transported through nC structures. Transport of proteins may temporarily alter the downstream expression of recipient cells, acting as a mechanism of acquired drug resistance or pathological angiogenesis. The ability of metastatic cells to transfer biomolecules that may transform recipient cells holds implications on how tumors manipulate the surrounding cell population to promote tumorigenesis. Furthermore, Qdot transfer holds interesting implications on how nanoChannel-mediated communication can be capitalized on for novel therapeutic strategies. One possibility is that

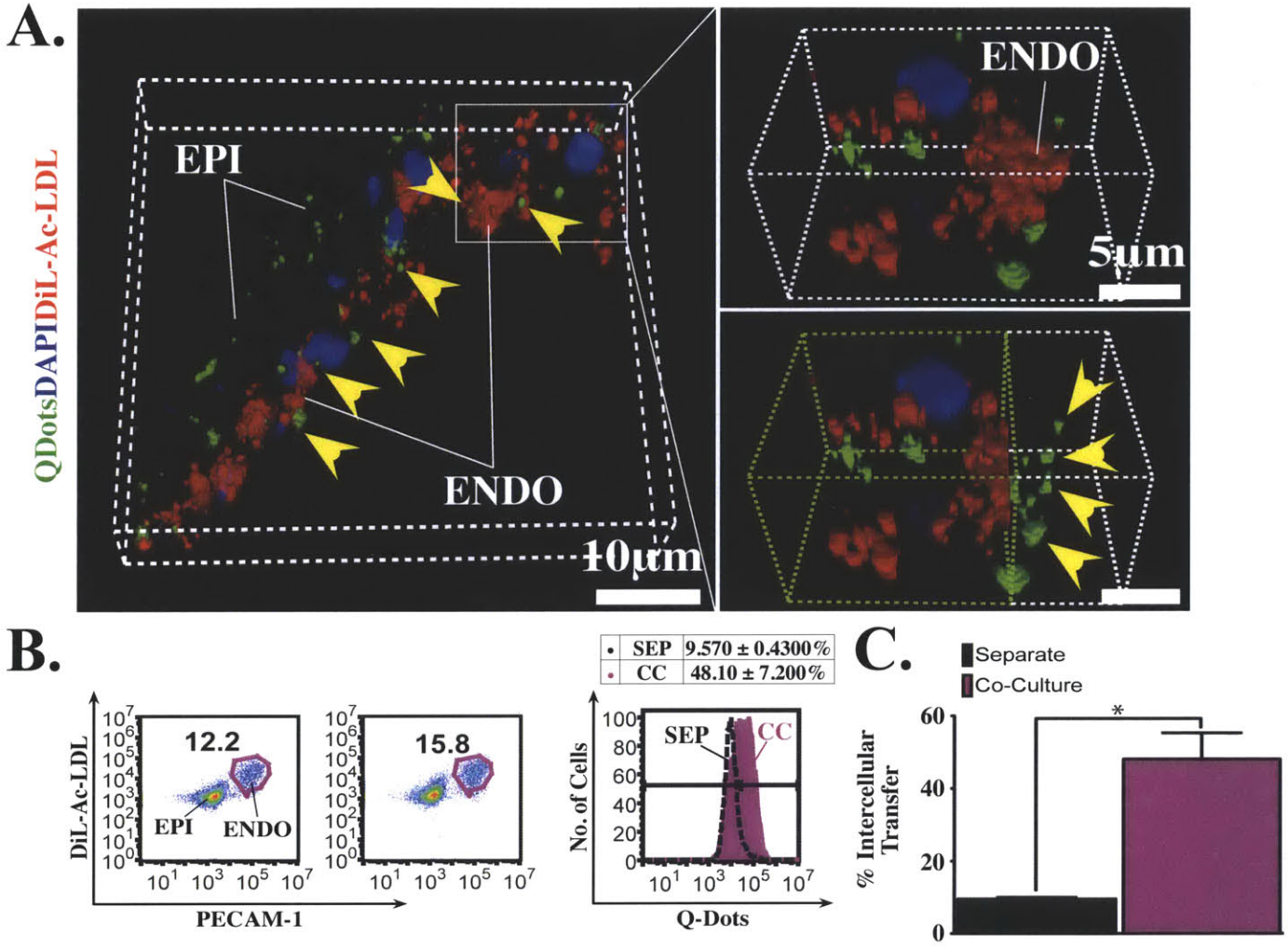

Figure 4-22: Intercellular transport of Qdots through nCs. (A) 3D volume reconstruction illustrating quantum dot nanoparticles in DiL-Ac-LDL labeled endothelial cells. Yellow arrowheads indicate endothelial cells containing transferred nanoparticles. (B/C) Intercellular transfer of Q-dots was confirmed via flow cytometry. In co-cultures, 48.10±7.200% of the endothelial cell population was positive for quantum dots compared to 9.570±0.4300% in separate cultures ($p<0.05$).

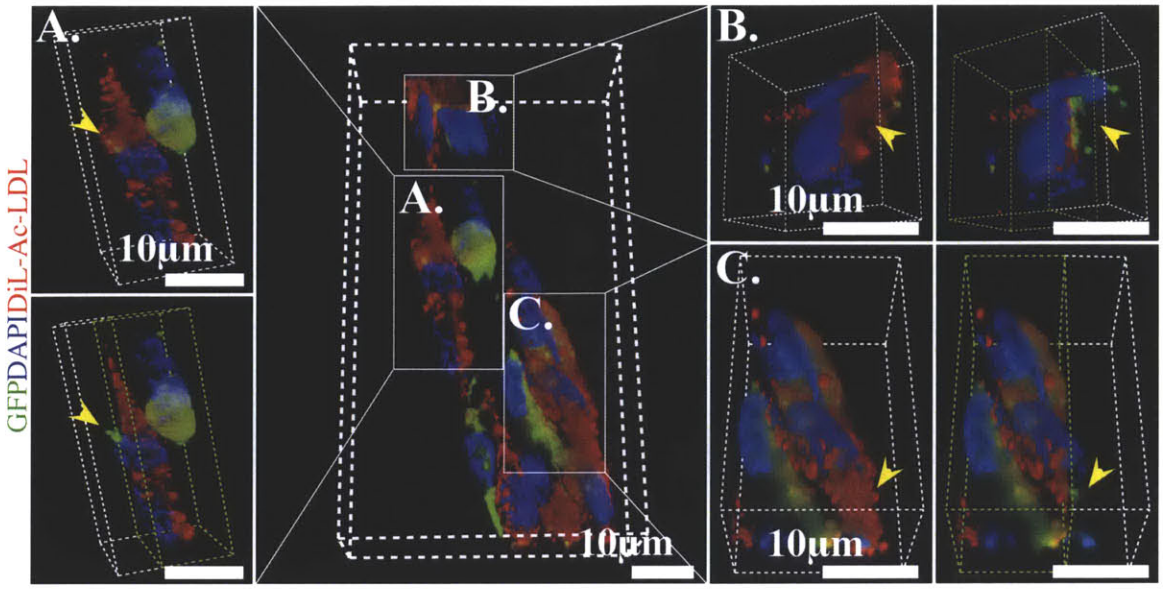

Figure 4-23: Intercellular transport of GFP through nCs. nCs provide a mechanism of transfer of soluble cytoplasmic proteins. GFP is detected within endothelial cells (indicated with yellow arrow heads).

nanoparticles can be uptaken by the cancer cells and transferred to other malignant cells as well as the surrounding stroma. There may be therapeutic strategies that can take advantage of this novel form of intercellular communication, especially capitalizing on the propensity of metastatic cells to form connections with the endothelium.

NanoChannels are also a conduit for organelle transfer. **Figure 4-24** summarizes the results from studies examining organelle transport through nCs. These studies were performed by co-culturing two populations of MDA-MB-231 cells **(Figure 4-24A)**. Half of the population was stained with a fluorescent cell membrane dye (CMD+ve), while the other half of the population was stained with a fluorescent dye that labels lysosomes (CMD-ve). The two cell populations were co-cultured for 24hrs and the prescence of fluorescently labelled lysosomes was determined in each population **(Figure 4-24B and C)**. As expected, in separate cultures, the CMD+ve population was negative for fluorescently labelled lysosomes

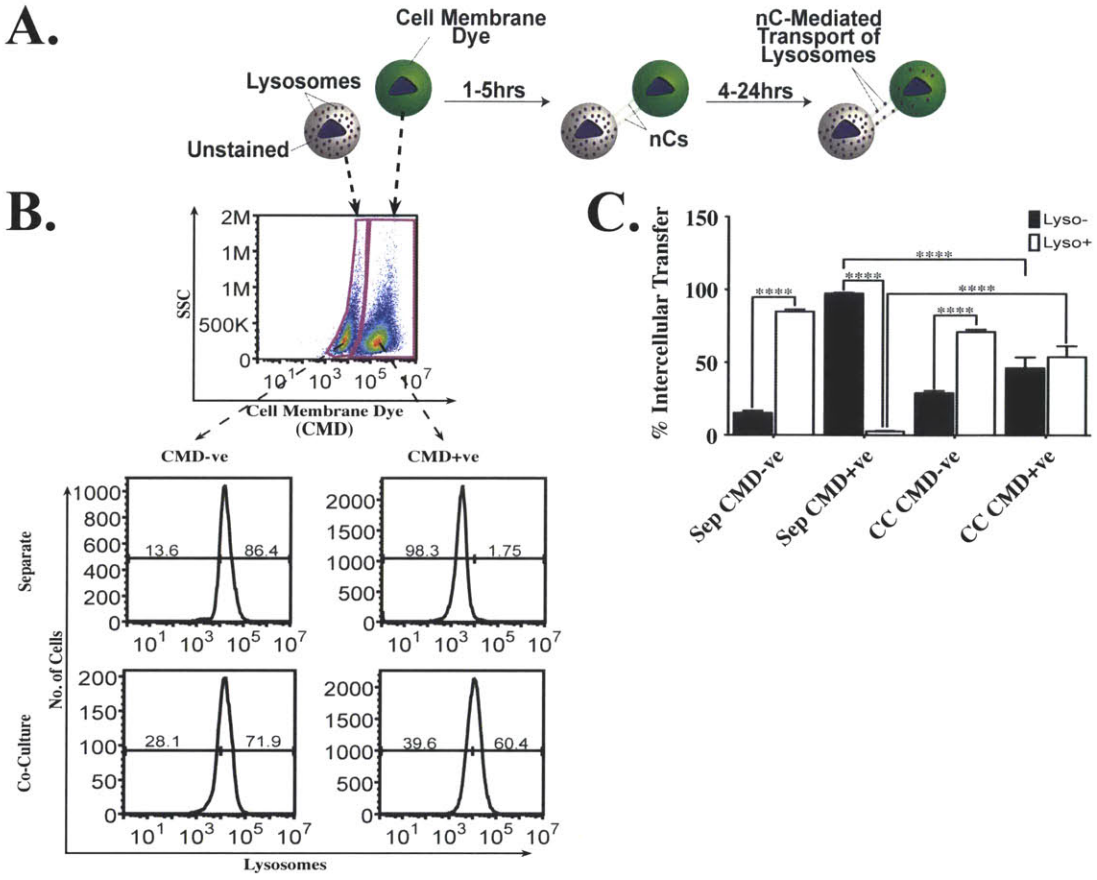

Figure 4-24: Organelle transfer through nanoChannels. (A) Schematic illustrating experimental design used to detect intercellular transfer of lysosomes through nC structures. MDA-MB-231 cells were fluorescently labeled with LysoTracker Red and then co-cultured with MDA-MB-231 cells labeled with a green cell membrane dye (CMD) at a 1:1 ratio. (B/C) Fluorescently labeled lysosomes were tracked using flow cytometry. The presence of fluorescently labeled lysosomes were assessed in CMD+ve and CMD-ve cells. In co-culture, 53.867±7.451% of the CMD+ve cells were positive for fluorescently labeled lysosomes ($p<0.0001$), compared to 2.613±0.478% of the CMD+ve cells in the separate cultures. The detection of labeled lysosomes in CMD+ve cells is likely due to the natural autofluorescence background of endothelial cells.

with only 2.613±0.478% of the population detected as positive (likely secondary to the natural autofluorescence of endothelial cells). In contrast, a high percentage of (53.867±7.451%) the cell population in co-cultures was positive for stained lysosomes. Furthermore, the increase of labelled organelles in these cells was mirrored by a cognate decrease in lysosomes in the CMD-ve group. This dcrease is likely due to transfer of lysosomes from the CMD-ve cells in co-culture and to the CMD+ve cells. Recall that this group represents the half of the co-culture population originally labelled with a fluorescent lysosomal dye. Although not explicitly demonstrated nanoChannels are likely the mechanism by which transport of lysosomes occurs in this model system.

NanoChannel-mediated communication appears to be universally conserved mechanism of intercellular communication. Stromal cells are also able to form nC structures by which intercellular contents can be communicated. **Figure 4-25A** illustrates nanoChannels or nanoChannel-like structures formed between endothelial cells. A projection formed by an endothelial cell **(Figure 4-25A3)** can be seen bypassing two breast epithelial cells **(white arrows, Figure 4-25A2)** to instead form a connection with a distant endothelial cell **(yellow dotted arrow, Figure 4-25A2)**. Since a full characterization was not done on these structures, it is unclear if these projections are nanoChannels or another related structure. Regardless of their identify, these structures too function in intercellular communication. When loaded with CFSE, the HUVEC endothelial cells were able to transfer intercellular contents to metastatic MDA-MB-231 breast epithelial cells. However, the percentage of the population receiving this reverse transfer was lower than communication from metastatic epithelial cells to the endothelium **(Figure 4-25B/C)**. This may be the result of endothelial cells preferentially forming connections with other endothelial cells, possibly in response to the same growth factors that drive metastatic cells to preferentially form nanoChannel connections with the endothelium.

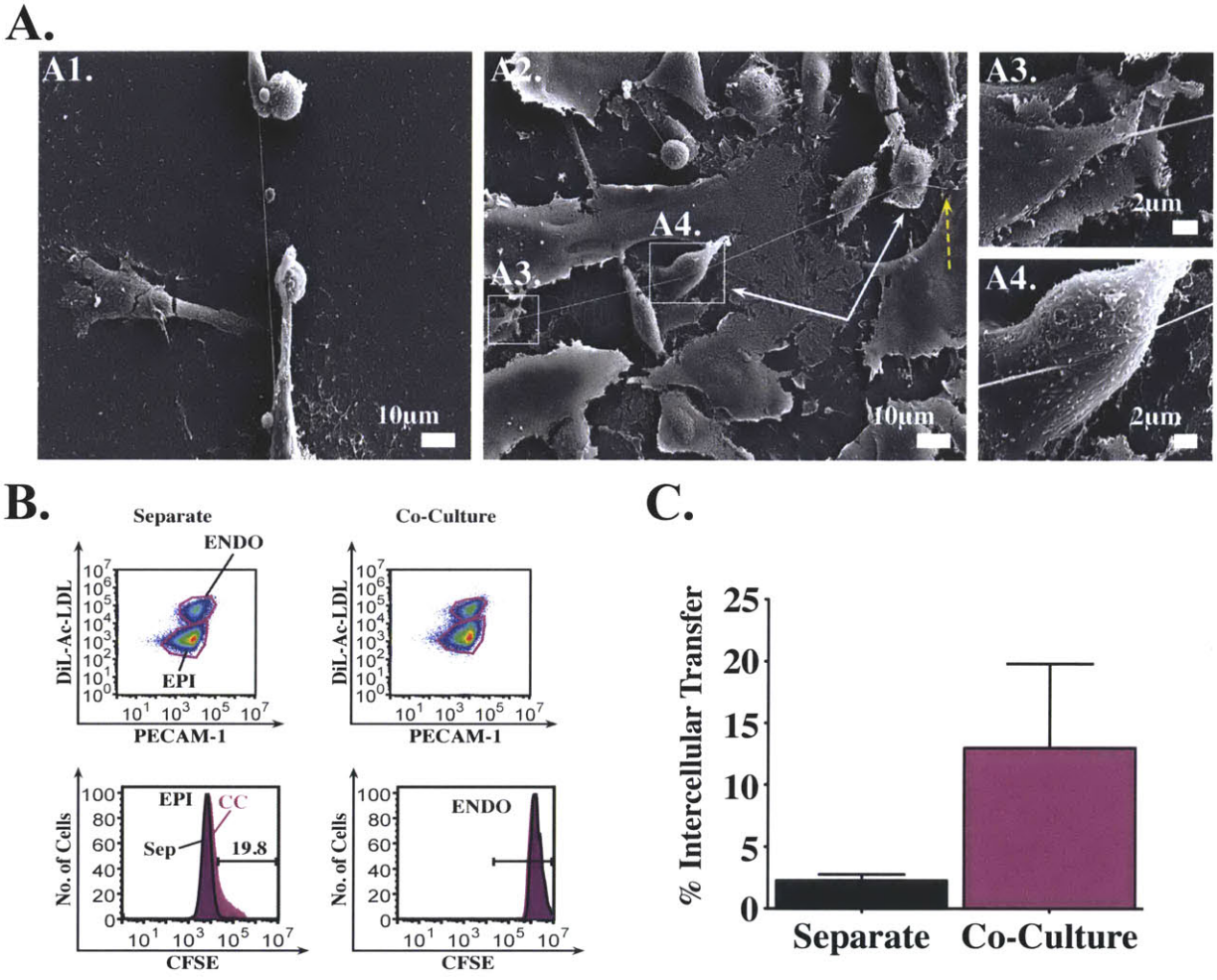

Figure 4-25: Reverse transfer through nanoChannel like structures. (A) SEM micrographs show connections formed between two endothelial cells. (B) Schematic and (C) graph of intercellular transfer from endothelial cells to metastatic breast epithelial cells. Only a small percentage of the epithelial cell population received intercellular communication from the endothelium.

4.4 Disruption of nanoChannels using cytoskeletal polymerization inhibitors

NanoChannel-mediated communication allows for the transport of a diverse array of intercellular contents, including small molecules, cytoplasmic proteins, organelles, and synthetic materials. To further validate the role of nanoChannels in intercellular communication, we hypothesized that pharmacological inhibitors that blocked polymerization of α/β-Tubulin and F-Actin cytoskeletal proteins would disrupt nanoChannel structures. To validate this hypothesis, we tested effects of the α/β-Tubulin cytoskeletal inhibitor, docetaxel, and the F-actin cytoskeletal inhibitors, latrunculin A and cytochalasin D, on nanoChannel formation by MDA-MB-231 cells. **Graphs 4-26 A, B, and C** illustrate results from dose titrations with latrunculin A, docetaxel, and cytochalasin D, respectively, examining the effects of these drugs on intercellular transport. The drugs were tested in MDA-MB-231 monoculture, where half of the MDA-MB-231 cell population was labeled with CFSE and the other half was unlabeled. The metastatic epithelial cells were pretreated with inhibitors for 24 hours prior to adding the cells to the culture as outlined in **Figure 4-17**. The percent of the cells receiving intercellular transfer was quantified and plotted. The data was normalized to control.

At low concentrations all the cytoskeletal inhibitors decreased intercellular transfer. Interestingly, at high concentrations the percent of intercellular concentration actually increased in some of the drug groups. It's unclear why this increase occurred, however, there are two likely factors responsible for this trend. The first is that nanoChannel projections are increased due to stress. High concentrations of drug may induce physiological stresses that result in projection formation which in turn leads to increased intercellular transfer. Similar cytoskeletal projections were found to increase in response to stress conditions. The second possibility is that high concentrations of drug destabilize the cytoskeletal membrane so much that the membrane actually disrupts. In this case CFSE would be able to freely diffuse from the cell to the recipient cell population independent of the presence

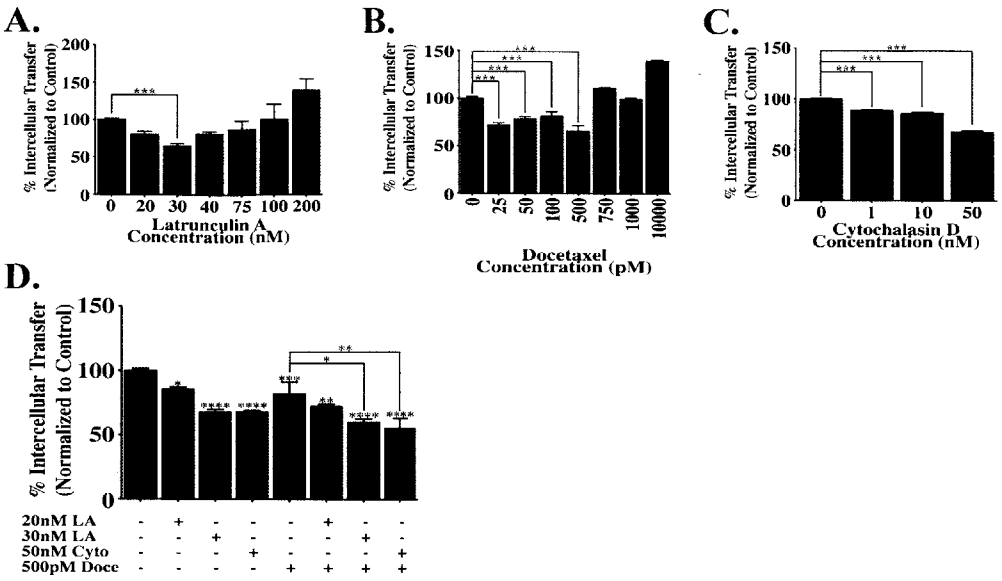

Figure 4-26: Optimization of pharmacological inhibition of nanoChannel structures. Dose titrations with cytoskeletal polymerization inhibitors (A) latrunculin A, (B) docetaxel, and (C) cytochalasin D were performed in a MDA-MB-231 monoculture system. (D) Combination of the α/β-Tubulin and F-Actin polymerization inhibitors resulted in decreased intercellular communication compared to each drug alone.

of nanoChannel projections.

The most effective concentration of each drug was selected and a combination of α/β-Tubulin and F-Actin polymerization inhibitors were tested. Combinations of the inhibitors achieved slightly greater inhibition compared to either drug alone **Graphs 4-26D**.

These optimization studies next enabled testing of the cytoskeletal polymerization inhibitors in an epithelial-endothelial co-culture format. From the therapeutic perspective of metastatic cancer, it is much more advantageous to disrupt epithelial-endothelial cell-cell communication. Therefore, we tested the optimized combinations in the co-culture platform. The data is summarized in **Figure 4-27 and Figure 4-28**.

MDA-MB-231 cells were pre-treated for 24 hours with a combination of docetaxel (500pM) with latrunculin A (30nM) or cytochalasin D (50nM), before addition to the endothelial vessels as described in **Figure 4-17**. Combination of the

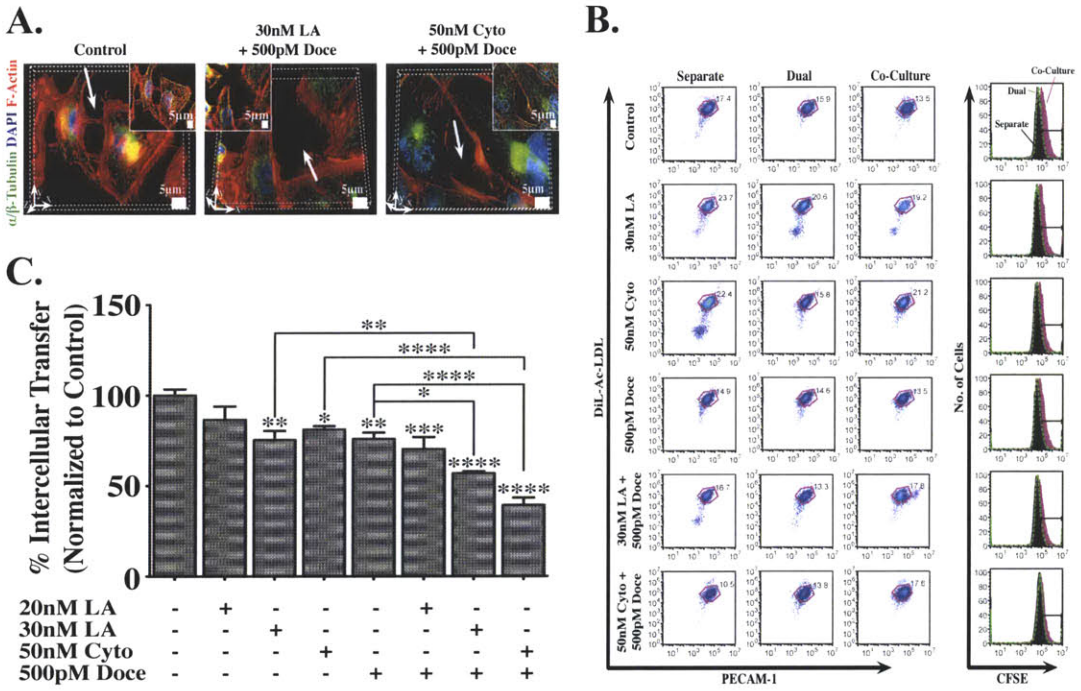

Figure 4-27: Combination of α/β-Tubulin and F-Actin polymerization inhibitors disrupt nanoChannel-mediated communication between metastatic breast epithelial cells and the endothelium. (A) NanoChannels are visibly disrupted after exposure to cytoskeletal polymerization inhibitors. (B/C) Drug combinations with small molecule inhibitors of F-actin (latrunculin A and cytochalasin D) and microtubules (docetaxel) were used to disrupt nC structures leading to a decrease in intercellular communication ($p<0.0001$)

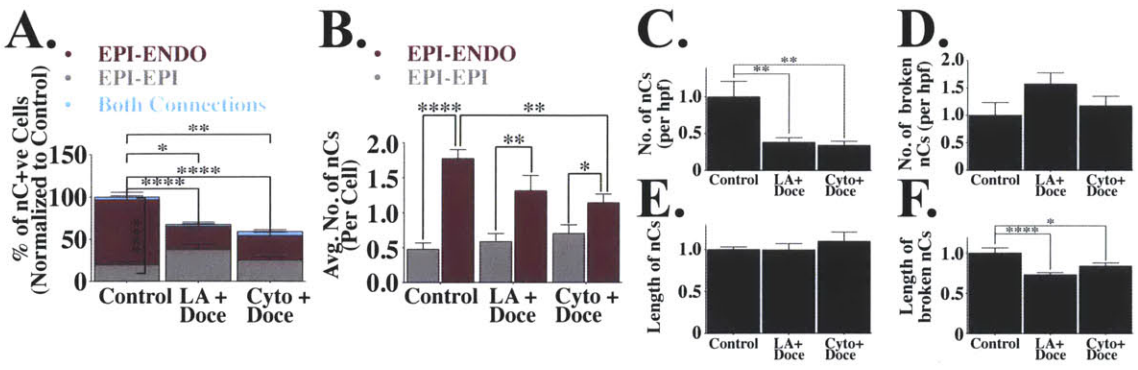

Figure 4-28: Quantification of nanoChannel disruption by cytoskeletal polymerization inhibitors. Drug combinations with small molecule inhibitors of cytoskeletal components F-actin (latrunculin A and cytochalasin D) and microtubules (docetaxel) were used to disrupt nC structures leading to (A) a decrease in percentage of EPI-ENDO nC+ve cells ($p<0.0001$), and (B) reduction in the number of nC structures per cell. (C-F) Drug treatment prevented the formation of nCs ($p<0.01$) (C) and also affected lengthening of the structures ($p<0.0001$). High power field (hpf)

cytoskeletal inhibitors disrupted nanoChannel structures as shown in **Figure 4-27A**. This data supported decreased intercellular transfer quantified using flow cytometry. **Figure 4-27 B and C** show a schematic and graph summarizing the percent of the HUVEC population receiving intercellular transfer at each concentration. As shown in **Figure 4-27C**, there was a significant reduction in nanoChannel-mediated communication following drug treatment. Physical disruption of nanoChannel structures **(Figure 4-27A)** corresponded to a decrease in nC functional activity. Intercellular transfer of CFSE decreased by $42.0\pm2.8\%$ ($p<0.0001$) and $56.6\pm0.4\%$ ($p<0.0001$) following pre-treatment of metastatic cells with combination of docetaxel (500pM) with latrunculin A (30nM) or cytochalasin D (50nM), respectively. Furthermore, drug treatment inhibited the total number of nC structures **(Figure 4-28C)**, as well as, the length of immature nanoChannels **(Figure 4-28F)**. However, there was no effect on the length of mature (tethered) nanoChannels **(Figure 4-28E)**. Taken together these data suggest that drug treatment prevents both initiation and lengthening of nCs but once intact structures are formed they are not disrupted by drug. Additionally, heterotypic epithelial-endothelial nCs were more

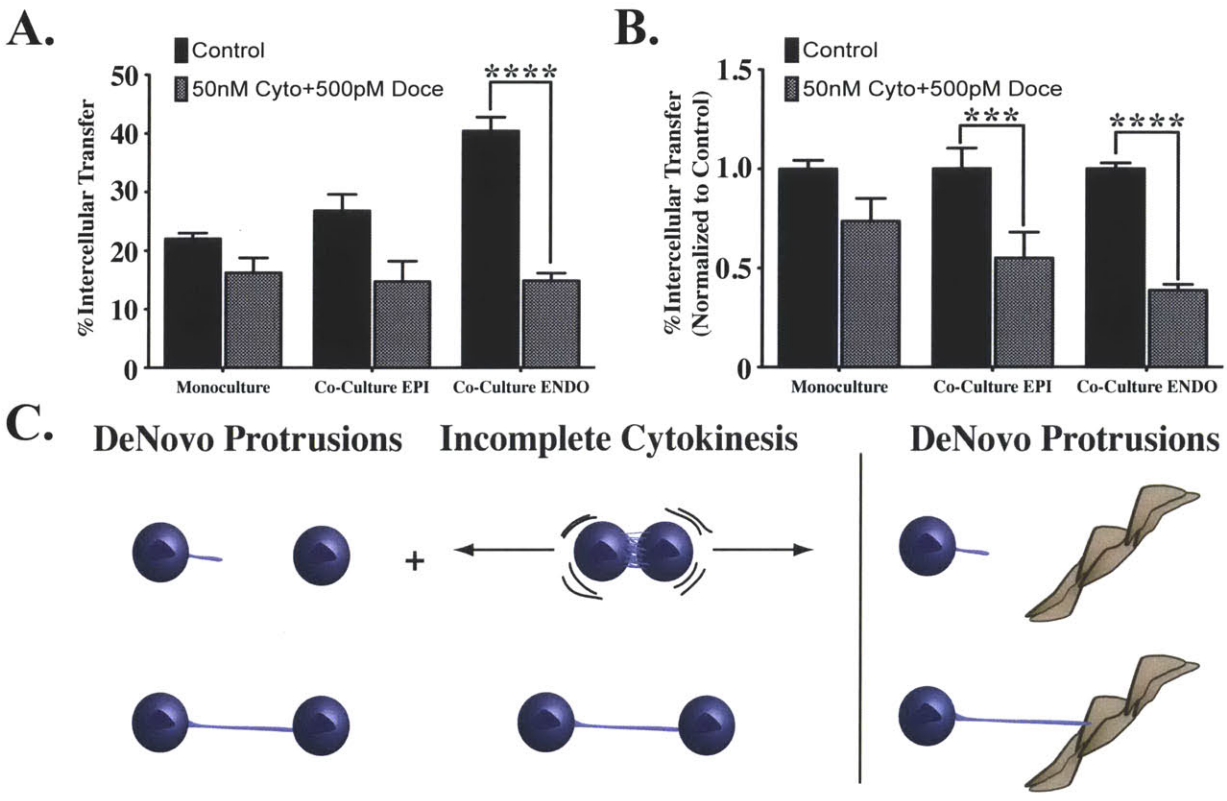

Figure 4-29: Heterotypic versus homotypic nC structures. (A/B) Inhibiting actin tubulin cytoskeletal has a greater effect on nanoChannels formed in heterotypic EPI-EPI co-cultures (MDA-MB-231/HMEC) and heterotypic EPI-ENDO co-cultures (MDA-MB-231/HUVEC) than homotypic EPI-EPI co-cultures (MDA-MB-231/MDA-MB-231). (C) This difference may highlight differences in mechanisms of formation of heterotypic vs. homotypic nCs.

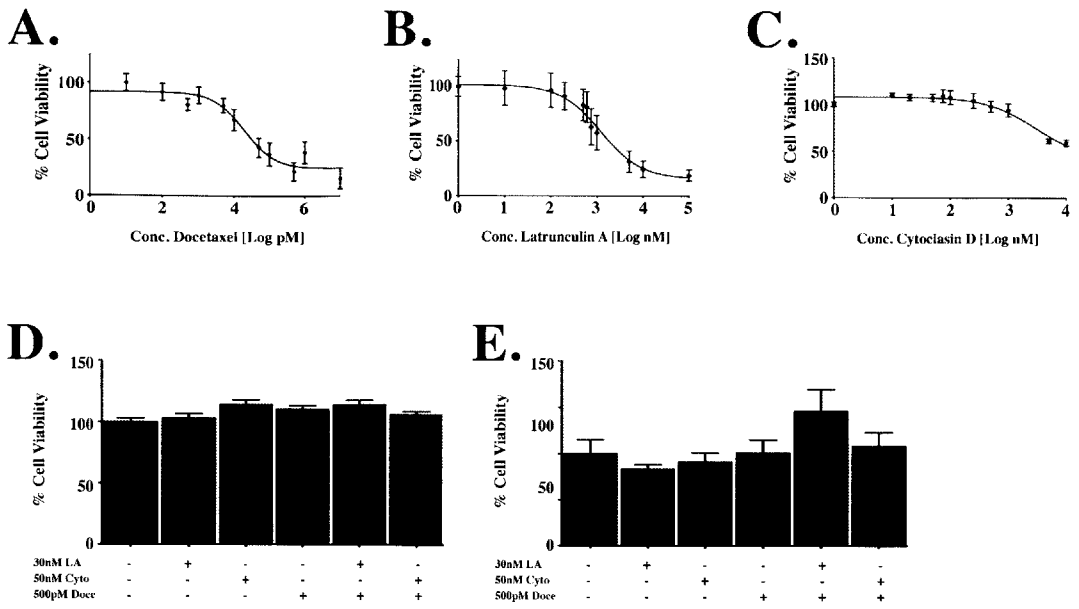

Figure 4-30: Treatment with low-dose F-Actin and tubulin polymerization inhibitors does not affect cell viability. (A-C) Graphs show concentration effect curve for docetaxel, latrunculin A, and cytochalasin D in MDA-MB-231. (D-E) Viability studies using combination of F-actin and tubulin polymerization inhibitors showed no effect on cell proliferation at (D) 24h and (E) 48hrs.

sensitive to the combination of actin-tubulin cytoskeletal inhibitors as evident by reduction in the number of nanoChannel+ve cells by <60% ($p<0.0001$) **(Figure 4-28A)**, as well as, a decrease in the average number of EPI-ENDO nanoChannels formed per cell, compared to homotypic EPI-EPI nanoChannels **(Figure 4-28B)**. The differential drug effects may arise from distinct mechanisms of formation of EPI-EPI and EPI-ENDO connections. EPI-ENDO nanoChannels likely form only through *de novo* protrusions mediated by actin-tubulin cytoskeletal machinery, while EPI-EPI connections may be the result of *de novo* projections, as well as, remnants of incomplete cytokinesis. Inhibition of cytoskeletal projections in heterotypic culture is more effective at reducing nanoChannel communication as shown in **Figure 4-29**. This result further emphasizes that nCs in homotypic versus heterotypic cultures likely resulting from different mechanisms.

4.4.1 Cytoskeletal polymerization inhibitors do not affect cellular proliferation, cellular migration, or induce apoptosis

To confirm that inhibition of intercellular communication was due specifically to disruption of nanoChannels rather than non-specific drug effects, we studied the effects of these inhibitors on cellular proliferation, cellular migration, and apoptosis at drug concentrations found to effectively inhibit nanoChannel formation. If drug inhibition significantly disrupted cellular physiology, the decline in intercellular transfer could potentially be a consequence to cellular death or an inability of cells to migrate and interact with the endothelium. These outcomes would be independent of nanoChannel formation and would not validate the role of nCs in intercellular transport. **Figure 4-30, Figure 4-31, Figure 4-32** provide the results of studies examining changes in proliferation, migration, and cell viability, respectively, in response to drug treatment.

Graphs 4-30 A, B, and C show the results of dose titrations with docetaxel, latrunculin A, and cytochalasin D, respectively, on cellular proliferation. Cell viability was measured using an MTS (3-(4,5-dimethylthiazol-2-yl)-5-(3-carboxymethoxyphenyl)-2-(4-sulfophenyl)-2H-tetrazolium) assay. The MTS assay is a colorimetric method for assessing cell viability. The MTS tetrazolium reagent is reduced by NADPH or NADH to produce a colored formazan product. NADPH and NADH are produced by dehydrogensase enzymes present in metabolically active cells. The quantity of colored formazan product can be measured using absorption spectroscopy and is directly proportional to the number of living cells in the culture.

NanoChannel formation is inhibited at low drug concentrations with minimal effects on cellular viability. There were no changes in cell viability for each of the drug concentrations utilized in the aforementioned studies (i.e. 500pM docetaxel, 30nM latrunculin A, and 50nM cytochalasin D). These conclusions are highlighted by dose-titration plots which show no change in cell viability at the concentrations used to inhibit nanoChannels **(Graphs 4-30 A, B, and C)**. Furthermore, even drug combinations had no effect on the percentage of viable cells. **Graphs 4-30 D and E**

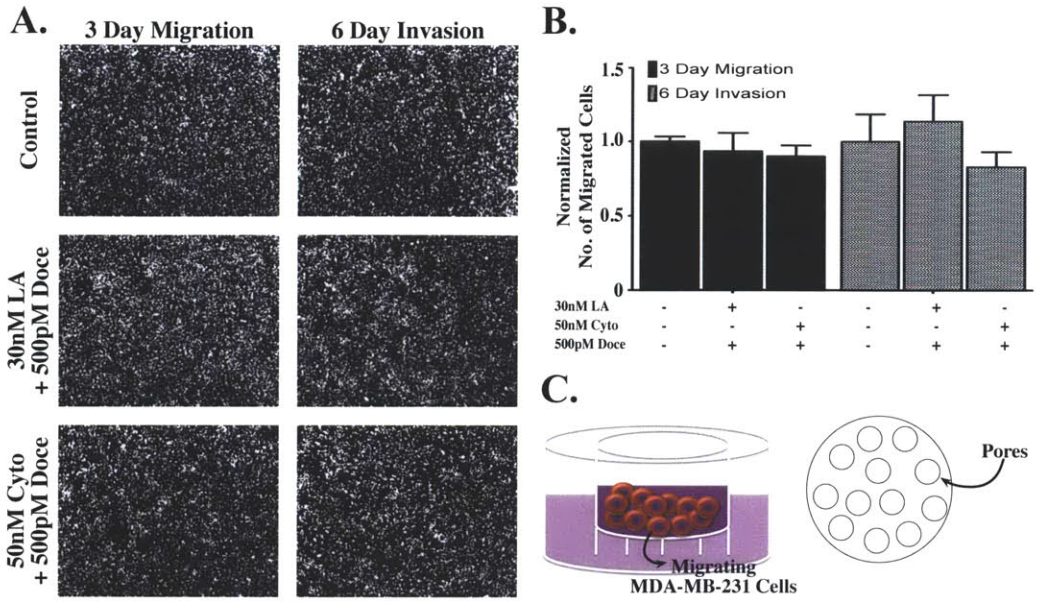

Figure 4-31: Treatment with low-dose F-actin and tubulin polymerization inhibitors does not affect cellular migration or invasion. (A) Images and (B) results from migration assay. Drug treatment did not affect cellular migration or invasion as assessed using a Boyden chamber assay. (A) Images were taken of migrated cells that have crossed the membrane toward the bottom chamber. (B) To test invasion, basement membrane was added to the Boyden Chambers, in contrast to migration studies, which are performed without basement membrane matrix. (C) Schematic illustration of Boyden Chambers. Cells can migrate from the top to the bottom chambers through membrane pores.

summarize results from viability studies at 24 and 48 hrs, respectively, performed at the drug concentrations used to inhibit nanoChannels using single inhibitors as well as drug combinations.

Similar results were observed when assessing drug effects on cellular migration or invasion. **Figure 4-31** show the results from Boyden chamber migration studies. **Figure 4-31C** is a schematic representation of the Boyden Chamber studies. The Boyden chambers are similar to the dual chambers described previously. However, in these studies, 8μm pore size chambers were used that enabled the cells to freely migrate from the top to the bottom chamber. The images in **Figure 4-31A** show the migrated cells that have crossed the membrane pores. Both migration and invasion assays were conducted. The migration assays were performed over three days without addition of a basement membrane matrix to the Boyden cham-

ber. In contrast, the invasion assays were performed over six days with basement membrane added. The migration assay measures the inherent ability of cells to move, while the invasion assay assesses both migration and invasion. The invasion assays are performed with matrix added to the wells, as a result, in order for cells to move from the top to bottom chambers, the cells must be able to proteolytically breakdown the matrix. This requirement provides a surrogate measure of invasive capacity.

Drug treatment at the concentrations of interest did not affect cellular migration or invasion **(Figure 4-31B)**. This is an important result because the ability of cells to interact with the endothelium in 3D cultures requires preserved migratory and invasive properties. Furthermore, formation of nC structures seems to be strongly correlated with intact EEC interactions. Consequently, nC structure formation is linked to invasive and migratory capacities. Drug treatment does not affect these properties, further emphasizing that the pharmacological inhibition of intercellular communication is nanoChannel specific.

Finally, the effect of drug treatment on apoptosis was assessed using an annexin V assay. Annexin V binds to phosphatidylserine residues on the surface of cells that are present during cellular apoptosis. **Figure 4-32** summarizes the results of this analysis. **Figure 4-32A** shows representative images of annexin V staining. Fluorescence was quantified over several images and summarized in **Figure 4-32B**. The results of this analysis show that drug treatment did not induce apoptosis in the cells 24 hours post drug treatment. The results of the proliferation, migration, and viability studies further emphasize that drug treatment specifically inhibited nanoChannel formation and that the observed decrease in intercellular communication was due to nC inhibition and not non-specific drug effects.

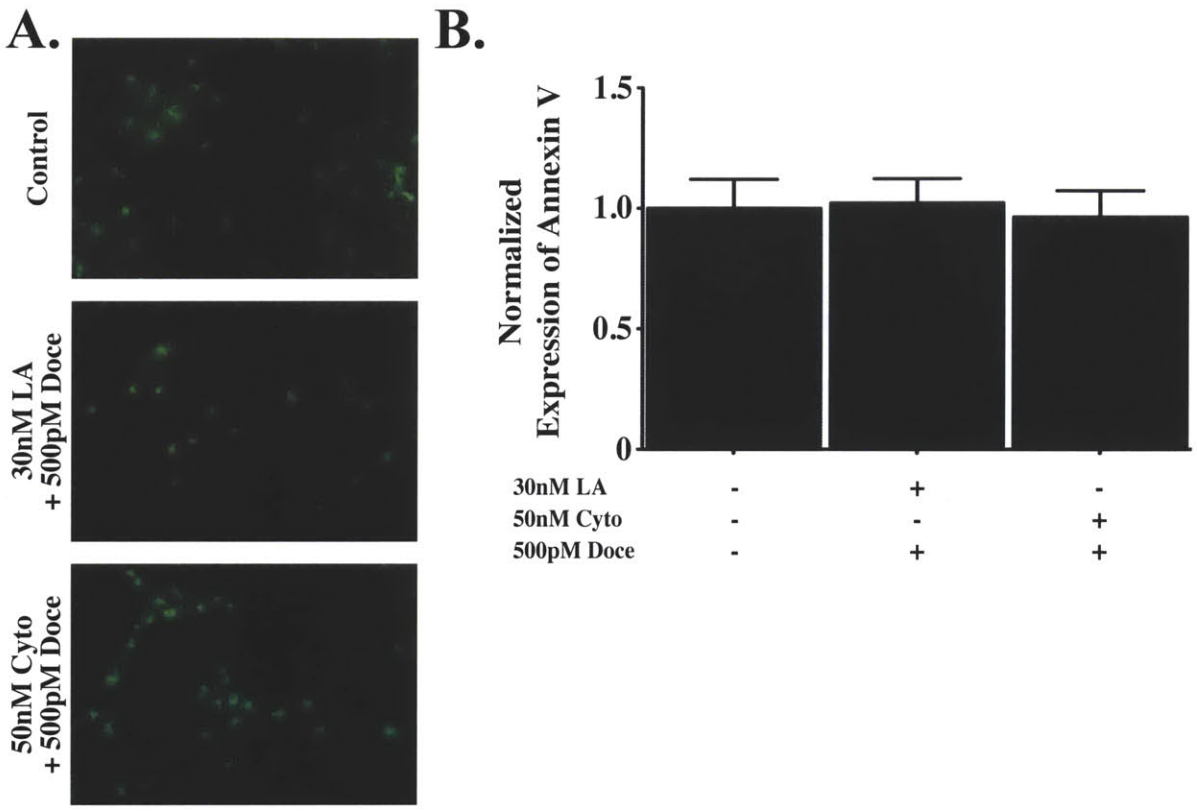

Figure 4-32: Treatment with low-dose F-actin and tubulin polymerization inhibitors does not induce apoptosis. (A) Images and (B) quantification of Annexin V staining used to assess induction of apoptosis by the inhibitors. The combination of F-actin and tubulin polymerization inhibitors did not induce apoptosis following 24 hours of drug exposure. The data was collected 24 hours after drug was removed.

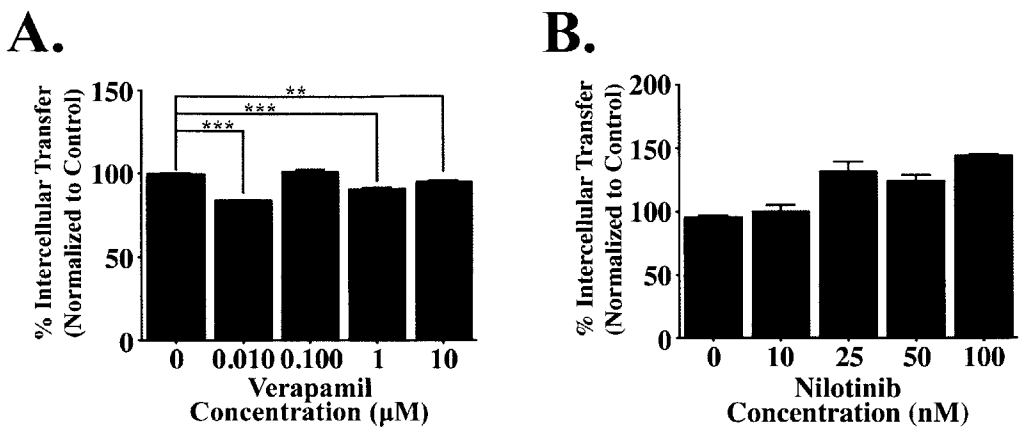

Figure 4-33: Exocytosis inhibitors do not affect intercellular transfer through nCs. Pre-treatment of MDA-MB-231 cells with verapamil and nilotinib had no effect on intercellular communication. These drugs target multidrug resistant transporters that are known to expel small molecules (such as CFSE or drugs) from the cells. The limited effect of these drugs further support that that observed intercellular transfer is likely not do to endocytosis-exocytosis mechanisms.

4.4.2 Pharmacological inhibition of potential endocytosis/exocytotic mechanism

Dual chambers were introduced into the study design as a mechanism to exclude endocytotic and exocytotic mechanisms of intercellular communication. However, to directly probe these mechanisms we also utilized pharmacological inhibitors of these mechanisms. Verapamil and nilotinib were selected because these drugs are inhibitors of efflux transporters. Multidrug resistance (MDR) is a common characteristic seen in many cancer tumor types. MDR is caused by efflux of drugs by ATP-binding cassette transporters, the most common being P-glycoprotein. Verapamil is a voltage dependent calcium channel blocker that was found to inhibit efflux pumps such as P-glycoprotein[310]. Nilotinib is a tyrosine kinase inhibitor also found to inhibit multidrug resistance transporters[311]. Cancer cells express high levels of multidrug resistant pumps[312], therefore we postulated that CFSE may be pumped out of the cells using these transporters, resulting in the observed intercellular transfer. In order to exclude exocytotic mechanisms, we performed dose

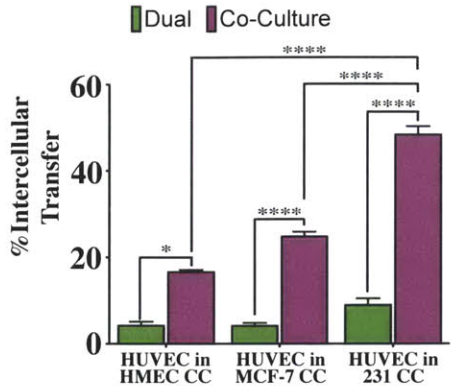

Figure 4-34: Intercellular transfer in normal, tumorigenic, and metastatic cells lines. Normal mammary epithelial cells (HMEC) and tumorigenic cells (MCF-7) transport intercellular contents significantly less than metastatic cells. This result correlates with quantification results showing fewer projections with the endothelium in primary and tumorigenic cell lines compared to metastatic cells.

titrations with each of the two inhibitors prior to co-culture. There were minimal effects on percent intercellular transfer with verapamil and no effect with nilotinib. These results are analogous to results seen with dual chambers (**Figure 4-33**).

4.5 Comparison of nC-mediated communication in primary, tumorigenic, and metastatic cell lines

We have shown the ability of metastatic breast epithelial cells to form nC connections with the endothelium. Metastatic cells preferentially form nC connections with endothelial cells compared to other epithelial cells. However, does this phenotype correspond to functional activity of the nCs? To address this question, we examined the ability of normal and tumorigenic breast epithelial cells, HMEC and MCF-7, respectively, to transfer intercellular contents through nanoChannels. The results of this analysis are given in **Figure 4-34 and Figure 4-35**.

All the cell types show intercellular transfer in co-culture cells compared to control dual chambers (**Figure 4-34**). Primary epithelial cells transfer intercellular contents to 12.39$\pm$1.079% of the endothelial cell population. Compare that to

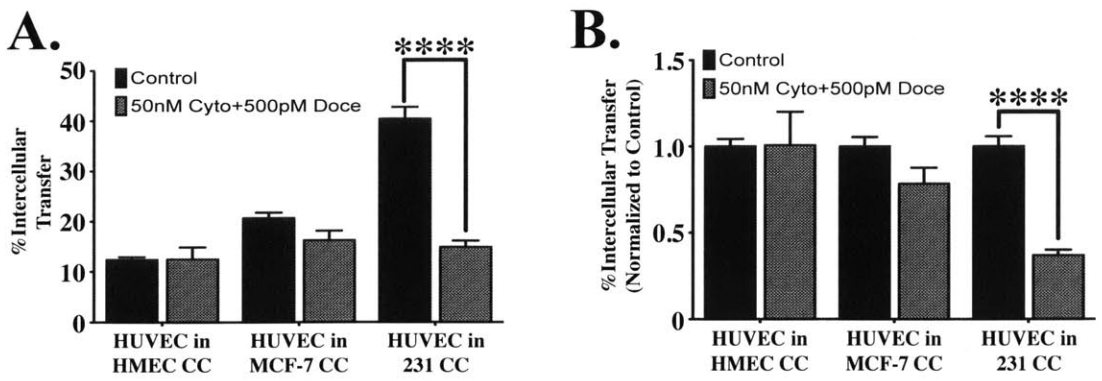

Figure 4-35: Inhibiting cytoskeletal protein polymerization does not reduce intercellular transport in normal and tumorigenic, non-metastatic epithelial cells. (A) Percent intercellular transfer in endothelial cells following pretreatment of breast epithelial cells with cytoskeletal inhibitors. Normal and tumorigenic cell lines show no inhibition of intercellular transfer with drug, implying that this communication may be due to alternative mechanisms. (B) Percent intercellular transfer normalized to control.

16.34±2.1% and 39.374±2.496% transfer of intercellular contents by tumorigenic and metastatic cells, respectively. There is an enhanced ability of metastatic cells to transfer intercellular contents to endothelial cells compared to primary and tumorigenic cells **(Figure 4-34)**. The results of this analysis correlates with previously described quantification of nC structures showing an increase in both percentage of nC expressing cells and number of nC structures per cell in metastatic cell lines compared to normal and tumorigenic non-metastatic cells **(Figure 4-15)**.

We assessed the ability of cytoskeletal polymerization inhibitors cytochalasin D and docetaxel to inhibit intercellular transfer in the primary and tumorigenic cell lines **(Figure 4-35)**. Interestingly, these inhibitors were not able to inhibit intercellular transfer in the primary epithelial cell co-cultures and only resulted in minimal inhibition in the tumorigenic cells. This data suggest that the intercellular transfer observed in endothelial cell co-cultures with primary and tumorigenic epithelial cells may not be nanoChannel mediated. An alternative hypothesis is that nanoChannel structures in these cell populations may not be composed of both

tubulin and actin cytoskeletal proteins therefore are not susceptible to inhibition with these inhibitors.

4.6 NanoChannel-mediated communication occurs in co-cultures with primary human dermal microvascular blood and lymph endothelial cells

We next examined nanoChannels formed by MDA-MB-231 cells in co-culture with primary human dermal microvascular blood and lymph endothelial cells. These cells represent matched pairs isolated from human plasma. The ability for MDA-MB-231 cells to form nC connections with true primary epithelial cells further highlights the clinical relevance of the observed phenotype and supports the notion that nCs may play a role in metastatic progression.

Figure 4-36 illustrates epithelial-endothelial cell co-cultures with the primary epithelial cells. **Figure 4-36A** shows scanning electron micrographs of monocultures and co-cultures with primary endothelial cells. Co-culture images capture interactions between MDA-MB-231 cells and primary human blood and lymph endothelial vessels. Similar to phenotypes with HUVEC endothelial cells, the presence of metastatic epithelial cells increases endothelial angiogenic parameters leading to widening and lengthening of vessel structures. Furthermore, like HUVEC co-cultures, there is a high degree of epithelial-endothelial cell interactions. The MDA-MB-231 cells were observed preferentially interacting with the endothelium, elongating along the vessel structures (solid white arrows). In contrast to the blood endothelium, the primary lymph cells formed disorganized vessel structures with less cell-cell adhesion compared to vascular endothelial vessels, correlating with physiological differences between lymphatic and vascular endothelium. NanoChannels form between metastatic cells and both types of primary human endothelial cells (dashed white arrows).

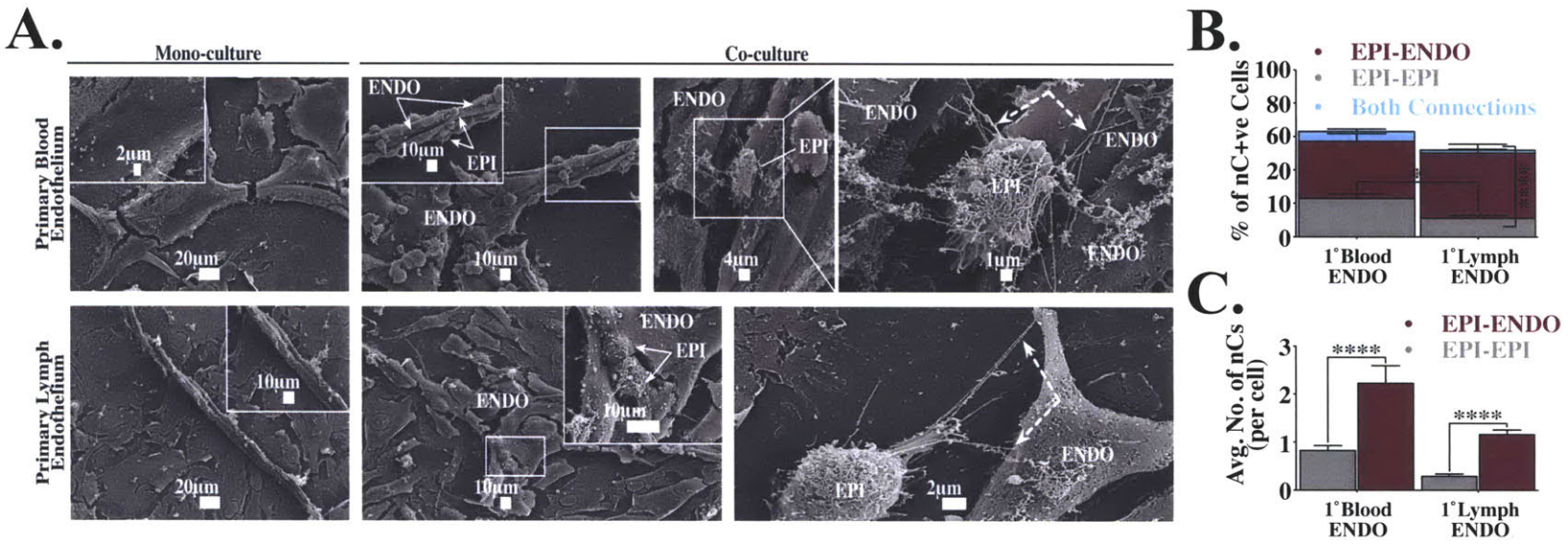

Figure 4-36: Metastatic breast cancer cells form nanoChannel connections with primary human blood and lymph endothelial vessels. (A) SEM images capture interactions between MDA-MB-231 cells and primary human blood and lymph endothelial vessels. Similar to phenotypes observed in 3D co-cultures with HUVEC vessels, MDA-MB-231 cells were observed elongating along the primary endothelial vessel structures (white arrows). There is significant vessel widening in vascular and lymphatic endothelial vessel co-cultures compared to monoculture. The lymph endothelial cells formed disorganized vessel structures with less cell-cell adhesion compared to vascular endothelial vessels, correlating with physiological difference between vascular and lymphatic endothelium. In agreement with previous results, nanoChannel structures formed between metastatic cells and primary endothelial cells (dotted white arrows). (B) As previously described, MDA-MB-231 cells preferentially formed nanoChannel structures with primary blood endothelial cells and primary lymph endothelial cells at a ratio of 1.503 ± 0.266 and 3.525 ± 0.690 ($p<0.0001$) compared to other epithelial cells, respectively. Statistical analysis performed using a 2-way ANOVA ($n>300$). (C) There is also an increase in nC structures formed per cell in EPI-ENDO interactions compared to EPI-EPI interactions, 2.695 ± 0.560 ($p<0.0001$) and 4.057 ± 0.783 ($p<0.0001$), respectively. Statistical analysis was performed using a 2-way ANOVA ($n>300$).

MDA-MB-231 cells preferentially formed nC structures with primary blood endothelial cells and primary lymph endothelial cells at a ratio of 1.503±0.266 and 3.525±0.690 ($p<0.0001$) compared to other epithelial cells, respectively. This data directly correlates with trends observed in HUVEC co-cultures **(Figure 4-36B)**. Furthermore, there was also an increase in nC structures formed per cell in EPI-ENDO interactions compared to EPI-EPI interactions, 2.695±0.560 ($p<0.0001$) and 4.057±0.783 ($p<0.0001$), respectively **(Figure 4-36C)**.

nC-mediated intercellular transfer also occurred between metastatic cells and primary endothelial cells (yellow arrowheads) **(Figure 4-37)**. Fluorescence imaging show CFSE within the endothelial cell compartment **(yellow arrow heads, Figure 4-37A)**. These results were quantified using flow cytometry. The percentage of CFSE+ve cells in dual-labeled endothelial cell populations was determined **(Figure 4-37B and C)**. MDA-MB-231 cells were also co-cultured with smooth muscle cells to demonstrate that the nC-mediated communication is specific to endothelial cells and does not occur with other stromal cells. Vascular endothelial cells were identified with immunostaining for PECAM-1/DiL-Ac-LDL, Thrombomodulin/DiL-Ac-LDL, or PECAM-1/Thrombomodulin. Lymph endothelial cells were identified with immunostaining for PECAM-1/DiL-Ac-LDL, LYVE-1/DiL-Ac-LDL, or PECAM-1/LYVE-1. **Graph 4-37C** shows percentage of CFSE+ve endothelial cells averaged over three studies. In both primary blood and primary lymph endothelial co-cultures there was significant intercellular transfer compared to control. However, in co-cultures with smooth muscle cells there was no transfer of CFSE between cell types. These data further highlight that nC-mediated communication may underly important interactions between metastatic cells and the endothelium which are unique from interactions with other stromal cells.

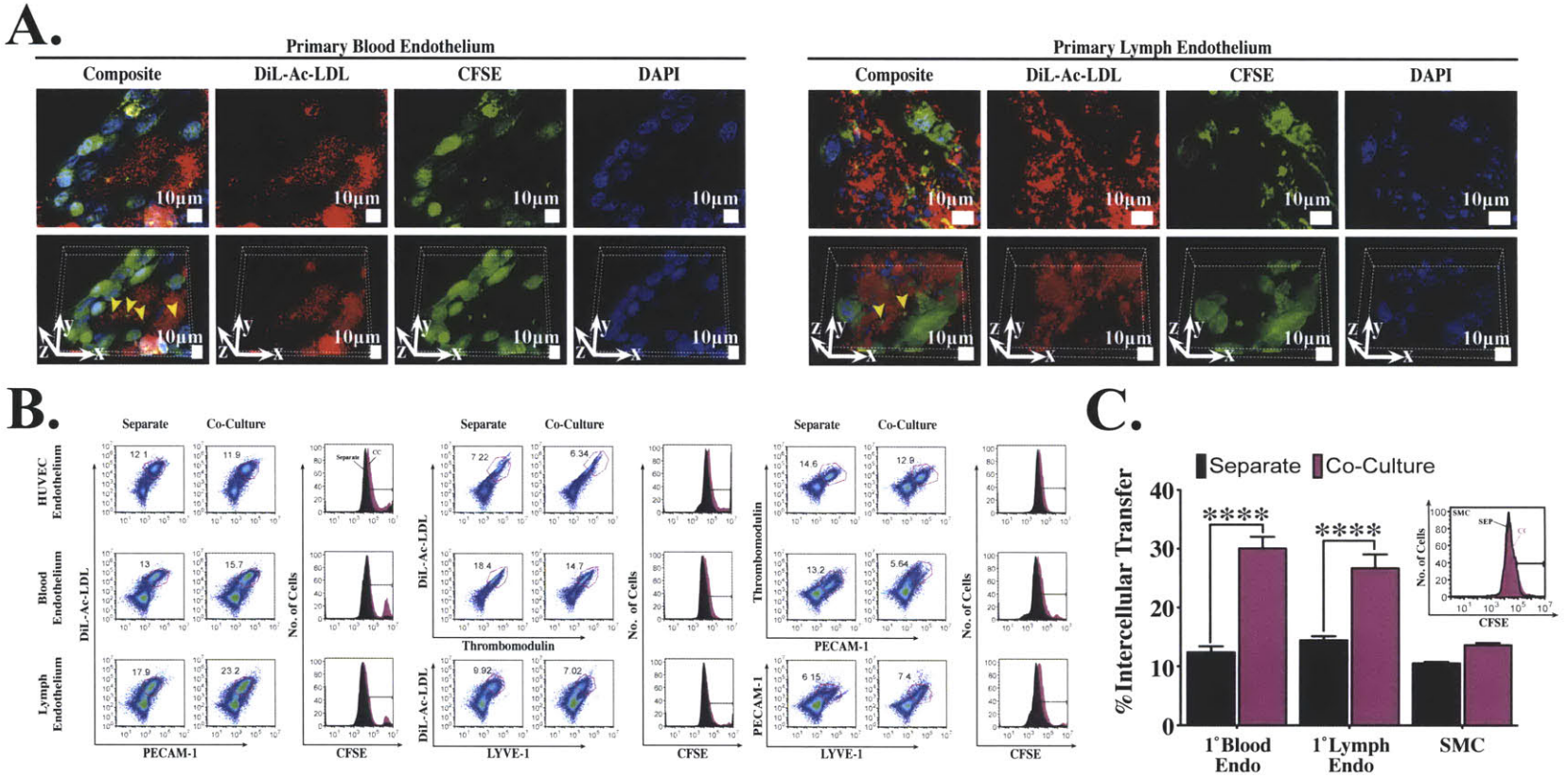

Figure 4-37: NanoChannels transfer intercellular cargo to primary endothelial cells. (A) nC-mediated intercellular transfer occurs between metastatic cells and primary endothelial cells through nanoChannel structures (yellow arrow heads). (B) Intercellular transfer was quantified using flow cytometry to determine the percentage of CFSE+ve cells in dual-labeled endothelial cell populations. Vascular endothelial cells were identified with immunostaining for PECAM-1/DiL-Ac-LDL, Thrombomodulin/DiL-Ac-LDL, or PECAM-1/Thrombomodulin. Lymph endothelial cells were identified with immunostaining for PECAM-1/DiL-Ac-LDL, LYVE-1/DiL-Ac-LDL, or PECAM-1/LYVE-1. (C) Percentage of CFSE+ve endothelial cells were averaged over three studies. Removing background signal, 17.76%±1.099% of the primary endothelial cell population and 12.29%±2.075% of the primary lymph endothelial cell population were CFSE+ve. Statistical analysis was performed using a 2-way ANOVA and Bonferroni post-test.

4.7 Conclusion

In summary, this chapter describes a novel form of heterotypic intercellular communication between cancer cells and the host endothelium, wherein tumor cells can transfer intercellular contents through nanoscale projections directly into neighboring endothelial cells. NanoChannel connections can transport a diverse array of intercellular contents, including small molecules, cytoplasmic proteins, organelles, and synthetic nanoparticles. NanoChannels have unique length scales and cytoskeletal composition that differentiates these structures from other cytoskeletal projections.

Interestingly, metastatic cells form more nC structures than primary and tumorigenic cells. Furthermore these connections preferentially form with the endothelium. nC-mediated communication can be inhibited by cytoskeletal polymerization inhibitors at concentrations that do not affect cellular proliferation, cellular migration, or induce apoptosis.

NanoChannel communication exhibits interesting properties which may enhance metastatic progression. In order to better understand nC-mediated communication, we next sought to explore transport of genetic materials through these structures. Intercellular communication of genetic material offers a powerful mechanism by which nC-mediated communication by metastatic cells can produce physiological changes in the endothelium that promote cancer progression.

Chapter 5

NanoChannel-mediated communication is a mechanism for miRNA transport

Multiple studies have highlighted the role of microRNAs as signaling regulators in tumor progression and angiogenesis[313]. For example, targeting miR-10b and miR-196b leads to significant defects in angiogenesis-mediated tumor growth[314]. Additionally, miR-10b is highly expressed in metastatic breast cancer cells and positively regulates cell migration and invasion[315]. Similarly, miR-132 was reported to be highly expressed in the endothelium of human tumors and hemangiomas but was undetectable in normal endothelium[102].

Intercellular communication of cytoplasmic RNAs has been recently identified as a powerful mechanism of cell-cell communication. These studies have focused on the role of carrier-mediated signaling (e.g. exosomes, ectosomes) in mediating tumor-endothelial interplay through the trafficking of microRNAs during metastatic progression[135]. For example, microRNAs packaged in microvesicles were transferred from tumor to endothelial cells and have been shown to prime the latter for morphological changes[142]. Furthermore, microRNAs have been shown to directly regulate endothelial cell recruitment in metastasis. MiR-126 has been identified as a negative regulator of endothelial cell recruitment, acting through

the IGFBP2/IGF1/IGF1R and GAS6/MERTK signaling pathways[287]. Endogenous suppression of miR-126, present in many cancers, enhances recruitment of the endothelium, while overexpression of miR-126 has been shown to inhibit endothelial cell recruitment[287]. To further emphasize the reciprocal interactions between metastatic cells and the endothelium, miR-126 activity can be directly regulated by the endothelium[287]. Interestingly, the use of antagomirs, engineered oligonucleotides, led to microRNA silencing in an *in vivo* context[306].

Transport of microRNAs through nanoChannels presents a novel mechanism of RNA-mediated intercellular communication. Unlike previously described mechanisms of genetic intercellular communication[135], communication of miRNA through nCs offers a highly specific and controlled mechanism by which a tumor cell can regulate stromal populations in a profound and persistent manner. Unlike exosomal transfer of microRNAs, miRNA transport through nanoChannels would be highly specific and localized, enabling a metastatic cell to directly alter neighboring cells. This mode of communication combines the advantage of specificity offered by the direct modes of cell-cell communication that require physical contact, with the versatility, diversity of cargo, and the long-range effects offered by indirect forms of cell-cell communication. Communication through nCs may potentially be a mechanism utilized by tumor cells to transform stromal populations. It is commonly know that the stroma of a tumor is genetically altered[274]. However, the mechanism underlying these transformations are largely unknown. Of particular interest in cancer progression and metastasis is how tumor cells initiate the angiogenic switch and the conversion of normal endothelium to pathological endothelium. It has long been established that the endothelium of tumor is transformed[122]. However, the mechanisms by which this transformation occurs have yet to be established[122].

5.1 NanoChannels are a mechanism for physical intercellular translocation of miRNAs

Our previous data revealed that in addition to CFSE, nanoChannels facilitated the trafficking of nanostructures **(Figure 4-22)**, proteins (GFP) **(Figure 4-23)**, and even organelles (lysosomes) **(Figure 4-24)**; therefore, we rationalized that maximal amplification of signaling could potentially be created through the transfer of microRNAs. We investigated whether nanoChannels can act as a physical bridge for microRNA-mediated intercellular communication by assessing nanoChannel-mediated transport of miR-132. MicroRNA 132 was chosen as a proof of concept because it has been implicated in pathological angiogenesis as a regulator of the angiogenic switch[129]. MicroRNA 132 functions through p120RasGAP to induce neovascularization[129]. Its expression was found to be high in embryonic stem cell models and also in the endothelium of tumors and hemangiomas[129]. In contrast, expression of miR-132 in normal healthy endothelium was found to be low. MiR-132 acts by inhibiting p120RasGAP, which increases RAS activity, inducing angiogenesis[129]. P120RasGAP is expressed in normal but not tumor endothelium. Lastly, inhibition of miR-132 with an α-mir resulted in restoration of p120RasGAP expression. This leads to inhibition of angiogenesis and a decrease in tumor burden in an orthotopic metastatic breast cancer model[129].

Figure 5-1 is an overview of microRNA transfer studies. MicroRNAs are transfected into the MDA-MB-231 cells followed by treatment with cytoskeletal inhibitors. The metastatic breast epithelial cells are then added to the pre-formed endothelial tubes and co-cultured for 36hrs. Following co-culture, the endothelial cells are isolated from the matrix for subsequent analysis. The percentage of miRNA+ve cells, effects of pharmacological inhibition of nCs, and the functional activity of the microRNAs are then determined.

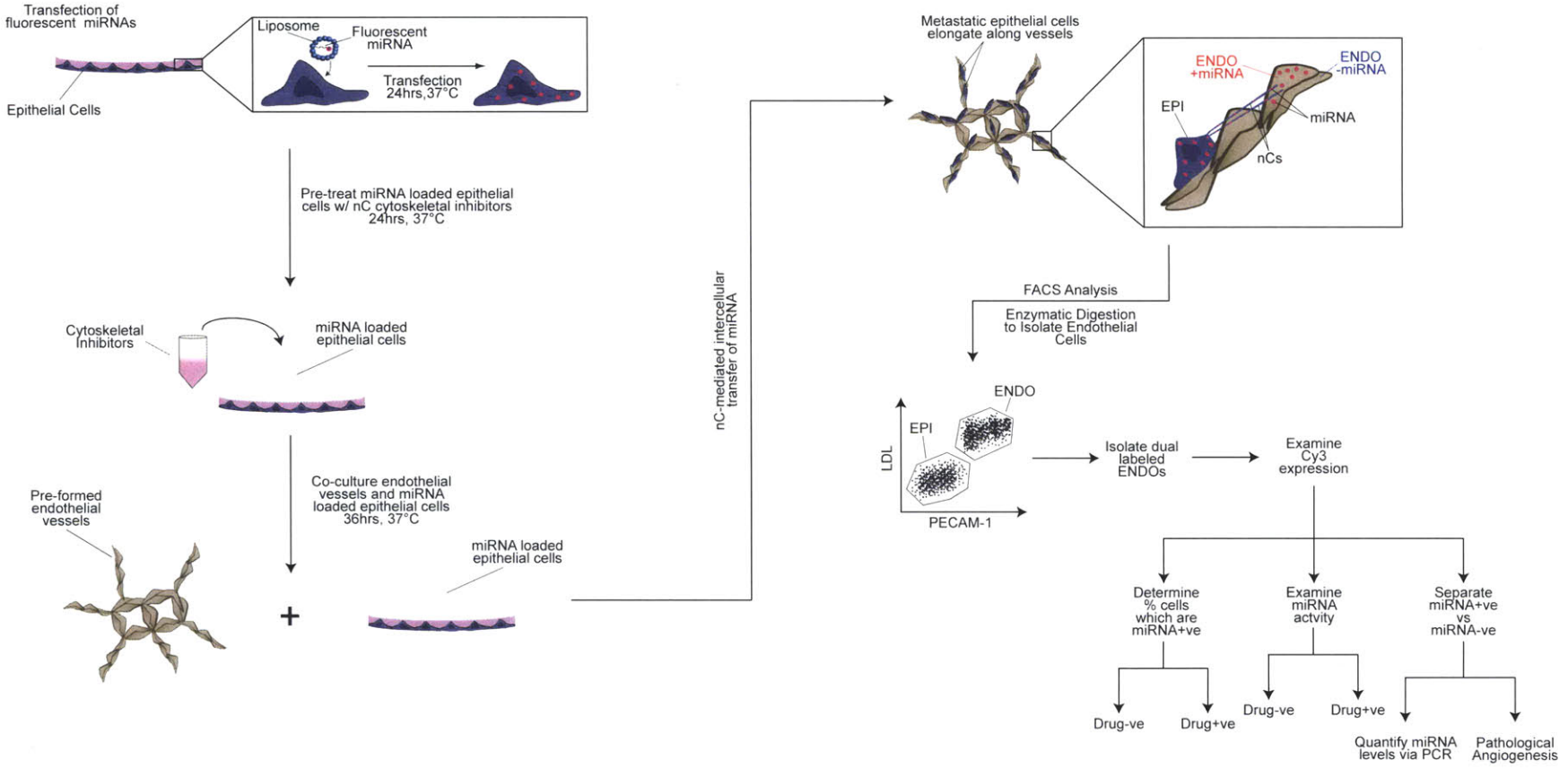

Figure 5-1: Experimental overview of miRNA studies. Schematic of experimental design used to evaluate nC-mediated intercellular transfer of microRNAs.

Transport of microRNA was initially analyzed using confocal fluorescence microscopy. Control microRNA and miR-132 are labeled with Cy3. Control microRNA and miR-132 were transfected in the MDA-MB-231 cells. The Cy3-labeled microRNAs were detected within the nanoChannels, 36hrs post co-culture incubation. **Figure 5-2** provides representative images of nanoChannel-mediated microRNA transport in both a 2D and 3D co-culture format. After co-culturing LDL (green) labeled endothelial cells with MDA-MB-231 cells containing Cy3-labeled miRNAs, the co-cultures were counterstained with phalloidin (purple) and DAPI + WGA (blue). The images show microRNAs within nanoChannel structures traveling toward an endothelial cell (white arrows). MicroRNAs within the cytoplasm of endothelial cells are indicated with yellow arrow heads. Transport of microRNAs through nCs does not appear to be regulated. NanoChannels allow for the transport of a control miRNA and miR-132.

MicroRNA transfer was quantified using flow cytometry in a similar manner as CFSE transfer. **Figures 5-3A and B** show schematic and graph of flow cytometry results, respectively. Co-cultures with untransfected MDA-MB-231 cells, MDA-MB-231 cells transfected with miR-132, and control miRNA were analyzed. Again, LDL and PECAM-1 dual-labeled endothelial cells were isolated and the percentage of endothelial cells expressing fluorescently labeled microRNAs were quantified. **Figure 5-3B** shows the percent of the endothelial cell population receiving intercellular transfer averaged over several studies.

Trafficking of miRNAs was observed in both the miR-132 ($p<0.01$) and control miRNA ($p<0.05$) groups at 36hrs as indicated by a shift in the co-culuture curve (pink) compared to background fluorescence seen in the duals (green) **(Figure 5-3A)**. There was $9.66\pm1.01\%$ and $23.98\pm2.60\%$ of the endothelial cell population receiving intercellular transfer in the control miRNA dual and co-culture groups, respectively. Similarly, $8.82\pm0.53\%$ and $21.18\pm1.93\%$ of the endothelial cell population receiving intercellular transfer in the miR-132 dual and co-culture groups, respectively. Compare this to percent seen in the untransfected groups, $7.49\pm1.04\%$ and $6.85\pm0.93\%$ in the dual and co-culture groups, respectively. As expected, no

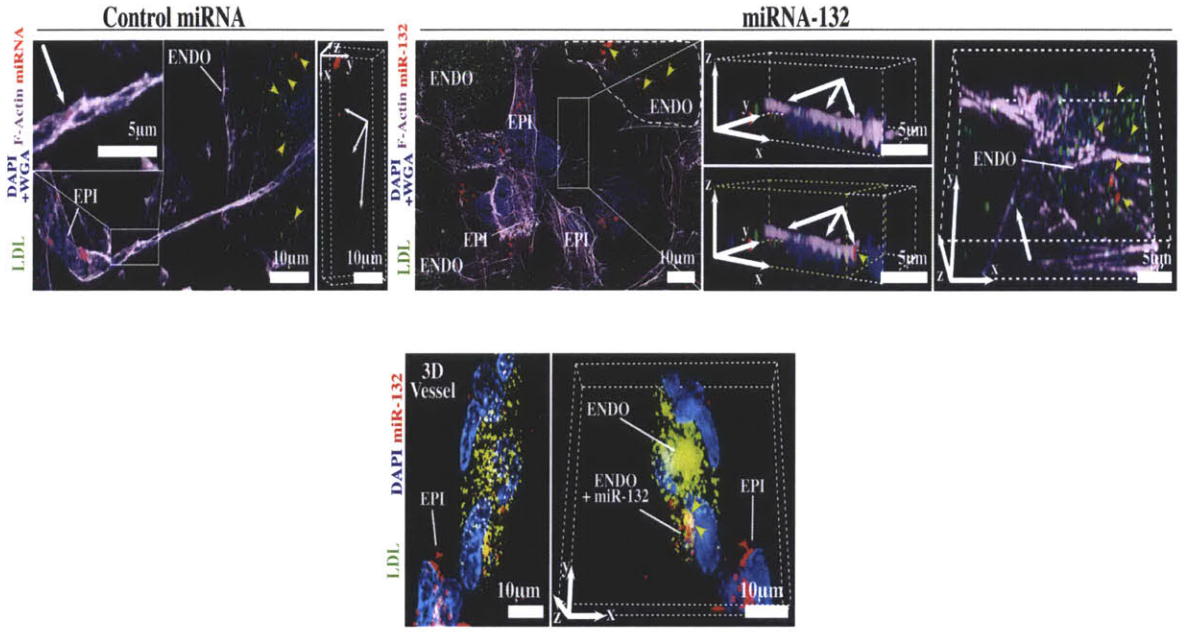

Figure 5-2: NanoChannels are a mechanism for physical translocation of miRNAs. Confocal images showing nanoChannel (nC)-mediated transfer of control miRNA and miR-132 from MDA-MB-231 cells (EPI) to endothelial cells (ENDO). LDL (green) labeled endothelial cells were co-cultured with Cy3-labeled miRNA transfected MDA-MB-231. Co-cultures were counterstained with phalloidin (purple) and DAPI + WGA (blue). nCs (white arrows) are conduits for direct cell-to-cell transfer of miRNAs to endothelial cells (yellow arrow heads). 3D reconstructions show miRNAs within the nC structures.

shift was seen in co-cultured samples in the untransfected groups. There is no statistical difference between measurements made in dual cultures from the control miRNA and miR-132 groups and co-cultures from the untransfected groups. These results emphasize that there is no intercellular transfer observed in dual cultures secondary to an endocytotic/exocytotic mode of intercellular communication.

To confirm that miRNA transfer was occurring through nanoChannels and not an alternative mechanism, pharmacological disruption of the nC projects with cytoskeletal polymerization inhibitors was performed. Similarly to the studies performed with CFSE, a combination of low dose α/β-Tubulin and F-Actin polymerization inhibitors were used to disrupt miRNA transfer through nC structures. The results of inhibition of nC-meditated intercellular transfer after pre-treatment with docetaxel (500pM) combined with latrunculin A (30nM) or cytochalasin D (50nM) are given in **Figure 5-3**. The horizontal black lines in **Figure 5-3A** indicates the percent of intercellular transfer in co-culture groups after drug treatment. **Figure 5-3B** shows that intercellular transport of miRNAs reverted to baseline (dual groups) after treatment with a combination of tubulin and actin inhibitors, validating the role of nanoChannels in miRNA trafficking. Compare this to no change in the untransfected group.

5.1.1 Kinetics of miRNA transfer

Interestingly, trafficking of miRNAs occurred less frequently and more slowly than diffusion-mediated transport of CFSE. **Figure 5-3B** shows percent intercellular transfer for the untransfected, control miRNA (24hrs), control miRNA (36hrs), and miR-132 (36hrs) experimental groups. A lower percentage of the endothelial cell population received intercellular transfer of miRNAs compared to CFSE transfer. In studies examining CFSE transfer, 43.30$\pm$2.35% ($p<0.0001$) of the endothelial cell population was found to be CFSE+ve, compared to 15.47$\pm$1.46% in the dual cultures. Correcting for background by removing the percent intercellular transfer observed in the duals, approximately 30% of the endothelial cell population re-

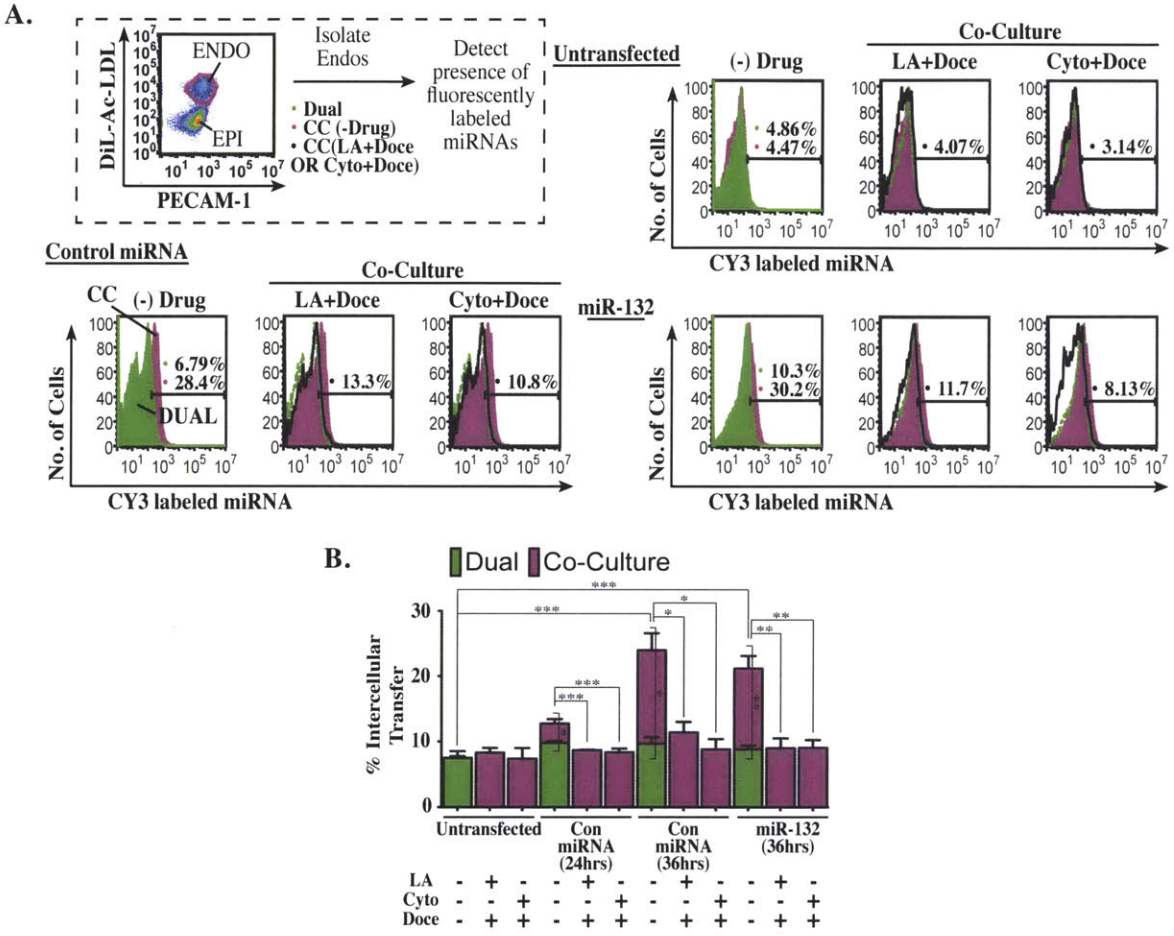

Figure 5-3: NanoChannel-mediated miRNA transport confirmed with flow cytometry. (A) Schema and (B) graph show quantification of nC-mediated microRNA transfer using flow cytometry. In co-culture (dual cultures were included as controls), endothelial cell populations were isolated and percentage of miRNA+ve cells were determined. Pharmacological disruption of nC structures inhibited miRNA transfer.

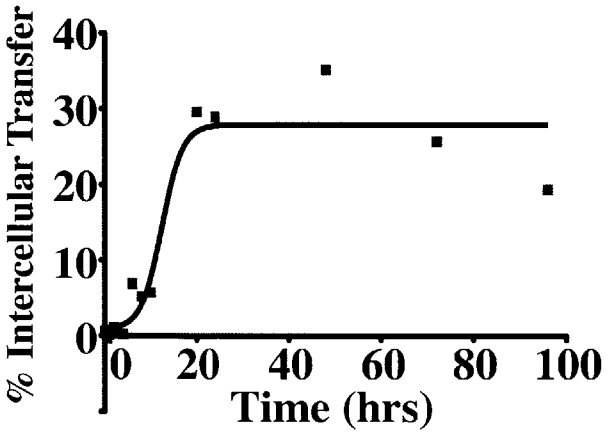

Figure 5-4: Revist of CFSE transport over time.

ceived intercellular transfer of cytoplasmic contents, while approximately 15% of the endothelial cell population received transported miRNAs. Furthermore, there was a significant increase in miRNA transfer at 36hrs compared to the observed transfer at 24hrs. This contrast the results seen with CFSE transfer where intercellular transfer of CFSE remained fairly constant after 24hrs **(Figure 5-4)**. The difference in transport kinetics in miRNA trafficking may indicate that an alternative mechanism may be involved in miRNA transport through nC structures. For example, there may be regulatory mechanism underlying miRNA transport through nCs. However, it is not likely specific to any particular miRNA sequence since transport dynamics of the control and miR-132 groups are similar. Alternatively, the difference in kinetics of intercellular transport may be due to detection limitations of the Cy3-labeled miRNAs. Possibly a higher concentration of miRNAs is required in order to achieve a signal-to-noise ratio allowing for sufficient and reproducible detection. However, this hypothesis is not likely because microRNA signal could be detected at 24hrs over baseline. Therefore, assuming that these alternative mechanisms are not occurring, the difference observed between CFSE

and miRNA transport may point to an active transport mechanism for trafficking of miRNAs via motor proteins, such as myosin V. Indeed, transport of RNA by motor proteins has been reported in other systems[314].

Using a similar approach as adapted to study the kinetics of CFSE transfer, we developed a model of nC-mediated miRNA transport. Again, we used fluorescence intensity as a surrogate measure of concentration. The MDA-MB-231 cells were transfected with a known concentration of 50μM of labeled oligonucleotide. Using the relationship given by:

$$\frac{X}{MedianFl._{HUVEC}} = \frac{Concentration_{SeparateMDA}}{MedianFl._{MDA}},$$

where $Concentration_{SeparateMDA}$ is the initial intercellular concentration of miRNA inside the MDA-MB-231 cells in separate cultures, $\boldsymbol{X}$ is the average miRNA concentration of the HUVEC population, and $\boldsymbol{MedianFl._{SeparateMDA}}$ and $\boldsymbol{MedianFl._{HUVEC}}$ are the median intensity values of the $MDA_{separate}$ and HUVEC peaks, respectively; we estimate that at 36hrs, the final concentration of miRNA is approximately 30μm.

Figure 5-5A predicts miRNA transport kinetics through nCs. Similar to CFSE transfer, we predict diffusion of miRNAs will begin at approximately 5hrs after intact nanoChannels are formed and continue for 36hrs, reaching a concentration of 30μm in the endothelial cells. We then compared this prediction to plots generated using the previously derived model from Fick's second law that yielded the following expression **(Figure 5-5B,C)**:

$$C = C_o(1 - \text{erf}\,\frac{x}{2\sqrt{Dt}}),$$

where $\boldsymbol{C_o}$ is the initial miRNA concentration loaded in MDA-MB-231 cells in M units, $\boldsymbol{t}$ is time in s, $\boldsymbol{D}$ is diffusion constant in units of m^2/s, and $\boldsymbol{x}$ is length in units of m. **Table 4.2** provides diffusion coefficients for miRNA in water and cytoplasm. However, from the previous analysis we determined that in nanoChannels

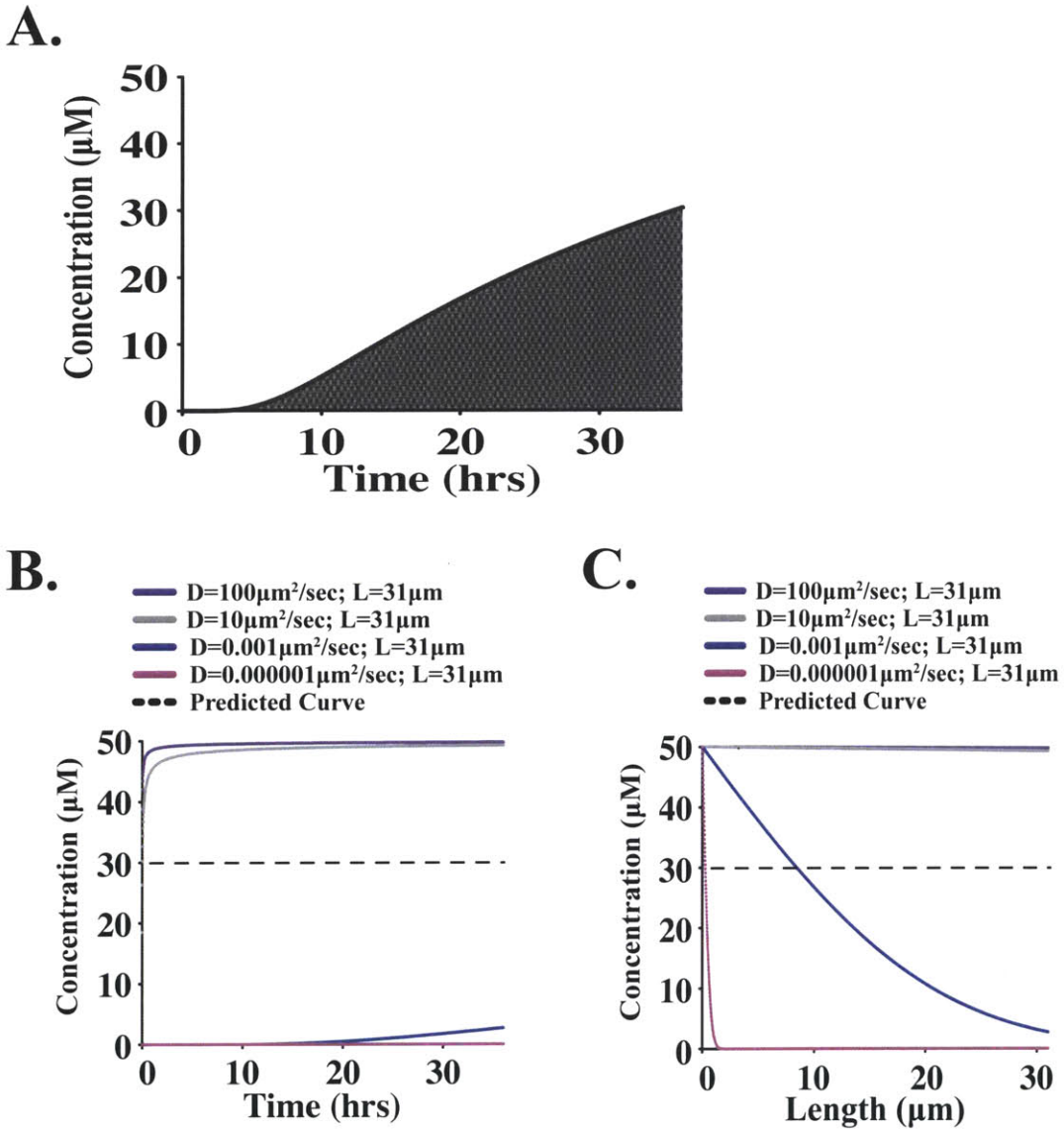

Figure 5-5: Kinetics of miRNA transport through nCs. (A) Predicted concentration versus time plot of miRNA diffusive transport through nCs. (B/C) The predicted curve was compared to a theoretical diffusion model. (B) Plot of concentration versus time and (C) length comparing the theoretical model to the predicted data.

the effective diffusion coefficient is given by the expression,

$$D_e = \frac{D\epsilon_t\delta}{\tau},$$

where ϵ_t is the porosity, δ is the constrictivity, and τ represents the tortuosity, and may be 4 to 7 orders of magnitude smaller than diffusion coefficients determined in free space. The effective diffusion coefficient may be decreased due to complex geometry and spatial constraints present within nCs. Furthermore, the size of fluorescently conjugated miRNA molecules is significantly bigger than CFSE molecules. Recall that constrictivity may further limit diffusive transport of miRNAs through nCs. Constrictivity, accounts for spatial constraints due to particle size.

Figures 5-5B and C illustrate the results of this analysis, plotting concentration versus time and length, respectively. There is a significant difference in transport dynamics in free diffusion of miRNAs in water (purple line) and cytoplasm (gray line) compared to diffusion of miRNAs through nanoChannels (blue and pink lines). These results clearly show that in the time scales of interest, diffusion alone cannot achieve the expected concentration of miRNAs in the endothelial cells. Even when accounting for an appropriate effective diffusion coefficient, diffusion alone cannot achieve the concentration of microRNAs measured within endothelial cells. This discrepancy highlights the possibility that an additional mechanism may be involved in miRNA transport through nCs.

Molecular motor proteins are responsible for the transport of a diverse array of cellular cargo including proteins, lipids, organelles, and miRNAs. They function in a wide array of critical cellular processes such as cell division, signal transduction, and embryonic development[316]. There are three classes of cytoskeletal motor proteins: myosin, an actin-based motor, and dynein and kinesin, two microtubule motors[316] **(Figure 5-6)**. All motor proteins are composed of a dimer of two heavy chains with an ATP catalytic domain that enables their function. They each have diverse functions, however, with several similarities. The majority of kinesin mo-

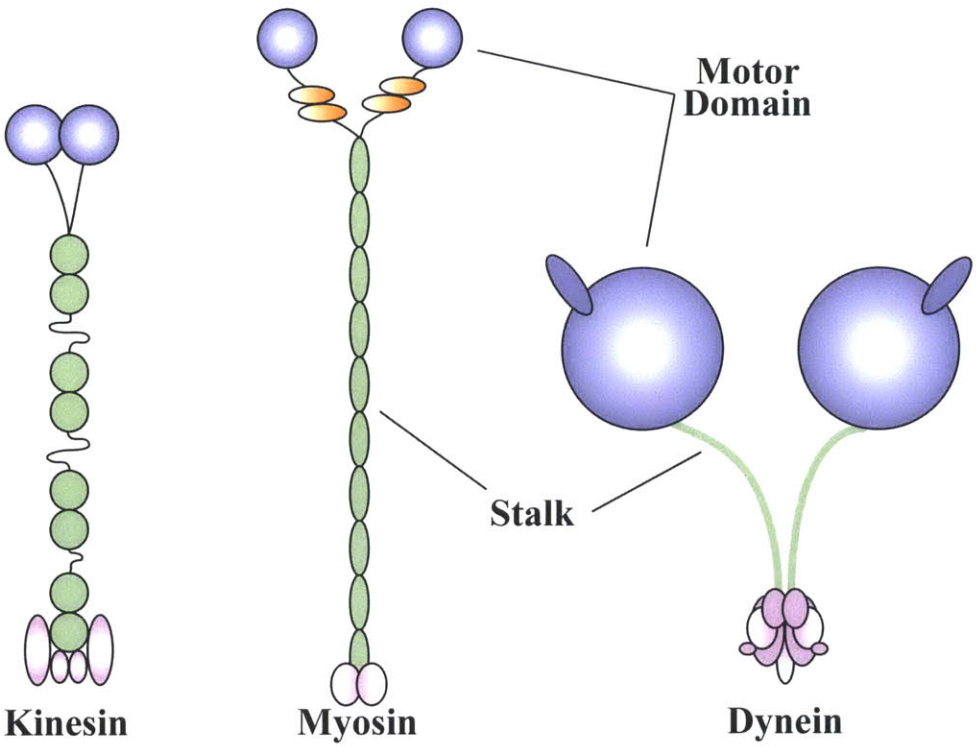

Figure 5-6: Molecular motor proteins are responsible for transport of diverse cargo. There are three classes of motor proteins: myosin, an actin-based motor, and dynein and kinesin, two microtubule motors.

tors are unidirectional walking toward the positive end of the microtubule, typically toward the periphery of the cell. This transport is referred to as anterograde transport[316]. In contrast, dynein motors move toward the negative end of the microtubule in a retrograde fashion[316]. Microtubule motor proteins maintain their interaction with tubulin through electrostatic force between the positively charged head of the motor protein and the negatively charged carboxyl groups on tubulin. The myosin family of molecular motors hold diverse functions ranging from muscle movement to organelle transport[316]. Myosin V is a unique member of this family that has been recently implicated in miRNA transport[308]. Kinesin and myosin V are both processive motors, meaning they are able to continuously move down the cytoskeletal protein without dissociating[317].

In this analysis we will use myosin V to model active transport through nanoChannels. However, any of these motors may be implicated since nanoChannels con-

tain both actin and tubulin cytoskeletal components. Myosin V mediated transport along actin filaments is considered bi-directional due to the network of cross-linked actin fibers. Furthermore, studies have also shown that microtubule motors also exhibit bi-direction transport. Using the mathematical description derived by Smith et al[318], we modeled combined diffusion and active transport through nCs. This model makes the following assumptions:

1. One-dimensional motion
2. A particle is considered a motor protein bound to an miRNA molecule
3. Particles move at a steady velocity
4. Binding and detachment from filaments can be modeled with first-order rate kinetics
5. Transport is bi-directional
6. Motion occurs directly following binding
7. Maximum loading of motor proteins
8. Starting concentration in the endothelium of labeled miRNA is zero

The result of this analysis yields a facilitation factor given by the expression:

$$F = \frac{L}{2l_{off}}(1 + \frac{l_{on}}{l_{off}}),$$

where $\boldsymbol{F}$ is the flux facilitation over free diffusion, $\boldsymbol{L}$ is nanoChannel length in units of m, $\boldsymbol{l_{off}}$ is the mean path free length in units of m, $\boldsymbol{l_{on}}$ is the mean path length on a filament in units of m. l_{on} and l_{off} can be determined from the following relationships, v/k' and $(\frac{D}{k})^{\frac{1}{2}}$, respectively, where $\boldsymbol{v}$ is the motor speed of particles on the filaments in units of *m/s*, $\boldsymbol{D}$ is the diffusion coefficient in units of m^2/s, and $\boldsymbol{k}$ and $\boldsymbol{k'}$ are the attachment and detachment rates to filaments of one polarity,

respectively, with units of *1/s*. This relationship can be used to scale the diffusion-only transport to predict the combined contribution of both diffusion and active transport.

Figure 5-7 illustrates the results of this analysis. **Figure 5-7A** models the transport of miRNAs with increasing motor protein speed ranging from 40nm/s - 400nm/s. As the motor protein speed increases, there is significant enhancement of miRNA transport speed. It is clear that in order for the concentration of miRNA to reach the predicted value in the endothelium, an active transport mechanism is required. Due to the complex geometry of nanoChannels, diffusion is severely impeded **(Figure 5-7B, blue)**. It's only when an active transport mechanism is included **(Figure 5-7B, pink)** does the model more closely resemble experimental results. The summed contribution of both active and passive transport is given by the solid black line. Compare this curve to the predicted transport curve (dashed line).

Active transport dominates in the context of severely limited diffusion. There are some unique aspects of the transport dynamics predicted with this analysis. First, there is a longer lag in transport than with diffusion-only transport. This might result from the requirement of both an intact nC structure as well as an intact cytoskeletal transport chain.

Interestingly, miRNAs are transported to less endothelial cells than CFSE. This may be due to a variety of reasons. First, miRNA transport may be regulated compared to non-specific intercellular contents such as CFSE. An additional consideration is the timescale of the experiment. If miRNA transport kinetics are dependent on an active transport mechanism it may require more time to achieve intercellular transport of a larger percent of the endothelial cell population. There is a significant time delay in transport observed in the active transport models. This can be rationalized by the requirement of both an intact nC structure, as well as an intact cytoskeletal transport chain. It's possible that nCs are formed between cells but that no miRNAs are transported due to a lack of an intact cytoskeletal transport network. This is especially true for longer nanoChannels. **Figure 5-5C** shows transport in longer nanoChannels. It requires significantly more time to achieve

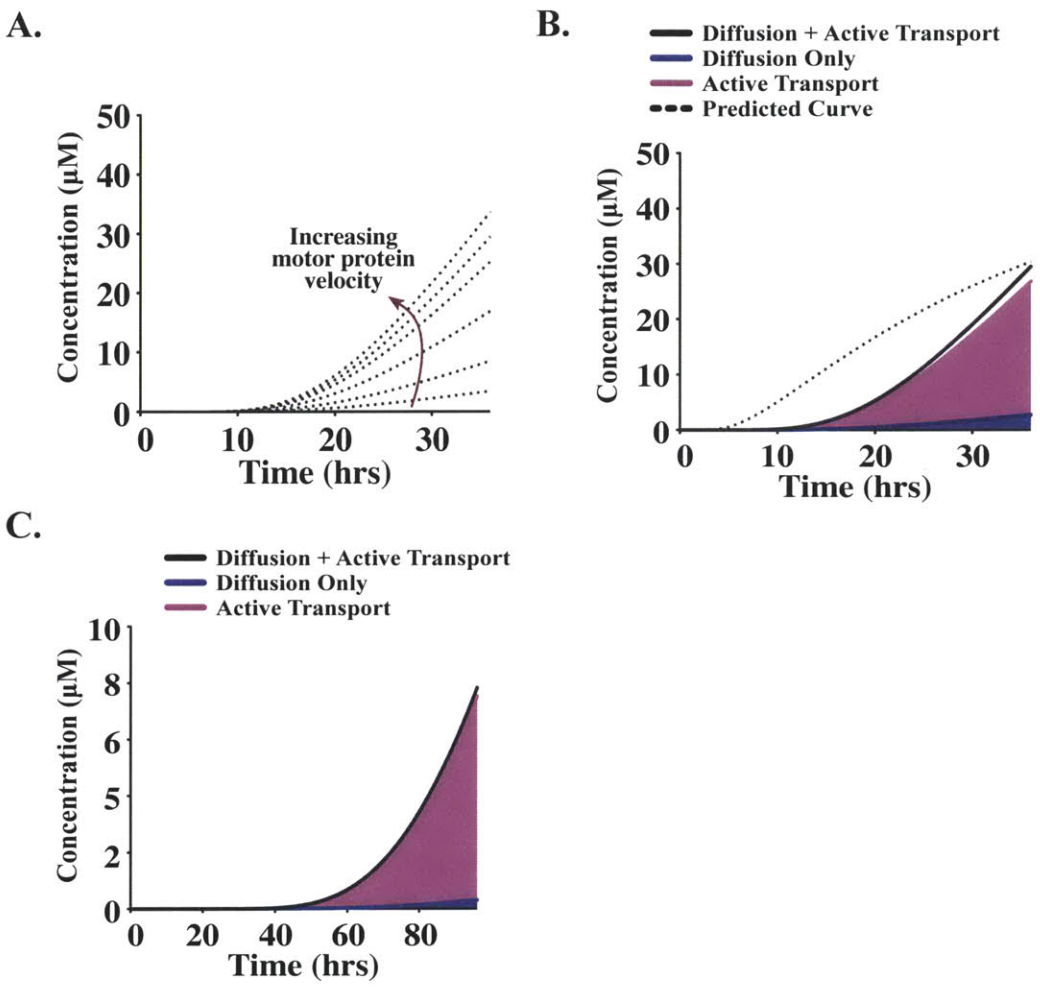

Figure 5-7: Modeling active transport. An active transport mechanism may be responsible for the transport of miRNAs through nCs. (A) Graph plotting increased concentration versus time with increasing motor protein speed. (B) Transport kinetics through nanoChannels combining contributions from both active and passive transport mechanisms. (C) Only with an active transport mechanisms within nanoChannels can the theoretical model match the concentration of miRNAs in endothelial cells measured experimentally.

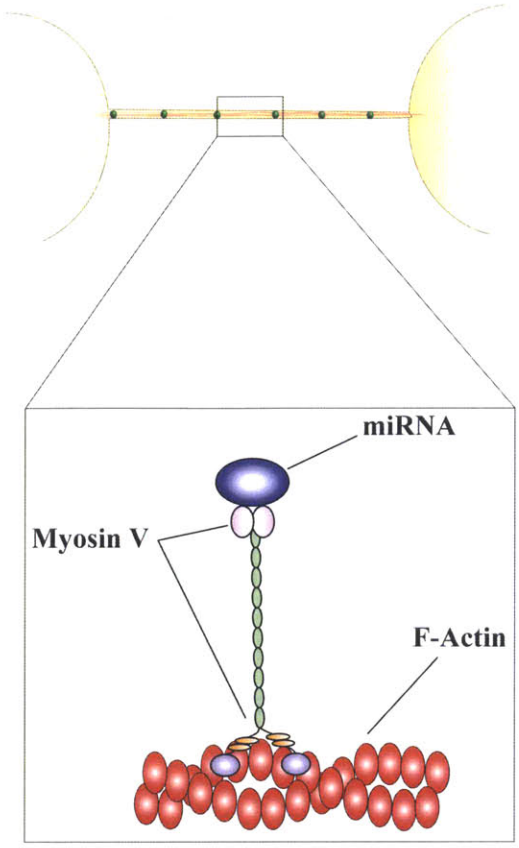

Figure 5-8: Proposed active transport mechanism of miRNAs. MiRNAs may be transported down nanoChannels using motor proteins.

detectable levels of miRNA for longer nanoChannel structures. **Figure 5-5C** shows that it take up to 96hours hours for miRNAs to travel down longer nanoChannels. Possibly, we could detect transport of miRNAs to a higher percentage of the endothelial cell population at longer time points. In nanoChannels, it may be that at early time points, diffusion dominates. However, at longer times, active transport begins to dominate through nCs, providing significant additive benefits compared to diffusion alone. **Figure 5-8** illustrates active transport of miRNAs through nanoChannels.

5.1.2 Transport of miRNAs are confirmed using PCR

Using a fluorescently tagged miRNA oligonucleotide, we have demonstrated that nanoChannels are a mechanism of microRNA transport. We next sought to quan-

tify the transferred oligonucleotide sequence via PCR. Quantification of the miRNA sequence using PCR was used to further confirm the presence of oligonucleotide. This confirmation is important because it excludes the possibility that the flow cytometry and imaging studies are detecting a dissociated fluorescent tag instead of the oligonucleotide sequence of interest.

We began by determining the appropriate endogenous control to use in quantifying transport of miR-132. **Figure 5-9** shows Ct values for ubiquitously expressed endogenous controls in endothelial cells. It was critical to choose an endogenous control that was not regulated by the epithelial-endothelial interactions that occur in co-culture. There was no difference in expression of RNU44 and hsa-mir-16-1 in dual and monoculture conditions, however, there was a significant difference in RNU48 expression in the two culture formats. These results indicate that RNU48 expression may be regulated by soluble factors secreted by epithelial cells, and therefore is not an appropriate endogenous control to use. Either RNU44 or hsa-mir-16-1 would be appropriate to use in our studies. We eventually concluded that RNU44 was the best candidate.

Figure 5-10 shows the results of the PCR analysis. MDA-MB-231 cells were transfected with miR-132 and α-miR-132 oligonucleotides prior to addition to endothelial cell vessels. After 36 hours, the LDL and PECAM-1 dual labeled endothelial cell populations were isolated and sorted into miRNA+ve and miRNA-ve groups. The expression of miR-132 in these groups was compared to HUVEC monoculture controls.

Metastatic cells increase expression of miR-132 through two mechanisms: soluble factors acting through the VEGFR pathway[129] and direct nC-mediated transport of microRNAs. nC-mediated transport of miR-132 and α-miR-132 led to a 5x increase (solid red) ($p<0.0001$) and 26x decrease in miR-132 expression ($p<0.0001$) compared to miRNA-ve samples, solid blue bar and striped blue bar, respectively. This corresponds to an increase of $544.1\pm52.79\%$ ($p\leq0.0001$) and decrease of $3262\pm943\%$ ($p\leq0.01$) in copies miR-132 oligonucleotides, for the miR-132 and α-miR-132 groups, respectively. This data further strengthens the previous results, demonstrating the

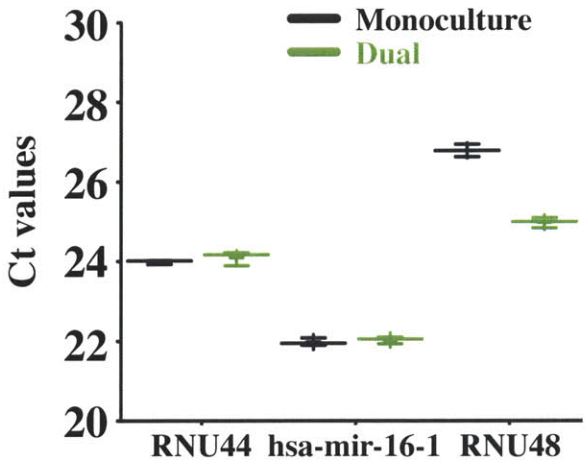

Figure 5-9: Selecting an endogenous control. The endogenous control used to analyze expression of miR-132 was selected based on minimal differences in expression in monoculture versus co-culture. Ideally, expression of the endogenous control in the endothelium will not be changed by the presence of metastatic cells.

role of nCs in miRNA transport. These results indicate that actual oligonucleotide was transferred. As expected, miR-132 groups showed an increase in miR-132 expression, while α-miR-132 showed a decrease.

In previous studies, microRNA-132 expression has been shown to be regulated in a VEGFR dependent manner[129]. Consistent with the findings implicating MDA-MB-231 conditioned media-induced activation of the VEGFR pathway, miR-132 expression is up-regulated from baseline in dual cultures. Compare the miR-132 expression in HUVEC monoculture control (gray bar) and dual (solid green bar). This data suggests that the miR-132 pathway is activated by soluble factors released by MDA-MB-231 cells. This activation was inhibited by α-miR-132 oligonucleotide (striped green bar) ($p<0.0001$).

Direct transfection of miR-132 (black) and α-miR-132 (light blue) in endothelial cells act as positive and negative controls, respectively. Fold change in these studies was determined compared to endothelial cell transfection with control miRNA

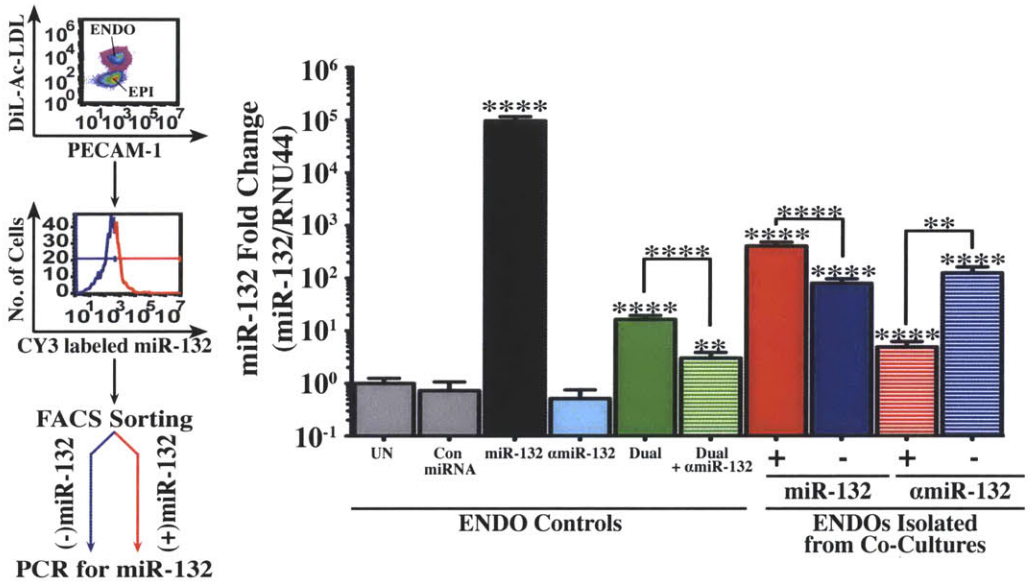

Figure 5-10: PCR of miR-132 confirms transport of miRNAs via nCs. Schema shows experimental design for RT-PCR detection of miR-132 in endothelial cells under different experimental conditions. MDA-MB-231 cells transfected with miR-132 and α-miR-132 were co-cultured with endothelial tubes. FACS isolated endothelial cell populations were analyzed for expression of miR-132. MiR-132+ve cell populations (solid red) show 5x increase compared to miR-132-ve populations (solid blue)($p<0.0001$), while α-miR-132+ve cells (striped red) show 26x decrease in miR-132 expression ($p<0.0001$) compared to α-miR-132-ve cells (striped blue). Direct transfection of miR-132 (black) and α-miR-132 (light blue) in endothelial cells act as positive and negative controls, respectively. Upregulation of miR-132 from baseline was observed in dual culture due to VEGFR pathway activation (solid green) which could be inhibited with α-miR-132 (striped green). Fold change was determined compared to endothelial cell transfection with control miRNA (gray).

(gray). As expected, miR-132 expression was similar in the miRNA-ve cell populations from both miR-132-ve and α-miR-132-ve co-culture group. This is not surprising because this population represents the cells that did not receive intercellular oligonucleotides. Surprisingly, however, the miR-132 expression in miRNA-ve cell population was 446.5±55.65% ($p<0.01$) and 685.0±146.8% ($p<0.001$) higher in the miR-132 and α-miR-132 groups, respectively, than levels of miR-132 expression in dual chambers. These results suggest that additional mechanisms may be regulating miR-132 expression in co-cultures. One possibility is that physical contact between the metastatic cells and the endothelial vessels increases expression of miR-132 through nC transport of intercellular contents, but not the fluorescently labeled microRNA. Studies examining transport of CFSE suggests that intercellular communication through nanoChannels occurs more frequently then is captured with fluorescently labeled microRNAs. Presumably, there may be other intercellular contents that are transported through nCs that affect miR-132 expression other than the assayed oligonucleotide.

5.2 Transported miRNAs have functional activity

To confirm that the transported microRNAs were physiologically active, endothelial cells receiving intercellular transfer were isolated from co-cultures, and the downstream targets of miR-132 were assayed via flow cytommetry. Recent work has shown that miR-132 leads to increased Ras activation through down regulation of p120RasGAP[129]. Endothelial cells receiving nC-mediated transport of miR-132 showed a decrease in expression of p120RasGAP and an increase in pAKT (S473) **(Figure 5-11)**. The reverse was observed when using α-miR-132 oligonucleotide **(Figure 5-11A)**. These finding correlate with miR-132 inhibition of p120RasGAP and subsequent activation of the Ras pathway leading to up-regulation of pAKT. These results were confirmed via PCR **(Figure 5-11B)**. **Figure 5-12** shows p120RasGAP and pAKT (S473) expression in both the MDA-MB-231 and HUVEC cell populations. The miR-132 group is indicated in black, the control group in gray, and the

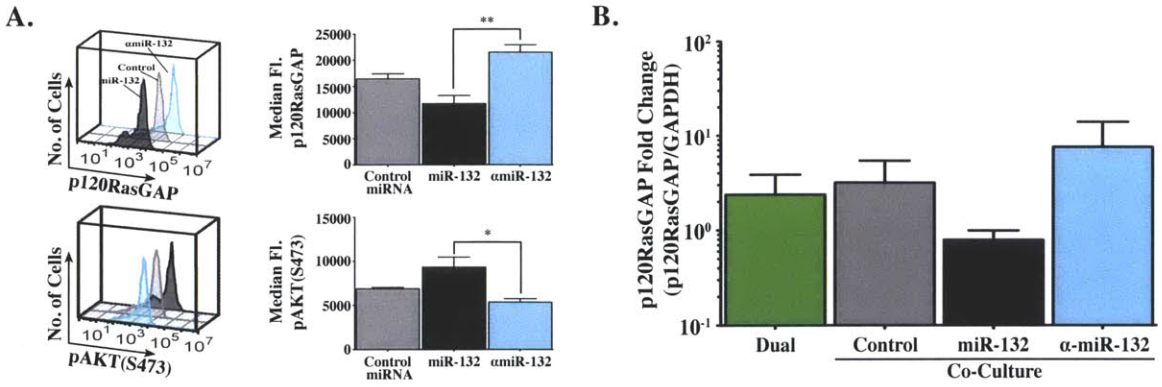

Figure 5-11: NanoChannels transport physiologically active miRNA oligonucleotides. (A) FACS analysis shows nC-mediated transfer of miRNAs leads to changes in p120RasGAP and pAkt (S473) expression downstream in endothelial cell populations isolated from co-cultures. Bar graphs show decreased p120RasGAP expression in the miR-132+ve cell populations and increased expression in the α-miR-132+ve cell populations, while further downstream miR-132 positively regulated pAKT expression. Data shown is mean $\pm$ SEM. (B) Expression of p120RasGAP was confirmed via PCR.

α-miR-132 group in light blue. Expression patterns in both the MDA-MB-231 and HUVEC cells are analogous, the only difference being slightly lower expression of miR-132 in the epithelial cells compared to the endothelial cell population. This data implies that the microRNAs transfected into the MDA-MB-231s are being expressed, resulting in changes in downstream pathways measured by p120RasGAP and pAKT (S473). This data would suggest that the microRNAs once transfected into the cells are released into the cytoplasm of the MDA-MB-231s, where they can exert cellular activity. Contrast this to transport of the microRNAs if they remained in the transfected lipid vesicles. In this situation, expression of miR-132 oligonucleotide in MDA-MB-231 population would likely not mirror what is seen in the HUVEC endothelial cell population because the microRNAs would be trapped within the transfected lipid vesicles. Therefore, these microRNAs would be unable to exert effects on cellular expression. Taking all this data together suggests that physiologically active microRNAs are transported through nanoChannels and transport of these oligonucleotides can be inhibited using cytoskeletal

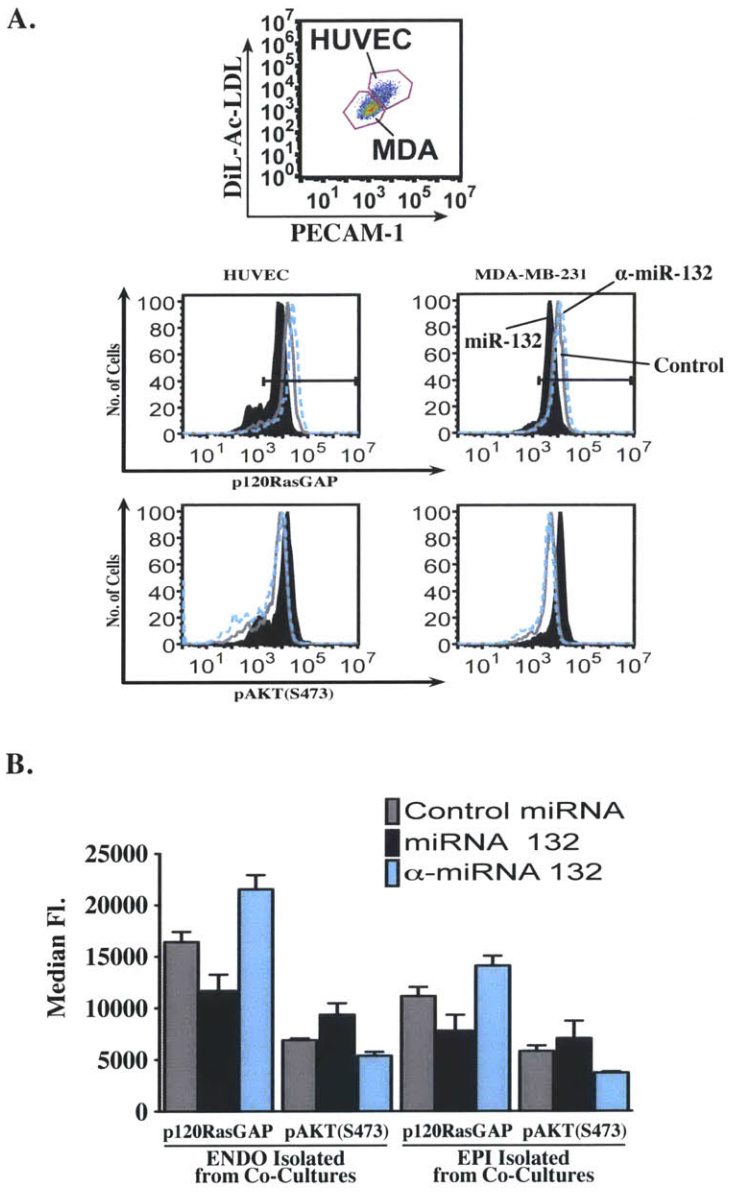

Figure 5-12: P120RasGAP and pAKT expression in MDA-MB-231 and HUVEC endothelial cells. The expression of p120RasGAP and pAKT in MDA-MB-231 cells mirrored expression patterns in HUVEC endothelial cells, suggesting that microRNAs are physiologically active within the metastatic cells. This data would suggest that the microRNAs once transfected into the cells are released into the cytoplasm of the MDA-MB-231 cells, where they can exert cellular activity. (A) Schema and (B) graph examining expression in MDA-MB-231 and HUVEC cells.

small molecule inhibitors.

Finally, in order to confirm that changes in p120RasGAP expression was occurring due to transport of miR132 through nanoChannels and not the result of VEGFR receptor activation by soluble factors secreted from MDA-MB-231 cells, we analyzed p120RasGAP expression in co-culture after inhibition of the VEGFR pathway. The schematic and graph **(Figure 5-13A,B)** show expression of p120RasGAP in HUVEC control sub-populations, dual populations, and co-culture populations both with and without VEGFR inhibitor. As previously described, the HUVEC monocultures are indicated with purple bars, the dual populations are indicated with light green bars, and co-culture populations are indicated with pink bars.

Figure 5-13A and B show no change in p120RasGAP expression in dual groups compared to co-culture populations. Furthermore, when treated with a VEGFR inhibitor, no change in p120RasGAP expression in either dual or co-culture population. Together this data supports previous studies concluding that p120RasGAP regulation is due to nanoChannel mediated transport of microRNAs and not through transfer of soluble factors from the MDA-MB-231 to the endothelial cell population, in turn activating the VEGFR pathway.

The vessel structures were also quantified to ensure that treatment with VEGFR inhibitors did not affect endothelial tube morphology which may indirectly alter p120RasGAP expression through an nC independent pathway. It was important to ensure that the cells were physiologically viable and that the inhibitors were only affecting the VEGFR receptor pathway leaving other functions in the endothelial cells untouched. As described in **Chapter 3**, the nodal area, vessel length, and vessel width were quantified after exposure to 0.1μM and 1μM of the VEGFR inhibitor, vatalinib.

The results of this analysis is given in **Figure 5-13C**, which highlights that there are no significant changes in any of the angiogenic parameters after drug treatment. Therefore, we can conclude that the physical form of the vessel structures are not altered by drug treatment, despite significant inhibition of VEGFR phosphorylation at 6 hours.

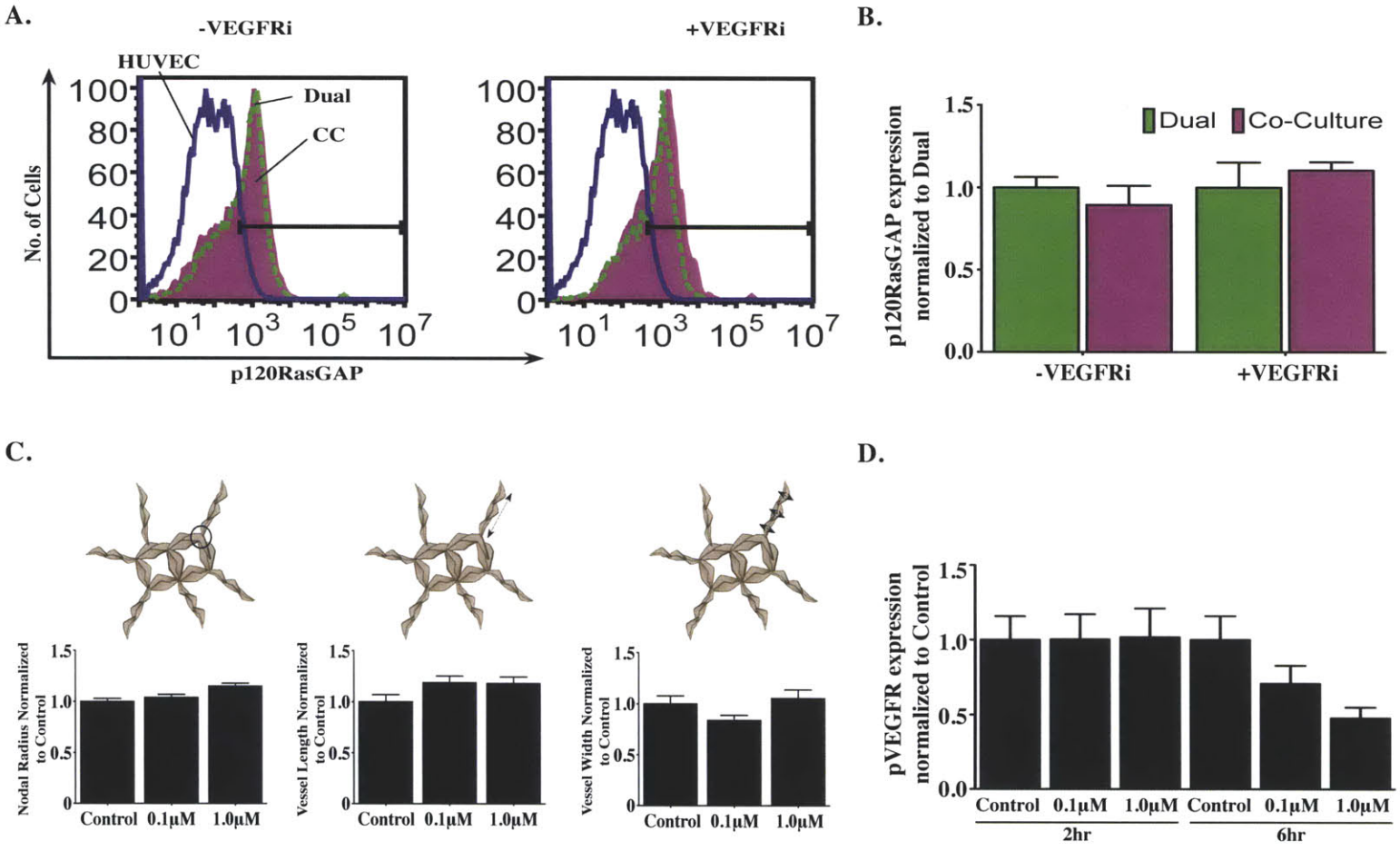

Figure 5-13: Inhibiting VEGFR signaling does not alter measured p120RasGAP expression in endothelial cells. (A) FACS data examining p120RasGAP expression following inhibition with vatalinib. (B) The VEGFRi did not alter p120RasGAP expression in dual versus co-cultures, indicating that the increase in p120RasGAP seen in miR-132 studies is due to miRNA transfer and not through a VEGFR mechanism. (C) Low dose inhibition of VEGFR signaling does not alter normal endothelial cell morphology in co-cultures. (D) The concentrations of drug used in these studies inhibited VEGFR signaling as measured by detection of VEGFR phosphorylation via western blot.

5.3 Conclusion

Transport of the microRNAs through nanoChannels is a unique mode of intercellular communication because nCs enable directed and specific transport of intercellular materials via a highly controlled mechanism allowing one population to transform neighboring cell populations in a very potent and long term manner. In contrast to similar forms of cell-cell communication, for example exosomes, this mechanism of miRNA transfer demonstrates functional activity of this communication in the secondary cell population. Much of the work done examining exosomal transfer of RNAs demonstrate very little functional activity of transported RNAs. Instead these studies emphasize the role of the released nucleotides as biomarkers of disease as opposed to mediators of disease. Much insight can be gained from understanding the mechanisms that underlie miRNA transport and cancer pathogenesis, as well as downstream effects of this form of communication. If indeed microRNA transport through nanoChannels is mediating a transformation of endothelial cell populations, this offers a unique and underexplored opportunity to target both tumor angiogenesis as well as metastatic progression.

The ability of nC structures to transport microRNAs offers a potent mechanism by which metastatic cells can utilize nanoChannels in order to promote cancer pathogenesis. What is unique about transport of microRNAs is that unlike transport of proteins or other small molecules, a microRNA can exert its effect for long durations of time, and since one microRNA regulates many pathways, the effects of a transported microRNA can be quite pronounced, unlike the singular effect, for example, of the transport of one particular protein.

Chapter 6

NanoChannel-mediated communication occurs *in vivo* and may present a novel mechanism for pathological angiogenesis

6.1 Introduction

The pioneering work of Juda Folkman established the intimate connection between cancer progression and angiogenesis. His work and the work of others have demonstrated that tumor growth is strongly regulated by the 'angiogenic switch.' Tumors will cease to grow unless they can successfully recruit vessels to provide the blood flow necessary to meet the metabolic demands of a quickly growing tumor. Not only are tumors able to recruit endothelium, but it has been established that the endothelium in a tumor is genetically altered compared to normal endothelium[122]. However, there is no definitive mechanism explaining how this transformation occurs.

We have previously described a model system that characterizes the unique interactions between metastatic cells and the endothelium. Using this model system,

we elucidated a novel form of communication through thin cytoskeletal projections called nanoChannels. NanoChannels can transport a variety of contents including small molecules, soluble proteins, organelles, and most interestingly miRNAs.

In our continued characterization of nCs, we sought to understand if nanoChannel-mediated communication leads to physiological changes in the endothelium consistent with pathological angiogenesis. We also sought to demonstrate the occurrence of nC-mediated transport in an *in vivo* context.

6.2 Evidence of *in vivo* nanoChannel-mediated communication

We hypothesized that metastatic cells transfer intercellular cargo to endothelial cells *in vivo*, and that disruption of these structures reduces metastatic lesions by preventing endothelial-epithelial cell interactions that are important for intravasation and extravasation.

To determine the role of nanoChannel mediated cellular transfer *in vivo*, we injected CFSE loaded MDA-MB-231 cells intravenously in CD1 nude mice. The animals were then sacrificed at 18, 24, 48, and 72hrs. Lung and liver tissue was isolated from each mouse and the presence of injected metastatic cancer cells was determined using H&E staining **(Figure 6-1)**. At the time points of interest, there was very little evidence of invasion of the MDA-MB-231 cells in the liver tissue, therefore, only representative images from H&E stained lung samples are given in **Figure 6-1**. Metastatic MDA-MB-231 cells can been seen in the lung tissue at 18hrs. At early time points, predominantly single cells are observed in the lung tissue. Within the vessel structures, cancer cells are evident identified by their large cell bodies, multiple nuclei, and alignment along the side of the endothelial cell vessel. By 24hrs small groups of metastatic cells can be seen within the mouse endothelial vessels. By 48hrs and 72hrs there is evidence of micrometastases forming within

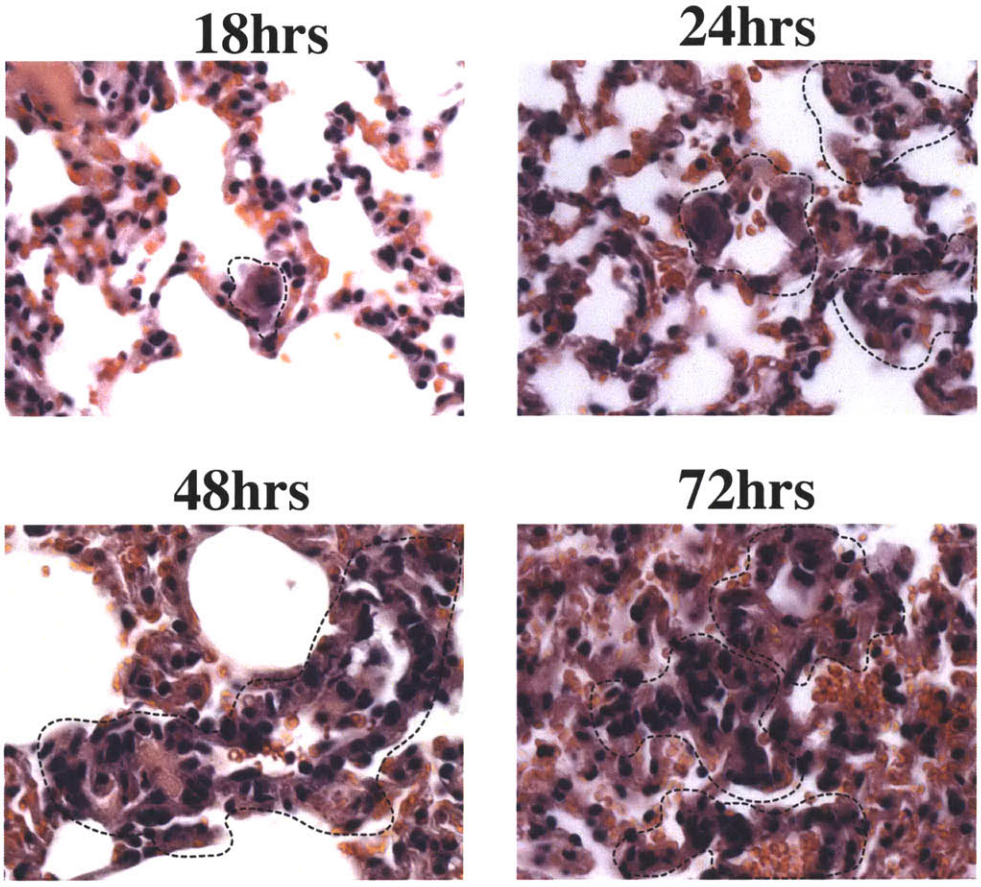

Figure 6-1: H&E images isolated from mouse experimental lung metastasis model. Metastatic MDA-MB-231 cells can be seen within the mouse lung parenchyma at 18hr, 24hr, 48hr, and 72hr. The MDA cells are highlighted with a dashed black outline. At 18 hours single cells can be seen within the lung tissue, by 24hrs small groups of cells are isolated, at 48 and 72 hr there is evidence of small micrometastases forming.

the tissue. Hemorrhage can be seen within the lung tissue at late time points, which is evidence of microemboli formation.

Once the presence of the metastatic cells within the lung tissue was confirmed, evidence of *in vivo* intercellular communication was examined. To begin this analysis, lung tissue was stained with VWF, CD34, and CD31 markers used to identify the endothelial cells. Confocal images of the mouse lung tissue isolated at the time points given above were used to identify nanoChannel-mediated communication. **Figure 6-2** provides representative confocal images of immunostained lung tissues. In these images, MDA-MB-231 cells are seen in green and the endothelial cell vessels are highlighted in red and marked with dashed outlines. NanoChannel projections can be seen forming as early as 18 hrs. The nanoChannels are outlined with a solid white line and yellow arrows show evidence of transport. By 24hrs, the metastatic breast epithelial cells can be seen leaving and extravasating outside the endothelial vessels into the lung parenchyma. By 48 hrs small micrometastases are being formed. Cells can been seen in clumps along the vessel, potentially within a thrombus, or also beginning to invade the surrounding lung parenchyma. At this time point, there is evidence of several nanoChannel projections showing a significant amount of transfer in the neighboring endothelial cell populations. By 72hrs, frank micrometasteses were found within the lung parenchyma. The endothelial vessels are indicated with dashed white lines and the micrometasteses are outlined with dashed yellow lines. SEM images illustrate nCs *in vivo* **(Figure 6-3**, which under close inspection appear identical to projections detected *in vitro* **(Figure 6-4)**.

Evidence of intercellular transfer identified in the confocal images was further validated by isolating lung endothelial cells and quantifying the percentage of CFSE+ve cells using FACS. **Figure 6-5** summarizes the results of this analysis. Endothelial cells were isolated using magnetic CD31 beads and the percentage of CFSE+ve cells were measured 48hrs post injection. Not surprisingly only a small, but significant, percentage of the endothelial cell population was CFSE+ve. This gave increased confidence that the observed intercellular transfer was likely

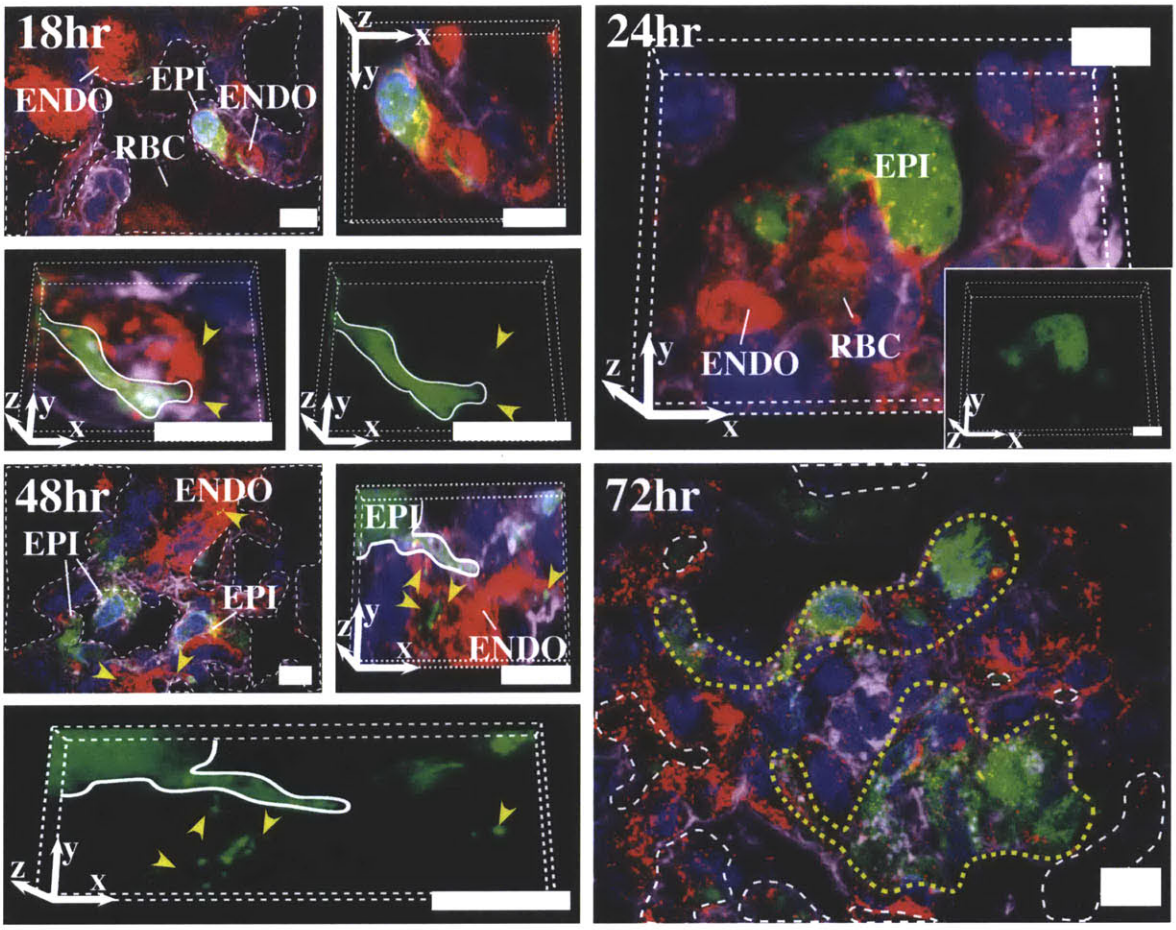

Figure 6-2: Nanochannel (nC)-mediated transfer of intercellular contents in an *in vivo* metastatic breast cancer model. MDA-MB-231 cells were loaded with CFSE (green) and injected into the tail vein of CD1 nude mice. The mice were sacrificed at the indicated time points and the lungs were removed, fixed, and stained. Endothelial cells (red) were triple-stained with vWF, CD34, and PECAM-1 (white dashed outline). 3D confocal reconstructions demonstrate nCs penetrating the endothelial cells and transferring CFSE dye (white solid outline). Examples of intercellular transfer are indicated with yellow arrowheads. MDA-MB-231 cells can be seen migrating out of the endothelial vessels 24hrs post-injection. Micrometastases began to form by 72hrs (yellow dashed outline).

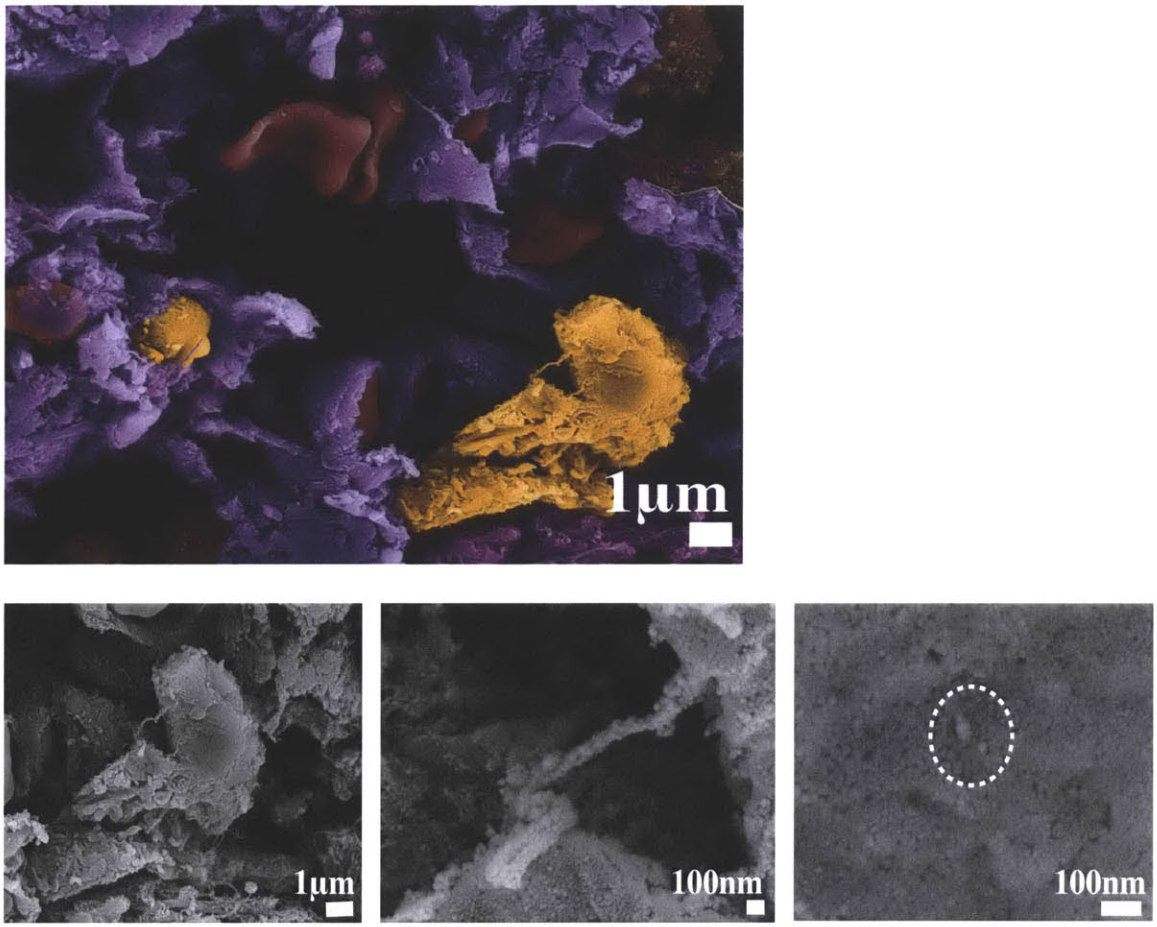

Figure 6-3: *In vivo* nanoChannel projections captured with SEM micrographs. The figure shows a metastatic breast epithelial cell, highlighted in yellow, extending an nC projection to the endothelium, highlighted in purple. The endothelium is identified due to the presence of red blood cells in the endothelial cell lumen. Metastatic breast epithelial cells are loaded with gold nanoparticles in order to identify these cells in the tissue.

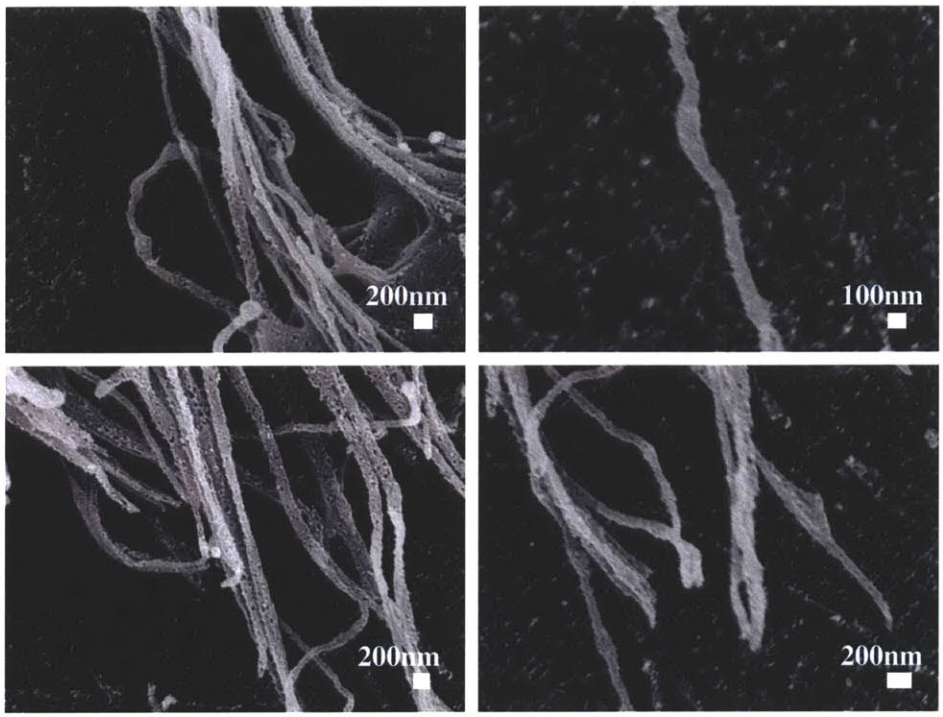

Figure 6-4: High magnification view of nanoChannels *in vitro*. High magnification SEM micrographs show nanoChannels extending from metastatic breast epithelial cells to the endothelium in *in vitro* cultures. These nanoChannels look similar to structures observed *in vivo*, which further confirms that the structures observed in the *in vitro* model system are similar to the structures that are formed *in vivo*.

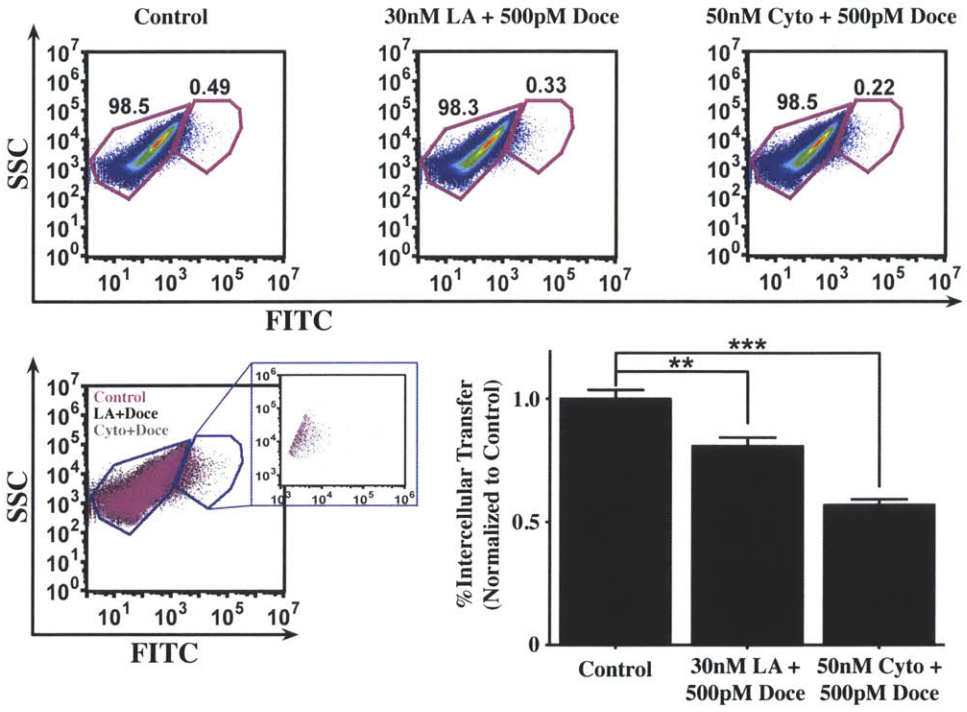

Figure 6-5: *In vivo* intercellular transfer was reduced after pre-treatment with cytoskeletal polymerization inhibitors. Endothelial cells were isolated from mouse lungs 48hrs post-injection and the level of transfer was quantified using FACS. Intercellular transfer was reduced by 43% ($p<0.001$).

nanoChannel-mediated.

To definitely confirm that nCs were involved in the observed transport *in vivo*, the MDA-MB-231 cells were pre-treated with cytoskeletal polymerization inhibitors prior to systemic injection within the mouse. Small molecule pharmacological inhibition of nanoChannels with 500pM Docetaxel combined with either 30nM Latrunclin A or 50nM Cytoklasin D significantly decreased the intercellular transfer of CFSE *in vivo* **(Figure 6-5)**, suggesting that indeed this observed intercellular transfer is of nanoChannel origin. Interestingly, low metronomic dose of taxanes have been reported to be clinically effective[315] , which could potentially arise from the disruption of nanoChannel-mediated intercellular communication.

6.3 Communication through nanoChannels leads to increase in pathological angiogenesis both *in vitro* and *in vivo*

Tumor endothelium is physiologically distinct from endothelium found in healthy tissue exhibiting both genotypic and phenotypic alterations. We next evaluated if nanoChannel-mediated intercellular communication can modify a normal endothelial cell by examining changes in expression of pathological angiogenic markers. We evaluated expression of two of the most ubiquitously expressed pathological angiogenesis markers CD137 and CD276[307]. CD137 and CD276 have been shown to be upregulated in tumor endothelium as well as in other states of pathological angiogenesis, for example, in chronic inflammation[307]. We analyzed expression of CD137 and CD276 in endothelial intercellular transfer+ve and intercellular transfer-ve cell populations. **Figure 6-6** summarizes the results of this analysis. Interestingly, we observed an overexpression of CD137 and CD276 in endothelial cells *in vivo* that were positive for physical intercellular communication. The upregulation of tumor endothelial markers CD137 and CD276 becomes very prominent when analyzing intercellular+ve versus intercellular-ve population **(Figure 6-6)** .

We then tested if the upregulation of pathological angiogenic markers can be inhibited with cytoskeletal polymerization inhibitors **(Figure 6-7)**. Indeed pretreatment of MDA-MB-231 cells with 500pM docetaxel combined with either 30nM latrunculin A or 50nM cytochalasin D decreased both the percentage of cells expressing CD137 and CD276 and the number of CD137 and CD276 receptors on the cell surface as measured by a decrease in median fluorescence. Taken together these results reaffirm that the observed increase in expression of pathological angiogenesis markers is secondary to communication through nC projections.

An upregulation of pathological angiogenesis markers in endothelial cells receiving communication from the metastatic MDA-MB-231 cells was also observed

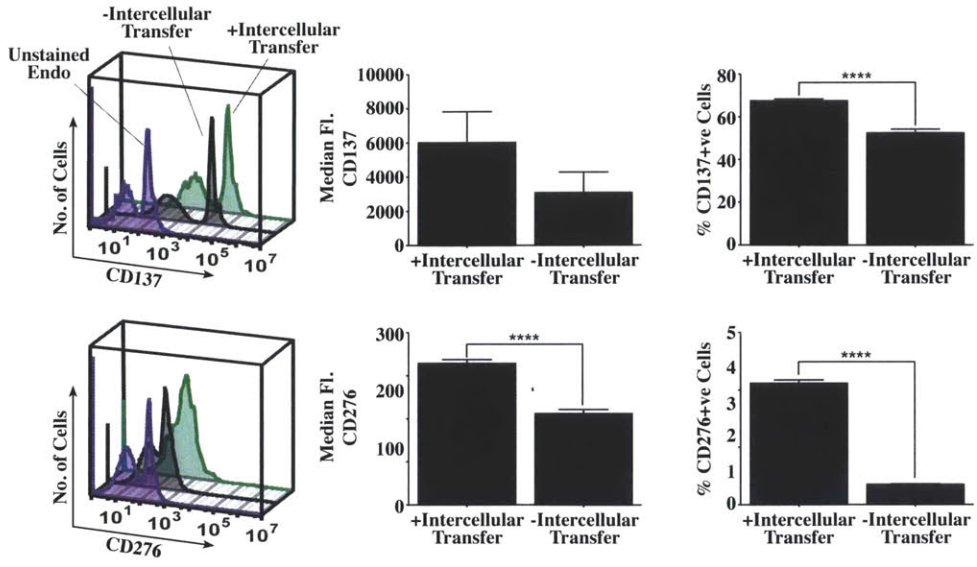

Figure 6-6: NanoChannel-mediated communication leads to increase in pathological angiogenic markers in human endothelial cells *in vivo*. Analogous to *in vitro* results, segregation of cells receiving nC-mediated intercellular transfer shows significantly higher expression of pathological angiogenic markers in intercellular transfer+ve cells.

in vitro **(Figure 6-8)**. This upregulation, similarly to what was seen with the *in vivo* cells, could be disrupted using cytoskeletal inhibitors. **Figure 6-8** highlights the results of this analysis. HUVEC endothelial control cells in monoculture are indicated in purple, HUVEC cells isolated from dual cultures are indicated in green, and HUVEC cells isolated from co-cultures are indicated in pink. The cytochalasin D and docetaxel drug treatment group is represented by the gray curve and latrunculin A and docetaxel are indicated in black. The graph shows that in co-culture the percentage of CD137+ve and CD276+ve endothelial cells was greater then in dual groups. Furthermore, the number of CD137+ve and CD276+ve cells were decreased by drug treatment.

Similarly to results observed *in vivo*, the upregulation of pathological angiogenesis markers become much more pronounced when comparing intercellular transfer+ve and intercellular transfer-ve cell populations. Given that the percentage of the endothelial cells receiving transport is much smaller than the negative intercel-

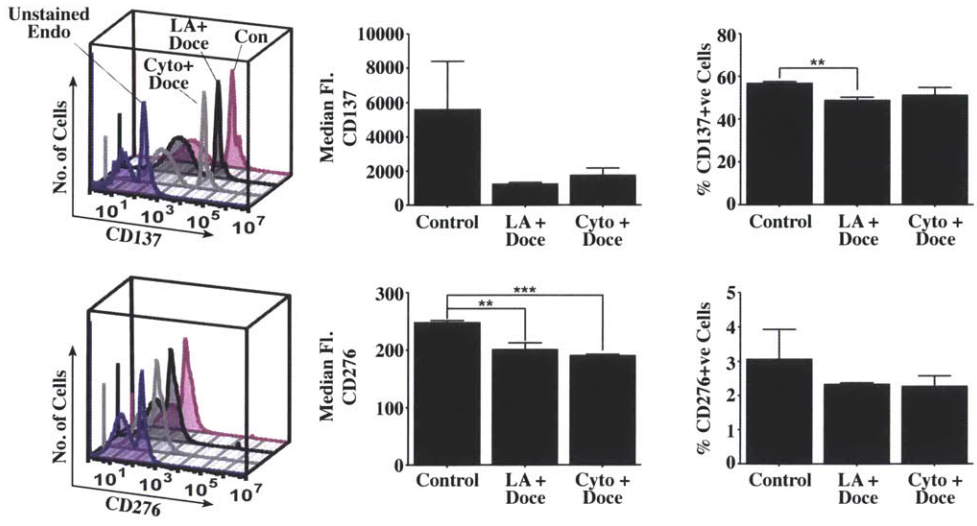

Figure 6-7: Upregulation of pathological angiogenic markers can be inhibited through pharmacological inhibition of nCs. FACS analysis of *in vivo* samples illustrate expression of pathological angiogenic markers CD137 and CD276 in the isolated endothelial cells, which was decreased with pharmacological inhibition of nC projections.

lular population, its easy to underestimate the change in expression of these markers when analyzing whole endothelial cell populations. However, by segregating the two endothelial cell populations into plus and minus transport, the signal-to-noise ratio is improved and the dramatic effects of this form of communication can fully be appreciated.

Upregulation of these markers may potentially enhance metastatic invasion. For example, recent studies have reported that activation of CD137 can increase endothelial cell surface expression of adhesion molecules such as intercellular adhesion molecule (ICAM)-1, vascular cell adhesion molecule (VCAM)-1, and E-selectin, which play a critical role in invasion[319]. Similarly, expression of CD276 (B7-H3), a cell surface transmembrane glycoprotein, was related to migration and invasion in melanoma and ductal and lobular breast cancer[320,321].

Figure 6-9 is a schematic overview postulating how nanoChannel-mediated communication fits into the metastatic cascades. The metastatic cascade starts with

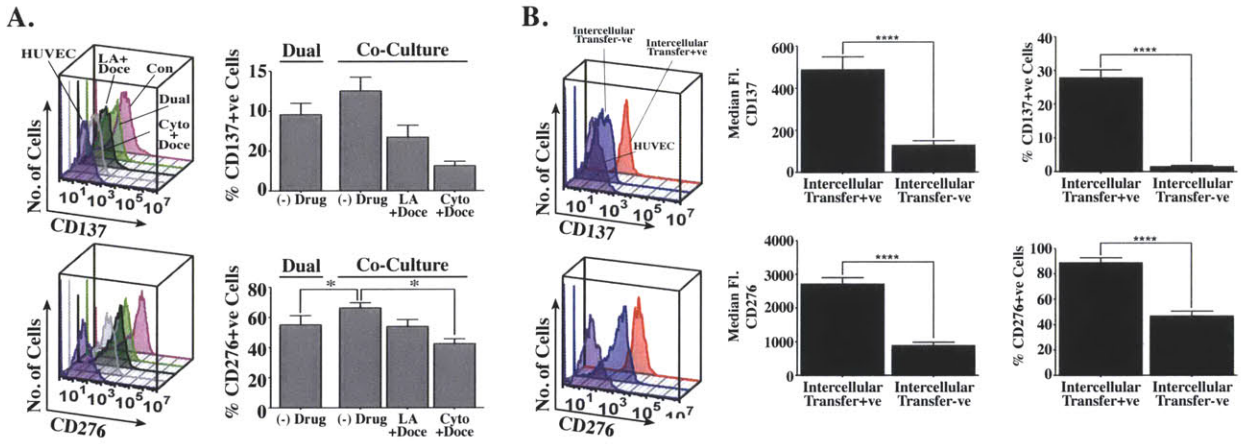

Figure 6-8: NanoChannel-mediated communication leads to increase in pathological angiogenic markers in human endothelial cells *in vitro*, which can be inhibited with pharmacological inhibition of nC projections. (A) Tumor endothelial markers CD137 and CD276 are upregulated in co-cultures, presumably through nC-mediated intercellular transport. This upregulation of pathological angiogenesis markers can be disrupted using combination of F-actin and tubulin polymerization inhibitors. (B) Segregation of intercellular transfer+/-ve cell populations show significantly higher expression of pathological angiogenic markers in intercellular transfer+ve cells.

formation of the primary tumor and invasion into the surrounding tissue. This is followed by elongation of the breast epithelial cells along the vessels and formation of the nanoChannel structure. The nanoChannel structures transport intercellular contents into the endothelium which may aid in metastatic progression.

There are two ways that nanoChannel-mediated communication may enhance metastatic cell invasion. The first mechanism is through long-term transformation of the endothelium into a pathological phenotype. The second mechanism requires quick induction of transient changes in the endothelial cells that in real-time enhance metastatic invasive potential. One example of this is nC-mediated endothelial cell retraction. There is evidence to suggest that nanoChannels may function in endothelial cell retraction through cdc42[108,322]. Previous work has shown that cdc42 expression in metastatic breast epithelial cells can lead to endothelial cell retraction through a β-1 integrin pathway[108]. Cdc42 has also been implicated in formation and extension of nanoChannel structures[322]. Its interesting to contemplate how expression of cdc42 in the breast epithelial cell population can lead to a change in a second population (i.e. the endothelial cells). One potential mechanism of how these two elements can be connected is through communication of intercellular contents through nanoChannels. For example, cdc42 might be an important mediator of nanoChannel formation. When cdc42 is overexpressed, more nanoChannels are formed, leading to increased intercellular transport. The intercellular contents might include miRNAs, proteins, etc. that lead to changes in the endothelial cell biology which result in endothelial cell retraction and promote the transmigration of the metastatic breast cancer cells across the endothelial cell barrier. Understanding alternative consequences to nanoChannel mediated communication in cancer is the next step in the project and I will discuss some potential ideas in **Chapter 7**.

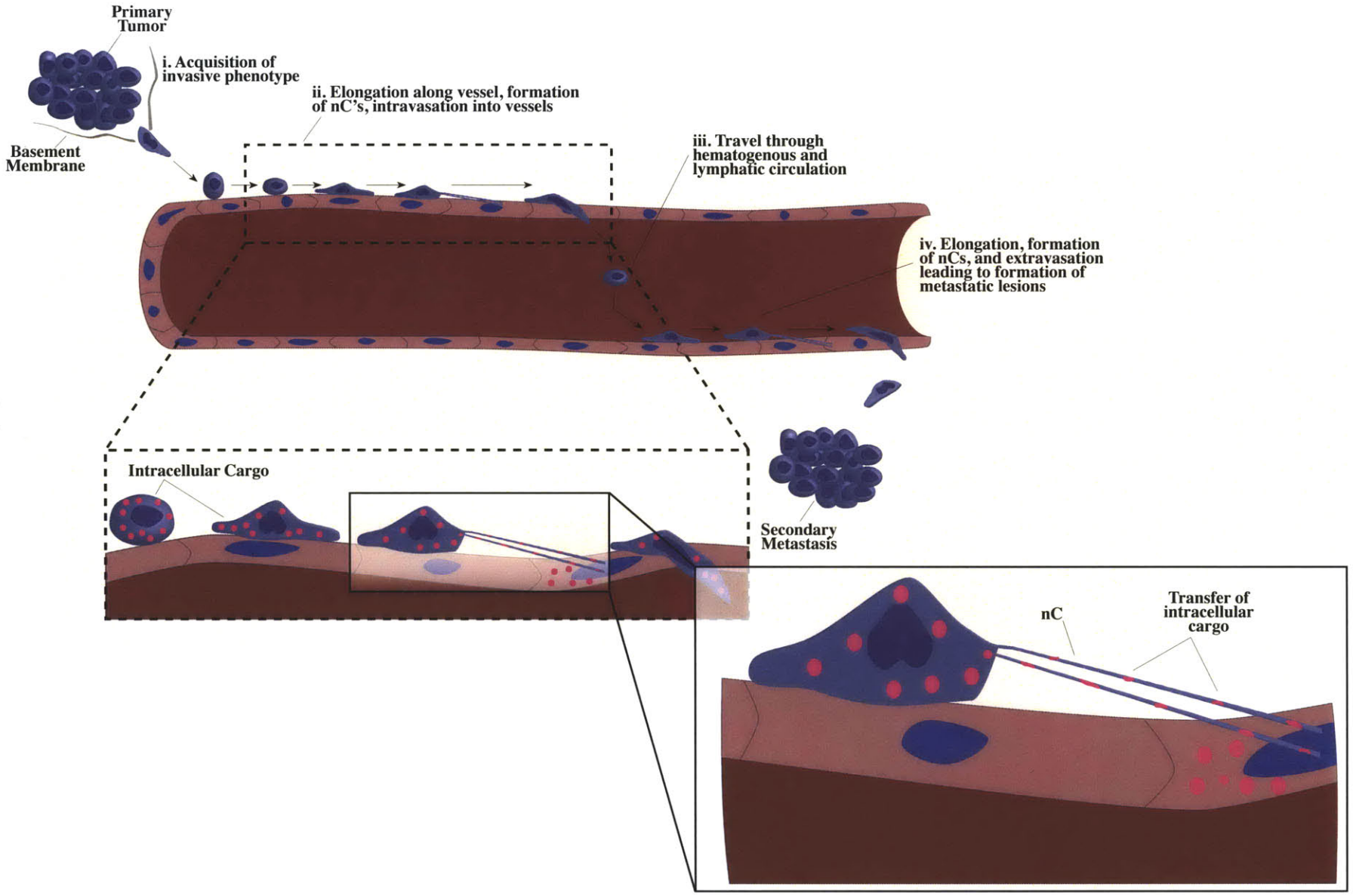

Figure 6-9: Schematic illustration of potential role of nCs in metastatic progression.

6.4 Conclusion

In summary, we describe a novel form of heterotypic intercellular communication between cancer cells and the host endothelium, where tumor cells can physically hijack and transform normal endothelial cells to a pathological angiogenesis phenotype. We define this process as *metastatic parasitism*. NanoChannel-mediated transfer of microRNAs may emerge as a new signaling mechanism in metastasis, which may function to prime the endothelium to facilitate transmigration of tumor cells and/or recruitment of vasculature to growing metastases. Indeed, elucidation of microRNAs transported through the nanoChannels presents a powerful opportunity to both explain mechanisms underlying pathological angiogenesis and for the development of metastasis-specific therapeutics. Interestingly, the ability to disrupt nanoChannels with sub-lethal doses of F-actin and tubulin inhibitors posits whether the clinical benefits of metronomic dosing[315] could arise from the disruption of this intercellular communication. Further mechanistic understanding of the nCs can offer the potential for novel strategies for the management of invasive disease, which are currently associated with dismal 5-year survival rates[8]. Important questions underlying mechanisms of nC formation, endogenous microRNA transport, and downstream changes in the endothelial cell populations remain to be addressed. However, the exploration of nanoChannels in the spread of invasive cancer introduces new insight into mechanisms exploited by cancer cells to facilitate cancer progression by directly manipulating the surrounding cell populations to promote pathogenesis.

Chapter 7

Future Directions

7.1 Summary of Work

Disease can be classified into two paradigms: diseases that can be cured and those which are managed. Modern medicine is well adept in treating localized disease - disease with one singular cause, affecting one singular organ system, and with one singular treatment, typically resulting in a cure. Infectious diseases are classic examples of the localized disease paradigm. These diseases are commonly treated with a single or combination of drug therapies that target well-defined biological mechanisms. In contrast, modern medicine is not well adept at treating non-localized, multi-system diseases. Systemic diseases are not one single disease, but instead a constellation of diseases, typically having multiple etiologies, and unfortunately due to their complexity, limited therapies. This results in diseases that cannot be cured, falling into the category of chronic disease and managed care. Examples of non-localized diseases include autoimmune disorders, chronic heart failure, and cancer metastasis.

Great strides have been made in the war against cancer that have led to significant improvements on 5-year survival rates for many cancers, transforming cancer from a death sentence to a chronic disease. However, the final-frontier in cancer, metastatic invasion, continues to present formidable obstacles that must be traversed to achieve further improvements on cancer treatment outcomes. Metas-

tasis is difficult to treat because like cancer at the primary site, metastatic disease is not one singular disease, but instead a constellation of several diseases, that are as numerous as the diversity of tumor types. Metastatic cancer is a systemic disease that leads to physiological disruptions of a wide range of cellular processes. Therefore, identifying and targeting the dominant pathways that control cancer progression remains a great challenge.

Mechanisms of cancer metastasis occur deep in the body, regulated by systemic interactions with the tissue microenvironment. Furthermore, the possible paths traversed by each invasive cell may potentially be as numerous as the signaling pathways that regulate cellular proliferation or metabolism. In order to advance knowledge of mechanisms underlying cancer metastasis, the fields of science and engineering must develop new cell-based and imaging tools that allow for isolation of discrete mechanisms involved in the metastatic cascade.

Cancer metastasis can be broadly divided into three distinct stages: development and invasion of the primary tumor, interactions with the endothelium, and seeding of the secondary tumor site. These stages offer three separate opportunities for therapeutic intervention. Currently the majority of existing drug therapies are targeted toward the growth of the primary tumor, therefore targeting the later two stages of metastasis presents several untapped therapeutic opportunities. However, elucidation of mechanisms underlying metastatic colonization remain fledgling, making this stage less desirable as a therapeutic target. Furthermore, tissue colonization is dependent on the biology of the primary tumor, as well as the biology of the new microenvironment making colonization a very complex systems biology problem. Lastly, drug therapies inhibiting metastatic colonization would target the late stages of metastasis. Arguably, greater therapeutic benefits could be achieved by targeting molecular events early in disease progression.

In contrast to the limited opportunities to target metastatic colonization, the current state of technology is ripe for making significant advances in our understanding of mechanisms regulating interactions between metastatic cells and the endothelium. Targeting this stage of the metastatic cascade may enable develop-

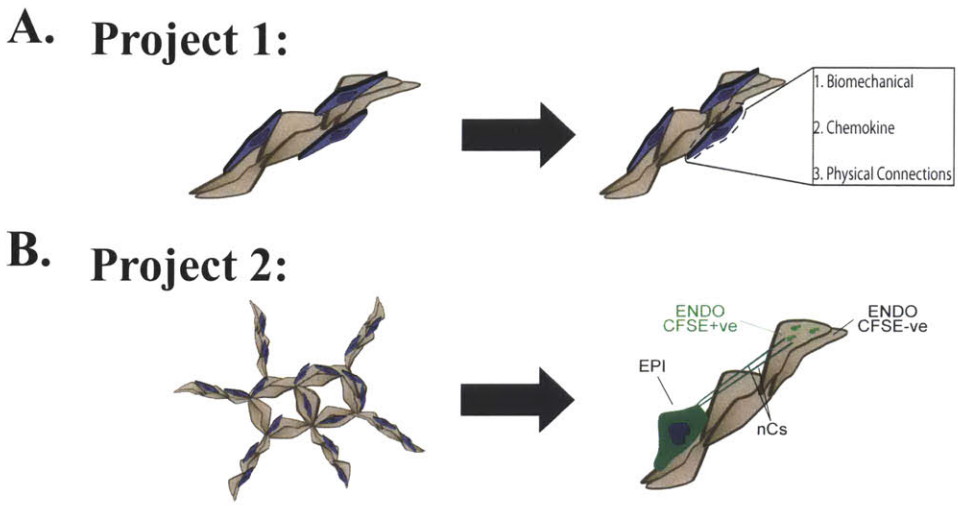

Figure 7-1: Summary of work. (A) An epithelial-endothelial co-culture system captures interactions between metastatic cells and the endothelium. (B) This model system enabled discovery of nanoChannel connections. These structures function in intercellular communication between metastatic cells and the endothelium.

ment of cancer therapies targeted toward early stages of metastasis.

Interactions with the endothelium occur during two distinct pathological events: intravasation/extravastion and the recruitment of angiogenic vessels by the primary tumor and the newly formed metastases. To this end, we have described the engineering of a three-dimensional, cell-based, co-culture model system used to study population and single cell interactions between metastatic epithelial cells and the endothelium. The primary motivation in developing this system is centered on the critical role the endothelium serves in cancer progression.

Our engineered 3D epithelial-endothelial co-culture system allows for the study of novel interaction phenotypes between epithelial cells and the endothelium **(Figure 7-1)**. We have demonstrated that this model system enables identification of molecular pathways that regulate these interactions and also provides a platform for probing these pathways using commonly available molecular biology techniques such as RNAi and small molecule pharmacological inhibitors. In the future, the model system may prove to be a valuable tool in screening potential therapeutics that not only target the tumor and angiogenic compartments individually, but

also target the intersection of these two compartments, a feature that has emerged to be a critical aspect of cancer progression. However, the most powerful aspect of the model is the window it offers into the typically occult process of metastasis. The ability to directly observe interactions between two cell types that physiologically should never come into direct contact offers witness to the formation of a symbiotic relationship that may provide powerful clues into the connection between aberrant cell-cell relationships and cancer metastasis. The power of observation, unlike other techniques used in science, introduces an opportunity to discover phenomenon without *a priori* knowledge of a phenomenon. It provides the purest form of inquisition guided not by previous knowledge or assumptions, but instead by direct observations.

Our observations of these cell-cell interactions enabled the identification of novel cytoskeletal projections extending between the metastatic cells and the endothelium. These projections, coined *nanoChannels*, seem to primarily function in intercellular communication **(Figure 7-1)**. However, they may also be involved in other yet to be explored mechanisms of cell-cell interactions. Communication of intercellular contents through these channels is a powerful mode of cellular communication that I would argue is distinct from other forms of cell-cell communication.

Unlike other forms of intercellular communication, nanoChannel projections allow for a level of tunability and specificity that cannot be achieved with similar forms of intercellular communication. For example, membrane vesicles transport similar cargo as nanoChannels, such as cytoplasmic RNAs. However, unlike membrane vesicles which are released from a cell to be taken up by a neighboring cell in a non-specific and seemingly random manner, communication via nanoChannels allows a singe cell to communicate directly with another single cell in a highly regulated and defined fashion. The ability to communicate with surrounding cells with specificity, combined with the wide array of transported biomolecules through nCs, highlights the unique nature of this communication. It also introduces many interesting questions regarding the function of nanoChan-

nels in cancer. What is the role of nCs in normal cellular physiology? How can this mode of communication be exploited by tumor cells in order to enhance cancer spread? For example, our data has shown that intercellular transfer through nanoChannels leads to the development of a pathological phenotype in the endothelium. However, could this form of communication serve other roles in metastatic invasion? For example, could nC-mediated communication enhance endothelial cell retraction to promote transendothelial cell migration? Presumably, a metastatic cell could arrest within a vessel and then rapidly, and specifically transport intercellular contents that alter the biomechanics of the endothelium in a manner that enhances the ability of metastatic cells to intravasate or extravasate. Alternatively, contents transported through nCs could transform the endothelium to not only enhance the metastatic potential of that particular cell, but potentially also make the endothelium more permissive for colonization by future metastatic cells. Lastly, nanoChannels may also function in primary tumor biology. We have demonstrated that nCs can promote cancer progression by quieting surrounding healthy cells. Communication of intercellular contents from tumor cells through nanoChannels leads to a decrease in cellular proliferation of normal breast epithelial cells. Just as pathogens enhance the spread of disease by monopolizing resources in order to outcompete normal cells, tumor cells can directly manipulate their surrounding environment to enhance survival.

The introduction of nanoChannels as a novel route of intercellular communication incites a wide array of questions and also presents therapeutic opportunities to target early and late stages of metastatic progression. However, to fully understand the importance of this mode of communication, future research on the subject is critical. Of particular importance is understanding the downstream consequences of nC-transport both in the primary tumor and in metastasis. How are these structures formed? Would inhibition of these structures lead to improved therapeutic outcomes? What drives these structures to form with high specificity with the endothelium? In the following section, I identify the critical questions regarding expansion of this body of work to address the role of nanoChannels in

metastasis and address possible therapeutic strategies for disrupting these projections.

7.2 Downstream consequence of nanoChannel transport

Transport of cytoplasmic contents through nanoChannels may have profound consequences in the primary tumor and in metastatic progression. Transfer of miRNAs through these structures presents a mechanism for long-term transformation of recipient cell types. Unlike other biological macromolecules, such as proteins with a limited half-life, transport of miRNAs leads to lasting and persistent changes. A single miRNA can target multiple mRNAs affecting several cellular pathways.

Although other forms of intercellular communication can transport miRNAs, such as exosomes, these mechanisms may not be capable of actively regulating metastasis at the level of tumor-endothelial interactions in the same manner as nCs. Membrane vesicles are non-specifically released by cells and the direction of transport is not directly controlled. For example, tumor cells that arrest within a capillary may release extracellular vesicles. However, what determines the ability of this mechanism to promote cancer is the probability that these vesicle will be uptaken by the endothelial cells. This probability in turn is dependent on the local concentration of vesicles near the cell of interest. It's unlikely that a high local concentration of exosomes can be achieved by metastatic cells within the blood stream. Exosomes randomly released by the cells are more likely to diffuse into the blood stream than be uptaken by surrounding endothelial cells.

Consider this analogy: transfer of genetic material via exosomes is analogous to insemination in plants while transfer of genetic material through nanoChannels is analogous to insemination in mammals. Take dandelions in a field. Dandelions are constantly releasing pollen, however in a strong wind, the majority of the pollen

released does not fall at the base of the plant, but instead is carried great distances. Exosomes in this analogy are like dandelion seeds. Contrast this to how insemination occurs in mammals. NanoChannels form direct connections between cells that can withstand the shear stress of blood flow. Formation of direct cell-cell connections greatly enhances the likelihood that intercellular contents will actually be transported into the specific cell of interest. Not only do nanoChannels allow for transport of potent regulatory biomolecules, but they also enhance the ability of cells to tightly regulate dispersion of these biomolecules that cannot be achieved through other modes of intercellular communication.

Given these unique characteristics of nanoChannels, what are the potential downstream consequences of this communication and how can these consequences be tested? NanoChannels likely serve dual functions in metastasis, broadly characterized into direct and indirect metastasis priming mechanisms. A direct mechanism is one that increases the metastatic potential of the communicating cell, while indirect mechanisms prime for subsequent metastatic invasions. An example of a direct mechanism is nC communication enhancing transendothelial migration. Previous studies have demonstrated that tumor cells can change the biomechanical properties of the endothelium, leading to increased transendothelial migration. In other studies, metastatic cells have been shown to promote endothelial cell retraction through β-1 integrins and cdc42. However, the mechanisms by which these phenomena occur have not been elucidated, introducing interesting considerations regarding the possible role nCs may play in creating this pro-metastatic phenotype. The forefront question is *how does expression of proteins by metastatic cells, promote biomechanical changes in the endothelium?* Our studies have shown that β-1 integrins are important for endothelial-epithelial cell-cell interactions. In addition, cdc42 is an actin cytoskeletal regulatory protein that has been implicated in formation of tunneling nanotubes, which are cytoskeletal projections with similar properties as nanoChannels. Therefore, it may be the case that expression of β-1 integrins and cdc42 is correlated with formation of nanoChannel projections and also that the cytoplasmic contents transported through these structures cause

changes in the biomechanical properties of endothelial cells.

NanoChannels indirectly contribute to metastatic invasion through transformation of the endothelium. Our work has shown that nanoChannels promote development of a pathological phenotype by endothelial cells. These pathological vessels, in turn, feed the growing metastatic lesion promoting development of frank metastases. Furthermore, pathological vessels are physically distorted characterized by irregular, leaky vessel structures. Those leaky vessels may make it easier for tumor cells to escape the endothelium and enter surrounding tissues. Lastly, transformation of the endothelium primes formation of future metastases by creating a pre-metastatic niche. Tumor endothelial cells have been linked to creation of a pre-metastatic niche through secretion of soluble factors, particularly pro-inflammatory signals. These signals recruit other tumor stromal cells, such as macrophages, that promote growth of metastatic lesions.

Investigating these hypotheses involves identifying phenotypic and genetic changes in the endothelium that occur as a result of communication through nanoChannels. Studies examining changes in cellular biomechanical properties would shed tremendous insight into the role nCs play in directly enhancing invasion by promoting transendothelial cell migration. Furthermore, examination of changes in cytoskeletal regulatory proteins may provide insight into endothelial cell retraction. An analysis of which specific microRNAs are transported may elucidate mechanisms explaining the origin of these changes in the endothelium. Studies have shown the endothelium of tumors is genetically transformed[274]. Potentially secondary to mutations caused by this miRNA transport. Other transported biomolecules may also be implicated in this transformation. Examining alterations in cytokine secretion may also shed light into the pro-metastatic role of nanoChannels, which may function through the formation of a pre-metastatic niche or via promotion of angiogenesis.

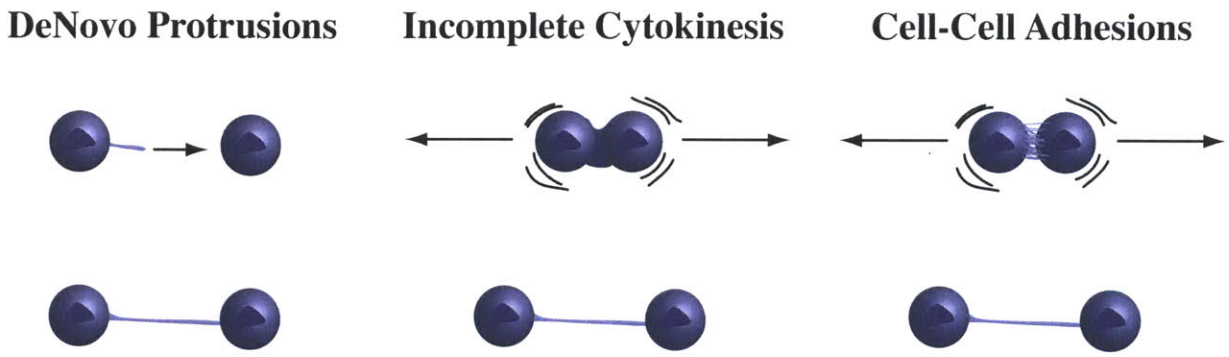

Figure 7-2: Mechanism of formation of nC structures. There are several possible mechanisms by which nanoChannels form, *de novo* protrusion formation, remnants of incomplete cytokinesis, and extensions of cell-cell adhesions.

7.3 Mechanism of formation of nC structures

NanoChannels introduce a new mechanism by which cellular transformation occurs called *metastatic parasitism*. The unique nature of this mode of communication potentially highlights these structures as druggable targets in cancer. However, development of nC specific therapeutics requires an understanding of how nCs are formed. NanoChannel formation is complex involving biological pathways regulating cytokine sensing, cytoskeletal rearrangement, and membrane fusion. There are several possible mechanisms by which nanoChannels form. The first mechanism is *de novo* protrusion formation **(Figure 7-2)**. This requires initiation and extension of a nanoChannel structure by one cell that eventually contacts a neighboring cell. *De novo* protrusion formation is likely the mechanism underlying formation of heterotypic nC-mediated communication. NanoChannels structures may also be remnants of incomplete cellular cytokinesis resulting from cell division. Alternatively, nanoChannels may form from tight cell-cell adhesion connections that remain intact as cells move further and further apart. In metastasis, the relevant function of nanoChannels is in heterotypic cell-cell interactions. Therefore, the most significant therapeutic opportunity lies in impeding *de novo* protrusion formation.

The steps of *de novo* protrusion formation can be divided into five stages with

distinct mechanisms: dynamic motions in the membrane, response to external nC promoting stimulus, initiation and extension of a projection, and fusion with the secondary cell membrane. These steps are summarized in **(Figure 7-3)**. Insight into the initial steps of nC protrusion formation may be gained by examining formation of other cytoskeletal projections such as filopodia or tunneling nanotubes. The initial steps of nC protrusion formation likely occur due to dynamic Brownian motions in the membrane that generate small projections. These motions are an inherent property of the membrane and are also likely the first step in initiation of similar cytoskeletal projections, such as filopodia. These small projections may contain cytokine receptors. Detection of an nC growth stimulus by these receptors may stimulate initiation and extension of these projections. Extension of the growing projection probably occur in response to chemotactic gradients of nC promoting factors secreted in high concentrations by endothelial cells.

Cytoskeletal regulatory proteins such as M-Sec, RalA, and the exocyst, have been implicated in the formation of similar cytoskeletal projections[323]. M-Sec is homologous to the Sec6 subunit of the exocyst[323]. M-Sec and RalA have been found to co-localize with the exocyst complex[322]. This protein complex regulates F-Actin remodeling required for protrusion formation. Formation of nanoChannel connections likely involves similar cytoskeletal regulatory molecules and therefore may be targeted with drugs inhibiting cytoskeletal regulatory proteins. For example, preliminary data shows that treatment of MDA-MB-231 cells with an aurora kinase inhibitor (Tozasertib) and a TNFα inhibitor (Pomalidomide) decreased intercellular transfer through nanoChannels **(Figure 7-4)**. The aurora kinases are known regulators of the actin cytoskeleton[324], while TNFα has been implicated in regulation of the exocyst complex[325]. Interestingly, activation of Fas ligand caspase signaling has been implicated in TNT formation by regulating Rho GTPase signaling[326]. This data suggests that screening for small molecules inhibitors of cytoskeletal regulators may yield drugs that effectively disrupt communication through nanoChannels.

The final step in nanoChannel formation involves fusion with the endothelial

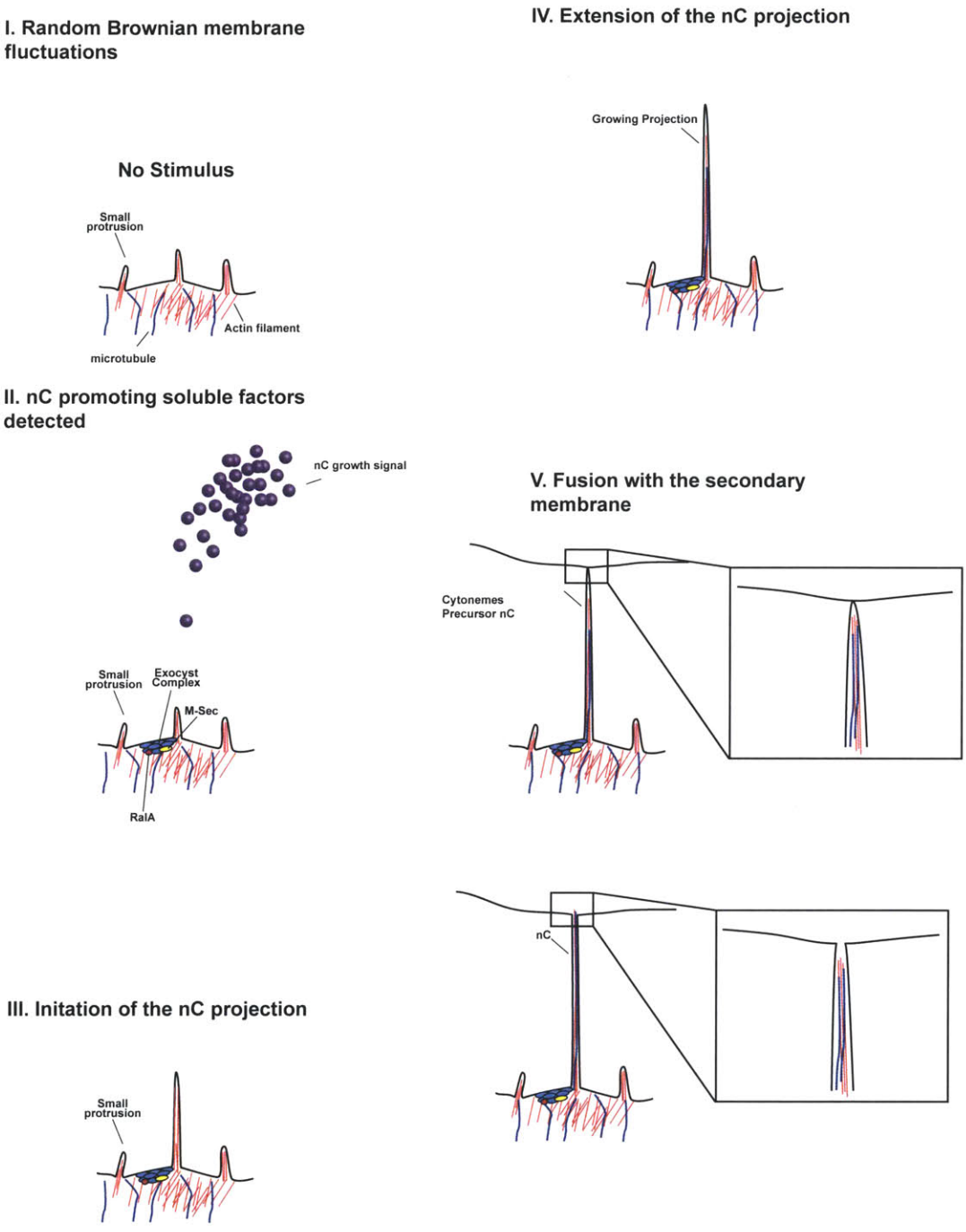

Figure 7-3: Formation of *de novo* nanoChannel protrusions. NanoChannel formation is theorized to involve five distinct steps. Brownian membrane fluctuations lead to formation of small protrusions that in response to soluble factors result in initiation and extension of nC projections toward the stimulus. The final step involves fusion with the endothelial cell membrane.

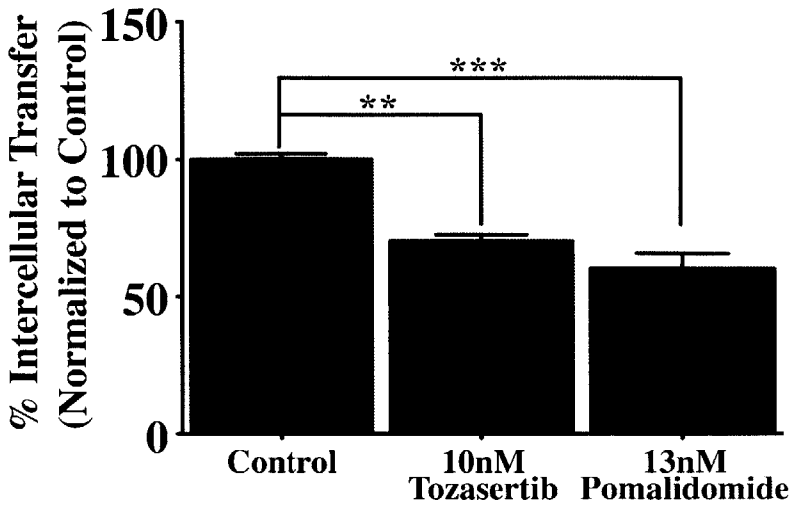

Figure 7-4: Inhibitors of aurora kinase and TNFα decrease intercellular transfer through nanoChannels. Aurora kinase inhibitor (Tozasertib) and a TNFα inhibitor (Pomalidomide) decreased intercellular transfer through nanoChannels.

cell membrane. Cytonemes or filopodial bridges are unfused closed-end tubular projections that may be precursors of nanoChannels. Fusion of the nanoChannel projections may occur through a clathrin-mediated pathway. A dose titration with chlorpromazine, a clathrin-mediated endocytosis inhibitor, resulted in a dramatic reduction in intercellular communication that correlated with increasing drug concentration **(Figure 7-5)**. In this experiment, the endothelial cells were treated with the endocytosis inhibitor chlorpromazine prior to seeding in the matrix. Dual chamber studies and pharmacological inhibition of exocytosis in the MDA-MB-231 cells show minimal effects on percent intercellular transfer. Furthermore, in both the 0.4μm and 3μm pore studies, extracellular vesicles can be seen in contact with the endothelial cells. These vesicles, however, are not endocytosed by the cells and do not result in a change in intercellular communication, excluding the involvement of an endocytotic/exocytotic mechanism as the source of the observed intercellular communication. Therefore, decline in intercellular transfer after treatment of endothelial cells with chlorpromazine likely results from defects in

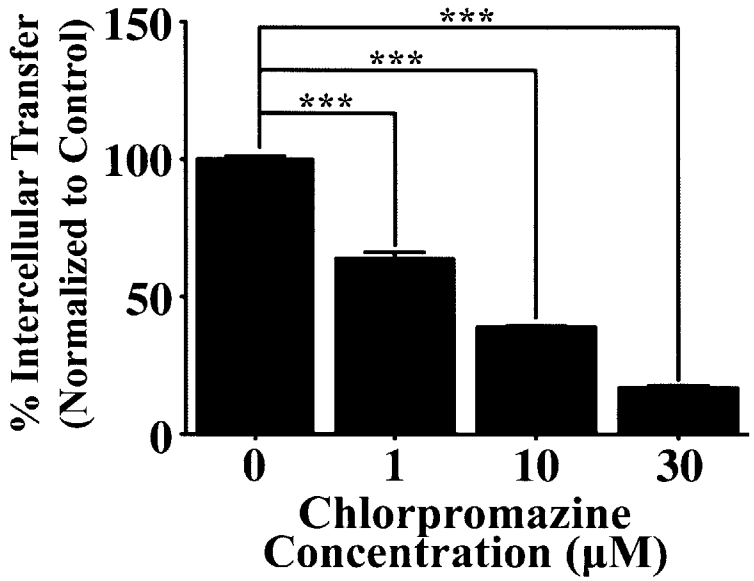

Figure 7-5: Clathrin mediated endocytosis inhibitor prevents nanoChannel fusion with the endothelial membrane. Increasing concentrations of chlorpromazine leads to a dose-dependent inhibition of intercellular transport through nCs by preventing membrane fusion.

nanoChannel fusion with the endothelial cell membrane **(Figure 7-5)**. Fusion of extracellular vesicles such as exosomes have also been shown to involve the clathrin pathway[327]. These results suggest possible overlaps regarding how nanoChannels and exosomes are formed.

7.3.1 Therapeutic implications: Targeting exosomes and membrane projections

Biogenesis of exosomes is a complex process and an active area of investigation. Reports on the roles of molecules involved in exosome formation vary in different cellular model systems, suggesting that exosome biogenesis may involve unique mechanisms in different cell types[328]. Exosome formation is signaled by ubiquitination of the cytosolic tails of receptors destined for degradation, which results in the formation of intralumenal vesicles (ILVs) through coordinated interactions of protein complexes collectively referred to as ESCRT (endosomal sorting complex

required for transport)[328]. ESCRT is believed to function in targeting the receptor to the intraluminal vesicle, playing critical roles in insuring appropriate protein composition of exosomes[135,328]. However, it's unclear of the exact role of ESCRT in all cell types or if other molecules may perform similar functions[328]. Annexins and RAB GTPases (RAB11, RAB27, and RAB35) proteins are involved in trafficking and secretion of exosomes[135,163,328]. The specific role of each RAB proteins in the formation of exosomes is unknown, further complicated by the possibility of cell type-to-cell type variability in function[328]. In the final steps (fusion with the plasma membrane and release into the extracellular environment) SNARE proteins are believed to play critical functions, however, the exact composition of this complex is unknown[328].

Exosomes commonly contain proteins involved in signal transduction such as protein kinases and G proteins. Heat shock proteins HSP70 and HSP90 are also commonly found within exosomes along with the Tetraspanins family of transmembrane proteins, such as CD9, CD63, CD81, and CD82[163]. The exact function of the tetraspanins is unknown but they are believed to be involved in large protein networks[163]. Exosomes have a specific lipid composition composed of cholesterol, ceramide and spingolipids, which may function in proper exosome release. For example ceramide is involved in exosome release and inhibition of ceramide synthesis reduces exosome production[135].

There are potential mechanistic overlaps between formation of nC structures and release of exosomes that present therapeutic opportunities for simultaneous dual targeting of both mechanisms. For example, each of these structures is regulated by cytoskeletal proteins. Future work may involve elucidating cytoskeletal regulators that function in both modes of communication. Another possibility is examining mechanisms that regulate the nature of the cargo transported by each of these modes because there are many functional overlaps that exist such as the ability of these structures to transport nucleic acids. However, the most similarities are probably found when considering how these structures fuse with the secondary membrane. Due to similarities in dimension, exosomes and nanoChannels

are likely indistinguishable to recipient cells. From the perspective of the recipient cell, the radius of a nanoChannel is much much smaller than the radius of the cell, therefore, an approaching nanoChannel likely appears similar to an approaching exosome. When these two structures interact with the recipient cell, it's likely that the cells respond similarly to both. Given our preliminary results, this shared mechanism involves clathrin-mediated endocytosis. However it's also possible that other mechanisms are involved, such as phagocytic mechanisms or membrane fusion.

7.4 Conclusion

Much of the work examining transport of miRNAs have focused on exosomes as the primary carriers. However, exosomes, like other extracellular vesicles, are randomly released into the microenvironment. This introduces questions about the efficiency of transport of miRNAs within extracellular vesicles and if transport of these molecules through other encapsulated structures, such as membrane bridges, offer additional specificity. There are many functional, and perhaps mechanistic, overlaps between intercellular communication through membrane bridges and extracellular vesicles. This introduces the question of what advantage does having both of these mechanisms provide cells. Potentially, exosomal mediated transport function more in long-range, low-specificity communication, while communication through membrane bridges better enables short-range, high-specificity communication.

Furthermore, these models likely have overlapping mechanisms of formation. Therefore, one potential therapeutic strategy may be to simultaneously target both membrane bridges and extracellular vesicles. In addition, each of these mechanisms exhibit both pro- and anti-tumorgienic properties. Could a viable therapeutic strategy be to induce intercellular communication through these mechanisms that are protective against tumor growth? Furthermore, can these mechanisms be explored for the delivery of anti-tumorigenic therapies, similar to strategies being

pursued for delivery of siRNAs[329]. To answer these questions and others requires a better understanding of the function of these structures. How are formed? What regulates the intercellular cargo they carry? What stimuli leads to secretion of exosomes versus formation of membrane bridges? What are the functional overlaps between these two modes of communication? How are they different? Are there mechanistic overlaps that will provide an opportunity for therapeutic intervention?

Appendix A

Matlab Code

```
% 2 PARAMETER INDEX
%    -Analysis of Normal, Tumorgenic and Metastatic cell lines
%    -Epithelial-Endothelial Disassociation Index (EEDI)
%    -Elongation Index (EI)
%
% Last modified: yamicia Jun 20, 2013 16:25:00
%-------------------------------------------------------------------------

clear;clc;close all;

if exist('yami_data.mat')
    load('yami_data.mat');
else
    lines = {'HMEC','MCF10A','MCF7','SKBR3','MDA_MB_231','MDA_MB_468',...
        'M_4T1'};
    cols = {'A','B','C','D','E','F','G','H','I','J'};
    % Normal (2), Tumorogenic (2), and Metastatic (3) cell lines being
    % analyzed for the 2 parameter index

    for i = 1:length(lines)
        inter.(lines{i}) = xlsread('Yami_Data.xlsx','EEDI',...
            [cols{i},'2:',cols{i},'1000']);
```

```
23          elongation.(lines{i}) = xlsread('Yami_Data.xlsx','EI',...
24              [cols{i},'2:',cols{i},'1000']);
25      end
26
27      save('yami_data.mat');
28  end
29
30  for i = 1:length(lines)
31      if(length(elongation.(lines{i})) >= length(inter.(lines{i})))
32          elong.(lines{i}) = convert2elong(elongation.(lines{i}),...
33              inter.(lines{i}));
34      else
35          elong.(lines{i}) = elongation.(lines{i});
36          inter.(lines{i}) = convert2elong(inter.(lines{i}),...
37              elongation.(lines{i}));
38      end
39  end
40
41  % Average and Standard Deviation for both EEDI and EI across all seven cell
42  % lines.
43  for i = 1:length(lines)
44      avg_inter.(lines{i}) = mean(inter.(lines{i}));
45      std_inter.(lines{i}) = std(inter.(lines{i}));
46      avg_elong.(lines{i}) = mean(elong.(lines{i}));
47      std_elong.(lines{i}) = std(elong.(lines{i}));
48  end
49
50  % Normal Lines
51  avg_inter.norm = mean([avg_inter.HMEC,avg_inter.MCF10A]);
52  avg_elong.norm = mean([avg_elong.HMEC,avg_elong.MCF10A]);
53  std_inter.norm = rms([std_inter.HMEC,std_inter.MCF10A]);
54  std_elong.norm = rms([std_elong.HMEC,std_elong.MCF10A]);
55  % Tumorgenic Lines
56  avg_inter.tumr = mean([avg_inter.MCF7,avg_inter.SKBR3]);
57  avg_elong.tumr = mean([avg_elong.MCF7,avg_elong.SKBR3]);
58  std_inter.tumr = rms([std_inter.MCF7,std_inter.SKBR3]);
```

```
std_elong.tumr = rms([std_elong.MCF7,std_elong.SKBR3]);
% Metastatic Lines
avg_inter.meta = mean([avg_inter.MDA_MB_231,avg_inter.MDA_MB_468,...
    avg_inter.M_4T1]);
avg_elong.meta = mean([avg_elong.MDA_MB_231,avg_elong.MDA_MB_468,...
    avg_elong.M_4T1]);
std_inter.meta = rms([std_inter.MDA_MB_231,std_inter.MDA_MB_468,...
    std_inter.M_4T1]);
std_elong.meta = rms([std_elong.MDA_MB_231,std_elong.MDA_MB_468,...
    std_elong.M_4T1]);

lines = [lines {'norm'} {'tumr'} {'meta'}];


% Plotting
t = 0:0.01:2*pi;
xlswrite('Yami_Data.csv',lines,'ellipse_x','A1');
xlswrite('Yami_Data.csv',lines,'ellipse_y','A1');
for i = 1:length(fieldnames(avg_elong))
    x{i} = [std_inter.(lines{i})*cos(t) + avg_inter.(lines{i})]';
    y{i} = [std_elong.(lines{i})*sin(t) + avg_elong.(lines{i})]';
end

save export_data.mat x y lines;
xlswrite('Yami_Data.csv',x{i},'ellipse_x',[cols{i},'2:',cols{i},'1000']);
xlswrite('Yami_Data.csv',y{i},'ellipse_y',[cols{i},'2:',cols{i},'1000']);

figure(1);
clr = [0 0 255; 0 127 0; 255 0 0; 0 191 191; 191 0 191; 191 191 0;...
    0 0 0]/255;
clr2 = [0 0 255; 0 127 127;0 255 0]/255;
hold on;
for i = 1:length(fieldnames(avg_elong))
    h = plot(x{i},y{i});
    if i<=7
        set(h,'Color',clr(i,:),'LineWidth',1);
```

```
    else
        set(h,'Color',clr2(i-7,:),'LineWidth',2.5);
    end
end
title('Elongation vs. Interaction');xlabel('Interaction');...
    ylabel('Elongation');
axis([0 1 -1 7]);
grid on; legend('HMEC','MCF10A','MCF7','SKBR3','MDA-MB-231',...
    'MDA-MB-468','4T1','Normal','Tumorgenic','Metastatic');
```

```
function elong = convert2elong(elongation,offr)

lower = floor(length(elongation)/length(offr));
numup = mod(length(elongation),length(offr));
if numup ~=0
    upper = lower+1;
else
    upper = lower;
end
num = upper;

elong = zeros(size(offr));
c = 1;
for i = 1:length(offr)
    for j = 1:num
        elong(i) = elong(i) + elongation(c);
        c = c+1;
    end
    elong(i) = elong(i)/num;
    if i >= numup
        num = lower;
    end
end
```

```
% CFSE Transfer Kinetics
%    Calculates kinetics transfer through nanotubes, at various diffusion
%    rates.
%
% Last modified: yamicia Jun 25, 2013 13:20:00
%-------------------------------------------------------------------------

clear;clc;close all;

x = 0:0.01:177; % um
t = 0:1/60:96;  % hour
% D = 10;       % um^2/sec -- protein in cytoplasm; miRNA in cytoplasm
% D = 100;      % um^2/sec -- small protein in water; miRNA in water
D = 0.001;      % um^2/sec -- small molecule in water
v = 0.350;      % speed in um/sec
k = 0.05;
k_1 = 0.5;
L = 72;
L_on = v/k_1;
L_off = (D/2*k)^(1/2);

C = zeros(size(x));
Cend = zeros(size(t));
C0 = 50000;  %nM

% Time-evolving graph, indicating transfer of CFSE in time
for i = 1:length(t)

    C = C0*erfc(x/(2*sqrt(D*t(i)*3600)));%*(L/2*L_off)*(1+(L_on/L_off));
    Cend(i) = C(end);

    figure(1);
    plot(x,C);
    grid on;
    title(['time = ',num2str(round(t(i))),' out of ',num2str(t(end)),' hours']);
    axis([min(x) max(x) 0 C0]);
```

```
37      xlabel('Distance [\mum]');ylabel('Concentration [nM]');
38      drawnow;
39  end
40
41  % Concentration in Epithelial cell over time.
42  figure(2)
43  plot(t,Cend);
44  grid on;
45  title('Concentration vs. Time')
46  axis([min(t) max(t) 0 C0]);
47  xlabel('Concentration [nM]');ylabel('Time [hrs]');
```

Appendix B

Materials and Methods

B.1 Cell Culture

HUVEC cells (ATCC) were cultured on 0.1% gelatin in EBM-2 (Lonza) supplemented with bullet kit (Lonza) and 0.1% antibiotic/antimycotic (A/A) (Life Technologies). Human primary Blood and Lymph endothelial cells, collected from plasma, were cultured on collagen (1:60) in MCDB 131 supplemented with 5% MVGS (Life Technologies), 1% L-alanyl-L-glutamine (Life Technologies), and 1% A/A. MDA-MB-231 (ATCC), MDA-MB-435 (ATCC), MCF-7 (ATCC), 4306, 4412, LLC, and B16 cells were cultured in DMEM supplemented with 10% FBS and 1% A/A. MDA-MB-468 cells were cultured in DMEM supplemented with 5% FBS and 1% A/A. SKBR3 (ATCC) were cultured in McCoys 5A (Life Technologies) supplemented with 15% FBS and 1% A/A. SKOV3 and HT29 cells were cultured in McCoys 5A supplemented with 10% FBS and 1% A/A. PC3, PC3M, PC3LN4, AT2.1, AT3.1, AT6.1, and 4T1 cells were cultured in RPMI supplemented with 10% FBS and 1% A/A. HMEC (Life Technologies) and MCF10a cells were cultured in MEBM (Lonza) supplemented with MEGM bullet kit (Lonza) and 1% A/A.

B.2 MicroRNA Labeling & Transfection

The Cy-3 labeled control miRNA was purchased from Life Technologies. miRNA-132 (Life Technologies) and α-miRNA-132 (Life Technologies) were labeled using Label IT miRNA Labeling Kit (Mirus) according to manufacturers protocol. Cells were transfected with Control microRNA (Life Technologies), miRNA-132 (Life Technologies), and α-miRNA-132 (Life Technologies). The microRNAs were transfected with siPORT NeoFX transfection reagent (Life Technologies) at a concentration of 50nM and 1x Opti-MEM I (Life Technologies). All transfections were completed according to manufacturers protocols for 24 hours.

B.3 Pharmacological Inhibition

Cells were incubated with a combination of cytoskeletal pharmacological inhibitors Latrunculin A (Sigma) or, Cytochalasin D (Sigma), and Docetaxal (Sigma) in complete media for 24hrs post 6-18hrs of serum deprivation.

B.4 Co-Culture Protocol

1. Appropriately coat well with Matrigel® is diluted with COLD sterile PBS – 50% Matrigel®; 50% PBS for 3D samples or gelatin for 2D samples

2. After 30 minutes of incubation at 37°C, for 2D samples, remove gelatin before adding endothelial cells, and the cells are ready to plate for 3D samples

3. Incubate endothelial cells with DiL-Ac-LDL reagent (1:100) (Life Technologies) in complete media for 1hr

4. Plate the endothelial cells in their respective media, and incubate the HUVEC and primary human dermal microvascular blood endothelial cells for 4-6 hours, or the primary human dermal microvascular lymph endothelial cells for 24 hours

5. Load epithelial cells with GFP, CellTrace CFSE (Life Technologies), Qtracker (Life Technologies), LysoTracker (Live Technologies), or MicroRNAs (Life Technologies) according to manufacturers specifications

6. Add stained epithelial cells to preformed vessels in their respective media, and incubate for 24-96 hours before further analysis

Matrigel per well:

1. 12 well - 400μL

2. 24 well 250μL

3. 12 well Dual chamber - 400μL bottom chamber, 118μL top chamber

Total Volume of Media per well:

1. 12 well - 2ml total volume

2. 24 well 1ml total volume

3. 12 well Dual chamber - 1.5mL bottom chamber, 0.5mL top chamber

Cells to add per well:

1. 2D: MDA-MDA/MDA-HUVEC add 150,000 cells/well (Of each type: Total number of cells = 300,000) in a 12 well plate

2. MDA-MDA/MDA-HUVEC add 75,000 cells/well (Of each type: Total Number of cells = 150,000) in a 24 well plate

3. 3D: MDA-MDA add 200,000 cells/well (Of each type: Total number of cells = 400,000) in a 12 well plate

4. MDA-HUVEC add 200,000 cells/well (Of each type: Total number of cells = 400,000) in a 12 well plate

5. MDA-BLOOD add 275,000 cells/well (Of each type: Total number of cells = 550,000) in a 12 well plate

6. MDA-LYMPH add 275,000 cells/well (Of each type: Total number of cells = 550,000) in a 12 well plate

7. MDA-MDA add 200,000 cells/well (Of each type: Total number of cells = 400,000) in a 24 well plate

8. MDA-HUVEC add 100,000 cells/well (Of each type: Total number of cells = 200,000) in a 24 well plate

B.5 Flow Cytommetry Sample Collection and Analysis

1. Incubate samples in trypsin EDTA (10x) (Sigma) for 20min at 37°C. Collect the samples, and incubate the remaining samples in the well again in trypsin EDTA (10x) (Sigma) for 20 minutes at 37°C.

2. Collect the remaining samples, and centrifuge for 15 minutes at 450rcf

3. Remove supernatant, and fix the diffuse pellet in 1mL of 4% Para-formaldehyde (PFA) for 20 minutes

4. Centrifuge samples after fixation for 15 minutes at 450rcf, and resuspend in 100μL staining buffer (0.1% Sodium Azide (Sigma), 5% FBS, 1% BSA (Sigma) in PBS)

5. Stain samples with one or more of the following antibodies: Rb pAB to CD31 (abcam, ab28364), Purified Mouse Anti-Human CD141 (BD Bioscience, 559780), Monoclonal Anti-human LYVE-1-APC (R&D Systems, FAB20892A), CD137 (abcam, ab3169), CD276 (abcam, ab89133), p120RasGAP (Santa Cruz Biotechnology, sc-63), or pAKT (Cell Signaling, 4051s).

6. Once samples are analyzed, use Cflow Plus (or Flowjo) software to plot double+ve endothelial cells, and check for the presence of CFSE, Qtracker, LysoTracker, or miRNAs.

B.6 In Vivo Studies

1. Drug treat MDA-MB-231 cells
2. Stain cells with CFSE per manufacturer's protocols
3. Inject cells into CD1 Nude Mice through tail vein injection
4. Sacrifice mice at 18hrs, 24hrs, 48hrs, or 72hrs.
5. Harvest lungs, and store or add magnetic CD31 beads for endothelial cell isolation
6. Stain samples with CD 137 or CD 276, and sort using a BD FACS Aria IIu SORP

B.7 Immunocytochemistry (ICC) Protocol

1. Remove about half the volume of excess media (siphon out using vacuum if it is a 2D sample or use Kim wipes to remove excess media by capillary action if it is a 3D sample)
2. Add 4% PFA (diluted in PBS) to the samples, and incubate at room temperature for 15 minutes.
3. Remove PFA, and wash once for 5 min in PBS.
4. Add 1mg/ml $NaBH_4$ (dissolved in PBS) to the samples, and incubate at room temperature for 10 min.
5. Remove $NaBH_4$, and wash once in PBS for 5 min.
6. Add buffer A (0.1% Tween + 0.1% Triton in PBS) and incubate at room temperature for 10 minutes.
7. Remove buffer A, and wash twice in PBS for 5 minutes each.

8. Add buffer B (1% BSA + 0.5% Sodium Azide (g/ml) in PBS) and incubate at room temperature for 1 hour.

9. Remove buffer B, and wash twice in PBS for 5 minutes each.

10. Add 200μL primary antibody (per well in a 24 well plate) (diluted in buffer B) and incubate overnight at 4°C, or at room temperature for 3 hours.

11. Remove primary antibody, and wash thrice in PBS for 5 minutes each.

12. Add secondary antibody (diluted in buffer B) and incubate at room temperature for 1 hour.

13. Remove secondary antibody, and wash thrice in PBS for 5 minutes each.

14. Add 200μL phalloidin to each well (1:100 dilution in PBS i.e. 1μL in 100μL PBS), and incubate at room temperature for one hour.

15. Remove phalloidin, and wash twice with PBS, for 5 min each.

16. Counterstain with DAPI (1:10000 in PBS i.e. 1μL in 10mL PBS) for 3 minutes at room temperature.

17. Remove DAPI and wash thrice in PBS for 5 minutes each.

18. Mount the coverslips with a drop of antifade onto slides.

Cells were stained with on or more of the following: rhodamine phalloidin (Life Technologies, R415), Alexa-fluor 647 phalloidin (Life Technologies, A22287), α/β Tubulin antibody (Cell Signaling, 2148s), Myosin (Life Technologies, 3402S), Wheat Germ Agglutinin (WGA)-CF405S conjugate (Biotium, 29027-1), Alexa Fluor 647 Conjugate WGA (Life Technologies, W32466).

B.8 Immunohistochemistry (IHC) Protocol

B.8.1 Deparaffinization

1. Place the slides on a slide rack in the staining vials.
2. Wash slides with 100% Xylene 2x3 minutes
3. Wash slides with 1:1 100% Xylene: 100% EtOH for 3 minutes
4. Wash slides with 100% EtOH 2x3 minutes
5. Wash slides with 95% EtOH for 3 minutes diluted in distilled water
6. Wash slides with 70% EtOH for 3 minutes
7. Wash slides with 50% EtOH for 3 minutes
8. Wash slides with running cold tap water to rinse sections. Keep slides in running water to prevent sections from drying out until antigen retrieval can be performed

B.8.2 Quench Aldehydes with $NaBH_4$

1. Wash slides in FRESH $NaBH_4$. Dissolve 1 mg/mL $NaBH_4$ in TBS. While the solution is still fizzing, submerge the slides. *Note* Take $NaBH_4$ from bottom of bottle. Fill bottle with Argon and store in dessicator until needed.
2. Wash 3 times for 10 minutes each

B.8.3 Antigen Retrieval

1. Make Sodium Citrate Buffer (10 mM sodium citrate, 0.05% Tween 20, pH 6.0): 2.94 g Tri-sodium citrate (dihydrate), 1 L distilled water, Mix to dissolve. Adjust pH to 6.0 with 1N HCl, add 0.5 mL Tween 20 and mix. Store at 4°C until needed.

2. Put slides in glass plate holders and fill with citrate buffer until samples are submerged

3. Heat the buffer to 100°C for 30 minutes in the fume hood. Let slides cool for 20 minutes at room temperature, otherwise the samples will come off the slides!

B.8.4 Antibody Staining

Day 1:

1. Make 10x TBS Recipe: 24g Tris Base, 88g NaCl, 900 mL dH20, Adjust pH to 7.6 with 12N HCl, bring final volume to 1L with distilled water

2. Wash slides 2x5minutes in TBS plus 0.025% Triton X-100 with gentle agitation

3. Block slides with 10% FBS and 1% BSA in 1x TBS for 2 hours at room temperature

4. Drain slides for a few seconds (do not rinse) and wipe around the sections with tissue paper

5. Apply primary antibodies (1:50 Rabbit anti-human CD31, 1:300 Von Willebrand Factor) in 1x TBS with 1% BSA. Incubate overnight at 4C

Day 2:

1. Rinse slides 2x5 minutes in TBS plus 0.025% Triton X-100 with gentle agitation

2. Apply secondary antibody (Alexa Fluor 568 anti-rabbit) at 1:1000 dilution in TBS plus 1% BSA for one hour at room temperature.

3. Wash slides 3 times for 5 minutes in TBS plus 0.025% Triton X-100

4. Incubate slides for 10 minutes in 1:100,000 DAPI diluted in TBS

5. Wash slides 2 times for 5 minutes in 1x HBSS
6. Incubate slides 10 minutes in 1:200 Alexa Fluor 647 Conjugate WGA diluted in HBSS
7. Wash slides 2 times for 5 minutes in 1x HBSS
8. Check slides under microscope to verify staining!
9. Apply cover slip over sample with mounting medium. Let dry for a few days at room temperature covered from light.

B.9 Scanning Electron Microscopy (SEM)

B.9.1 Sample Preparation Protocol

1. Make 2X Sodium cacodylate buffer: 0.2 M sodium cacodylate, 4% gluteraldehyde, 3% PFA, 10% Sucrose
2. Make 2X osmium tetroxide in aqueous buffer: 2% osmium tetroxide in diH20
3. Mix both 2X sodium cacodylate buffer and 2X osmium tetroxide right before use to get final working buffer.
4. Fix sample for 2 hours in SEM fixative, and change fixative at least 2-3 times, or when it turns dark brown-black.
5. Wash once for 5 minutes with sodium cacodylate solution.
6. Successively incubate at room temperature in the following ethanol solutions: 50%, 70%, 85%, 90%, 95%, and 100% for 5-10 minutes each.
7. Wash with 100% ethanol for 10 minutes again.
8. Store in 100% ethanol until ready. Sample can be kept in ethanol overnight if plate is sealed with Para film. If kept overnight, replace with fresh ethanol prior to critical point drying.

9. Bring to facility for critical point drying (Autosamdri 815 critical point dryer) and sputter coating (Cressington 208HR sputter coating with Au or Pt/Pd).

B.9.2 SEM Quantification

1. Imaging was done on a Jeol 5600LV SEM, Zeiss EVO SEM, or Zeiss FESEM Ultra55 microscope.

2. For each image count: total number of cancer cells, cancer cells with nCs, cancer cells without nCs, total number of nCs, total number of epi-epi nCs, epi-endo nCs, number of cells forming epi-epi nCs, epi-endo nCs, and number of cells positive for both epi-epi and epi-endo nCs.

3. Measure the length and width of the nCs using the CarlZeiss TIF annotation editor. Measure the width at 3 different positions across the length of the nCs and calculate the average width.

B.10 Cell Viability

MTS (3-(4,5-dimethylthiazol-2-yl)-5-(3-carboxymethoxyphenyl)-2-(4-sulfophenyl)-2H-tetrazolium) Assays: MDA-MB-231 cells were plated in a 96 well plate, and drug treated for 24 hours. MTS reagent (Life Technologies) was added to the sample and the plate was analyzed using a BioTek Epoch Microplate Spectrophotometer. Drug treated MDA-MB-231 cells were treated with Alexa Fluor 488 Annexin V (Life Technologies), incubated with endothelial cells, and imaged after 24hrs. The fluorescence of each image was measured and compared between the treatment groups.

B.11 PCR

B.11.1 Primer Design

p120RasGAP and GAPDH primers (IDT) were designed using mRNA reference sequences from NCBI database and Life Technologies OligoPerfect Designer software. Primer specificity was analyzed using NCBI PrimerBLAST. Primer self-dimerization and hetero-dimerization were analyzed using IDT OligoAnalyzer per iQ SYBR Green Supermix (Biorad) PCR assay experimental conditions. GAPDH Forward: 5 AGTCAGCCGCATCTTCTTTT 3 GAPDH Reverse: 5 GAGGTCAATGAAGGGGTCAT 3 p120RasGAP Forward: 5 TAACAGCATTGGGGACATCA 3 p120RasGAP Reverse: 5 TTGCCATCCACTGTGTCATT 3 SYBR Green PCR Assay: Co-cultured cells were sorted using BD FACS Aria IIu SORP. After total RNA extraction and quantification, cDNA was created using iScriptTM cDNA Synthesis Kit (Bio-Rad) per manufacturers protocol. Real-time PCR was performed on MyiQ Real time PCR Detection System (Bio-Rad) using iQ SYBR Green Supermix (Bio-Rad) per manufacturers protocol for p120RasGAP and GAPDH primers.

B.11.2 miRNA PCR Assay

Co-cultured cells were sorted using BD FACS Aria IIu SORP. miRNAs were extracted from mono-cultured and sorted cells using the mirVana miRNA isolation kit (Life Technologies) per the manufacturers protocol, and quantified using the Take3 Micro-Volume plate (BioTek). cDNA was created using the Taqman miRNA Reverse Transcription kit (Life Technologies) per manufacturers protocol for RNU44 and hsa-mir-132 Reverse Transcription primers. PCR was performed using Taqman Universal PCR Master Mix II, no UNG (Life Technologies) and Taqman Small RNA Assay (Life Technologies) for RNU44 and hsa-mir-132 on MyiQ Real-Time PCR Detection System (BioRad).

B.12 Transmission Electron Microscopy

Cells were fixed in 2.5% gluteraldehyde, 3% paraformaldehyde with 5% sucrose in 0.1M sodium cacodylate buffer (pH 7.4), pelletted, and post fixed in 1% OsO_4 in veronal-acetate buffer. The cell pellet was stained in block overnight with 0.5% uranyl acetate in veronal-acetate buffer (pH 6.0), then dehydrated and embedded in Embed-812 resin. Sections were cut on a Reichert Ultracut E microtome with a Diatome diamond knife at a thickness of 50 nm, stained with uranyl acetate, and lead citrate. The sections were examined using an FEI Tecnai spirit at 80KV and photographed with an AMT CCD camera.

B.13 Imaging

Fluorescence imaging was performed on a Nikon Eclipse Ti camera (Nikon Instruments) with NIS Elements Imaging Software (3.10) using Plan Apo 40X/0.95 air (∞/0.11-0.23, WD 0.25-0.17) DIC , Plan Apo 20X/0.75 air objective lenses (Nikon). The system has the capacity to do Z-stack images that can be processed using deconvolution software to generate 3D reconstruction images. Confocal fluorescence imaging was done on a PerkinElmer Ultraview Spinning Disk Confocal Microscope with Velocity acquisition software and Hammamatsu ORCA-ER CCD camera using Plan Apo 100X/1.4 oil DIC (∞/0.17) and Plan Apo 63X/1.4 oil DIC (∞/0.17) objective lenses (Zeiss). Contrast and brightness parameter adjustments were applied across the whole image or equally across all the comparison groups when necessary.

B.14 Quantification

Fluorescent Imaging: Used NIS Elements Software: Quantification of angiogenic parameters and endothelial-epithelial cell interaction was conducted using images taken at 4x magnification. For each frame, one brightfield and one FITC image was

captured for quantification.

B.14.1 Angiogenic Parameters

1. Nodes were first identified A node is classified as the intersection of 2 or more vessel structures.

2. The area of all nodes in the image were measured using either the circular or ellipse measurement tool for the circular nodes or the semi-axis measurement, respectively.

3. Tube lengths were measured as a vessel between the circumferences of two nodes.

4. If only part of the tube is captured in an image, the length of the tube is measured between the circumference of the node of origin and the end of the tube as seen in the image. Tubes shorter than 100μm in length that extend outside the image are not quantified as they will be covered in a different image.

5. The widths of the tubes were measured by taking three measurements along each vessel, making sure the measurements captured the heterogeneity in size.

B.14.2 Interaction Index

1. Using the brightfield image, a Region of Interest (ROI) is drawn, enclosing the network (all nodes and vessels). When drawing an ROI around the network, any cells that were in contact with the network, or laying directly on the network, are included in the ROI. If a cell was found adjacent to the ROI, but not in direct contact with the node or vessel it was excluded from the ROI.

2. Using the ROI feature, 3 small rectangular ROIs were drawn in regions with no cells.

3. All 4 ROIs were copied to the respective FITC image and the background fluorescence was removed by subtracting the maximum fluorescent intensity of the three rectangular ROIs from the total intensity of the image.

4. The sum intensity of the ROI enclosing the network is noted as the intensity of the cells that are ON the networks. Fluorescence intensity was assumed to be an estimate of cell number as the average intensity of each cell is assumed to be the same.

B.14.3 Elongation

1. Images of fixed and stained cells (rhodamine phalloidin, CFSE and DAPI) in co-culture were captured at a higher magnification (20x and 40x) to measure individual cells.

2. 300 cells on the vessels and 100 cells off the vessels were measured using the semi-axis feature.

3. The ratio of major axis to minor axis of the on cells was compared to the average major/minor axis ratio of the off cells.

B.14.4 Drug Study Quantification

B.14.4.1 Fluorescent Imaging

Fluorescent imaging was performed on a Nikon eclipse Ti camera using NIS Elements Imaging Software (3.10) using 20X objective lens to capture a minimum of 300 cells from 5 replicate co-culture samples for each group (Control, Lat-A+Doce and Cyto-D+Doce). Lengths of the complete and broken nCs were measured using the same software.

B.14.4.2 SEM

SEM imaging was done using Zeiss FESEM Ultra55 microscope for 3D co-cultured cells (n=104) and using Nikon eclipse Ti camera using NIS Elements Imaging Software (3.10) for the Fluorescence nanoChannels (n=63) and other projections (n=72) to capture nanoChannels. Length and width of the nanoChannels was measured using the CarlZeiss TIF annotation editor. Width was measured at 3 different positions across the length of the nanoChannels and average width was calculated for the comparison of length and width of the groups. Quantification imaging was done using Zeiss FESEM Ultra55 microscope in the magnification range 1.75KX to 2.25KX to capture minimum 300 cells from 6 replicate co-culture samples for each cell line. For each image the total number of cancer cells, number of cancer cells with nanoChannels, number of cancer cells without nanoChannels, total number of nanoChannels, number of epi-epi nanoChannels, number of epi-endo nanoChannels, number of cells forming epi-epi nanoChannels, number of cells forming epi-endo nanoChannels and number of cells positive for both epi-epi and epi-endo nanoChannels were counted. Average number of total nanoChannels, epi-epi nanoChannels and epi-endo nanoChannels per cell were calculated.

B.15 Migration

3 drug treatment groups were plated to examine migration, invasion, and intravasation:

1. Control
2. Lat A/Doce
3. Cyto D/Doce

B.15.1 Protocol

1. Plate 300,000 HUVEC cells into the bottom well of a 24 well plate

2. Next, plate matrigel® diluted 1:4 in cold PBS in the top chambers for invasion and intravasation.

3. In the top chambers of the wells examining intravasation, plate 100,000 HUVEC cells for 24 hours prior to plating the MDA-MB-231 cells.

4. Once the HUVECs have formed a monolayer beneath the matrigel, add 300,000 of the MDA-MB-231 cells to the top chamber of each well. (3 replicates per condition).

5. After 48-72 hours of incubation, fix the cells in the top chamber with 4% PFA.

6. Once fixed, use a Q-tip to clean out all contents from the inside of the chamber, and place the top chambers in DAPI for 5 minutes to stain the cells that have migrated to the bottom of the chamber.

7. Image each chamber, at 4x magnification, taking 26-27 images per well (this should be enough to cover the entire chamber), making sure to focus on the underside of the chambe, where the migrated cells lay.

B.16 Endothelial Cell Isolation

B.16.1 Bead Preparation

1. Prepare beads the day before isolation: Sheep anti rat beads (Invitrogen #110.35) with Rat anti mouse CD31 (Pharmigen #55337 0.5mg/mL).

2. Wash Beads beadwash: PBS+ antibiotic/antimycotic (1:100) + 0.1% BSA(1.66mL/500mL) (Sigma A9576-50ml).

3. Place on rotator overnight at 4°C (or 1 hour at room temperature).

4. Prepare Collagenase: Type I (Worthington #4197) 0.2g% in DPBS +Ca/Mg, mix at 37°C for 1 hour and then filter (0.22 micron).

5. Coat 4 plates with gelatin (0.1%) for 30 minutes at 37°C.

6. Harvest tissue into 25 mLs of DMEM+ pen/strep (1%) and keep on ice.

7. Pour off media into waste and rinse tissue in tube 2X with DPBS.

8. Pour tissue into sterile dish with a little of the DPBS (Tip: if extra blood clots, cut lungs in half and rinse again, also press on lung to expel any blood).

9. Dissect off all extra tissue (Tip: tissue to be removed appears lighter in color), then transfer to clean dish.

10. Remove all extra liquid and mince tissue with scissors until the consistency of pate or garlic (Tip: wipe off scissors before mincing step. There will be small chunks and this ok, take approx 1 minute.)

11. Add 10 mLs of collagenase to plate, mix with 5 mL pipet and transfer to new 50 ml tube; wash the plate with another 10 mLs and pool. (Tip: If more than 4 hearts use 25 mL of collagenase) Parafilm cap in place.

12. Place in hybridization oven at 37°C for 30 minutes with slow revolution or on rocker. (Tip: After 30 minutes check, if clumps dont appear to be feathered incubate another 5 minutes but no longer).

B.16.2 Endothelial Separation

1. Pipet tissue and collagenase up and down 15 times with 20 or 30 mL syringe and 14 G cannula (Tip: do not create extra bubbles).

2. Drip over cell strainer into BD tube (Tip: drip slowly to prevent liquid block).

3. Rinse tube and filter with DPBS into BD tube.

4. Spin at 800 rpm for 8 minutes (Tip: no faster as high speed spin damages cells).

5. Place tube in magnet, wait 1-2 minutes, remove liquid with 1mL pipet.

6. Add 850mL fresh beadwash, mix and transfer to sterile tube and place in magnet.

7. Repeat 5 times, the last time resuspend pellet in 100μL in sterile eppendorf tube. These can be stored up to 2 weeks at 4°C. (Tip: if you leave beads in magnet too long they become difficult to resuspend).

8. Remove supernatant from tissue pellet with pipet (not vacuum) as much as easily removable. Gently resuspend in remaining volume.

9. Add 2 mLs bead wash to pellet, resuspend using 5ml pipet and transfer to polystyrene tube (Falcon 2058, 12X75 sterile snap caps). (Tip: DO NOT transfer any white clumps so use 5ml pipet horizontally and watch carefully, dumping any clumps back into the original tube.)

10. Rinse original tube with 1mL beadwash and pool, again watching carefully for any clumps of tissue.

11. Add beads: (Tip: fine line between enough and too many beads).

12. Cap and parafilm tube and place on rotator for 15 minutes at room temperature.

13. Put tube into magnet (Tip: remove parafilm and cap first) leave for 2 minutes.

14. Do not remove the tube from magnet. Remove supernatant and save in sterile tube (just in case) (Tip: keep pipet to front of tube away from the beads).

15. Pull tube out of magnet and add 3 mLs of bead wash, vigorously mix 4-5 times with 5 mL pipet (Tip: do not cause foaming of BSA).

16. Return to magnet, and wait for 2 minutes. Remove media with vacuum and add 3 mLs fresh bead wash and mix vigorously (outside of magnet).

17. Return to magnet and repeat 6-8 times, waiting 2 minutes between or alternating tubes so that the magnet has time to work.

18. Let sit in magnet for 1 minute.

19. Once endothelial cells are separated, resuspend cells for FACS analysis

Bibliography

[1] S. Kumar and V. M. Weaver, "Mechanics, malignancy, and metastasis: the force journey of a tumor cell," *Cancer Metastasis Reviews*, vol. 28, pp. 113–127, June 2009.

[2] A. Rustom, R. Saffrich, I. Markovic, P. Walther, and H. H. Gerdes, "Nanotubular highways for intercellular organelle transport," *Science*, vol. 303, pp. 1007–1010, February 2004.

[3] H. H. Gerdes and R. N. Carvalho, "Intercellular transfer mediated by tunneling nanotubes," *Current Opinion in Cell Biology*, vol. 20, pp. 470–475, August 2008.

[4] E. M. Kramer, N. L. Frazer, and T. I. Baskin, "Measurement of diffusion within the cell wall in living roots of Arabidopsis thaliana," *Journal of Experimental Botany*, vol. 58, pp. 3005–15, August 2007.

[5] R. Phillips, J. Kondev, and J. Theriot, *A Physical Biology of the Cell*. Garland Science, 2009.

[6] V. P. Zhdanov, "Conditions of appreciable influence of microRNA on a large number of target mRNAs," *Molecular BioSystems*, vol. 5, pp. 638–643, June 2009.

[7] C. L. Chaffer and R. A. Weinberg, "A Perspective on Cancer Cell Metastasis," *Science*, vol. 331, pp. 1559–1564, March 2011.

[8] P. S. Steeg, "Tumor metastasis: mechanistic insights and clinical challenges," *Nature Medicine*, vol. 12, pp. 895–904, August 2006.

[9] G. P. Gupta and J. Massagu, "Cancer Metastasis: Building a Framework," *Cell*, vol. 127, pp. 679–695, November 2006.

[10] N. Howlader, A. Noone, M. Krapcho, N. Neyman, R. Aminou, W. Waldron, S. Altekruse, C. Kosary, J. Ruhl, Z. Tatalovich, H. Cho, A. Mariotto, M. Eisner, D. Lewis, H. Chen, E. Feuer, K. Cronin, and B. Edwards, "SEER Cancer Statistics Review, 1975-2008, National Cancer Institute. based on November 2010 SEER data submission, posted to the SEER web site, `http://seer.cancer.gov/csr/1975_2008/`," 2011.

[11] S. C. Morgan and C. C. Parker, "Local treatment of metastatic cancer - killing the seed or disturbing the soil?," *Nat Rev Clin Oncol*, vol. 8, pp. 504–506, June 2011.

[12] A. Schroeder, D. A. Heller, M. M. Winslow, J. E. Dahlman, G. W. Pratt, R. Langer, T. Jacks, and D. G. Anderson, "Treating metastatic cancer with nanotechnology," *Nat Rev Cancer*, vol. 12, pp. 39–50, January 2012.

[13] D. Hanahan and R. A. Weinberg, "The Hallmarks of Cancer," *Cell*, vol. 100, pp. 57–70, January 2000.

[14] D. Hanahan and R. A. Weinberg, "Hallmarks of Cancer: The Next Generation," *Cell*, vol. 144, pp. 646–674, March 2011.

[15] D. Wirtz, K. Konstantopoulos, and P. C. Searson, "The physics of cancer: the role of physical interactions and mechanical forces in metastasis," *Nat Rev Cancer*, vol. 11, pp. 512–522, July 2011.

[16] J. Debnath and J. S. Brugge, "Modelling glandular epithelial cancers in three-dimensional cultures," *Nat Rev Cancer*, vol. 5, pp. 675–688, September 2005.

[17] C. Hebner, V. M. Weaver, and J. Debnath, "Modeling Morphogenesis and Oncogenesis in Three-Dimensional Breast Epithelial Cultures," *Annual Review of Pathology: Mechanisms of Disease*, vol. 3, pp. 313–339, February 2008.

[18] K. L. Schmeichel and M. J. Bissell, "Modeling tissue-specific signaling and organ function in three dimensions," *Journal of Cell Science*, vol. 116, pp. 2377–2388, June 2003.

[19] A. C. Society, "The History of Cancer. Accessed at `http://www.cancer.org/acs/groups/cid/documents/webcontent/002048-pdf.pdfonMay1,2013`," June 2012.

[20] P. Friedl and S. Alexander, "Cancer invasion and the microenvironment: plasticity and reciprocity," *Cell*, vol. 147, pp. 992–1009, November 2011.

[21] O. Warburg, "On the origin of cancer cells," *Science*, vol. 123, pp. 309–314, February 1956.

[22] S. G. Baker and B. S. Kramer, "Paradoxes in carcinogenesis: new opportunities for research directions," *BMC cancer*, vol. 7, p. 151, August 2007.

[23] C. Sonnenschein and A. M. Soto, "Theories of carcinogenesis: an emerging perspective," *Seminars in cancer biology*, vol. 18, pp. 372–377, October 2008.

[24] A. M. Soto and C. Sonnenschein, "The somatic mutation theory of cancer: growing problems with the paradigm?," *BioEssays : news and reviews in molecular, cellular and developmental biology*, vol. 26, pp. 1097–1107, October 2004.

[25] T. N. Seyfried and L. M. Shelton, "Cancer as a metabolic disease," *Nutrition and Metabolism*, vol. 7, p. 7, January 2010.

[26] C. Sonnenschein and A. M. Soto, "Somatic mutation theory of carcinogenesis: why it should be dropped and replaced," *Molecular Carcinogenesis*, vol. 29, pp. 205–211, December 2000.

[27] S. A. Frank, *Dynamics of cancer: incidence, inheritance, and evolution*. Princeton, N.J.: Princeton University Press, 2007.

[28] H. J. Curtis, "Formal discussion of: somatic mutations and carcinogenesis," *Cancer Research*, vol. 25, pp. 1305–1308, September 1965.

[29] L. Foulds, "The experimental study of tumor progression: a review," *Cancer Research*, vol. 14, pp. 327–339, June 1954.

[30] H. Zhang, B. S. Herbert, K. H. Pan, J. W. Shay, and S. N. Cohen, "Disparate effects of telomere attrition on gene expression during replicative senescence of human mammary epithelial cells cultured under different conditions," *Oncogene*, vol. 23, pp. 6193–6198, August 2004.

[31] J. F. Passos, G. Saretzki, and T. von Zglinicki, "DNA damage in telomeres and mitochondria during cellular senescence: is there a connection?," *Nucleic Acids Research*, vol. 35, pp. 7505–7513, December 2007.

[32] K. Chin, C. O. de Solorzano, D. Knowles, A. Jones, W. Chou, E. G. Rodriguez, W. L. Kuo, B. M. Ljung, K. Chew, K. Myambo, M. Miranda, S. Krig, J. Garbe, M. Stampfer, P. Yaswen, J. W. Gray, and S. J. Lockett, "In situ analyses of genome instability in breast cancer," *Nature Genetics*, vol. 36, pp. 984–988, September 2004.

[33] P. Fedi, A. Kimmelman, and S. A. Aaronson, *Growth Factor Signal Transduction in Cancer*. Hamilton (ON): BC Decker, 2000.

[34] N. Cheng, A. Chytil, Y. Shyr, A. Joly, and H. L. Moses, "Transforming growth factor-beta signaling-deficient fibroblasts enhance hepatocyte growth factor signaling in mammary carcinoma cells to promote scattering and invasion," *Molecular Cancer Research*, vol. 6, pp. 1521–1533, October 2008.

[35] P. P. DiFiore, J. H. Pierce, M. H. Kraus, O. Segatto, C. R. King, and S. A. Aaronson, "erbB-2 is a potent oncogene when overexpressed in NIH/3T3 cells," *Science*, vol. 237, pp. 178–182, July 1987.

[36] J. T. Zilfou and S. W. Lowe, "Tumor Suppressive Functions of p53," *Cold Spring Harbor Perspectives in Biology*, vol. 1, pp. a001883–a001883, November 2009.

[37] D. Menendez, A. Inga, and M. A. Resnick, "The expanding universe of p53 targets," *Nature Reviews. Cancer*, vol. 9, pp. 724–737, October 2009.

[38] J. M. Adams and S. Cory, "The Bcl-2 apoptotic switch in cancer development and therapy," *Oncogene*, vol. 26, pp. 1324–1337, February 2007.

[39] R. Mathew, V. Karantza-Wadsworth, and E. White, "Role of autophagy in cancer," *Nature Reviews. Cancer*, vol. 7, pp. 961–967, December 2007.

[40] A. Apel, H. Zentgraf, M. W. Buchler, and I. Herr, "Autophagy-A double-edged sword in oncology," *International Journal of Cancer*, vol. 125, pp. 991–995, September 2009.

[41] J. Folkman, "Tumor angiogenesis: therapeutic implications," *The New England Journal of Medicine*, vol. 285, pp. 1182–1186, November 1971.

[42] G. Bergers and L. E. Benjamin, "Tumorigenesis and the angiogenic switch," *Nature Reviews. Cancer*, vol. 3, pp. 401–410, June 2003.

[43] D. Hanahan and J. Folkman, "Patterns and emerging mechanisms of the angiogenic switch during tumorigenesis," *Cell*, vol. 86, pp. 353–364, August 1996.

[44] B. R. Zetter, "Angiogenesis and tumor metastasis," *Annual Review of Medicine*, vol. 49, pp. 407–424, February 1998.

[45] Y. Shing, J. Folkman, R. Sullivan, C. Butterfield, J. Murray, and M. Klagsbrun, "Heparin affinity: purification of a tumor-derived capillary endothelial cell growth factor," *Science*, vol. 223, pp. 1296–1299, March 1984.

[46] H. F. Dvorak, N. S. Orenstein, A. C. Carvalho, W. H. Churchill, A. M. Dvorak, S. J. Galli, J. Feder, A. M. Bitzer, J. Rypysc, and P. Giovinco, "Induction of a fibrin-gel investment: an early event in line 10 hepatocarcinoma growth mediated by tumor-secreted products," *Journal of Immunology*, vol. 122, pp. 166–174, January 1979.

[47] D. R. Senger, S. J. Galli, A. M. Dvorak, C. A. Perruzzi, V. S. Harvey, and H. F. Dvorak, "Tumor cells secrete a vascular permeability factor that promotes accumulation of ascites fluid," *Science*, vol. 219, pp. 983–985, February 1983.

[48] J. A. Nagy, A. M. Dvorak, and H. F. Dvorak, "VEGF-A and the induction of pathological angiogenesis," *Annual review of pathology*, vol. 2, pp. 251–275, October 2007.

[49] A. K. Olsson, A. Dimberg, J. Kreuger, and L. Claesson-Welsh, "VEGF receptor signalling - in control of vascular function," *Nature Reviews. Molecular Cell Biology*, vol. 7, pp. 359–371, May 2006.

[50] V. Baeriswyl and G. Christofori, "The angiogenic switch in carcinogenesis," *Seminars in Cancer Biology*, vol. 19, pp. 329–337, October 2009.

[51] J. Folkman, "Angiogenesis and apoptosis," *Seminars in cancer biology*, vol. 13, pp. 159–167, April 2003.

[52] R. K. Jain, "Normalization of tumor vasculature: an emerging concept in antiangiogenic therapy," *Science*, vol. 307, pp. 58–62, January 2005.

[53] J. Folkman, "Angiogenesis," *Annual Review of Medicine*, vol. 57, pp. 1–18, February 2006.

[54] J. S. Desgrosellier and D. A. Cheresh, "Integrins in cancer: biological implications and therapeutic opportunities," *Nature Reviews. Cancer*, vol. 10, pp. 9–22, January 2010.

[55] J. T. Parsons, A. R. Horwitz, and M. A. Schwartz, "Cell adhesion: integrating cytoskeletal dynamics and cellular tension," *Nature Reviews. Molecular Cell Biology*, vol. 11, pp. 633–643, September 2010.

[56] A. J. Ridley, H. F. Paterson, C. L. Johnston, D. Diekmann, and A. Hall, "The small GTP-binding protein rac regulates growth factor-induced membrane ruffling," *Cell*, vol. 70, pp. 401–410, August 1992.

[57] F. van Roy and G. Berx, "The cell-cell adhesion molecule E-cadherin," *Cellular and Molecular Life Sciences*, vol. 65, pp. 3756–3788, November 2008.

[58] T. Okada, M. Lopez-Lago, and F. G. Giancotti, "Merlin/NF-2 mediates contact inhibition of growth by suppressing recruitment of Rac to the plasma membrane," *The Journal of Cell Biology*, vol. 171, pp. 361–371, October 2005.

[59] M. Curto, B. K. Cole, D. Lallemand, C. H. Liu, and A. I. McClatchey, "Contact-dependent inhibition of EGFR signaling by Nf2/Merlin," *The Journal of Cell Biology*, vol. 177, pp. 893–903, June 2007.

[60] J. I. Partanen, A. I. Nieminen, and J. Klefstrom, "3D view to tumor suppression: Lkb1, polarity and the arrest of oncogenic c-Myc," *Cell Cycle*, vol. 8, pp. 716–724, March 2009.

[61] A. F. Hezel and N. Bardeesy, "LKB1; linking cell structure and tumor suppression," *Oncogene*, vol. 27, pp. 690–6919, September 2008.

[62] R. J. Shaw, "Tumor suppression by LKB1: SIK-ness prevents metastasis," *Science Signaling*, vol. 2, p. 55, September 2009.

[63] K. Polyak and R. A. Weinberg, "Transitions between epithelial and mesenchymal states: Acquisition of malignant and stem cell traits," *Nature Reviews. Cancer*, vol. 9, pp. 265–273, April 2009.

[64] R. Liu, X. Wang, G. Y. Chen, P. Dalerba, A. Gurney, T. Hoey, G. Sherlock, J. Lewicki, K. Shedden, and M. F. Clarke, "The prognostic role of a gene signature from tumorigenic breast-cancer cells," *The New England Journal of Medicine*, vol. 356, pp. 217–226, January 2007.

[65] N. Bloushtain-Qimron, J. Yao, E. L. Snyder, M. Shipitsin, L. L. Campbell, S. A. Mani, M. Hu, H. Chen, V. Ustyansky, J. E. Antosiewicz, P. Argani, M. K. Halushka, J. A. Thomson, P. Pharoah, A. Porgador, S. Sukumar, R. Parsons, A. L. Richardson, M. R. Stampfer, R. S. Gelman, T. Nikolskaya, Y. Nikolsky, and K. Polyak, "Cell type-specific DNA methylation patterns in the human breast," *Proceedings of the National Academy of Sciences of the United States of America*, vol. 105, pp. 14076–14081, September 2008.

[66] J. H. Taube, J. I. Herschkowitz, K. Komurov, A. Y. Zhou, S. Gupta, J. Yang, K. Hartwell, T. T. Onder, P. B. Gupta, K. W. Evans, B. G. Hollier, P. T. Ram, E. S. Lander, J. M. Rosen, R. A. Weinberg, and S. A. Mani, "Core epithelial-to-mesenchymal transition interactome gene-expression signature is associated with claudin-low and metaplastic breast cancer subtypes," *Proceedings of the National Academy of Sciences of the United States of America*, vol. 107, pp. 15449–15454, August 2010.

[67] M. Beltran, I. Puig, C. Pena, J. M. Garcia, A. B. Alvarez, R. Pena, F. Bonilla, and A. G. de Herreros, "A natural antisense transcript regulates Zeb2/Sip1 gene expression during Snail1-induced epithelial-mesenchymal transition," *Genes & Development*, vol. 22, pp. 756–769, March 2008.

[68] N. Dumont, M. B. Wilson, Y. G. Crawford, P. A. Reynolds, M. Sigaroudinia, and T. D. Tlsty, "Sustained induction of epithelial to mesenchymal transition activates DNA methylation of genes silenced in basal-like breast cancers," *Proceedings of the National Academy of Sciences of the United States of America*, vol. 105, pp. 14867–14872, September 2008.

[69] T. Brabletz, A. Jung, S. Reu, M. Porzner, F. Hlubek, L. A. Kunz-Schughart, R. Knuechel, and T. Kirchner, "Variable beta-catenin expression in colorectal cancers indicates tumor progression driven by the tumor environment," *Proceedings of the National Academy of Sciences of the United States of America*, vol. 98, pp. 10356–10361, August 2001.

[70] C. Franci, M. Takkunen, N. Dave, F. Alameda, S. Gomez, R. Rodriguez, M. Escriva, B. Montserrat-Sentis, T. Baro, M. Garrido, F. Bonilla, I. Virtanen, and A. G. de Herreros, "Expression of Snail protein in tumor-stroma interface," *Oncogene*, vol. 25, pp. 5134–5144, August 2006.

[71] C. C. Yates, C. R. Shepard, D. B. Stolz, and A. Wells, "Co-culturing human prostate carcinoma cells with hepatocytes leads to increased expression of E-cadherin," *British Journal of Cancer*, vol. 96, pp. 1246–1252, April 2007.

[72] P. Friedl and K. Wolf, "Tube travel: the role of proteases in individual and collective cancer cell invasion," *Cancer Research*, vol. 68, pp. 7247–7249, September 2008.

[73] J. Massague, "TGFB in Cancer," *Cell*, vol. 134, pp. 215–230, July 2008.

[74] B. Ozdamar, R. Bose, M. Barrios-Rodiles, H. R. Wang, Y. Zhang, and J. L. Wrana, "Regulation of the polarity protein Par6 by TGFbeta receptors controls epithelial cell plasticity," *Science*, vol. 307, pp. 1603–1609, March 2005.

[75] L. Yang, Y. Pang, and H. L. Moses, "TGF-beta and immune cells: an important regulatory axis in the tumor microenvironment and progression," *Trends in Immunology*, vol. 31, pp. 220–227, June 2010.

[76] S. A. Mani, W. Guo, M. J. Liao, E. N. Eaton, A. Ayyanan, A. Y. Zhou, M. Brooks, F. Reinhard, C. C. Zhang, M. Shipitsin, L. L. Campbell, K. Polyak, C. Brisken, J. Yang, and R. A. Weinberg, "The epithelial-mesenchymal transition generates cells with properties of stem cells," *Cell*, vol. 133, pp. 704–715, May 2008.

[77] A. P. Morel, M. Lievre, C. Thomas, G. Hinkal, S. Ansieau, and A. Puisieux, "Generation of breast cancer stem cells through epithelial-mesenchymal transition," *PloS one*, vol. 3, p. e2888, August 2008.

[78] C. Sheridan, H. Kishimoto, R. K. Fuchs, S. Mehrotra, P. Bhat-Nakshatri, C. H. Turner, R. G. Jr, S. Badve, and H. Nakshatri, "CD44+/CD24- breast cancer cells exhibit enhanced invasive properties: an early step necessary for metastasis," *Breast Cancer Research: BCR*, vol. 8, p. R59, October 2006.

[79] M. Shipitsin, L. L. Campbell, P. Argani, S. Weremowicz, N. Bloushtain-Qimron, J. Yao, T. Nikolskaya, T. Serebryiskaya, R. Beroukhim, M. Hu, M. K. Halushka, S. Sukumar, L. M. Parker, K. S. Anderson, L. N. Harris, J. E. Garber, A. L. Richardson, S. J. Schnitt, Y. Nikolsky, R. S. Gelman, and K. Polyak, "Molecular definition of breast tumor heterogeneity," *Cancer Cell*, vol. 11, pp. 259–273, March 2007.

[80] D. S. Micalizzi, S. M. Farabaugh, and H. L. Ford, "Epithelial-mesenchymal transition in cancer: parallels between normal development and tumor progression," *Journal of Mammary Gland Biology and Neoplasia*, vol. 15, pp. 117–134, June 2010.

[81] E. Vincan and N. Barker, "The upstream components of the Wnt signaling pathway in the dynamic EMT and MET associated with colorectal cancer progression," *Clinical & Experimental Metastasis*, vol. 25, pp. 657–663, March 2008.

[82] Z. Wang, S. Banerjee, Y. Li, K. M. Rahman, Y. Zhang, and F. H. Sarkar, "Down-regulation of notch-1 inhibits invasion by inactivation of nuclear factor-kappaB, vascular endothelial growth factor, and matrix metalloproteinase-9 in pancreatic cancer cells," *Cancer Research*, vol. 66, pp. 2778–2784, March 2006.

[83] J. M. Bailey, P. K. Singh, and M. A. Hollingsworth, "Cancer metastasis facilitated by developmental pathways: Sonic hedgehog, Notch, and bone

morphogenic proteins," *Journal of Cellular Biochemistry*, vol. 102, pp. 829–839, November 2007.

[84] E. H. Gort, A. J. Groot, E. van der Wall, P. J. van Diest, and M. A. Vooijs, "Hypoxic regulation of metastasis via hypoxia-inducible factors," *Current Molecular Medicine*, vol. 8, pp. 60–67, February 2008.

[85] P. A. Gregory, A. G. Bert, E. L. Paterson, S. C. Barry, A. Tsykin, G. Farshid, M. A. Vadas, Y. Khew-Goodall, and G. J. Goodall, "The miR-200 family and miR-205 regulate epithelial to mesenchymal transition by targeting ZEB1 and SIP1," *Nature Cell Biology*, vol. 10, pp. 593–601, May 2008.

[86] S. M. Park, A. B. Gaur, E. Lengyel, and M. E. Peter, "The miR-200 family determines the epithelial phenotype of cancer cells by targeting the E-cadherin repressors ZEB1 and ZEB2," *Genes & Development*, vol. 22, pp. 894–907, April 2008.

[87] P. A. Gregory, C. P. Bracken, A. G. Bert, and G. J. Goodall, "MicroRNAs as regulators of epithelial-mesenchymal transition," *Cell Cycle*, vol. 7, pp. 3112–3118, October 2008.

[88] O. C. Rodriguez, A. W. Schaefer, C. A. Mandato, P. Forscher, W. M. Bement, and C. Waterman-Storer, "Conserved microtubule-actin interactions in cell movement and morphogenesis," *Nature Cell Biology*, vol. 5, pp. 599–609, July 2003.

[89] A. Nrnberg, T. Kitzing, and R. Grosse, "Nucleating actin for invasion," *Nature Reviews. Cancer*, vol. 11, pp. 177–187, February 2011.

[90] T. D. Pollard and J. A. Cooper, "Actin, a central player in cell shape and movement," *Science*, vol. 326, pp. 1208–1212, November 2009.

[91] A. J. Ridley, M. A. Schwartz, K. Burridge, R. A. Firtel, M. H. Ginsberg, G. Borisy, J. T. Parsons, and A. R. Horwitz, "Cell migration: integrating signals from front to back," *Science*, vol. 302, pp. 1704–1709, December 2003.

[92] A. J. Ridley, "Life at the leading edge," *Cell*, vol. 145, pp. 1012–1022, June 2011.

[93] P. A. Coulombe and P. Wong, "Cytoplasmic intermediate filaments revealed as dynamic and multipurpose scaffolds," *Nature Cell Biology*, vol. 6, August 2004.

[94] T. A. Hely and D. J. Willshaw, "Short-term interactions between microtubules and actin filaments underlie long-term behaviour in neuronal growth cones," *Proc. R. Soc. B*, vol. 265, pp. 1801–1807, September 1998.

[95] A. W. Schaefer, N. Kabir, and P. Forscher, "Filopodia and actin arcs guide the assembly and transport of two populations of microtubules with unique dynamic parameters in neuronal growth cones," *The Journal of Cell Biology*, vol. 158, pp. 139–152, July 2002.

[96] N. Kabir, A. W. Schaefer, A. Nakhost, W. S. Sossin, and P. Forscher, "Protein kinase C activation promotes microtubule advance in neuronal growth cones by increasing average microtubule growth lifetimes," *The Journal of Cell Biology*, vol. 152, pp. 1033–1044, March 2001.

[97] F. Q. Zhou, C. M. Waterman-Storer, and C. S. Cohan, "Focal loss of actin bundles causes microtubule redistribution and growth cone turning," *The Journal of Cell Biology*, vol. 157, pp. 839–849, May 2002.

[98] N. M. Sherer and W. Mothes, "Cytonemes and tunneling nanotubules in cell-cell communication and viral pathogenesis," *Trends in Cell Biology*, vol. 18, pp. 414–420, September 2008.

[99] D. A. Lauffenburger and A. F. Horwitz, "Cell migration: a physically integrated molecular process," *Cell*, vol. 84, pp. 359–369, February 1996.

[100] P. A. DiMilla, K. Barbee, and D. A. Lauffenburger, "Mathematical model for the effects of adhesion and mechanics on cell migration speed," *Biophysical Journal*, vol. 60, pp. 15–37, July 1991.

[101] A. Mogilner and G. Oster, "Cell motility driven by actin polymerization," *Biophysical journal*, vol. 71, pp. 3030–3045, December 1996.

[102] F. L. Miles, F. L. Pruitt, K. L. van Golen, and C. R. Cooper, "Stepping out of the flow: capillary extravasation in cancer metastasis," *Clinical & experimental metastasis*, vol. 25, pp. 305–324, June 2008.

[103] S. E. Cross, Y. S. Jin, J. Tondre, R. Wong, J. Rao, and J. K. Gimzewski, "AFM-based analysis of human metastatic cancer cells," *Nanotechnology*, vol. 19, pp. 384003–384010, September 2008.

[104] S. E. Cross, Y. S. Jin, J. Rao, and J. K. Gimzewski, "Nanomechanical analysis of cells from cancer patients," *Nature Nanotechnology*, vol. 2, pp. 780–783, December 2007.

[105] C. T. Mierke, D. P. Zitterbart, P. Kollmannsberger, C. Raupach, U. Schlotzer-Schrehardt, T. W. Goecke, J. Behrens, and B. Fabry, "Breakdown of the endothelial barrier function in tumor cell transmigration," *Biophysical Journal*, vol. 94, pp. 2832–2846, April 2008.

[106] A. B. Al-Mehdi, K. Tozawa, A. B. Fisher, L. Shientag, A. Lee, and R. J. Muschel, "Intravascular origin of metastasis from the proliferation of endothelium-attached tumor cells: a new model for metastasis," *Nature Medicine*, vol. 6, pp. 100–102, January 2000.

[107] A. F. Chambers, I. C. MacDonald, E. E. Schmidt, V. L. Morris, and A. C. Groom, "Clinical targets for anti-metastasis therapy," *Advances in Cancer Research*, vol. 79, pp. 91–121, 2000.

[108] N. Reymond, J. H. Im, R. Garg, F. M. Vega, B. B. d'Agua, P. Riou, S. Cox, F. Valderrama, R. J. Muschel, and A. J. Ridley, "CDC42 promotes transendothelial migration of cancer cells through β1 integrin," *The Journal of Cell Biology*, vol. 199, pp. 653–668, November 2012.

[109] T. Dittmar, C. Heyder, E. Gloria-Maercker, W. Hatzmann, and K. S. Zanker, "Adhesion molecules and chemokines: the navigation system for circulating tumor (stem) cells to metastasize in an organ-specific manner," *Clinical & Experimental Metastasis*, vol. 25, pp. 11–32, September 2008.

[110] A. F. Chambers, A. C. Groom, and I. C. MacDonald, "Dissemination and growth of cancer cells in metastatic sites," *Nature Reviews. Cancer*, vol. 2, pp. 563–572, August 2002.

[111] G. Mannori, D. Santoro, L. Carter, C. Corless, R. M. Nelson, and M. P. Bevilacqua, "Inhibition of colon carcinoma cell lung colony formation by a soluble form of E-selectin," *The American Journal of Pathology*, vol. 151, pp. 233–243, July 1997.

[112] L. Weiss, "Biomechanical interactions of cancer cells with the microvasculature during hematogenous metastasis," *Cancer and Metastasis Reviews*, vol. 11, pp. 227–235, November 1992.

[113] Y. J. Kim, L. Borsig, N. M. Varki, and A. Varki, "P-selectin deficiency attenuates tumor growth and metastasis," *Proceedings of the National Academy of Sciences of the United States of America*, vol. 95, pp. 9325–9330, August 1998.

[114] S. Paget, "The Distribution of Secondary Growth in Cancer of the Breast," *The Lancet*, vol. 133, pp. 571–573, October 1889.

[115] I. J. Fidler, "The pathogenesis of cancer metastasis: The 'seed and soil' hypothesis revisited," *Nature Reviews. Cancer*, vol. 3, pp. 453–458, June 2003.

[116] S. C. Smith and D. Theodorescu, "Learning therapeutic lessons from metastasis suppressor proteins," *Nature Reviews. Cancer*, vol. 9, pp. 253–264, April 2009.

[117] H.-H. Gerdes, N. V. Bukoreshtliev, and J. F. V. Barroso, "Tunneling nanotubes: A new route for the exchange of components between animal cells," *FEBS letters*, vol. 581, pp. 2194–2201, May 2007.

[118] T. Elsdale and J. Bard, "Collagen substrata for studies on cell behavior," *The Journal of cell biology*, vol. 54, pp. 626–637, September 1972.

[119] D. E. Ingber and J. Folkman, "How does extracellular matrix control capillary morphogenesis?," *Cell*, vol. 58, pp. 803–805, September 1989.

[120] C. T. Mierke, "Cancer cells regulate biomechanical properties of human microvascular endothelial cells," *The Journal of Biological Chemistry*, vol. 286, pp. 40025–40037, November 2011.

[121] C. Urbich, A. Kuehbacher, and S. Dimmeler, "Role of microRNAs in vascular diseases, inflammation, and angiogenesis," *Cardiovascular Research*, vol. 79, pp. 581–588, September 2008.

[122] S. Anand and D. A. Cheresh, "MicroRNA-mediated regulation of the angiogenic switch," *Current Opinion in Hematology*, vol. 18, pp. 171–176, May 2011.

[123] J. A. Joyce and J. W. Pollard, "Microenvironmental regulation of metastasis," *Nature Reviews. Cancer*, vol. 9, pp. 239–252, April 2009.

[124] P. Lu, V. M. Weaver, and Z. Werb, "The extracellular matrix: a dynamic niche in cancer progression," *The Journal of Cell Biology*, vol. 196, pp. 395–406, February 2012.

[125] K. R. Johnson, J. L. Leight, and V. M. Weaver, "Demystifying the effects of a three-dimensional microenvironment in tissue morphogenesis," *Methods in Cell Biology*, vol. 83, pp. 547–583, March 2007.

[126] H. F. Dvorak, "Tumors: wounds that do not heal. Similarities between tumor stroma generation and wound healing," *The New England Journal of Medicine*, vol. 315, pp. 1650–1659, December 1986.

[127] J. S. Palumbo, K. E. Talmage, J. V. Massari, C. M. L. Jeunesse, M. J. Flick, K. W. Kombrinck, Z. Hu, K. A. Barney, and J. L. Degen, "Tumor cell-associated tissue factor and circulating hemostatic factors cooperate to increase metastatic potential through natural killer cell-dependent and-independent mechanisms," *Blood*, vol. 110, pp. 133–141, July 2007.

[128] J. A. Nagy, S. H. Chang, S. C. Shih, A. M. Dvorak, and H. F. Dvorak, "Heterogeneity of the tumor vasculature," *Seminars in Thrombosis and Hemostasis*, vol. 36, pp. 321–331, April 2010.

[129] S. Anand, B. K. Majeti, L. M. Acevedo, E. A. Murphy, R. Mukthavaram, L. Scheppke, M. Huang, D. J. Shields, J. N. Lindquist, P. E. Lapinski, P. D. King, S. M. Weis, and D. A. Cheresh, "MicroRNA-132-mediated loss of p120RasGAP activates the endothelium to facilitate pathological angiogenesis," *Nature Medicine*, vol. 16, August 2010.

[130] D. R. Welch, "Technical considerations for studying cancer metastasis in vivo," *Clinical & Experimental Metastasis*, vol. 15, pp. 272–306, May 1997.

[131] K. Hida, Y. Hida, D. N. Amin, A. F. Flint, D. Panigrahy, C. C. Morton, and M. Klagsbrun, "Tumor-associated endothelial cells with cytogenetic abnormalities," *Cancer Research*, vol. 64, pp. 8249–8255, November 2004.

[132] K. Hida and M. Klagsbrun, "A new perspective on tumor endothelial cells: unexpected chromosome and centrosome abnormalities," *Cancer Research*, vol. 65, pp. 2507–2510, April 2005.

[133] K. Hida, Y. Hida, and M. Shindoh, "Understanding tumor endothelial cell abnormalities to develop ideal anti-angiogenic therapies," *Cancer Science*, vol. 99, pp. 459–466, March 2008.

[134] C. W. Melnyk, A. Molnar, and D. C. Baulcombe, "Intercellular and systemic movement of RNA silencing signals," *The EMBO journal*, vol. 30, pp. 3553–3563, August 2011.

[135] M. Mittelbrunn and F. Snchez-Madrid, "Intercellular communication: diverse structures for exchange of genetic information," *Nature Reviews. Molecular Cell Biology*, vol. 13, pp. 328–335, April 2012.

[136] S. E. Andaloussi, I. Mger, X. O. Breakefield, and M. J. A. Wood, "Extracellular vesicles: biology and emerging therapeutic opportunities," *Nature Reviews. Drug Discovery*, vol. 12, pp. 347–357, April 2013.

[137] D. Tirziu, F. J. Giordano, and M. Simons, "Cell Communications in the Heart [Basic Science for Clinicians]," *Circulation*, vol. 122, pp. 928–937, August 2010.

[138] P. D. Arkwright, F. Luchetti, J. Tour, C. Roberts, R. Ayub, A. P. Morales, J. J. Rodriguez, A. Gilmore, B. Canonico, S. Papa, and M. D. Esposti, "Fas stimulation of T lymphocytes promotes rapid intercellular exchange of death signals via membrane nanotubes," *Cell Research*, vol. 20, pp. 72–88, January 2010.

[139] M. Mack, A. Kleinschmidt, H. Bruhl, C. Klier, P. J. Nelson, J. Cihak, J. Plachy, M. Stangassinger, V. Erfle, and D. Schlondorff, "Transfer of the chemokine receptor CCR5 between cells by membrane-derived microparticles: a mechanism for cellular human immunodeficiency virus 1 infection," *Nature Medicine*, vol. 6, pp. 769–775, July 2000.

[140] S. Ali and G. Lazennec, "Chemokines: novel targets for breast cancer metastasis," *Cancer Metastasis Reviews*, vol. 26, pp. 401–420, Dec 2007.

[141] H. Peinado, M. Aleckovic, S. Lavotshkin, I. Matei, B. Costa-Silva, G. Moreno-Bueno, M. Hergueta-Redondo, C. Williams, G. Garcia-Santos, C. Ghajar, A. Nitadori-Hoshino, C. Hoffman, K. Badal, B. A. Garcia, M. K. Callahan, J. Yuan, V. R. Martins, J. Skog, R. N. Kaplan, M. S. Brady, J. D. Wolchok, P. B. Chapman, Y. Kang, J. Bromberg, and D. Lyden, "Melanoma exosomes

educate bone marrow progenitor cells toward a pro-metastatic phenotype through MET," *Nature Medicine*, vol. 18, pp. 883–891, June 2012.

[142] V. Muralidharan-Chari, J. W. Clancy, A. Sedgwick, and C. D'Souza-Schorey, "Microvesicles: Mediators of extracellular communication during cancer progression," *Journal of Cell Science*, vol. 123, pp. 1603–1611, May 2010.

[143] H. G. Zhang and W. E. Grizzle, "Exosomes and cancer: A newly described pathway of immune suppression," *Clinical Cancer Research*, vol. 17, pp. 959–964, March 2011.

[144] V. Luga, L. Zhang, A. M. Viloria-Petit, A. A. Ogunjimi, M. R. Inanlou, E. Chiu, M. Buchanan, A. N. Hosein, M. Basik, and J. L. Wrana, "Exosomes mediate stromal mobilization of autocrine Wnt-PCP signaling in breast cancer cell migration," *Cell*, vol. 151, pp. 1542–1556, December 2012.

[145] N. Kosaka and T. Ochiya, "Unraveling the Mystery of Cancer by Secretory microRNA: Horizontal microRNA Transfer between Living Cells," *Frontiers in Genetics*, vol. 2, January 2012.

[146] S. Domhan, L. Ma, A. Tai, Z. Anaya, A. Beheshti, M. Zeier, L. Hlatky, and A. Abdollahi, "Intercellular communication by exchange of cytoplasmic material via tunneling nano-tube like structures in primary human renal epithelial cells," *PloS One*, vol. 6, p. 21283, June 2011.

[147] B. G. Zani and E. R. Edelman, "Cellular bridges: Routes for intercellular communication and cell migration," *Communicative & Integrative Biology*, vol. 3, pp. 215–220, May 2010.

[148] B. G. Zani, L. Indolfi, and E. R. Edelman, "Tubular bridges for bronchial epithelial cell migration and communication," *PloS one*, vol. 5, p. 8930, January 2010.

[149] S. Bloemendal and U. Kck, "Cell-to-cell communication in plants, animals, and fungi: A comparative review," *Naturwissenschaften*, November 2012.

[150] J. E. Trosko and R. J. Ruch, "Cell-cell communication in carcinogenesis," *Frontiers in Bioscience: A Journal and Virtual Library*, vol. 3, pp. 208–236, February 1998.

[151] A. Bafico, G. Liu, L. Goldin, V. Harris, and S. A. Aaronson, "An autocrine mechanism for constitutive Wnt pathway activation in human cancer cells," *Cancer Cell*, vol. 6, pp. 497–506, November 2004.

[152] R. L. Yauch, S. E. Gould, S. J. Scales, T. Tang, H. Tian, C. P. Ahn, D. Marshall, L. Fu, T. Januario, D. Kallop, M. Nannini-Pepe, K. Kotkow, J. C. Marsters, L. L. Rubin, and F. J. de Sauvage, "A paracrine requirement for hedgehog signalling in cancer," *Nature*, vol. 455, pp. 406–410, September 2008.

[153] A. B. Singh and R. C. Harris, "Autocrine, paracrine and juxtacrine signaling by EGFR ligands," *Cellular Signaling*, vol. 17, pp. 1183–1193, October 2005.

[154] B. J. Nickoloff, B. A. Osborne, and L. Miele, "Notch signaling as a therapeutic target in cancer: A new approach to the development of cell fate modifying agents," *Oncogene*, vol. 22, pp. 6598–6608, September 2003.

[155] P. Rizzo, C. Osipo, K. Foreman, T. Golde, B. Osborne, and L. Miele, "Rational targeting of Notch signaling in cancer," *Oncogene*, vol. 27, pp. 5124–5131, September 2008.

[156] S. Gurke, J. F. Barroso, and H. H. Gerdes, "The art of cellular communication: Tunneling nanotubes bridge the divide," *Histochemistry and Cell Biology*, vol. 129, pp. 539–550, May 2008.

[157] K. Al-Nedawi, B. Meehan, R. S. Kerbel, A. C. Allison, and J. Rak, "Endothelial expression of autocrine VEGF upon the uptake of tumor-derived microvesicles containing oncogenic EGFR," *Proceedings of the National Academy of Sciences of the United States of America*, vol. 106, pp. 3794–3799, March 2009.

[158] M. C. Henderson and D. O. Azorsa, "The Genomic and Proteomic Content of Cancer Cell-Derived Exosomes," *Frontiers in Oncology*, vol. 2, pp. 3794–3799, April 2012.

[159] M. E. Dinger, T. R. Mercer, and J. S. Mattick, "RNAs as extracellular signaling molecules," *Journal of Molecular Endocrinology*, vol. 40, pp. 151–159, April 2008.

[160] C. Harding, J. Heuser, and P. Stahl, "Endocytosis and intracellular processing of transferrin and colloidal gold-transferrin in rat reticulocytes: demonstration of a pathway for receptor shedding," *European Journal of Cell Biology*, vol. 35, pp. 256–263, November 1984.

[161] B.-T. Pan and R. M. Johnstone, "Fate of the transferrin receptor during maturation of sheep reticulocytes in vitro: Selective externalization of the receptor," *Cell*, vol. 33, pp. 967–978, July 1983.

[162] A. Turchinovich, L. Weiz, and B. Burwinkel, "Extracellular miRNAs: The mystery of their origin and function," *Trends in Biochemical Sciences*, vol. 37, pp. 460–465, November 2012.

[163] C. Thery, L. Zitvogel, and S. Amigorena, "Exosomes: composition, biogenesis and function," *Nature Reviews. Immunology*, vol. 2, pp. 569–579, August 2002.

[164] A. J. Maule, "Plasmodesmata: structure, function and biogenesis," *Current Opinion in Plant Biology*, vol. 11, pp. 680–686, December 2008.

[165] J. C. Palauqui, T. Elmayan, J. M. Pollien, and H. Vaucheret, "Systemic acquired silencing: transgene-specific post-transcriptional silencing is transmitted by grafting from silenced stocks to non-silenced scions," *The EMBO Journal*, vol. 16, pp. 4738–4745, August 1997.

[166] A. Molnar, C. W. Melnyk, A. Bassett, T. J. Hardcastle, R. Dunn, and D. C. Baulcombe, "Small Silencing RNAs in Plants Are Mobile and Direct Epigenetic Modification in Recipient Cells," *Science*, vol. 328, pp. 872–875, May 2010.

[167] L. A. Gregory, R. A. Ricart, S. A. Patel, P. K. Lim, and P. Rameshwar, "microRNAs, Gap Junctional Intercellular Communication and Mesenchymal Stem Cells in Breast Cancer Metastasis," *Current Cancer Therapy Reviews*, vol. 7, pp. 176–183, August 2011.

[168] A. Mendoza-Naranjo, G. Bouma, C. Pereda, M. Ramirez, K. F. Webb, A. Tittarelli, M. N. Lopez, A. M. Kalergis, A. J. Thrasher, D. L. Becker, and F. Salazar-Onfray, "Functional gap junctions accumulate at the immunological synapse and contribute to T cell activation," *Journal of Immunology*, vol. 187, pp. 3121–3132, September 2011.

[169] V. Valiunas, Y. Y. Polosina, H. Miller, I. A. Potapova, L. Valiuniene, S. Doronin, R. T. Mathias, R. B. Robinson, M. R. Rosen, I. S. Cohen, and P. R. Brink, "Connexin-specific cell-to-cell transfer of short interfering RNA by gap junctions," *The Journal of Physiology*, vol. 568, pp. 459–468, October 2005.

[170] E. Kizana, E. Cingolani, and E. Marban, "Non-cell-autonomous effects of vector-expressed regulatory RNAs in mammalian heart cells," *Gene Therapy*, vol. 16, pp. 1163–1168, September 2009.

[171] M. M. Saunders, M. J. Seraj, Z. Li, Z. Zhou, C. R. Winter, D. R. Welch, and H. J. Donahue, "Breast cancer metastatic potential correlates with a breakdown in homospecific and heterospecific gap junctional intercellular communication," *Cancer Research*, vol. 61, pp. 1765–1767, March 2001.

[172] J. Pasquier, P. Magal, C. Boulange-Lecomte, G. Webb, and F. L. Foll, "Consequences of cell-to-cell P-glycoprotein transfer on acquired multidrug resistance in breast cancer: A cell population dynamics model," *Biology Direct*, vol. 6, p. 5, January 2011.

[173] K. Gousset and C. Zurzolo, "Tunneling nanotubes: A highway for prion spreading?," *Prion*, vol. 3, pp. 94–98, June 2009.

[174] G. P. Dubey and S. Ben-Yehuda, "Intercellular Nanotubes Mediate Bacterial Communication," *Cell*, vol. 144, pp. 590–600, February 2011.

[175] D. M. Davis and S. Sowinski, "Membrane nanotubes: dynamic long-distance connections between animal cells," *Nature Reviews. Molecular Cell Biology*, vol. 9, pp. 431–436, June 2008.

[176] B. Onfelt, S. Nedvetzki, R. K. Benninger, M. A. Purbhoo, S. Sowinski, A. N. Hume, M. C. Seabra, M. A. Neil, P. M. French, and D. M. Davis, "Structurally distinct membrane nanotubes between human macrophages support long-distance vesicular traffic or surfing of bacteria," *Journal of Immunology*, vol. 177, pp. 8476–8483, December 2006.

[177] B. Onfelt, "Long-Distance Calls Between Cells Connected by Tunneling Nanotubules," *Science's STKE*, p. 55, December 2005.

[178] S. Sowinski, C. Jolly, O. Berninghausen, M. A. Purbhoo, A. Chauveau, K. Kohler, S. Oddos, P. Eissmann, F. M. Brodsky, C. Hopkins, B. Onfelt, Q. Sattentau, and D. M. Davis, "Membrane nanotubes physically connect T cells over long distances presenting a novel route for HIV-1 transmission," *Nature Cell Biology*, vol. 10, pp. 211–219, February 2008.

[179] B. Onfelt, S. Nedvetzki, K. Yanagi, and D. M. Davis, "Cutting Edge: Membrane nanotubes connect immune cells," *Journal of Immunology*, vol. 173, pp. 1511–1513, August 2004.

[180] S. C. Watkins and R. D. Salter, "Functional Connectivity between Immune Cells Mediated by Tunneling Nanotubules," *Immunity*, vol. 23, pp. 309–318, September 2005.

[181] C. Schiller, J. E. Huber, K. N. Diakopoulos, and E. H. Weiss, "Tunneling nanotubes enable intercellular transfer of MHC class I molecules," *Human Immunology*, vol. 74, pp. 412–416, April 2013.

[182] C. Schiller, K. N. Diakopoulos, I. Rohwedder, E. Kremmer, C. von Toerne, M. Ueffing, U. H. Weidle, H. Ohno, and E. H. Weiss, "LST1 promotes the assembly of a molecular machinery responsible for tunneling nanotube formation," *Journal of Cell Science*, vol. 126, pp. 767–777, February 2013.

[183] A. Chauveau, A. Aucher, P. Eissmann, E. Vivier, and D. M. Davis, "Membrane nanotubes facilitate long-distance interactions between natural killer cells and target cells," *Proceedings of the National Academy of Sciences of the United States of America*, vol. 107, pp. 5545–5550, March 2010.

[184] J. C. Stinchcombe, G. Bossi, S. Booth, and G. M. Griffiths, "The Immunological Synapse of CTL Contains a Secretory Domain and Membrane Bridges," *Immunity*, vol. 15, pp. 751–761, November 2001.

[185] B. J. Quah, V. P. Barlow, V. McPhun, K. I. Matthaei, M. D. Hulett, and C. R. Parish, "Bystander B cells rapidly acquire antigen receptors from activated B cells by membrane transfer," *Proceedings of the National Academy of Sciences of the United States of America*, vol. 105, pp. 4259–4264, March 2008.

[186] D. Wittig, X. Wang, C. Walter, H. H. Gerdes, R. H. Funk, and C. Roehlecke, "Multi-level communication of human retinal pigment epithelial cells via tunneling nanotubes," *PloS one*, vol. 7, p. 33195, March 2012.

[187] K. C. Vallabhaneni, H. Haller, and I. Dumler, "Vascular smooth muscle cells initiate proliferation of mesenchymal stem cells by mitochondrial transfer via tunneling nanotubes," *Stem cells and development*, vol. 21, pp. 3104–3113, November 2012.

[188] K. He, X. Shi, X. Zhang, S. Dang, X. Ma, F. Liu, M. Xu, Z. Lv, D. Han, X. Fang, and Y. Zhang, "Long-distance intercellular connectivity between cardiomyocytes and cardiofibroblasts mediated by membrane nanotubes," *Cardiovascular Research*, vol. 92, pp. 39–47, October 2011.

[189] Y. Wang, J. Cui, X. Sun, and Y. Zhang, "Tunneling-nanotube development in astrocytes depends on p53 activation," *Cell death and differentiation*, November 2010.

[190] Y. Zhang, D. Liu, X. Chen, J. Li, L. Li, Z. Bian, F. Sun, J. Lu, Y. Yin, X. Cai, Q. Sun, K. Wang, Y. Ba, Q. Wang, D. Wang, J. Yang, P. Liu, T. Xu, Q. Yan, J. Zhang, K. Zen, and C. Y. Zhang, "Secreted monocytic miR-150 enhances targeted endothelial cell migration," *Molecular Cell*, vol. 39, pp. 133–144, July 2010.

[191] G. Lachenal, K. Pernet-Gallay, M. Chivet, F. J. Hemming, A. Belly, G. Bodon, B. Blot, G. Haase, Y. Goldberg, and R. Sadoul, "Release of exosomes from differentiated neurons and its regulation by synaptic glutamatergic activity," *Molecular and Cellular Neurosciences*, vol. 46, pp. 409–418, February 2011.

[192] N. M. Sherer, "Long-distance relationships: do membrane nanotubes regulate cell-cell communication and disease progression?," *Molecular Biology of the Cell*, vol. 24, pp. 1095–1098, April 2013.

[193] L. Marzo, K. Gousset, and C. Zurzolo, "Multifaceted Roles of Tunneling Nanotubes in Intercellular Communication," *Frontiers in Physiology*, vol. 3, April 2012.

[194] E. A. Eugenin, P. J. Gaskill, and J. W. Berman, "Tunneling nanotubes: A potential mechanism for intercellular HIV trafficking," *Communicative & Integrative Biology*, vol. 2, pp. 243–244, May 2009.

[195] J. Mukerji, K. C. Olivieri, V. Misra, K. A. Agopian, and D. Gabuzda, "Proteomic analysis of HIV-1 Nef cellular binding partners reveals a role for exocyst complex proteins in mediating enhancement of intercellular nanotube formation," *Retrovirology*, vol. 9, p. 33, June 2012.

[196] N. Izquierdo-Useros, M. Naranjo-Gomez, I. Erkizia, M. C. Puertas, F. E. Borras, J. Blanco, and J. Martinez-Picado, "HIV and mature dendritic cells: Trojan exosomes riding the Trojan horse?," *PLoS Pathogens*, vol. 6, p. 1000740, March 2010.

[197] G. Lambert, L. Estevez-Salmeron, S. Oh, D. Liao, B. M. Emerson, T. D. Tlsty, and R. H. Austin, "An analogy between the evolution of drug resistance in bacterial communities and malignant tissues," *Nature Reviews. Cancer*, vol. 11, pp. 375–382, May 2011.

[198] T. Wei, A. Kikuchi, Y. Moriyasu, N. Suzuki, T. Shimizu, K. Hagiwara, H. Chen, M. Takahashi, T. Ichiki-Uehara, and T. Omura, "The spread of Rice dwarf virus among cells of its insect vector exploits virus-induced tubular structures," *Journal of Virology*, vol. 80, pp. 8593–8602, September 2006.

[199] M. Belting and A. Wittrup, "Nanotubes, exosomes, and nucleic acid-binding peptides provide novel mechanisms of intercellular communication in eukaryotic cells: implications in health and disease," *The Journal of Cell Biology*, vol. 183, pp. 1187–1191, December 2008.

[200] J. Skog, T. Wrdinger, S. van Rijn, D. H. Meijer, L. Gainche, W. T. Curry, B. S. Carter, A. M. Krichevsky, and X. O. Breakefield, "Glioblastoma microvesicles transport RNA and proteins that promote tumour growth and provide diagnostic biomarkers," *Nature Cell Biology*, vol. 10, pp. 1470–1476, December 2008.

[201] K. Al-Nedawi, B. Meehan, J. Micallef, V. Lhotak, L. May, A. Guha, and J. Rak, "Intercellular transfer of the oncogenic receptor EGFRvIII by microvesicles derived from tumour cells," *Nature Cell Biology*, vol. 10, pp. 619–624, May 2008.

[202] S. S. Sidhu, A. T. Mengistab, A. N. Tauscher, J. LaVail, and C. Basbaum, "The microvesicle as a vehicle for EMMPRIN in tumor-stromal interactions," *Oncogene*, vol. 23, pp. 956–963, January 2004.

[203] E. Lou, S. Fujisawa, A. Barlas, Y. Romin, K. Manova-Todorova, M. A. Moore, and S. Subramanian, "Tunneling Nanotubes: A new paradigm for studying intercellular communication and therapeutics in cancer," *Communicative and Integrative Biology*, vol. 5, pp. 399–403, July 2012.

[204] E. U. Wieckowski, C. Visus, M. Szajnik, M. J. Szczepanski, W. J. Storkus, and T. L. Whiteside, "Tumor-derived microvesicles promote regulatory T cell expansion and induce apoptosis in tumor-reactive activated CD8+ T lymphocytes," *Journal of Immunology*, vol. 183, pp. 3720–3730, September 2009.

[205] J. W. Kim, E. Wieckowski, D. D. Taylor, T. E. Reichert, S. Watkins, and T. L. Whiteside, "Fas ligand-positive membranous vesicles isolated from sera of

patients with oral cancer induce apoptosis of activated T lymphocytes," *Clinical Cancer Research*, vol. 11, pp. 1010–1020, February 2005.

[206] J. Wolfers, A. Lozier, G. Raposo, A. Regnault, C. Thery, C. Masurier, C. Flament, S. Pouzieux, F. Faure, T. Tursz, E. Angevin, S. Amigorena, and L. Zitvogel, "Tumor-derived exosomes are a source of shared tumor rejection antigens for CTL cross-priming," *Nature Medicine*, vol. 7, pp. 297–303, March 2001.

[207] V. Ciravolo, V. Huber, G. C. Ghedini, E. Venturelli, F. Bianchi, M. Campiglio, D. Morelli, A. Villa, P. D. Mina, S. Menard, P. Filipazzi, L. Rivoltini, E. Tagliabue, and S. M. Pupa, "Potential role of HER2-overexpressing exosomes in countering trastuzumab-based therapy," *Journal of Cellular Physiology*, vol. 227, pp. 658–667, February 2012.

[208] S. V. Ambudkar, Z. E. Sauna, M. M. Gottesman, and G. Szakacs, "A novel way to spread drug resistance in tumor cells: functional intercellular transfer of P-glycoprotein (ABCB1)," *Trends in Pharmacological Sciences*, vol. 26, pp. 385–387, August 2005.

[209] J. Pasquier, L. Galas, C. Boulange-Lecomte, D. Rioult, F. Bultelle, P. Magal, G. Webb, and F. L. Foll, "Different Modalities of Intercellular Membrane Exchanges Mediate Cell-to-cell P-glycoprotein Transfers in MCF-7 Breast Cancer Cells," *The Journal of Biological Chemistry*, vol. 287, pp. 7374–7387, March 2012.

[210] I. Nazarenko, S. Rana, A. Baumann, J. McAlear, A. Hellwig, M. Trendelenburg, G. Lochnit, K. T. Preissner, and M. Zoller, "Cell surface tetraspanin Tspan8 contributes to molecular pathways of exosome-induced endothelial cell activation," *Cancer Research*, vol. 70, pp. 1668–1678, February 2010.

[211] V. Vasioukhin, P. Anker, P. Maurice, J. Lyautey, C. Lederrey, and M. Stroun, "Point mutations of the N-ras gene in the blood plasma DNA of patients with myelodysplastic syndrome or acute myelogenous leukaemia," *British Journal of Haematology*, vol. 86, pp. 774–779, April 1994.

[212] J. Pasquier, B. Guerrouahen, H. A. Thawadi, P. Ghiabi, M. Maleki, N. Abu-Kaoud, A. Jacob, M. Mirshahi, L. Galas, S. Rafii, F. L. Foll, and A. Rafii, "Preferential transfer of mitochondria from endothelial to cancer cells through tunneling nanotubes modulates chemoresistance," *Journal of Translational Medicine*, vol. 11, p. 94, April 2013.

[213] A. Levchenko, B. M. Mehta, X. Niu, G. Kang, L. Villafania, D. Way, D. Polycarpe, M. Sadelain, and S. M. Larson, "Intercellular transfer of P-glycoprotein mediates acquired multidrug resistance in tumor cells," *Proceedings of the National Academy of Sciences of the United States of America*, vol. 102, pp. 1933–1938, February 2005.

[214] X. Chen, H. Liang, J. Zhang, K. Zen, and C. Y. Zhang, "Secreted microRNAs: a new form of intercellular communication," *Trends in Cell Biiology*, vol. 22, pp. 125–132, March 2012.

[215] H. Valadi, K. Ekstrom, A. Bossios, M. Sjostrand, J. J. Lee, and J. O. Lotvall, "Exosome-mediated transfer of mRNAs and microRNAs is a novel mechanism of genetic exchange between cells," *Nature cell biology*, vol. 9, pp. 654–659, June 2007.

[216] L. Holmgren, A. Szeles, E. Rajnavolgyi, J. Folkman, G. Klein, I. Ernberg, and K. I. Falk, "Horizontal transfer of DNA by the uptake of apoptotic bodies," *Blood*, vol. 93, pp. 3956–3963, June 1999.

[217] D. M. Pegtel, K. Cosmopoulos, D. A. Thorley-Lawson, M. A. van Eijndhoven, E. S. Hopmans, J. L. Lindenberg, T. D. de Gruijl, T. Wurdinger, and J. M. Middeldorp, "Functional delivery of viral miRNAs via exosomes," *Proceedings of the National Academy of Sciences of the United States of America*, vol. 107, pp. 6328–6333, April 2010.

[218] M. A. Cortez, C. Bueso-Ramos, J. Ferdin, G. Lopez-Berestein, A. K. Sood, and G. A. Calin, "MicroRNAs in body fluids–the mix of hormones and biomarkers," *Nature Reviews. Clinical Oncology*, vol. 8, pp. 467–477, June 2011.

[219] X. Chen, Y. Ba, L. Ma, X. Cai, Y. Yin, K. Wang, J. Guo, Y. Zhang, J. Chen, X. Guo, Q. Li, X. Li, W. Wang, Y. Zhang, J. Wang, X. Jiang, Y. Xiang, C. Xu, P. Zheng, J. Zhang, R. Li, H. Zhang, X. Shang, T. Gong, G. Ning, J. Wang, K. Zen, J. Zhang, and C. Y. Zhang, "Characterization of microRNAs in serum: a novel class of biomarkers for diagnosis of cancer and other diseases," *Cell Research*, vol. 18, pp. 997–1006, October 2008.

[220] M. Mittelbrunn, C. Gutirrez-Vzquez, C. Villarroya-Beltri, S. Gonzlez, F. Snchez-Cabo, M. ngel Gonzlez, A. Bernad, and F. Snchez-Madrid, "Unidirectional transfer of microRNA-loaded exosomes from T cells to antigen-presenting cells," *Nature Communications*, vol. 2, p. 282, April 2011.

[221] E. Hergenreider, S. Heydt, K. Treguer, T. Boettger, A. J. Horrevoets, A. M. Zeiher, M. P. Scheffer, A. S. Frangakis, X. Yin, M. Mayr, T. Braun, C. Urbich, R. A. Boon, and S. Dimmeler, "Atheroprotective communication between endothelial cells and smooth muscle cells through miRNAs," *Nature Cell Biology*, vol. 14, pp. 249–256, February 2012.

[222] A. Fire, S. Xu, M. K. Montgomery, S. A. Kostas, S. E. Driver, and C. C. Mello, "Potent and specific genetic interference by double-stranded RNA in Caenorhabditis elegans," *Nature*, vol. 391, pp. 806–811, February 1998.

[223] W. M. Winston, C. Molodowitch, and C. P. Hunter, "Systemic RNAi in C. elegans requires the putative transmembrane protein SID-1," *Science*, vol. 295, pp. 2456–2459, Mar 29 2002.

[224] W. D. O. Hamilton and D. C. Baulcombe, "Infectious RNA Produced by in vitro Transcription of a Full-length Tobacco Rattle Virus RNA-1 cDNA," *Journal of General Virology*, vol. 70, pp. 963–968, April 1989.

[225] J. N. Culver and W. O. Dawson, "Tobacco mosaic virus coat protein: an elicitor of the hypersensitive reaction but not required for the development of mosaic symptoms in Nicotiana sylvestris," *Virology*, vol. 173, pp. 755–758, December 1989.

[226] P. Dunoyer, G. Schott, C. Himber, D. Meyer, A. Takeda, J. C. Carrington, and O. Voinnet, "Small RNA duplexes function as mobile silencing signals between plant cells," *Science*, vol. 328, pp. 912–916, May 2010.

[227] A. Carlsbecker, J.-Y. Lee, C. J. Roberts, J. Dettmer, S. Lehesranta, J. Zhou, O. Lindgren, M. A. Moreno-Risueno, A. Vatn, S. Thitamadee, A. Campilho, J. Sebastian, J. L. Bowman, Y. Helariutta, and P. N. Benfey, "Cell signalling by microRNA-165/6 directs gene dose-dependent root cell fate," *Nature*, vol. 465, pp. 316–321, April 2010.

[228] N. Kosaka, H. Iguchi, and T. Ochiya, "Circulating microRNA in body fluid: a new potential biomarker for cancer diagnosis and prognosis," *Cancer science*, vol. 101, pp. 2087–2092, October 2010.

[229] R. Ma, T. Jiang, and X. Kang, "Circulating microRNAs in cancer: origin, function and application," *Journal of Experimental & Clinical Cancer Research*, vol. 31, p. 38, April 2012.

[230] P. S. Mitchell, R. K. Parkin, E. M. Kroh, B. R. Fritz, S. K. Wyman, E. L. Pogosova-Agadjanyan, A. Peterson, J. Noteboom, K. C. O'Briant, A. Allen, D. W. Lin, N. Urban, C. W. Drescher, B. S. Knudsen, D. L. Stirewalt, R. Gentleman, R. L. Vessella, P. S. Nelson, D. B. Martin, and M. Tewari, "Circulating microRNAs as stable blood-based markers for cancer detection," *Proceedings of the National Academy of Sciences of the United States of America*, vol. 105, pp. 10513–10518, July 2008.

[231] O. F. Laterza, L. Lim, P. W. Garrett-Engele, K. Vlasakova, N. Muniappa, W. K. Tanaka, J. M. Johnson, J. F. Sina, T. L. Fare, F. D. Sistare, and W. E. Glaab, "Plasma MicroRNAs as sensitive and specific biomarkers of tissue injury," *Clinical Chemistry*, vol. 55, pp. 1977–1983, Nov 2009.

[232] K. C. Vickers, B. T. Palmisano, B. M. Shoucri, R. D. Shamburek, and A. T. Remaley, "MicroRNAs are transported in plasma and delivered to recipient cells by high-density lipoproteins," *Nature cell biology*, vol. 13, pp. 423–433, April 2011.

[233] J. D. Arroyo, J. R. Chevillet, E. M. Kroh, I. K. Ruf, C. C. Pritchard, D. F. Gibson, P. S. Mitchell, C. F. Bennett, E. L. Pogosova-Agadjanyan, D. L. Stirewalt,

J. F. Tait, and M. Tewari, "Argonaute2 complexes carry a population of circulating microRNAs independent of vesicles in human plasma," *Proceedings of the National Academy of Sciences of the United States of America*, vol. 108, pp. 5003–5008, March 2011.

[234] K. Wang, S. Zhang, J. Weber, D. Baxter, and D. J. Galas, "Export of microRNAs and microRNA-protective protein by mammalian cells," *Nucleic Acids Research*, vol. 38, pp. 7248–7259, November 2010.

[235] J. A. Weber, D. H. Baxter, S. Zhang, D. Y. Huang, K. H. Huang, M. J. Lee, D. J. Galas, and K. Wang, "The microRNA spectrum in 12 body fluids," *Clinical Chemistry*, vol. 56, pp. 1733–1741, November 2010.

[236] C. H. Lawrie, S. Gal, H. M. Dunlop, B. Pushkaran, A. P. Liggins, K. Pulford, A. H. Banham, F. Pezzella, J. Boultwood, J. S. Wainscoat, C. S. Hatton, and A. L. Harris, "Detection of elevated levels of tumour-associated microRNAs in serum of patients with diffuse large B-cell lymphoma," *British Journal of Haematology*, vol. 141, pp. 672–675, May 2008.

[237] W. Zhu, W. Qin, U. Atasoy, and E. R. Sauter, "Circulating microRNAs in breast cancer and healthy subjects," *BMC Research Notes*, vol. 2, pp. 89–93, May 2009.

[238] Z. Hu, X. Chen, Y. Zhao, T. Tian, G. Jin, Y. Shu, Y. Chen, L. Xu, K. Zen, C. Zhang, and H. Shen, "Serum microRNA signatures identified in a genome-wide serum microRNA expression profiling predict survival of non-small-cell lung cancer," *Journal of Clinical Oncology: Official Journal of the American Society of Clinical Oncology*, vol. 28, pp. 1721–1726, April 2010.

[239] M. Boeri, C. Verri, D. Conte, L. Roz, P. Modena, F. Facchinetti, E. Calabro, C. M. Croce, U. Pastorino, and G. Sozzi, "MicroRNA signatures in tissues and plasma predict development and prognosis of computed tomography detected lung cancer," *Proceedings of the National Academy of Sciences of the United States of America*, vol. 108, pp. 3713–3718, March 2011.

[240] K. E. Resnick, H. Alder, J. P. Hagan, D. L. Richardson, C. M. Croce, and D. E. Cohn, "The detection of differentially expressed microRNAs from the serum of ovarian cancer patients using a novel real-time PCR platform," *Gynecologic Oncology*, vol. 112, pp. 55–59, January 2009.

[241] D. D. Taylor and C. Gercel-Taylor, "MicroRNA signatures of tumor-derived exosomes as diagnostic biomarkers of ovarian cancer," *Gynecologic Oncology*, vol. 110, pp. 13–21, July 2008.

[242] K. Wang, S. Zhang, B. Marzolf, P. Troisch, A. Brightman, Z. Hu, L. E. Hood, and D. J. Galas, "Circulating microRNAs, potential biomarkers for drug-induced liver injury," *Proceedings of the National Academy of Sciences of the United States of America*, vol. 106, pp. 4402–4407, March 2009.

[243] A. S. Ho, X. Huang, H. Cao, C. Christman-Skieller, K. Bennewith, Q. T. Le, and A. C. Koong, "Circulating miR-210 as a Novel Hypoxia Marker in Pancreatic Cancer," *Translational oncology*, vol. 3, pp. 109–113, April 2010.

[244] T. S. Wong, X. B. Liu, B. Y. Wong, R. W. Ng, A. P. Yuen, and W. I. Wei, "Mature miR-184 as Potential Oncogenic microRNA of Squamous Cell Carcinoma of Tongue," *Clinical Cancer Research*, vol. 14, pp. 2588–2592, May 2008.

[245] E. Moussay, K. Wang, J. H. Cho, K. van Moer, S. Pierson, J. Paggetti, P. V. Nazarov, V. Palissot, L. E. Hood, G. Berchem, and D. J. Galas, "MicroRNA as biomarkers and regulators in B-cell chronic lymphocytic leukemia," *Proceedings of the National Academy of Sciences of the United States of America*, vol. 108, pp. 6573–6578, April 2011.

[246] M. Tanaka, K. Oikawa, M. Takanashi, M. Kudo, J. Ohyashiki, K. Ohyashiki, and M. Kuroda, "Down-regulation of miR-92 in human plasma is a novel marker for acute leukemia patients," *PloS One*, vol. 4, p. 5532, May 2009.

[247] E. K. Ng, W. W. Chong, H. Jin, E. K. Lam, V. Y. Shin, J. Yu, T. C. Poon, S. S. Ng, and J. J. Sung, "Differential expression of microRNAs in plasma of patients with colorectal cancer: a potential marker for colorectal cancer screening," *Gut*, vol. 58, pp. 1375–1381, October 2009.

[248] Z. Huang, D. Huang, S. Ni, Z. Peng, W. Sheng, and X. Du, "Plasma microRNAs are promising novel biomarkers for early detection of colorectal cancer," *International Journal of Cancer*, vol. 127, pp. 118–126, July 2010.

[249] M. Miyachi, K. Tsuchiya, H. Yoshida, S. Yagyu, K. Kikuchi, A. Misawa, T. Iehara, and H. Hosoi, "Circulating muscle-specific microRNA, miR-206, as a potential diagnostic marker for rhabdomyosarcoma," *Biochemical and Biophysical Research Communications*, vol. 400, pp. 89–93, September 2010.

[250] M. Tsujiura, D. Ichikawa, S. Komatsu, A. Shiozaki, H. Takeshita, T. Kosuga, H. Konishi, R. Morimura, K. Deguchi, H. Fujiwara, K. Okamoto, and E. Otsuji, "Circulating microRNAs in plasma of patients with gastric cancers," *British Journal of Ciancer*, vol. 102, pp. 1174–1179, March 2010.

[251] N. J. Park, H. Zhou, D. Elashoff, B. S. Henson, D. A. Kastratovic, E. Abemayor, and D. T. Wong, "Salivary microRNA: Discovery, Characterization, and Clinical Utility for Oral Cancer Detection," *Clinical Cancer Research*, vol. 15, pp. 5473–5477, August 2009.

[252] E. C. Hung, R. W. Chiu, and Y. M. Lo, "Detection of circulating fetal nucleic acids: A review of methods and applications," *Journal of Clinical Pathology*, vol. 62, pp. 308–313, April 2009.

[253] S. Gilad, E. Meiri, Y. Yogev, S. Benjamin, D. Lebanony, N. Yerushalmi, H. Benjamin, M. Kushnir, H. Cholakh, N. Melamed, Z. Bentwich, M. Hod, Y. Goren,

and A. Chajut, "Serum microRNAs are promising novel biomarkers," *PloS One*, vol. 3, p. 3148, September 2008.

[254] G. D. Sorenson, D. M. Pribish, F. H. Valone, V. A. Memoli, D. J. Bzik, and S. L. Yao, "Soluble normal and mutated DNA sequences from single-copy genes in human blood," *Cancer Epidemiology, Biomarkers & Prevention*, vol. 3, pp. 67–71, January 1994.

[255] X. Xue, Y. M. Zhu, and P. J. Woll, "Circulating DNA and lung cancer," *Annals of the New York Academy of Sciences*, vol. 1075, pp. 154–164, September 2006.

[256] N. Bruhn, T. Beinert, C. Oehm, B. Jandrig, I. Petersen, X. Q. Chen, K. Possinger, and M. Fleischhacker, "Detection of microsatellite alterations in the DNA isolated from tumor cells and from plasma DNA of patients with lung cancer," *Annals of the New York Academy of Sciences*, vol. 906, pp. 72–82, April 2000.

[257] H. Schwarzenbach, V. Muller, N. Stahmann, and K. Pantel, "Detection and characterization of circulating microsatellite-DNA in blood of patients with breast cancer," *Annals of the New York Academy of Sciences*, vol. 1022, pp. 25–32, June 2004.

[258] H. Nawroz, W. Koch, P. Anker, M. Stroun, and D. Sidransky, "Microsatellite alterations in serum DNA of head and neck cancer patients," *Nature medicine*, vol. 2, pp. 1035–1037, September 1996.

[259] B. Taback, S. Saha, and D. S. Hoon, "Comparative analysis of mesenteric and peripheral blood circulating tumor DNA in colorectal cancer patients," *Annals of the New York Academy of Sciences*, vol. 1075, pp. 197–203, September 2006.

[260] A. A. Kamat, A. K. Sood, D. Dang, D. M. Gershenson, J. L. Simpson, and F. Z. Bischoff, "Quantification of total plasma cell-free DNA in ovarian cancer using real-time PCR," *Annals of the New York Academy of Sciences*, vol. 1075, pp. 230–234, September 2006.

[261] A. V. Lichtenstein, H. S. Melkonyan, L. D. Tomei, and S. R. Umansky, "Circulating nucleic acids and apoptosis," *Annals of the New York Academy of Sciences*, vol. 945, pp. 239–249, September 2001.

[262] I. Muller, K. Urban, K. Pantel, and H. Schwarzenbach, "Comparison of genetic alterations detected in circulating microsatellite DNA in blood plasma samples of patients with prostate cancer and benign prostatic hyperplasia," *Annals of the New York Academy of Sciences*, vol. 1075, pp. 222–229, September 2006.

[263] K. K. Vdovichenko, S. I. Markova, and A. S. Belokhvostov, "Mutant Form of BRAF Gene in Blood Plasma of Cancer Patients," *Annals of the New York Academy of Sciences*, vol. 1022, pp. 228–231, January 2004.

[264] H. H. Schlechte, C. Stelzer, S. Weickmann, M. Fleischhacker, and G. Schulze, "TP53 gene in blood plasma DNA of tumor patients," *Annals of the New York Academy of Sciences*, vol. 1022, pp. 61–69, June 2004.

[265] S. A. Leon, B. Shapiro, D. M. Sklaroff, and M. J. Yaros, "Free DNA in the serum of cancer patients and the effect of therapy," *Cancer Research*, vol. 37, pp. 646–650, March 1977.

[266] S. Holdenrieder and P. Stieber, "Therapy control in oncology by circulating nucleosomes," *Annals of the New York Academy of Sciences*, vol. 1022, pp. 211–216, June 2004.

[267] G. Lindstedt, P. A. Lundberg, S. Iwarsson, and J. Lindberg, "Circulating heat-labile DNA binder(s) in chronic active hepatitis and rheumatoid arthritis," *International Journal of Clinical C hemistry*, vol. 62, pp. 183–185, July 1975.

[268] B. Schmidt, S. Weickmann, C. Witt, and M. Fleischhacker, "Integrity of cell-free plasma DNA in patients with lung cancer and nonmalignant lung disease," *Annals of the New York Academy of Sciences*, vol. 1137, pp. 207–213, August 2008.

[269] M. Chiba, M. Kimura, and S. Asari, "Exosomes secreted from human colorectal cancer cell lines contain mRNAs, microRNAs and natural antisense RNAs, that can transfer into the human hepatoma HepG2 and lung cancer A549 cell lines," *Oncology Reports*, vol. 28, pp. 1551–1558, November 2012.

[270] T. Kogure, W. L. Lin, I. K. Yan, C. Braconi, and T. Patel, "Intercellular nanovesicle-mediated microRNA transfer: A mechanism of environmental modulation of hepatocellular cancer cell growth," *Hepatology*, vol. 54, pp. 1237–1248, October 2011.

[271] M. Katakowski, B. Buller, X. Wang, T. Rogers, and M. Chopp, "Functional microRNA is transferred between glioma cells," *Cancer Research*, vol. 70, pp. 8259–8263, November 2010.

[272] K. Ohshima, K. Inoue, A. Fujiwara, K. Hatakeyama, K. Kanto, Y. Watanabe, K. Muramatsu, Y. Fukuda, S. Ogura, K. Yamaguchi, and T. Mochizuki, "Let-7 microRNA family is selectively secreted into the extracellular environment via exosomes in a metastatic gastric cancer cell line," *PloS One*, vol. 5, p. 13247, October 2010.

[273] G. V. Glinsky, A. B. Glinskii, O. Berezovskaya, B. A. Smith, P. Jiang, X. M. Li, M. Yang, and R. M. Hoffman, "Dual-color-coded imaging of viable circulating prostate carcinoma cells reveals genetic exchange between tumor cells in vivo, contributing to highly metastatic phenotypes," *Cell Cycle*, vol. 5, pp. 191–197, January 2006.

[274] F. Moinfar, Y. G. Man, L. Arnould, G. L. Bratthauer, M. Ratschek, and F. A. Tavassoli, "Concurrent and independent genetic alterations in the stromal and epithelial cells of mammary carcinoma: implications for tumorigenesis," *Cancer Research*, vol. 60, pp. 2562–2566, May 2000.

[275] A. Bergsmedh, A. Szeles, M. Henriksson, A. Bratt, M. J. Folkman, A. L. Spetz, and L. Holmgren, "Horizontal transfer of oncogenes by uptake of apoptotic bodies," *Proceedings of the National Academy of Sciences of the United States of America*, vol. 98, pp. 6407–6411, May 2001.

[276] J. Ehnfors, M. Kost-Alimova, N. L. Persson, A. Bergsmedh, J. Castro, T. Levchenko-Tegnebratt, L. Yang, T. Panaretakis, and L. Holmgren, "Horizontal transfer of tumor DNA to endothelial cells in vivo," *Cell Death and Differentiation*, vol. 16, pp. 749–757, May 2009.

[277] M. C. Deregibus, V. Cantaluppi, R. Calogero, M. L. Iacono, C. Tetta, L. Biancone, S. Bruno, B. Bussolati, and G. Camussi, "Endothelial progenitor cell derived microvesicles activate an angiogenic program in endothelial cells by a horizontal transfer of mRNA," *Blood*, vol. 110, pp. 2440–2448, October 2007.

[278] S. Fischer, M. Nishio, S. C. Peters, M. Tschernatsch, M. Walberer, S. Weidemann, R. Heidenreich, P. O. Couraud, B. B. Weksler, I. A. Romero, T. Gerriets, and K. T. Preissner, "Signaling mechanism of extracellular RNA in endothelial cells," *FASEB Journal*, vol. 23, pp. 2100–2109, July 2009.

[279] M. Baj-Krzyworzeka, R. Szatanek, K. Weglarczyk, J. Baran, B. Urbanowicz, P. Branski, M. Z. Ratajczak, and M. Zembala, "Tumour-derived microvesicles carry several surface determinants and mRNA of tumour cells and transfer some of these determinants to monocytes," *Cancer Immunology, Immunotherapy*, vol. 55, pp. 808–818, July 2006.

[280] M. Fabbri, A. Paone, F. Calore, R. Galli, E. Gaudio, R. Santhanam, F. Lovat, P. Fadda, C. Mao, G. J. Nuovo, N. Zanesi, M. Crawford, G. H. Ozer, D. Wernicke, H. Alder, M. A. Caligiuri, P. Nana-Sinkam, D. Perrotti, and C. M. Croce, "MicroRNAs bind to Toll-like receptors to induce prometastatic inflammatory response," *Proceedings of the National Academy of Sciences of the United States of America*, vol. 109, pp. 2110–6, July 2012.

[281] C. Grange, M. Tapparo, F. Collino, L. Vitillo, C. Damasco, M. C. Deregibus, C. Tetta, B. Bussolati, and G. Camussi, "Microvesicles released from human renal cancer stem cells stimulate angiogenesis and formation of lung premetastatic niche," *Cancer Research*, vol. 71, pp. 5346–5356, August 2011.

[282] F. Wen, A. Shen, A. Choi, E. W. Gerner, and J. Shi, "Extracellular DNA in pancreatic cancer promotes cell invasion and metastasis," *Cancer Research*, May 2013.

[283] P. K. Lim, S. A. Bliss, S. A. Patel, M. Taborga, M. A. Dave, L. A. Gregory, S. J. Greco, M. Bryan, P. S. Patel, and P. Rameshwar, "Gap junction-mediated import of microRNA from bone marrow stromal cells can elicit cell cycle quiescence in breast cancer cells," *Cancer Research*, vol. 71, pp. 1550–1560, March 2011.

[284] J. Palma, S. C. Yaddanapudi, L. Pigati, M. A. Havens, S. Jeong, G. A. Weiner, K. M. Weimer, B. Stern, M. L. Hastings, and D. M. Duelli, "MicroRNAs are exported from malignant cells in customized particles," *Nucleic Acids Research*, vol. 40, pp. 9125–9138, October 2012.

[285] D. J. Gibbings, C. Ciaudo, M. Erhardt, and O. Voinnet, "Multivesicular bodies associate with components of miRNA effector complexes and modulate miRNA activity," *Nature Cell Biology*, vol. 11, pp. 1143–1149, September 2009.

[286] H. F. Dvorak, "Vascular permeability factor/vascular endothelial growth factor: A critical cytokine in tumor angiogenesis and a potential target for diagnosis and therapy," *Journal of Clinical Oncology*, vol. 20, pp. 4368–4380, November 2002.

[287] K. J. Png, N. Halberg, M. Yoshida, and S. F. Tavazoie, "A microRNA regulon that mediates endothelial recruitment and metastasis by cancer cells," *Nature*, vol. 481, pp. 190–194, December 2011.

[288] P. D. Bos, D. X. Nguyen, and J. Massagu, "Modeling metastasis in the mouse," *Current Opinion in Pharmacology*, vol. 10, pp. 571–577, October 2010.

[289] A. Albini and R. Benelli, "The chemoinvasion assay: a method to assess tumor and endothelial cell invasion and its modulation," *Nature Protocols*, vol. 2, pp. 504–511, March 2007.

[290] M. J. Bissell and D. Radisky, "Putting tumours in context," *Nat Rev Cancer*, vol. 1, pp. 46–54, October 2001.

[291] L. G. Griffith and M. A. Swartz, "Capturing complex 3D tissue physiology in vitro," *Nature Reviews. Molecular Cell Biology*, vol. 7, pp. 211–224, March 2006.

[292] D. M. Bissell, D. M. Arenson, J. J. Maher, and F. J. Roll, "Support of cultured hepatocytes by a laminin-rich gel. Evidence for a functionally significant subendothelial matrix in normal rat liver," *The Journal of Clinical Investigation*, vol. 79, pp. 801–812, March 1987.

[293] J. T. Emerman and D. R. Pitelka, "Maintenance and induction of morphological differentiation in dissociated mammary epithelium on floating collagen membranes," *In vitro*, vol. 13, pp. 316–328, May 1977.

[294] E. D. Hay and J. W. Dodson, "Secretion of collagen by corneal epithelium. I. Morphology of the collagenous products produced by isolated epithelia grown on frozen-killed lens," *The Journal of Cell Biology*, vol. 57, pp. 190–213, April 1973.

[295] T. Elsdale and J. Bard, "Cellular Interactions in Mass Cultures of Human Diploid Fibroblasts," *Nature*, vol. 236, pp. 152–155, March 1972.

[296] E. Cukierman, R. Pankov, D. R. Stevens, and K. M. Yamada, "Taking cell-matrix adhesions to the third dimension," *Science*, vol. 294, pp. 1708–1712, November 2001.

[297] V. M. Weaver, "Reversion of the Malignant Phenotype of Human Breast Cells in Three-Dimensional Culture and In Vivo by Integrin Blocking Antibodies," *The Journal of Cell Biology*, vol. 137, pp. 231–245, April 1997.

[298] F. Wang, R. K. Hansen, D. Radisky, T. Yoneda, M. H. Barcellos-Hoff, O. W. Petersen, E. A. Turley, and M. J. Bissell, "Phenotypic Reversion or Death of Cancer Cells by Altering Signaling Pathways in Three-Dimensional Contexts," *Journal of the National Cancer Institute*, vol. 94, pp. 1494–1503, October 2002.

[299] O. W. Petersen, L. Ronnov-Jessen, A. R. Howlett, and M. J. Bissell, "Interaction with basement membrane serves to rapidly distinguish growth and differentiation pattern of normal and malignant human breast epithelial cells," *Proceedings of the National Academy of Sciences of the United States of America*, vol. 89, pp. 9064–9068, October 1992.

[300] H. K. Kleinman, M. L. McGarvey, J. R. Hassell, V. L. Star, F. B. Cannon, G. W. Laurie, and G. R. Martin, "Basement membrane complexes with biological activity," *Biochemistry*, vol. 25, pp. 312–318, January 1986.

[301] G. H. Underhill, G. Peter, C. S. Chen, and S. N. Bhatia, "Bioengineering Methods for Analysis of Cells In Vitro," *Annual Review of Cell and Developmental Biology*, vol. 28, pp. 385–410, November 2012.

[302] M. A. Karsdal, P. Hjorth, K. Henriksen, T. Kirkegaard, K. L. Nielsen, H. Lou, J. M. Delaisse, and N. T. Foged, "Transforming growth factor-beta controls human osteoclastogenesis through the p38 MAPK and regulation of RANK expression," *The Journal of Biological Chemistry*, vol. 278, pp. 44975–44987, November 2003.

[303] M. J. Bissell, A. Rizki, and I. S. Mian, "Tissue architecture: The ultimate regulator of breast epithelial function," *Current opinion in cell biology*, vol. 15, pp. 753–762, December 2003.

[304] T. Shibue and R. A. Weinberg, "Integrin β1-focal adhesion kinase signaling directs the proliferation of metastatic cancer cells disseminated in the lungs,"

Proceedings of the National Academy of Sciences of the United States of America, vol. 106, pp. 10290–10295, June 2009.

[305] M. A. Pollmann, Q. Shao, D. W. Laird, and M. Sandig, "Connexin 43 mediated gap junctional communication enhances breast tumor cell diapedesis in culture," *Breast Cancer Research*, vol. 7, pp. R522–34, May 2005.

[306] J. Krutzfeldt, N. Rajewsky, R. Braich, K. G. Rajeev, T. Tuschl, M. Manoharan, and M. Stoffel, "Silencing of microRNAs in vivo with 'antagomirs'," *Nature*, vol. 438, pp. 685–689, December 2005.

[307] S. Seaman, J. Stevens, M. Y. Yang, D. Logsdon, C. Graff-Cherry, and B. S. Croix, "Genes that distinguish physiological and pathological angiogenesis," *Cancer Cell*, vol. 11, pp. 539–554, June 2007.

[308] S. L. Reck-Peterson, D. W. P. Jr, M. S. Mooseker, and J. A. Mercer, "Class V myosins," *Biochimica et Biophysica Acta*, vol. 1496, pp. 36–51, March 2000.

[309] E. Atilgan, D. Wirtz, and S. X. Sun, "Mechanics and dynamics of actin-driven thin membrane protrusions," *Biophysical Journal*, vol. 90, pp. 65–76, January 2006.

[310] K. Yusa and T. Tsuruo, "Reversal mechanism of multidrug resistance by verapamil: Direct binding of verapamil to P-glycoprotein on specific sites and transport of verapamil outward across the plasma membrane of K562/ADM cells," *Cancer Research*, vol. 49, pp. 5002–5006, September 1989.

[311] A. K. Tiwari, K. Sodani, C. L. Dai, A. H. Abuznait, S. Singh, Z. J. Xiao, A. Patel, T. T. Talele, L. Fu, A. Kaddoumi, J. M. Gallo, and Z. S. Chen, "Nilotinib potentiates anticancer drug sensitivity in murine ABCB1-, ABCG2-, and ABCC10-multidrug resistance xenograft models," *Cancer Letters*, vol. 328, pp. 307–317, January 2013.

[312] W. C. Yen and W. W. Lamph, "The selective retinoid X receptor agonist bexarotene (LGD1069, Targretin) prevents and overcomes multidrug resistance in advanced breast carcinoma," *Molecular Cancer Therapeutics*, vol. 4, pp. 824–834, May 2005.

[313] L. Ma, J. Teruya-Feldstein, and R. A. Weinberg, "Tumour invasion and metastasis initiated by microRNA-10b in breast cancer," *Nature*, vol. 449, pp. 682–688, October 2007.

[314] J. Shan, T. P. Munro, E. Barbarese, J. H. Carson, and R. Smith, "A molecular mechanism for mRNA trafficking in neuronal dendrites," *The Journal of Neuroscience*, vol. 23, pp. 8859–8866, October 2003.

[315] R. S. Kerbel and B. A. Kamen, "The anti-angiogenic basis of metronomic chemotherapy," *Nature Reviews. Cancer*, vol. 4, pp. 423–436, June 2004.

[316] G. Woehlke and M. Schliwa, "Walking on two heads: the many talents of kinesin," *Nature Reviews. Molecular Cell Biology*, vol. 1, pp. 50–58, October 2000.

[317] K. M. Trybus, "Myosin V from head to tail," *Cellular and Molecular Life Sciences*, vol. 65, pp. 1378–1389, May 2008.

[318] D. A. Smith and R. M. Simmons, "Models of motor-assisted transport of intracellular particles," *Biophysical Journal*, vol. 80, pp. 45–68, January 2001.

[319] A. Palazon, A. Teijeira, I. Martinez-Forero, S. Hervas-Stubbs, C. Roncal, I. Penuelas, J. Dubrot, A. Morales-Kastresana, J. L. Perez-Gracia, M. C. Ochoa, L. Ochoa-Callejero, A. Martinez, A. Luque, J. Dinchuk, A. Rouzaut, M. Jure-Kunkel, and I. Melero, "Agonist anti-CD137 mAb act on tumor endothelial cells to enhance recruitment of activated T lymphocytes," *Cancer Research*, vol. 71, pp. 801–811, February 2011.

[320] J. Wang, K. K. Chong, Y. Nakamura, L. Nguyen, S. K. Huang, C. Kuo, W. Zhang, H. Yu, D. L. Morton, and D. S. B. Hoon, "B7-H3 Associated with Tumor Progression and Epigenetic Regulatory Activity in Cutaneous Melanoma," *Journal of Investigative Dermatology*, Aprilv 2013.

[321] C. Liu, J. Liu, J. Wang, Y. Liu, F. Zhang, W. Lin, A. Gao, M. Sun, Y. Wang, and Y. Sun, "B7-H3 expression in ductal and lobular breast cancer and its association with IL-10," *Molecular Medicine Reports*, 2012.

[322] K. Hase, S. Kimura, H. Takatsu, M. Ohmae, S. Kawano, H. Kitamura, M. Ito, H. Watarai, C. C. Hazelett, C. Yeaman, and H. Ohno, "M-Sec promotes membrane nanotube formation by interacting with Ral and the exocyst complex," *Nature Cell Biology*, vol. 11, pp. 1427–1432, November 2009.

[323] Y. Zhao and W. Guo, "Secure nanotubes with RalA and Exocyst," *Nature Cell Biology*, vol. 11, pp. 1396–1397, 2009.

[324] Y. W. Heng and C. G. Koh, "Actin cytoskeleton dynamics and the cell division cycle," *The International Journal of Biochemistry & Cell Biology*, vol. 42, pp. 1622–1633, October 2010.

[325] K. Sugihara, S. Asano, K. Tanaka, A. Iwamatsu, K. Okawa, and Y. Ohta, "The exocyst complex binds the small GTPase RalA to mediate filopodia formation," *Nature Cell Biology*, vol. 4, pp. 73–78, January 2002.

[326] S. Kimura, K. Hase, and H. Ohno, "Tunneling nanotubes: emerging view of their molecular components and formation mechanisms," *Experimental Cell Research*, vol. 318, pp. 1699–1706, August 2012.

[327] S. J. Gould, A. M. Booth, and J. E. Hildreth, "The Trojan exosome hypothesis," *Proceedings of the National Academy of Sciences of the United States of America*, vol. 100, pp. 10592–10597, September 2003.

[328] A. Bobrie, M. Colombo, G. Raposo, and C. Thery, "Exosome secretion: Molecular mechanisms and roles in immune responses," *Traffic*, vol. 12, pp. 1659–1668, December 2011.

[329] C. Wolfrum, S. Shi, K. N. Jayaprakash, M. Jayaraman, G. Wang, R. K. Pandey, K. G. Rajeev, T. Nakayama, K. Charrise, E. M. Ndungo, T. Zimmermann, V. Koteliansky, M. Manoharan, and M. Stoffel, "Mechanisms and optimization of in vivo delivery of lipophilic siRNAs," *Nature Biotechnology*, vol. 25, pp. 1149–1157, October 2007.